Regulation of *C. elegans* behavior and physiology by the hypoxia-response pathway

by

Corinne L. Pender

B.S. Biology
California Institute of Technology, 2009

Submitted to the Department of Biology
in Partial Fulfillment of the Requirements for the Degree of

Doctor of Philosophy

at the

Massachusetts Institute of Technology

June 2018

Signature of Author: _____
Department of Biology
March 13, 2018

Certified by: _____
H. Robert Horvitz
Professor of Biology
Thesis Supervisor

Accepted by: _____
Amy E. Keating
Professor of Biology
Co-Chair, Biology Graduate Committee

Regulation of *C. elegans* behavior and physiology by the hypoxia-response pathway

By Corinne L. Pender

Submitted to the Department of Biology on March 13, 2018
in Partial Fulfillment of the Requirements for the Degree of
Doctor of Philosophy in Biology

Abstract

The transcriptional response controlling adaptation to internal and environmental hypoxia is broadly conserved in animals. The key mediator of this response is the transcription factor HIF (hypoxia-inducible factor), which is active only in hypoxia due to the function of its negative regulators, the prolyl hydroxylase EGLN and the E3 ubiquitin ligase complex recognition subunit pVHL. HIF drives transcription of hundreds of targets that promote hypoxia adaptation. Recent work has also described important and broad roles for HIF outside of the traditional hypoxia response, including functions in immunity, oxidative and other stress responses, and behavior; how HIF targets drive these aspects of animal physiology is poorly understood. In this dissertation, I describe genetic analyses of the nematode *C. elegans* that have provided insight into the function of HIF targets in regulating animal physiology and behavior.

The EGLN family was defined by the *C. elegans* homolog, EGL-9. Prior to the identification of EGL-9 as a HIF hydroxylase, our laboratory discovered the *egl-9* gene from studies of egg-laying behavior. *egl-9* loss-of-function mutants, in which HIF is constitutively active, are egg-laying defective; the mechanism regulating egg laying downstream of HIF has been unknown. From a screen for suppressors of the *egl-9(lf)* egg-laying defect, we identified the gene *cyp-36A1*, which encodes a cytochrome P450 enzyme and is likely a direct transcriptional target of HIF. In addition to modulating egg-laying behavior downstream of HIF, CYP-36A1 controls expression of more than a third of HIF-upregulated genes and regulates multiple stress responses. A screen for suppressors of *cyp-36A1(lf)* identified the nuclear hormone receptor NHR-46. We propose that CYP-36A1 functions as a hormone biosynthetic enzyme for the ligand of this receptor, thus mediating gene expression changes that alter stress physiology and behavior. We also found site-of-action and genetic evidence for at least one additional pathway acting downstream of EGL-9 and HIF-1 to regulate egg-laying behavior. These studies have identified novel HIF effectors that broadly affect physiology and behavior in *C. elegans*, and reveal new avenues for future work on regulation of HIF-controlled biology.

Thesis Supervisor: Dr. H. Robert Horvitz
Title: Professor of Biology

Biographical Note

Education

Massachusetts Institute of Technology — Cambridge, MA
PhD, Biology — Expected June 2018

California Institute of Technology — Pasadena, CA
BS, Biology, Graduation with Honors — June 2009

Awards

Caltech Axline Merit Scholar (2005 – 2009)
Caltech London Scholar (University College London; 2007)

Research Experience

MIT Department of Biology — Cambridge, MA
Graduate student — Sept. 2011 – June 2018
Advisor: Dr. H. Robert Horvitz

- Identified a novel hormone signaling pathway that acts downstream of the HIF hypoxia-response pathway to regulate *C. elegans* behavior, stress responses, and gene expression
- Identified additional genes involved in regulation of *C. elegans* egg laying
- Studied the role of biogenic amines in regulating locomotory responses to food availability

Arbor Vita Corporation — Fremont, CA
Research associate — Sept. 2009 – April 2011

- Worked on development of a lateral flow test for avian influenza
- Developed a cell-based assay for identifying novel stroke therapeutics

Caltech Department of Biology — Pasadena, CA
Amgen Scholar — April – Aug. 2007
Advisor: Dr. Paul Patterson

- Worked on establishing a habituation procedure for functional magnetic resonance imaging (fMRI) in conscious mice
- Conducted preliminary neuroimaging studies

Rossum Family Summer Research Fellow — July 2006 – March 2007
Advisor: Dr. Ralph Adolphs

- Investigated differences between social and non-social learning in humans using fMRI

Teaching Experience

MIT Department of Biology — Cambridge, MA
Undergraduate Cell Biology, Teaching Assistant — Fall 2014
Graduate Genetics, Teaching Assistant — Fall 2012

Caltech Department of Biology — Pasadena, CA
The Biology and Biophysics of Viruses, Teaching Assistant — Spring 2009
The Biology and Biophysics of Viruses, Teaching Assistant — Spring 2008

Publications

Pender, C.L. & Horvitz, H.R. The HIF hypoxia-response pathway drives hormonal signaling to modulate *C. elegans* stress resistance and behavior (submitted)

Ma, D.K., Rothe, M., Zheng, S., Bhatla, N., **Pender, C.L.**, Menzel, R., & Horvitz, H.R. Cytochrome P450 drives a HIF-regulated behavioral response to reoxygenation by *C. elegans*. *Science* 341.6145 (2013): 554-558.

Paquin, N., Murata, Y., Froehlich, A., Omura, D.T., Ailion, M., **Pender, C.L.**, Constantine-Paton, M., & Horvitz, H.R. The conserved VPS-50 protein functions in dense-core vesicle maturation and acidification and controls animal behavior. *Current Biology* 26.7 (2016): 862-871.

Presentations (talks)

Pender, C.L. & Horvitz, H.R. A cytochrome P450 and nuclear hormone receptor control hypoxia-regulated behaviors. MIT Building 68 Annual Retreat, Falmouth, MA, June 2017.

Pender, C.L. & Horvitz, H.R. HIF-1 regulates behavior and stress response by controlling the activity of a cytochrome P450 and NHR. Boston Area Worm Meeting, Cambridge, MA, May 2017.

Pender, C.L. & Horvitz, H.R. CYP-36A1 acts downstream of the EGL-9/HIF-1 hypoxia-response pathway to regulate *C. elegans* egg-laying behavior. International *C. elegans* meeting, Los Angeles, CA, June 2015.

Pender, C.L., Kim., H. and Adolphs, R. Investigating neural correlates of social conditioning in humans using fMRI. Southern California Conference for Undergraduate Research, Los Angeles, CA, November 2006.

Presentations (Posters)

Pender, C.L. & Horvitz, H.R. A cytochrome P450 and nuclear hormone receptor control hypoxia-regulated behaviors and stress responses. Modulation of Neural Circuits and Behavior Gordon Conference, Newry, ME, June 2017.

Pender, C.L. & Horvitz, H.R. The EGL-9/HIF-1 hypoxia-response pathway controls the activity of a cytochrome P450 to regulate behavior and immune response. *C. elegans* neuroscience meeting, Nagoya, Japan, July 2016.

Pender, C.L. & Horvitz, H.R. Regulation of egg-laying behavior by the conserved EGL-9/HIF-1 hypoxia-response pathway. *C. elegans* neuroscience meeting, Madison, WI, July 2014.

Pender, C.L. & Horvitz, H.R. Regulation of egg-laying behavior by EGL-9. International *C. elegans* meeting, Los Angeles, CA, June 2013.

Acknowledgments

First and foremost, I would like to thank my advisor, Bob. It has been a privilege to work with such an exceptional scientist during my graduate career, and I feel truly grateful to have had that opportunity. He has given me the independence to explore my own path, while being supportive of both my science and career at every step. I would also like to thank my thesis committee, Matt Vander Heiden and Troy Littleton, who have provided invaluable advice that has shaped my work over the years, and have given me the encouragement to have confidence in myself as a scientist. Frank Solomon has been a wonderful mentor and friend from the beginning; his advice and wit have made life easier along the way. I am also grateful to the other faculty I have taught with or who have otherwise been important in my graduate education: Adam Martin, David Housman, Lenny Guarente, Dennis Kim, and Angelika Amon.

The Horvitz lab has been family to me throughout grad school, and I want to thank everyone who has made me feel at home coming into work. My baymate Nick P taught me about worm neuroscience and has an admirable willingness to help with any and every problem. Dengke and Nikhil were both forces of creativity and brilliance in the lab, and have been sources of friendship and support in the years since. Josh has kept room 433 entertaining in the last few years, as has Calista, more recently. Anna, Akiko, Eugene, Holly, Kaitlin, Na, Nick A, and Rita have made life in the lab and lunchroom more fun every day. The enthusiasm that both Nick B and Kirk have for science is inspiring; I have always appreciated the positive attitude they bring to the lab. Vivek has been a star lab citizen in his desire to help others and his thoughtful approach to science. My “lab sibling” and roommate Steve is second to none in his ability to understand my stupid jokes and willingness to follow any absurd or profound line of conversation wherever it goes. I must also thank our friends in the Kim lab, especially Zoë, Josh, Dan, and Spencer, who have made the fourth floor of building 68 the truly special place it is.

Life at MIT would not have been the same without my friends. I feel extremely lucky to have had such a wonderful group of people as co-adventurers on this grad school journey. In particular, Aaron Hosios, Alex Godfrey, Doug Cattie, Grace Chen, Jamie Kwasnieski, Jonathan Coravos, Mike Erickson, Sean McGeary, Stephen Eichhorn, and Tom O’Grady have been incredible friends and endless sources of fun, inspiration and support throughout the last seven years. Each of these friendships has meant so much to me, and over these years I have grown more as a person than I could have ever expected in large part because of them.

Finally, I would like to thank my family. Their constant love, encouragement, and support made the idea of traveling down this sometimes-difficult road seem possible, and made every moment of celebration more joyous. As the family continues to grow, I can’t wait to see all of the fun times the future has in store for us.

Table of Contents

Chapter One

Introduction

I. Introduction

Beginning 2.5 billion years ago, the atmosphere of our planet underwent a major shift in its composition due to the release of oxygen as a byproduct of photosynthesis. Aerobic organisms subsequently harnessed the released molecular oxygen as the terminal electron acceptor in the electron transport chain, allowing for the efficient generation of energy in the form of ATP by oxidative phosphorylation. The higher efficiency of oxidative phosphorylation for energy production facilitated the evolution of complex multicellular organisms, including animals, which depend absolutely on oxygen for their survival (Lane and Martin, 2010). Because of the fundamental importance of oxygen to normal animal physiology, delivery of molecular oxygen throughout the body and maintenance of oxygen homeostasis are critical. In some animals, such as in the nematode *Caenorhabditis elegans*, oxygen can reach all tissues by passive diffusion; in other cases, more elaborate systems of oxygen delivery have evolved, as can be seen in the complex cardiovascular and respiratory systems of larger animals. Unlike these oxygen delivery systems, the molecular mechanism mediating oxygen homeostasis, i.e. the response to low oxygen (hypoxia), is remarkably conserved throughout animals. This molecular pathway underlies responses to environmental and internal hypoxia as well as aspects of the development of the oxygen delivery systems themselves. At the core of this hypoxia-response pathway are the oxygen-sensing prolyl hydroxylase EGLN, the E3 ubiquitin ligase pVHL, and the transcription factor HIF (hypoxia-inducible factor). In this introduction, I will describe the discovery of this pathway (section II), provide an overview of the current knowledge of the function of each of the key pathway components in mammals (section III), and describe studies of this pathway in the nematode *C. elegans* (section IV).

II. The identification of a pathway that controls hypoxia-dependent gene expression

A. The hypoxia-inducible factor HIF regulates hypoxia-induced gene expression

Classic physiology studies established two major responses to environmental hypoxia in mammals: modulation of ventilation and increased production of red blood cells (Bunn and Poyton, 1996). The former represents a rapid response to hypoxia that is regulated by the carotid body chemosensory organ, the molecular mechanism of which is still poorly understood (Chang, 2017). The latter is a slower response that is driven by increased production of the hormone erythropoietin (Epo), an essential growth factor necessary for erythropoiesis, or red blood cell production (Jelkmann, 1992). The discovery of increased Epo mRNA levels in hypoxia-exposed hepatoma cells led to the development of this system as an important model for understanding transcriptional regulation by hypoxia (Goldberg et al., 1987). A major breakthrough in understanding the mechanism of Epo transcriptional regulation occurred with the identification of a 3' regulatory element, called a "hypoxia-responsive element" (HRE), required for Epo induction in hepatoma cells (Beck et al., 1991; Pugh et al., 1991; Semenza et al., 1991), shortly followed by the identification and characterization by Semenza and colleagues of a factor that binds this 3' sequence to regulate Epo expression (Semenza and Wang, 1992; Wang and Semenza, 1995). This factor, named HIF1 (for hypoxia-inducible factor), was found to consist of HIF1α and HIF1β subunits (Wang et al., 1995).

HRE and HIF1 were quickly shown to be important for regulating hypoxia-induced gene expression in contexts other than Epo expression in hepatoma cells. Fusing the Epo 3' enhancer to reporter genes confers hypoxia sensitivity to expression of those genes (Semenza et al., 1991); this hypoxia- and HRE-dependent control of gene expression was observed even when such

reporter gene/Epo 3' enhancer fusions were transfected into non-hepatoma cell types, suggesting that the oxygen-sensing mechanism must be broadly present, rather than confined to a small number of specialized tissues (Maxwell et al., 1993). Additionally, a variety of other genes were shown to be endogenously regulated by hypoxia in a HIF-dependent manner, including those encoding glycolytic enzymes (Semenza et al., 1994), the glucose transporter GLUT1 (Bashan et al., 1992; Ebert et al., 1995), and vascular endothelial growth factor (VEGF) (Manalo et al., 2005). It thus became apparent that HIF is a major player in the transcriptional response to hypoxia, and significant efforts began to identify the oxygen-sensing mechanism responsible for HIF's hypoxia-dependent activity.

B. pVHL controls O_2-dependent degradation of HIF

Analysis of HIFα and HIFβ mRNA and protein in normoxia (21% O_2) versus hypoxia determined that stabilization of the HIFα protein was primarily responsible for the induction of HIF activity in hypoxia, whereas the HIFβ protein is constitutively present (Huang et al., 1996). Subsequent work found that the ubiquitin/proteasome pathway controls degradation of HIFα and requires an oxygen-dependent degradation domain (ODDD) in HIFα (Huang et al., 1998). The mechanism of proteasome-dependent HIFα degradation was ultimately revealed by studies of the hypoxia response in a different system, renal carcinoma cells mutant for the von Hippel-Lindau (VHL) tumor suppressor gene. Mutations in the *VHL* gene are associated with a hereditary cancer syndrome characterized by a predisposition to develop renal carcinomas, retinal angiomas, and other tumor types (Kaelin, 2007). Hypoxia-inducible genes, including *VEGF* and *GLUT1*, are constitutively expressed in *VHL(lf)* renal carcinoma cells, suggesting that the pVHL protein encoded by the *VHL* gene functions in the oxygen-sensing pathway (Gnarra et al., 1996; Iliopoulos et al., 1996). Ratcliffe and colleagues found that HIFα is constitutively stabilized in

VHL(lf) cells, that pVHL and HIFα physically interact (Maxwell et al., 1999), and that the molecular function of pVHL is as the recognition component of a ubiquitin ligase complex that ubiquitylates sequences within the HIFα ODDD (Cockman et al., 2000). Ratcliffe, Kaelin and colleagues then determined that pVHL specifically interacts with a HIFα fragment containing a hydroxylated proline (Ivan et al., 2001; Jaakkola et al., 2001), and hypothesized the existence of a prolyl hydroxylase that makes the modification and might function as a direct oxygen sensor.

C. EGLN is required for pVHL and O_2-dependent HIF degradation

The prolyl hydroxylation of HIF requires iron, molecular oxygen, ascorbate, and 2-oxoglutarate, and is inhibited by Co(II) or Ni(II). That these same activator/inhibitor interactions are observed for members of the 2-oxoglutarate-dependent oxygenases suggested that the enzyme that hydroxylates HIFα might be a member of this family (Jaakkola et al., 2001). From a series of experiments using the nematode *C. elegans* and *in vitro* analyses, Ratcliffe and colleagues identified the relevant prolyl hydroxylase (Epstein et al., 2001). First, they identified a HIFα homolog in *C. elegans*, *hif-1*, and showed that, like mammalian HIFα, HIF-1 protein stability is regulated by prolyl hydroxylation. They then examined HIF-1 stability in worms mutant for various prolyl hydroxylases, and found that loss-of-function mutants for the predicted prolyl hydroxylase gene *egl-9* had constitutively stabilized HIF-1 protein; *egl-9* had been identified by our laboratory as required for the regulation of egg laying (Trent et al., 1983) but had no previously known molecular function. They further demonstrated that recombinant EGL-9 can hydroxylate a proline on HIF-1 and that this hydroxylation facilitates interaction between the *C. elegans* pVHL homolog VHL-1 and HIF-1. Finally, they identified three human homologs of EGL-9, EGLN1, EGLN2, and EGLN3, which similarly hydroxylate the human HIFα homolog.

D. Summary of the core hypoxia-response pathway

The function of the core hypoxia-response pathway is thus as follows: in normoxia, EGL-9/EGLN hydroxylates a proline on the HIFα subunit, allowing it to be recognized by pVHL and targeted for proteasomal degradation. In hypoxia, HIFα is stabilized; together with its constitutively stable partner HIFβ, it drives a transcriptional response to hypoxia (Figure 1).

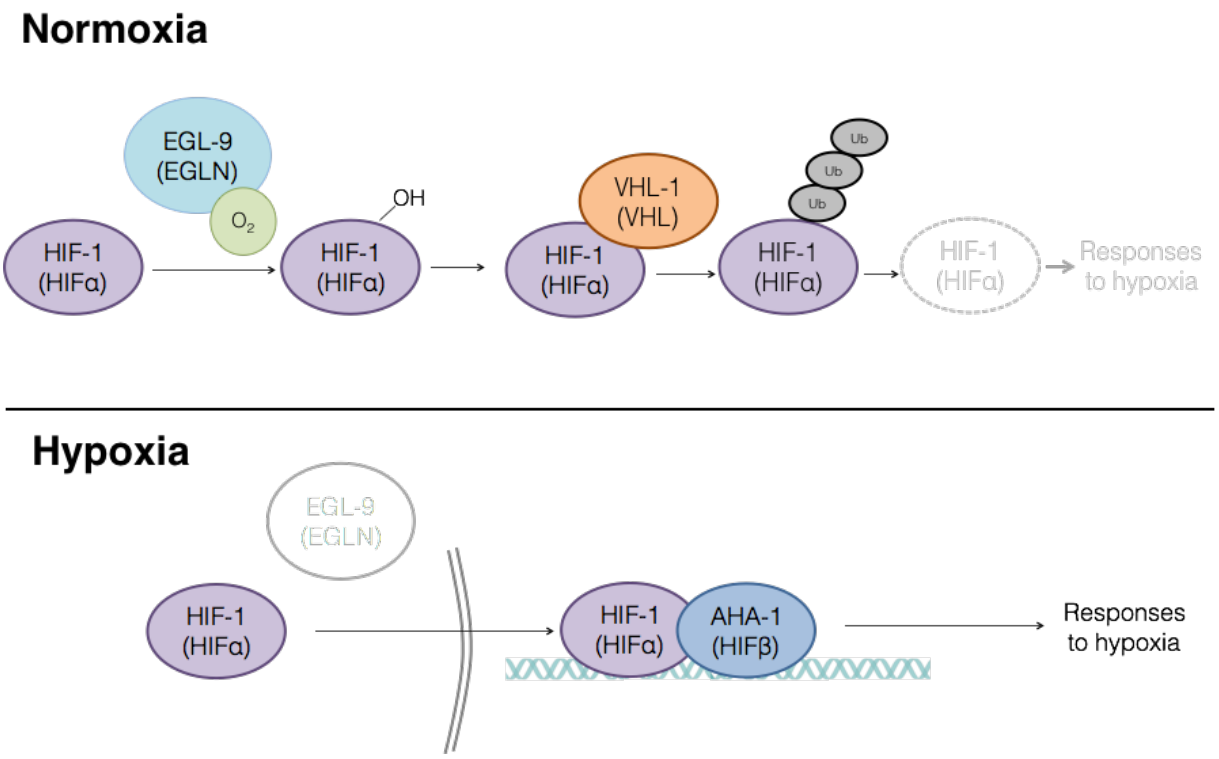

Figure 1. The EGLN/VHL/HIF hypoxia-response pathway. See text for details.

III. Function of the EGLN/VHL/HIF pathway in mammals

A. HIF regulates cellular, tissue, and organismal responses to hypoxia

i. The *HIFα* genes encode bHLH-PAS transcription factors

The HIF protein is a heterodimer consisting of a HIFα subunit, which is regulated by oxygen levels, and a HIFβ subunit, which is constitutively active. HIFα contains a bHLH (basic helix-loop-helix) domain, two PAS (Per-ARNT-Sim) domains, an oxygen-dependent degradation domain (ODDD), and two transactivation domains, called NTAD and CTAD. HIFβ also has bHLH and PAS domains, as well as a glutamine-rich transactivation domain (Burslem et al., 2017; Wu and Rastinejad, 2017). The bHLH and PAS domains function together to mediate dimerization of HIFα and HIFβ; the bHLH domains of HIFα and HIFβ also mediate binding to the core HRE (hypoxia-responsive element) motif, RCGTG (Wu et al., 2015). The ODDD, which overlaps with the NTAD, contains two prolines that are targets for EGLN-mediated hydroxylation (Ivan et al., 2001; Jaakkola et al., 2001; Masson et al., 2001; Wu and Rastinejad, 2017), and is thus essential for regulation of HIFα stability by oxygen. The transactivation domains recruit transcriptional coactivators; in particular, the CTAD interacts with CBP and p300 (Dames et al., 2002; Freedman et al., 2002), which promote transcription through histone acetylation and recruitment of RNA polymerase II (Vo and Goodman, 2001). Interestingly, the CTAD also contains a site of oxygen-dependent HIF regulation, mediated by another 2-oxoglutarate-dependent oxygenase, FIH1 (factor inhibiting HIF). FIH1, in the presence of oxygen, hydroxylates an asparagine near the C-terminus of HIFα, blocking the recruitment of p300/CBP (Lando et al., 2002). Thus, FIH1 regulates transcriptional activity of HIF, rather than stability. FIH1 is active at a lower O_2 concentration than EGLN (Koivunen et al., 2004), suggesting that FIH1 might function to inactivate HIFα at intermediate levels of oxygen.

Humans have three HIFα paralogs, HIF1α, HIF2α (EPAS), and HIF3α (Kaelin and Ratcliffe, 2008). HIF1α is ubiquitously expressed and is the primary regulator of transcriptional responses to hypoxia, whereas expression of HIF2α is enriched in specific tissues (Loboda et al., 2010). HIF3α encodes multiple splice variants (Makino et al., 2002); at least one variant, called IPAS, lacks transactivation domains and plays an inhibitory role in the hypoxia response by dimerizing with HIF1α and blocking its activity (Makino et al., 2001). HIF1β is the common partner for all HIFα subunits. HIF1β was originally identified as the aryl hydrocarbon receptor nuclear translocator (ARNT). ARNT heterodimerizes with a number of other partners, including the aryl hydrocarbon receptor (AHR), to form active transcription factors that function in a variety of processes, such as xenobiotic response (Kewley et al., 2004).

HIF1 and HIF2 recognize the same HRE but have an only partially overlapping set of targets due to differential activity of their transactivation domains (Hu et al., 2003, 2006; Mole et al., 2009); for example, HIF2α is more resistant to FIH1-mediated CTAD regulation (Bracken et al., 2006; Yan et al., 2007), and the NTAD of HIF1α is critical for regulation of HIF1-specific transcriptional changes (Hu et al., 2007). Throughout this introduction, I will indicate HIF1 and HIF2-specific functions where relevant, and will sometimes refer to HIF generically for effectors common to both.

ii. HIF functions in mammalian development

Exposure to hypoxia occurs during normal mammalian development (Lee et al., 2001), and low oxygen concentration is used in this context as a cue to drive tissue differentiation and other aspects of development (Dunwoodie, 2009). HIF is a critical player in mediating this hypoxia-dependent developmental progression, as is evidenced by the numerous embryonic defects observed in HIF-defective mutants. In mice, loss-of-function mutations in the *Hif1α* gene

result in embryonic lethality around day E10.5; the embryos appear abnormal beginning at day 8, and have multiple cardiovascular and neural defects (Iyer et al., 1998; Ryan et al., 1998; Yoon et al., 2006). *Hif1β* mutants are similarly inviable by embryonic day 10.5 (Kozak et al., 1997; Maltepe et al., 1997). Expression of *Hif1α* is observed beginning around day 8 (Iyer et al., 1998; Ryan et al., 1998), consistent with a role for HIF around this time. HIF2 also appears to be important for embryonic development, though the specific effect of mutation appears to depend on genetic background; in all cases *Hif2α* mutation reduces viability, but in different *Hif2α* mutant models death is observed as early as embryonic day 9.5 or as late as several months after birth; in all cases cardiovascular defects are present, and in some models other defects are observed as well (Compernolle et al., 2002; Peng et al., 2000; Scortegagna et al., 2003; Tian et al., 1998). The role of HIF in embryonic development also extends to the development of the placenta. *Hif1α* mutants, *Hif1α Hif2α* double mutants, and *Hif1β* mutants all have severe defects in placental development (Adelman et al., 2000; Dahl et al., 2005; Kozak et al., 1997).

Studies of conditional knockouts eliminating HIF function from specific tissues have been useful in further elucidating the role of HIF in development. Such studies have identified roles for HIF in development of a vast assortment of cell types: for example, cardiomyocytes (Huang et al., 2004), chondrocytes (Schipani et al., 2001), osteoblasts (Wang et al., 2007), neurons (Tomita et al., 2003), and B lymphocytes (Kojima et al., 2002); in many cases HIF functions to drive expression of other transcription factors that then regulate development of these cell types (Dunwoodie, 2009). HIF thus appears to be an important player in developmental processes beyond the cardiovascular system.

iii. HIF regulates metabolism

Because of the requirement for oxygen in oxidative phosphorylation, changing oxygen levels drive shifts in cellular metabolism, which in many cases depend on HIF. Numerous HIF targets function to promote glycolysis, downregulate number and activity of mitochondria, or otherwise regulate metabolism to compensate for the effects of hypoxia. Some of the earliest identified targets of HIF1 include glycolytic enzymes (aldolase A, enolase 1, and others) (Iyer et al., 1998; Semenza et al., 1996) and the glucose transporter GLUT1 (Iyer et al., 1998). HIF1 also promotes production of lactate as the end product of glycolysis through upregulation of its targets lactate dehydrogenase A, which converts pyruvate to lactate (Semenza et al., 1996), and the transporter MCT4, which mediates lactate efflux from the cell (Ullah et al., 2006). Further, pyruvate dehydrogenase, which is required for the conversion of pyruvate to acetyl-CoA and thus links glycolysis to the tricarboxylic acid (TCA) cycle and oxidative phosphorylation, is inhibited by HIF1 through the HIF target pyruvate dehydrogenase kinase 1, which phosphorylates and inhibits pyruvate dehydrogenase (Kim et al., 2006; Papandreou et al., 2006). The consequent reduction in glucose-derived acetyl-CoA is partially compensated for by HIF-dependent reductive carboxylation of glutamine to generate acetyl-CoA, which can be used as a precursor for lipid biosynthesis (Sun and Denko, 2014).

Regulation of mitochondrial number occurs both through upregulation of mitophagy and inhibition of mitochondrial biogenesis. The HIF1 targets BNIP3 and BNIP3L, both BCL2 protein family members, promote autophagy, including mitophagy (Bellot et al., 2009; Zhang et al., 2008), while the HIF1 target max-interacting protein 1 (MXI1) inhibits C-MYC activity, resulting in reduced generation of mitochondria (Zhang et al., 2007). HIF also regulates mitochondrial respiration by altering the composition of the electron transport chain. HIF1

promotes expression of the cytochrome *c* oxidase COX4-2 isoform and drives degradation of the COX4-1 isoform through upregulation of the mitochondrial protease LON; this COX4 isoform switch promotes more efficient transfer of electrons to oxygen in hypoxic cells. Another HIF1 target, the NADH dehydrogenase (ubiquinone) 1 alpha subcomplex, 4-like 2 (NDUFA4L2), inhibits complex I of the respiratory chain.

Interestingly, oxygen is not limiting for ATP production at 1% O_2 (Zhang et al., 2008). This finding, in conjunction with observations of reactive oxygen species (ROS)-induced toxicity associated with hypoxia in cells defective for HIF1, suggests that the metabolic shift orchestrated by HIF might serve primarily to reduce the generation of toxic ROS that are otherwise released by the respiratory chain during hypoxia due to inadequate availability of the terminal electron acceptor (Semenza, 2012), at least at 1% O_2.

iv. HIF controls cardiovascular system function

HIF plays an important role not only in the development of the cardiovascular system, as described above, but also in regulating its function during systemic or tissue hypoxia. Several HIF targets are angiogenic cytokines, such as vascular endothelial growth factor (VEGF), angiopoietins (ANGPT) 1 and 2, and stromal-derived factor (SDF1). These secreted factors cell non-autonomously promote angiogenesis (the generation of new blood vessels) by inducing proliferation and mobilization of endothelial cells, as well as recruitment of circulating progenitor cells (Ceradini et al., 2004; Forsythe et al., 1996; Kelly et al., 2003). Other HIF targets stimulate blood flow by promoting vasodilation. The HIF targets endothelial nitric oxide synthase (eNOS) and heme oxygenase-1 (HO1) generate nitric oxide and carbon monoxide, respectively, both of which promote relaxation of vascular smooth muscle, resulting in

vasodilation (Coulet et al., 2003). Hypoxia also promotes rapid systemic vasodilation through a mechanism that is likely HIF-independent (Bishop and Ratcliffe, 2015).

Interestingly, the vascular response depends on the specific tissue experiencing hypoxia; unlike most other blood vessels, the pulmonary vasculature undergoes HIF-dependent vasoconstriction due to altered expression of ion channels and the vasoconstriction-promoting peptide endothelin-1 (Bishop and Ratcliffe, 2015). This adaptive response shunts blood away from poorly ventilated lung tissue; however, it leads to pulmonary hypertension in chronic obstructive pulmonary disease, in which long-term smoking, exposure to environmental pollutants, or genetic factors result in hypoxia in most lung tissue (Semenza, 2009).

v. HIF promotes adaptation to high altitude

HIF promotes adaptations to systemic hypoxia, e.g. due to the environmental hypoxia associated with high altitude, by modulating both erythropoiesis (red blood cell production) and ventilation (breathing rate). The increase in erythropoesis represents a coordinated response by a suite of HIF targets. HIF2, and to a lesser extent, HIF1, promotes expression of Epo in the kidney and liver during hypoxia; this cytokine stimulates production of red blood cells in the bone marrow (Rankin et al., 2007). Expression of the Epo receptor is also increased by HIF, as are various targets that promote iron absorption from the intestine (e.g. the divalent metal transporter DMT1), iron transport through the blood (transferrin) and iron uptake by erythroid progenitor cells (the transferrin receptor); these HIF targets act in concert to promote generation of iron-rich erythrocytes (Semenza, 2010).

Environmental hypoxia induces a rapid increase in breathing rate (seconds-to-minutes timescale) which depends on oxygen-sensitive ion channels, such as K+ channels in the type I glomus cells of the carotid body that close during hypoxia, resulting in depolarization of the cell

(Lopez-Barneo et al., 1988). Though this response is known to be independent of HIF, the relevant oxygen sensing mechanism remains unknown. In addition to this rapid response, there is also a slower, HIF-dependent ventilatory acclimatization to chronic hypoxia. The mechanism of this increase in breathing rate, which occurs on the scale of hours to days, is complex; it likely involves the function of several HIF targets. In some cases, targets such as Epo, VEGF, endothelin-1, and heme oxygenase, which have clear functions in other aspects of the hypoxic response, also act in cells of the carotid body and/or central nervous system to regulate breathing rate (Powell and Fu, 2008; Prabhakar and Semenza, 2012). Additionally, the rate-limiting dopamine biosynthetic enzyme, tyrosine hydroxylase, is a HIF target, the expression of which in the carotid body is increased by hypoxia; this HIF-dependent regulation of dopamine production might play a role in the ventilatory acclimatization to chronic hypoxia (Lam et al., 2008).

Interestingly, several recent studies have identified polymorphisms in components of the HIF pathway, including EGLN1, HIF1α, and EPAS1 (HIF2α), from studies of adaptations to the high altitude environment of the Tibetan plateau (Beall et al., 2010; Simonson et al., 2010; Yi et al., 2010). These adaptations appear to result in reduced HIF activation (Lorenzo et al., 2014), consistent with the observation that these populations have a blunted hypoxia response (reduced erythropoiesis and pulmonary hypertension) and suggesting that long-term activation of HIF under environmental hypoxia is maladaptive.

vi. Non-canonical functions of HIF

In addition to its numerous functions in mediating adaptations to environmental and tissue hypoxia, HIF also regulates physiological changes that are less traditionally thought of as aspects of a hypoxia response. For example, regions of hypoxia are found in the adipose tissue in obese individuals (Pasarica et al., 2009), and HIF1 activation in the adipose tissue of mice fed a

high-fat diet drives inflammation and insulin resistance (Lee et al., 2014). HIF also has important functions in immunity. Infected and inflamed tissues are often sites of hypoxia, due to infiltration of inflammatory cells and presence of pathogen in bacterial infection, which results in HIF activation. Additionally, other aspects of infection, such as sequestration of iron by bacterial siderophores (Hartmann et al., 2008) and production of reactive oxygen species by macrophages (Shatrov, 2003), inhibit EGLN and thus induce HIF activity. Expression of *HIF1α* mRNA is also induced by NF-κB during inflammation (Fitzpatrick et al., 2011; Rius et al., 2008). HIF1 facilitates macrophage function by promoting expression of antimicrobial peptides, proteases, and inducible nitric oxide synthase, which generates antimicrobial nitric oxide (Peyssonnaux et al., 2005). HIF also promotes neutrophil-mediated inflammation (Thompson et al., 2014; Walmsley et al., 2005). Cells of the adaptive immune system are also regulated by HIF; for example, T cell proliferation and differentiation are controlled by HIF1 (Bhandari et al., 2013; Dang et al., 2011). Activation of HIF1 also promotes wound healing, including of burn wounds, by promoting angiogenic gene expression at the wound site (Liu et al., 2008; Zhang et al., 2010).

vii. Regulation of HIF – beyond EGLN and pVHL

Modulation of HIF activity occurs primarily through the activity of 2-oxoglutarate-dependent oxygenases: the EGLN prolyl hydroxylases control proteasomal degradation of HIF in a pVHL dependent pathway, while the asparaginyl hydroxylase FIH1 controls HIF activity, as discussed above. In addition, several other regulators of HIF levels and activity have been described, which control either expression of *HIF* mRNA, HIF protein synthesis, or stability of the HIF protein.

HIF1α mRNA expression is increased during the inflammatory response due to the activity of NF-κB, as described above (Fitzpatrick et al., 2011; Rius et al., 2008). *HIF2α* mRNA

is upregulated due to oxidative stress; for example, ROS-generating NADPH oxidase Nox4 promotes *HIF2α* expression (Maranchie and Zhan, 2005).

HIFα translation is regulated through multiple mechanisms. In proliferating cells, mTOR increases translation of HIF1α, resulting in normoxic induction of HIF1 target genes (Brugarolas et al., 2003; Düvel et al., 2010). In hypoxia, translation is globally downregulated due to inhibition of mTOR and phosphorylation of the eukaryotic initiation factor 2a (Wouters and Koritzinsky, 2008); HIF1α translation is protected from inhibition through a mechanism that is not well understood but might involve an internal ribosomal entry site (Lang et al., 2002; Young et al., 2008).

A variety of post-translational modifications (PTMs) regulate HIFα stability. HIFα can be polyubiquitinated and degraded independently of EGLN and pVHL through a mechanism involving the receptor of activated protein kinase C (RACK1) and heat shock protein 90 (HSP90). HSP90 normally blocks pVHL-independent HIF1α degradation by competing for a site on HIF1α otherwise recognized by RACK1. In the absence of HSP90, RACK1 recruits the Elongin-C/B ubiquitin ligase complex and targets HIF1α for degradation (Isaacs et al., 2002; Liu et al., 2007). SUMOylation of HIF also drives HIFα degradation by promoting VHL recognition independent of prolyl hydroxylation (Cheng et al., 2007). Several regulators modulate EGLN and VHL-dependent stability; for example, OS9 promotes hydroxylation of HIF1α (Baek et al., 2005), and VHL-interacting deubiquitinating enzyme 2 (VDU2) can deubiquitinate HIF1α (Li et al., 2005). HIF activity can also be regulated by PTMs; for example, phosphorylation of HIF1α by p42/p44 MAP kinases (ERKs) promotes HIF1 transcriptional activity (Richard et al., 1999).

B. pVHL primarily functions in the degradation of HIF

i. *VHL* encodes the recognition component of an E3 ubiquitin ligase complex

The von Hippel-Lindau tumor suppressor gene *VHL* was identified as the gene mutated in von Hippel-Lindau disease. This genetic disorder was first described by Treacher Collins, Eugen von Hippel and Arvid Lindau (Collins, 1894; von Hippel, 1904; Lindau, 1926), and is characterized by cysts and tumors in multiple tissues, including hemangioblastomas, pheochromocytomas, and renal cell carcinoma (Kaelin, 2007). VHL disease displays an autosomal dominant inheritance pattern, with development of tumors resulting from loss of heterozygosity at the *VHL* locus, or can arise sporadically (Maher et al., 1990). The pVHL protein encoded by *VHL* is the recognition component of an E3 ubiquitin ligase complex. Through its α domain, pVHL binds elongin C, which recruits elongin B, cullin-2 and the ubiquitin ligase RING box 1 (Rbx1) to form an SCF-like ubiquitin ligase complex; the pVHL β domain binds substrates (Kamura et al., 1999; Stebbins et al., 1999). Hydroxylated HIFα is the best characterized target of this ubiquitin ligase complex, and constitutive activation of HIF, particularly HIF2, is thought to be the primary mechanism of VHL disease progression. Inhibition of HIF in mouse models of VHL disease is sufficient to suppress tumor growth (Kondo et al., 2002, 2003; Zimmer et al., 2004); however, this does not preclude possible involvement of other pVHL targets in aspects of disease progression.

ii. Non-canonical functions of pVHL

In addition to the HIFα subunits, several other pVHL interactors have been identified. In some cases, the interaction requires EGLN activity and results in target degradation; for example, the NDRG3 protein is a target of EGLN1 hydroxylation and is degraded in a pVHL-dependent manner in hypoxia. Interestingly, hypoxic buildup of lactate is required for the stabilization of NDRG3; lactate directly binds NDRG3 and inhibits its degradation. Stabilized NDRG3 drives Raf/ERK signaling which promotes angiogenesis and cell growth (Lee et al., 2015). The β-2 adrenergic receptor is another target of both EGLN (in this case, EGLN3) and pVHL; turnover of this receptor is reduced in hypoxia (Xie et al., 2009). pVHL also mediates degradation of the RNA polymerase II subunits RPB1 and RPB7 (Kuznetsova et al., 2003; Na et al., 2003). In other cases, pVHL has ubiquitination-independent effects on its binding partners. For example, Jade-1 (gene for Apoptosis and Differentiation in Epithelia) is stabilized through its interaction with pVHL (Zhou et al., 2002); pVHL directly interacts with and inhibits the transcription factor Sp1 (Cohen et al., 1999; Mukhopadhyay et al., 1997); and pVHL appears to regulate mRNA stability in conjunction with the RNA-binding protein HuR (Datta et al., 2005).

VHL also appears to regulate the cytoskeleton and extracellular matrix (ECM) independently of HIF. Cells mutant for *VHL* have defects in fibronectin matrix assembly, unstable cytoskeleton, and other ECM/cytoskeletal defects (Hergovich et al., 2003; Hoffman et al., 2001; Kurban et al., 2006). These abnormalities are observed in a class of *VHL* mutants, type 2C, which are still able to regulate HIFα stability, suggesting that these defects are not downstream of HIF stabilization. Type 2C mutations result in increased risk of pheochromocytomas, suggesting that HIF-independent activity of VHL contributes to the pathogenesis of VHL disease (Hoffman et al., 2001). Additionally, a study of gene expression

regulation by VHL in *C. elegans* identified a set of genes regulated independently of HIF that appear to be involved in ECM formation (Bishop et al., 2004).

C. EGLN primarily functions in hydroxylation of HIF

i. The *EGLN* genes encode prolyl hydroxylases

The human genome encodes three HIF prolyl hydroxylase paralogs: *EGLN1*, *EGLN2*, and *EGLN3* (also called *PHD2, PHD1,* and *PHD3*, respectively) that are members of a family of ~70 human 2-oxoglutarate-dependent oxygenases. The EGLNs function as dioxygenases, i.e. they use molecular oxygen as a substrate and incorporate both oxygen atoms into products, with one oxygen used to hydroxylate a HIFα proline, and the other participating in the oxidative decarboxylation of 2-oxoglutarate to generate succinate and CO_2 (McNeill et al., 2002). The prolyl hydroxylase domain of the EGLNs that performs this reaction features eight beta-strands in a "jelly-roll" motif, which includes an Fe(II)-coordinating facial triad of two histidines and one aspartate in the active site. This coordinated iron binds molecular oxygen and 2-oxoglutarate; a reactive ferryl intermediate (Fe(IV) = O) forms in the decarboxylation of 2-oxoglutarate and subsequently oxidizes the target amino acid (McDonough et al., 2010). *EGLN1* also contain an N-terminal MYND (myeloid, Nervy and DEAF1) domain, the function of which has not been clearly defined. This zinc finger domain has been proposed to decrease EGLN1 catalytic activity (Choi, 2005) or stability (Barth et al., 2007), or alternatively, increase EGLN1 activity through recruitment of HSP90 or HSP90 cochaperones containing a PXLE motif recognized by the zinc finger (Song et al., 2013).

EGLN1 is the primary regulator of HIFα (Berra et al., 2003), but the other EGLNs also participate in degradation of HIFα and consequent HIF target regulation (Minamishima and Kaelin, 2010). The relatively greater physiological importance of EGLN1 is reflected in the

phenotypes associated with mutants of the *EGLN* genes: *EGLN1* null mutant mice are embryonic lethal, while *EGLN2* and *EGLN3* mutants are viable (Takeda et al., 2006). *EGLN1* also has the highest expression in normoxic cells (Appelhoff et al., 2004). The EGLNs have different expression patterns; all are expressed broadly, but *EGLN3* expression is highest in the heart, while *EGLN2* is enriched in the testes. *EGLN1* and *EGLN3* are both upregulated by hypoxia and appear to be targets of HIF (Appelhoff et al., 2004), suggesting the presence of a negative feedback loop. *EGLN2* expression is not regulated by hypoxia, but is induced by estrogen (Seth et al., 2002). Intracellular localization patterns are also varied, with EGLN1 found primarily in the cytoplasm, EGLN2 in the nucleus, and EGLN3 in both nucleus and cytoplasm (Metzen et al., 2003a). A fourth EGLN homolog, called PHD4 or P4H-TM, is localized to the ER; it can hydroxylate HIFα *in vitro* but is otherwise less well characterized than the other EGLNs (Koivunen et al., 2007a). P4H-TM inhibition affects HIF target levels *in vivo*, though this regulation could be indirect, as function of P4H-TM as a HIF hydroxylase has not been demonstrated in this context (Laitala et al., 2012). Activity on substrate also appears to be different among EGLN paralogs, with EGLN2 and EGLN3 having greater activity on HIF2α (Appelhoff et al., 2004).

ii. Regulation of EGLN beyond O_2 levels

In addition to its regulation by oxygen, EGLN prolyl hydroxylase activity is controlled by some metals, reactive oxygen species, and metabolites. As described above, iron is required for EGLN function, and as such, desferrioxamine and other iron chelators reduce EGLN activity and promote HIF stability and expression of HIF targets (Epstein et al., 2001). Ascorbate is also required for full EGLN catalytic activity, and is thought to function as a reducing agent for iron to generate Fe(II) from Fe(III), or, in the case of uncoupled reaction cycles, Fe(IV) (Schofield

and Ratcliffe, 2004). Conversely, reactive oxygen species inhibit EGLN activity, likely due to oxidation of iron (Gerald et al., 2004; Knowles et al., 2003; Pan et al., 2007). Co(II), Cu(II), Zn(II) and Mn(II) also inhibit EGLN, presumably due to replacement of Fe(II) in the EGLN catalytic core by these metals, which are unable to facilitate EGLN catalytic activity (Schofield and Ratcliffe, 2004). However, some evidence suggests that Co(II) might reduce levels of ascorbate and thus indirectly affect EGLN activity instead (Salnikow et al., 2004). EGLN1 activity is also sensitive to intracellular cysteine, depletion of which results in oxidative self-inactivation of EGLN1. Such cysteine depletion occurs in triple-negative breast cancer cells due to secretion of glutamate by these cells, which accumulates extracellularly and inhibits the xCT glutamate-cystine antiporter (Briggs et al., 2016).

Several TCA cycle intermediates also regulate EGLN catalytic activity. In particular, fumarate and succinate compete with 2-oxoglutarate at the EGLN active site and thus inhibit EGLN (Koivunen et al., 2007b). Cells mutant for fumarate hydratase (FH) or succinate dehydrogenase (SDH), which accumulate fumarate and succinate, respectively, have increased HIF activity, which can be reversed with exogenous 2-oxoglutarate (MacKenzie et al., 2007). Heterozygous germline mutations in FH are associated with hereditary leiomyomatosis and renal cell carcinoma, while mutations in SDH cause hereditary paraganglioma-pheochromocytoma syndrome (Pollard et al., 2003), suggesting that accumulation of these metabolites might promote tumorigenesis *in vivo*; however, further work is required to determine the extent to which the mechanism of tumorigenesis is HIF-dependent. Another metabolite that acts as a 2-oxoglutarate antagonist, 2-hydroxyglutarate, has been shown to accumulate in tumors due to neomorphic mutations in isocitrate dehydrogenase (Dang et al., 2009; Xu et al., 2011) or noncanonical use of 2-oxoglutarate as a substrate by lactate dehydrogenase or malate

dehydrogenase during hypoxia (Intlekofer et al., 2015; Oldham et al., 2015) or acidosis (Intlekofer et al., 2017; Nadtochiy et al., 2016).

Other regulators compete with oxygen to inhibit EGLN activity. HIF is induced by nitric oxide (Metzen et al., 2003b), and a crystal structure has shown that nitric oxide (NO) can replace oxygen in the active site of a 2-oxoglutarate-dependent dioxygenase (Zhang et al., 2002). However, the regulation of EGLN and HIF by nitric oxide is likely complex. For example, NO can also inhibit the electron transport chain, which increases oxygen levels in hypoxia by reducing oxygen utilization, thereby promoting EGLN activity (Hagen et al., 2003).

iii. Non-HIF targets of EGLN

Historically, studies of the function of the EGLN family have largely centered around their function as HIF hydroxylases, but recent work has begun to uncover noncanonical substrates that are hydroxylated by EGLN. As described above, some of these targets are targeted by pVHL for degradation as a consequence of their EGLN-mediated hydroxylation, similar to HIFα. In other cases, hydroxylation alters activity through other mechanisms. For example, the serine-threonine kinases AKT1 and AKT2, which promote cell proliferation, are hydroxylated by EGLN1, resulting in binding by pVHL and inhibition of AKT activity. Hypoxia or cancer-associated mutations in AKT that lead to reduced hydroxylation cause hyperactivation of AKT, thus linking EGLN1 to inhibition of AKT-dependent tumor growth. Interestingly, though pVHL inhibits the hydroxylated AKT, it does so through an E3 ligase-independent mechanism (Guo et al., 2016). Hydroxylation of a noncanonical EGLN2 substrate has the opposite effect on cell proliferation: EGLN2 hydroxylates the FOXO3a transcription factor, blocking FOXO3a interaction with the USP9x deubiquitinase. As a result, proteasomal degradation of FOXO3a is promoted and Cyclin D1, which is otherwise repressed by FOXO, is

upregulated. Loss of EGLN2 leads to decreased cell proliferation due to downregulation of Cyclin D1 (Zheng et al., 2014). Other noncanonical EGLN targets include acetyl-CoA carboxylase 2 (ACC2) and pyruvate kinase M2 (PKM2), both of which are hydroxylated by EGLN3; hydroxylation of ACC2 results in repression of fatty acid oxidation (German et al., 2016), while PKM2 hydroxylation promotes interaction between PKM2 and HIF1α and enhances HIF transcriptional activity (Luo et al., 2011).

D. The EGLN/pVHL/HIF pathway in disease

As described throughout this introduction, HIF regulates a wide range of processes that affect cardiovascular function, cell proliferation, immune response, and other aspects of physiology, and as a result, this pathway plays either a protective or pathogenic role in numerous diseases. Activation of HIF in mouse models is protective against ischemia in multiple contexts, including myocardial infarction (Shohet and Garcia, 2007), stroke (Wang et al., 2015), and limb ischemia (Aragonés et al., 2008; Bosch-Marce et al., 2007). Inhibition of EGLN or stabilization of HIFα also appears to at least partially mediate both ischemic preconditioning, in which exposure to mild hypoxia is protective against later, more severe ischemia to the heart or other tissues (Cai et al., 2008; Eckle et al., 2008), and remote ischemic preconditioning, in which exposure to hypoxia in one tissue protects against ischemia in a distant tissue (Cai et al., 2013; Olenchock et al., 2016). Several animal studies of EGLN inhibitors have shown efficacy in treating myocardial infarction, as measured by reduced infarct size and improved cardiac function (Bishop and Ratcliffe, 2015). However, activation of HIF is not strictly beneficial in the context of cardiovascular health. Sustained HIF1 or HIF2 activation is associated with cardiomyopathy (Bekeredjian et al., 2010; Hölscher et al., 2012; Moslehi et al., 2010), indicating that the possible therapeutic benefits of HIF activators must be balanced with the risk of

cardiomyopathy. Nevertheless, EGLN inhibitors are currently being explored in preclinical and clinical trials for multiple indications; the application that is closest to the clinic is for the treatment of anemia, as HIF activation promotes many aspects of red blood cell production, as described previously (Bishop and Ratcliffe, 2015).

The EGLN/pVHL/HIF pathway has also been implicated in the pathogenesis of cancer. As described above, pVHL has a well-established tumor suppressor function that appears to be mediated at least in part through its regulation of HIF. Additionally, even outside of the context of *VHL* loss of function, high levels of HIF1α or HIF2α are associated with higher mortality for numerous cancers (Chi et al., 2006; Winter et al., 2007). However, increased HIF might in some cases be an effect, rather than cause, of aggressive tumor growth, as faster-growing tumors might be more likely to outgrow their blood supply and thus have regions of hypoxia. HIF activation regulates many aspects of cancer biology, including tumor vascularization, metabolic changes, immune evasion, metastasis, and treatment resistance (Semenza, 2012). HIF1 and HIF2 appear to have different effects on tumor growth, with HIF2 clearly promoting tumor growth in the context of pVHL-defective clear cell renal carcinoma, versus a possible anti-tumorigenic role for HIF1 (Ratcliffe, 2013; Shen and Kaelin, 2013). Drugs that target HIF2α and its effectors, such as VEGF, are currently under clinical investigation (Ivan and Kaelin, 2017).

Finally, as described earlier, HIF has important functions in promoting inflammation and immunity. HIF inhibitors might thus be useful therapeutics for treating inflammatory disorders, such as arthritis, while HIF activators (e.g. EGLN inhibitors) could facilitate the treatment of infectious disease (Okumura et al 2012; Palazon et al, 2014).

IV. Studies of the EGLN/pVHL/HIF pathway in the nematode *C. elegans* have revealed novel roles for this pathway in controlling physiology and behavior

A. *C. elegans* as a system for studying the EGLN/pVHL/HIF pathway

The nematode *C. elegans* has proven to be a powerful system for exploring numerous aspects of animal development, behavior, and stress biology. The EGLN/pVHL/HIF hypoxia-response pathway is conserved in worms; in fact, the first pathway component to be discovered, EGLN (for homolog of EGL-9, i.e. EGg-Laying defective Nine), was identified for its role in regulating *C. elegans* egg-laying behavior. Studies of *C. elegans* were also critical in the identification of EGL-9 and its homologs as the dioxygenases that hydroxylate HIFα and thus mark HIFα for degradation (Epstein et al., 2001). The pathway is functionally conserved, as it is required for worms to adapt to hypoxia. For example, animals mutant in the *HIFα* homolog *hif-1* have reduced survival relative to wild-type animals when grown at 1% oxygen (Jiang et al., 2001).

Each pathway component has a single homolog in *C. elegans* (*egl-9, vhl-1, hif-1,* and *aha-1* as homologs of *EGLN, VHL, HIFα, and HIFβ,* respectively), thus simplifying genetic analysis of pathway function. Further, loss-of-function mutants in each of these genes is viable; by contrast, mouse loss-of-function mutants die during embryonic development, as described above, and although mutants of the *Drosophila HIF* homolog *Sima* are viable, flies mutant for the *EGLN* homolog *Fatiga* display larval lethality (Centanin et al., 2005). Consequently, analysis of HIF pathway function in other animals has largely focused on either heterozygotes or animals in which the pathway is activated or inactivated in a tissue-specific manner. Because the HIF pathway can be activated or inactivated in the entire animal while still allowing normal

development, *C. elegans* is an excellent model for analyzing the role of this pathway in integrative physiology of the entire animal. In addition to the ease of studying mutants, animals can also be easily exposed to environmental stressors that regulate the HIF pathway, e.g. hypoxia or oxidative stress. Because *C. elegans* does not have a circulatory system and gases are distributed among tissues by diffusion, levels of oxygen and other gases throughout the entire animal can be controlled (Ma and Ringstad, 2012).

In the following sections, I will describe two major areas of whole-organism physiology in which HIF plays a role, as demonstrated by studies of *C. elegans*: behavior and stress response.

B. EGL-9/HIF-regulated behavior

Worms are bacteriovores and are found growing in rotting plant matter, in which oxygen levels can fluctuate over short distances (Rogers et al., 2006). Oxygen is thus an important environmental cue for *C. elegans*, and as such the worm has multiple systems for responding behaviorally to O_2 fluctuations. Worms prefer an intermediate oxygen concentration of ~10% O_2 (vs. 21% atmospheric concentration) and will avoid higher or lower levels. This aerotaxis behavior is driven by guanylate cyclases, which sense oxygen through their associated heme group, and a well-defined neural circuit (Chang et al., 2006; Cheung et al., 2005; Gray et al., 2004). *C. elegans* also exhibit a locomotory response when shifted from normoxia to anoxia (0% O_2) or from anoxia to normoxia, displaying an increase in locomotion speed in both cases (the "O2-OFF" and "O2-ON" responses, respectively), both of which decay back to baseline after several minutes (Ma et al., 2012).

Aerotaxis, O2-OFF, and O2-ON behaviors are all responses to acute changes in oxygen concentration, occurring on a seconds-to-minutes timescale. EGL-9 and HIF-mediated

behavioral changes, on the other hand, represent adaptations to chronic hypoxia and occur over a longer timescale. One such behavioral change that occurs in hypoxia is the modulation of egg-laying behavior. Adult hermaphrodites exposed to 0.5% oxygen for 24 hours slow their egg-laying rate (Miller and Roth, 2009). *egl-9(lf)* mutants also inhibit egg laying, and do so in a *hif-1*-dependent manner (Bishop et al., 2004; Trent et al., 1983). *egl-9* has been shown to function in neurons and neuroendocrine cells to regulate this behavior (Chang and Bargmann, 2008), but the mechanism is otherwise unknown. Prolonged exposure to hypoxia regulates several other behaviors by modulating neural circuits in an EGL-9/HIF-dependent manner. For example, gustatory sensory perception of salt is enhanced following exposure to 1% O_2 for 12 hours. This perceptual change is due to HIF-dependent upregulation of the rate-limiting serotonin biosynthetic enzyme, tryptophan hydroxylase, in a neuron not otherwise involved in salt gustation, and this results in activation of a noncanonical chemosensory circuit (Pocock and Hobert, 2010). The authors of this study speculate that enhanced chemosensation might be part of a broader escape response that involves increased sensitivity to multiple environmental cues.

Interestingly, two of the acute oxygen responses described above are regulated by the HIF pathway. The neural circuit controlling aerotaxis behavior is altered in *egl-9(lf)* mutants or mutants pre-conditioned with chronic hypoxia. These animals prefer a lower oxygen concentration (8% vs. 10%) off of food and prefer lower oxygen concentration even in the presence of food; wild-type animals, on the other hand, avoid high (>14%) oxygen only in the absence of food (Chang and Bargmann, 2008). In this case, the neural circuit controlling aerotaxis is simplified, rather than expanded as in the chemosensory circuit, eliminating several neurons that normally feed into aerotaxis behavioral regulation (Chang and Bargmann, 2008). The O2-ON response is also regulated by chronic hypoxia. Activation of HIF suppresses the O2-

ON response through downregulation of a cytochrome P450 enzyme, CYP-13A12. This CYP mediates the O2-ON response by generating eicosanoids from polyunsaturated fatty acid precursors upon reoxygenation (Ma et al., 2013). Further work is required to determine the neural circuit controlling the O2-ON response, and how that circuit is modulated following chronic hypoxia exposure.

EGL-9-mediated behavioral changes can also occur through a HIF-independent mechanism in at least one case. EGL-9 hydroxylates the Mint ortholog LIN-10, blocking phosphorylation of LIN-10 by the proline-directed serine-threonine kinase CDK-5; unphosphorylated LIN-10 promotes trafficking of the GLR-1 AMPA receptor to the plasma membrane. In hypoxia-exposed worms or *egl-9(lf)* mutants, phosphorylation of LIN-10 inhibits GLR-1 recycling, resulting of accumulation of GLR-1 in endosomes and reduction in GLR-1-mediated reversal behavior (Park et al., 2012).

C. EGL-9/HIF-regulated stress responses

The EGL-9/HIF pathway has emerged as a central regulator of response and resistance to stressors beyond hypoxia itself. Even prior to the identification of EGL-9 as the prolyl hydroxylase regulating HIF-1, *egl-9* was identified from a screen for mutants resistant to lethal paralysis by the pathogenic bacterium *Pseudomonas aeruginosa* strain PAO1 (Darby et al., 1999). Subsequent work found that PAO1 toxicity is due to cyanide poisoning (Gallagher and Manoil, 2001), and that *egl-9* mutation mediates resistance due to upregulation of the HIF-1 target and cysteine synthase homolog *cysl-2*, which promotes cyanide detoxification (Budde and Roth, 2011). HIF also promotes resistance in other models of *Pseudomonas* pathogenesis. *egl-9(lf)* mutants are resistant to infection as measured by the "slow killing" assay on *Pseudomonas aeruginosa* strain PA14 (Bellier et al., 2009); toxicity in this model arises from intestinal

colonization (Tan et al., 1999). In a third model of *Pseudomonas* infection, the "liquid killing" model, iron chelation by the bacterial siderophore pyoverdin drives toxicity. *hif-1(lf)* mutants are hypersensitive to pathogenesis in this model, presumably due to defects in iron homeostasis caused by *hif-1* mutation. HIF activation also drives resistance to pore-forming toxins (PFTs), including crystal (Cry) proteins and *Vibrio cholerae* cytolysin; resistance to Cry protein requires upregulation of the HIF target nuclear hormone receptor 57 (*nhr-57*) (Bellier et al., 2009). However, the *egl-9(lf)* mutation appears to be detrimental in at least one infection model, as these mutant animals are hypersensitive to *Staphylococcus aureus* infection (Luhachack et al., 2012).

HIF-1 activation drives resistance to other stressors as well. Preconditioning worms with moderate heat stress (25°C) enhances their resistance to later, more severe heat stress (35°C), an effect that requires *hif-1*. *egl-9(lf)* and *vhl-1(lf)* mutants, in which HIF-1 is constitutively active, are resistant to 35°C even in the absence of preconditioning (Treinin et al., 2003); both mutants are also resistant to proteotoxic stress due to polyglutamine and β-amyloid aggregation (Mehta et al., 2009). This pathway also regulates endoplasmic reticulum proteostasis, as *vhl-1(lf)* mutants are resistant to tunicamycin and dithiothreitol, both of which induce ER stress (Bellier et al., 2009; Leiser et al., 2015). *egl-9(lf)* mutants are also resistant to oxidative stress through an unknown mechanism (Bellier et al., 2009) and hydrogen sulfide through upregulation of the sulfide:quinone reductase *sqrd-1*, which is required for sulfide oxidation (Budde and Roth, 2010). HIF also protects against DNA-damaged-induced apoptosis by upregulating expression of the secreted tyrosinase TYR-2 in the ASJ sensory neurons. TYR-2 cell-nonautonomously inhibits CEP-1, the homolog of the tumor suppressor p53, to protect germ cells from programmed cell death following ionizing radiation (Sendoel et al., 2010).

Pathways that promote stress resistance often also regulate longevity (Shore and Ruvkun, 2013), and the EGL-9/HIF pathway is no exception. Loss of function of *vhl-1* or *egl-9* extends lifespan (Mehta et al., 2009; Zhang et al., 2009). The lifespan extension of respiratory chain mutants also requires *hif-1*; increased ROS levels in these mutants activate HIF-1 and promote longevity (Lee et al., 2010). Intriguingly, activation of HIF-1 in only the nervous system is sufficient to increase lifespan. Neuronal HIF-1 promotes serotonin signaling that acts on the SER-7 serotonin receptor in the intestine, driving expression of the pro-longevity xenobiotic detoxification enzyme flavin-containing monooxygenase FMO-2 (Leiser et al., 2015). Surprisingly, *hif-1(lf)* also promotes longevity in a temperature-dependent manner; *hif-1(lf)* mutants are long lived at 25°C due to activation of the transcription factor and FOXO homolog DAF-16 (Leiser et al., 2011).

V. Summary and Thesis Outline

In summary, the conserved EGLN/HIF pathway functions broadly in regulating numerous aspects of the response to hypoxia and other stressors. The nematode *C. elegans* is a powerful system for genetic analysis of this pathway. In this dissertation, I will describe studies of the EGL-9/HIF-1 pathway in *C. elegans* that have identified new players that drive HIF-dependent gene expression and physiology. In Chapter 2, I discuss the identification of a hormone signaling pathway, consisting of a cytochrome P450 enzyme and nuclear hormone receptor, that controls egg-laying behavior, other behaviors and multiple stress responses downstream of HIF. In Chapter 3, I provide evidence for additional pathways acting in parallel to the hormone-signaling pathway to regulate HIF-dependent modulation of egg laying. In Chapter 4, I detail possible future directions for the analysis of the EGL-9/HIF-1 pathway in *C. elegans.*

This dissertation also includes two appendices that describe other studies to which I contributed. Appendix A details the discovery of another cytochrome P450 enzyme that controls a HIF-dependent locomotory behavior. Appendix B discusses the identification and characterization of a conserved protein, VPS-50, that controls behavioral state and regulates dense-core vesicle maturation.

Acknowledgments

I thank Aaron Hosios and Calista Diehl for helpful comments concerning this chapter.

References

Adelman, D.M., Gertsenstein, M., Nagy, A., Simon, M.C., and Maltepe, E. (2000). Placental cell fates are regulated in vivo by HIF-mediated hypoxia responses. Genes Dev. *14*, 3191–3203.

Appelhoff, R.J., Tian, Y.-M., Raval, R.R., Turley, H., Harris, A.L., Pugh, C.W., Ratcliffe, P.J., and Gleadle, J.M. (2004). Differential Function of the Prolyl Hydroxylases PHD1, PHD2, and PHD3 in the Regulation of Hypoxia-inducible Factor. J. Biol. Chem. *279*, 38458–38465.

Aragonés, J., Schneider, M., Geyte, K.V., Fraisl, P., Dresselaers, T., Mazzone, M., Dirkx, R., Zacchigna, S., Lemieux, H., Jeoung, N.H., et al. (2008). Deficiency or inhibition of oxygen sensor Phd1 induces hypoxia tolerance by reprogramming basal metabolism. Nat. Genet. *40*, 170–180.

Baek, J.H., Mahon, P.C., Oh, J., Kelly, B., Krishnamachary, B., Pearson, M., Chan, D.A., Giaccia, A.J., and Semenza, G.L. (2005). OS-9 Interacts with Hypoxia-Inducible Factor 1α and Prolyl Hydroxylases to Promote Oxygen-Dependent Degradation of HIF-1α. Mol. Cell *17*, 503–512.

Barth, S., Nesper, J., Hasgall, P.A., Wirthner, R., Nytko, K.J., Edlich, F., Katschinski, D.M., Stiehl, D.P., Wenger, R.H., and Camenisch, G. (2007). The Peptidyl Prolyl cis/trans Isomerase FKBP38 Determines Hypoxia-Inducible Transcription Factor Prolyl-4-Hydroxylase PHD2 Protein Stability. Mol. Cell. Biol. *27*, 3758–3768.

Bashan, N., Burdett, E., Hundal, H.S., and Klip, A. (1992). Regulation of glucose transport and GLUT1 glucose transporter expression by O_2 in muscle cells in culture. Am. J. Physiol.-Cell Physiol. *262*, C682–C690.

Beall, C.M., Cavalleri, G.L., Deng, L., Elston, R.C., Gao, Y., Knight, J., Li, C., Li, J.C., Liang, Y., McCormack, M., et al. (2010). Natural selection on EPAS1 (HIF2α) associated with low hemoglobin concentration in Tibetan highlanders. Proc. Natl. Acad. Sci. *107*, 11459–11464.

Beck, I., Ramirez, S., Weinmann, R., and Caro, J. (1991). Enhancer element at the 3'-flanking region controls transcriptional response to hypoxia in the human erythropoietin gene. J. Biol. Chem. *266*, 15563–15566.

Bekeredjian, R., Walton, C.B., MacCannell, K.A., Ecker, J., Kruse, F., Outten, J.T., Sutcliffe, D., Gerard, R.D., Bruick, R.K., and Shohet, R.V. (2010). Conditional HIF-1α Expression Produces a Reversible Cardiomyopathy. PLOS ONE *5*, e11693.

Bellier, A., Chen, C.-S., Kao, C.-Y., Cinar, H.N., and Aroian, R.V. (2009). Hypoxia and the hypoxic response pathway protect against pore-forming toxins in *C. elegans*. PLoS Pathog *5*, e1000689.

Bellot, G., Garcia-Medina, R., Gounon, P., Chiche, J., Roux, D., Pouysségur, J., and Mazure, N.M. (2009). Hypoxia-Induced Autophagy Is Mediated through Hypoxia-Inducible Factor Induction of BNIP3 and BNIP3L via Their BH3 Domains. Mol. Cell. Biol. *29*, 2570–2581.

Berra, E., Benizri, E., Ginouvès, A., Volmat, V., Roux, D., and Pouysségur, J. (2003). HIF prolyl-hydroxylase 2 is the key oxygen sensor setting low steady-state levels of HIF-1α in normoxia. EMBO J. *22*, 4082–4090.

Bhandari, T., Olson, J., Johnson, R.S., and Nizet, V. (2013). HIF-1α influences myeloid cell antigen presentation and response to subcutaneous OVA vaccination. J. Mol. Med. *91*, 1199–1205.

Bishop, T., and Ratcliffe, P.J. (2015). HIF Hydroxylase Pathways in Cardiovascular Physiology and Medicine. Circ. Res. *117*, 65–79.

Bishop, T., Lau, K.W., Epstein, A.C.R., Kim, S.K., Jiang, M., O'Rourke, D., Pugh, C.W., Gleadle, J.M., Taylor, M.S., Hodgkin, J., et al. (2004). Genetic analysis of pathways regulated by the von Hippel-Lindau tumor suppressor in *Caenorhabditis elegans*. PLoS Biol *2*, e289.

Bosch-Marce, M., Okuyama, H., Wesley, J.B., Sarkar, K., Kimura, H., Liu, Y.V., Zhang, H., Strazza, M., Rey, S., Savino, L., et al. (2007). Effects of Aging and Hypoxia-Inducible Factor-1 Activity on Angiogenic Cell Mobilization and Recovery of Perfusion After Limb Ischemia. Circ. Res. *101*, 1310–1318.

Bracken, C.P., Fedele, A.O., Linke, S., Balrak, W., Lisy, K., Whitelaw, M.L., and Peet, D.J. (2006). Cell-specific Regulation of Hypoxia-inducible Factor (HIF)-1α and HIF-2α Stabilization and Transactivation in a Graded Oxygen Environment. J. Biol. Chem. *281*, 22575–22585.

Briggs, K.J., Koivunen, P., Cao, S., Backus, K.M., Olenchock, B.A., Patel, H., Zhang, Q., Signoretti, S., Gerfen, G.J., Richardson, A.L., et al. (2016). Paracrine Induction of HIF by Glutamate in Breast Cancer: EglN1 Senses Cysteine. Cell *166*, 126–139.

Brugarolas, J.B., Vazquez, F., Reddy, A., Sellers, W.R., and Kaelin, W.G. (2003). TSC2 regulates VEGF through mTOR-dependent and -independent pathways. Cancer Cell *4*, 147–158.

Budde, M.W., and Roth, M.B. (2010). Hydrogen Sulfide Increases Hypoxia-inducible Factor-1 Activity Independently of von Hippel–Lindau Tumor Suppressor-1 in *C. elegans*. Mol. Biol. Cell *21*, 212–217.

Budde, M.W., and Roth, M.B. (2011). The Response of *Caenorhabditis elegans* to Hydrogen Sulfide and Hydrogen Cyanide. Genetics *189*, 521–532.

Bunn, H.F., and Poyton, R.O. (1996). Oxygen sensing and molecular adaptation to hypoxia. Physiol. Rev. *76*, 839–885.

Burslem, G.M., Kyle, H.F., Nelson, A., Edwards, T.A., and Wilson, A.J. (2017). Hypoxia inducible factor (HIF) as a model for studying inhibition of protein–protein interactions. Chem. Sci. *8*, 4188–4202.

Cai, Z., Zhong, H., Bosch-Marce, M., Fox-Talbot, K., Wang, L., Wei, C., Trush, M.A., and Semenza, G.L. (2008). Complete loss of ischaemic preconditioning-induced cardioprotection in mice with partial deficiency of HIF-1α. Cardiovasc. Res. *77*, 463–470.

Cai, Z., Luo, W., Zhan, H., and Semenza, G.L. (2013). Hypoxia-inducible factor 1 is required for remote ischemic preconditioning of the heart. Proc. Natl. Acad. Sci. U. S. A. *110*, 17462–17467.

Centanin, L., Ratcliffe, P.J., and Wappner, P. (2005). Reversion of lethality and growth defects in Fatiga oxygen-sensor mutant flies by loss of Hypoxia-Inducible Factor-α/Sima. EMBO Rep. *6*, 1070–1075.

Ceradini, D.J., Kulkarni, A.R., Callaghan, M.J., Tepper, O.M., Bastidas, N., Kleinman, M.E., Capla, J.M., Galiano, R.D., Levine, J.P., and Gurtner, G.C. (2004). Progenitor cell trafficking is regulated by hypoxic gradients through HIF-1 induction of SDF-1. Nat. Med. *10*, 858.

Chang, A.J. (2017). Acute oxygen sensing by the carotid body: from mitochondria to plasma membrane. J. Appl. Physiol. *123*, 1335–1343.

Chang, A.J., and Bargmann, C.I. (2008). Hypoxia and the HIF-1 transcriptional pathway reorganize a neuronal circuit for oxygen-dependent behavior in *Caenorhabditis elegans*. Proc. Natl. Acad. Sci. *105*, 7321–7326.

Chang, A.J., Chronis, N., Karow, D.S., Marletta, M.A., and Bargmann, C.I. (2006). A Distributed Chemosensory Circuit for Oxygen Preference in *C. elegans*. PLoS Biol *4*, e274.

Cheng, J., Kang, X., Zhang, S., and Yeh, E.T.H. (2007). SUMO-Specific Protease 1 Is Essential for Stabilization of HIF1α during Hypoxia. Cell *131*, 584–595.

Cheung, B.H.H., Cohen, M., Rogers, C., Albayram, O., and de Bono, M. (2005). Experience-Dependent Modulation of *C. elegans* Behavior by Ambient Oxygen. Curr. Biol. *15*, 905–917.

Chi, J.-T., Wang, Z., Nuyten, D.S.A., Rodriguez, E.H., Schaner, M.E., Salim, A., Wang, Y., Kristensen, G.B., Helland, Å., Børresen-Dale, A.-L., et al. (2006). Gene Expression Programs in Response to Hypoxia: Cell Type Specificity and Prognostic Significance in Human Cancers. PLOS Med. *3*, e47.

Choi, K.-O. (2005). Inhibition of the catalytic activity of HIF-1 -prolyl hydroxylase 2 by a MYND-type zinc finger. Mol. Pharmacol.

Cockman, M.E., Masson, N., Mole, D.R., Jaakkola, P., Chang, G.-W., Clifford, S.C., Maher, E.R., Pugh, C.W., Ratcliffe, P.J., and Maxwell, P.H. (2000). Hypoxia inducible factor-α binding and ubiquitylation by the von Hippel-Lindau tumor suppressor protein. J. Biol. Chem. *275*, 25733–25741.

Cohen, H.T., Zhou, M., Welsh, A.M., Zarghamee, S., Scholz, H., Mukhopadhyay, D., Kishida, T., Zbar, B., Knebelmann, B., and Sukhatme, V.P. (1999). An Important von Hippel-Lindau Tumor Suppressor Domain Mediates Sp1-Binding and Self-Association. Biochem. Biophys. Res. Commun. *266*, 43–50.

Collins, E.T. (1894). Intra-ocular growths (two cases, brother and sister, with peculiar vascular new growth, probably retinal, affecting both eyes). Trans Ophthalmol Soc UK *14*, 1894–149.

Compernolle, V., Brusselmans, K., Acker, T., Hoet, P., Tjwa, M., Beck, H., Plaisance, S., Dor, Y., Keshet, E., Lupu, F., et al. (2002). Loss of HIF-2α and inhibition of VEGF impair fetal lung maturation, whereas treatment with VEGF prevents fatal respiratory distress in premature mice. Nat. Med. *8*, 702.

Coulet, F., Nadaud, S., Agrapart, M., and Soubrier, F. (2003). Identification of Hypoxia-response Element in the Human Endothelial Nitric-oxide Synthase Gene Promoter. J. Biol. Chem. *278*, 46230–46240.

Dahl, K.D.C., Fryer, B.H., Mack, F.A., Compernolle, V., Maltepe, E., Adelman, D.M., Carmeliet, P., and Simon, M.C. (2005). Hypoxia-Inducible Factors 1α and 2α Regulate Trophoblast Differentiation. Mol. Cell. Biol. *25*, 10479–10491.

Dames, S.A., Martinez-Yamout, M., Guzman, R.N.D., Dyson, H.J., and Wright, P.E. (2002). Structural basis for Hif-1α/CBP recognition in the cellular hypoxic response. Proc. Natl. Acad. Sci. *99*, 5271–5276.

Dang, E.V., Barbi, J., Yang, H.-Y., Jinasena, D., Yu, H., Zheng, Y., Bordman, Z., Fu, J., Kim, Y., Yen, H.-R., et al. (2011). Control of TH17/Treg Balance by Hypoxia-Inducible Factor 1. Cell *146*, 772–784.

Dang, L., White, D.W., Gross, S., Bennett, B.D., Bittinger, M.A., Driggers, E.M., Fantin, V.R., Jang, H.G., Jin, S., Keenan, M.C., et al. (2009). Cancer-associated IDH1 mutations produce 2-hydroxyglutarate. Nature *462*, 739.

Darby, C., Cosma, C.L., Thomas, J.H., and Manoil, C. (1999). Lethal paralysis of *Caenorhabditis elegans* by *Pseudomonas aeruginosa*. Proc. Natl. Acad. Sci. U. S. A. *96*, 15202–15207.

Datta, K., Mondal, S., Sinha, S., Li, J., Wang, E., Knebelmann, B., Karumanchi, S.A., and Mukhopadhyay, D. (2005). Role of elongin-binding domain of von hippel lindau gene product on HuR-mediated VPF/VEGF mRNA stability in renal cell carcinoma. Oncogene *24*, 7850.

Dunwoodie, S.L. (2009). The Role of Hypoxia in Development of the Mammalian Embryo. Dev. Cell *17*, 755–773.

Düvel, K., Yecies, J.L., Menon, S., Raman, P., Lipovsky, A.I., Souza, A.L., Triantafellow, E., Ma, Q., Gorski, R., Cleaver, S., et al. (2010). Activation of a Metabolic Gene Regulatory Network Downstream of mTOR Complex 1. Mol. Cell *39*, 171–183.

Ebert, B.L., Firth, J.D., and Ratcliffe, P.J. (1995). Hypoxia and Mitochondrial Inhibitors Regulate Expression of Glucose Transporter-1 via Distinct Cis-acting Sequences. J. Biol. Chem. *270*, 29083–29089.

Eckle, T., Kohler, D., Lehmann, R., El Kasmi, K.C., and Eltzschig, H.K. (2008). Hypoxia-Inducible Factor-1 Is Central to Cardioprotection: A New Paradigm for Ischemic Preconditioning. Circulation *118*, 166–175.

Epstein, A.C.R., Gleadle, J.M., McNeill, L.A., Hewitson, K.S., O'Rourke, J., Mole, D.R., Mukherji, M., Metzen, E., Wilson, M.I., Dhanda, A., et al. (2001). *C. elegans* EGL-9 and mammalian homologs define a family of dioxygenases that regulate HIF by prolyl hydroxylation. Cell *107*, 43–54.

Fitzpatrick, S.F., Tambuwala, M.M., Bruning, U., Schaible, B., Scholz, C.C., Byrne, A., O'Connor, A., Gallagher, W.M., Lenihan, C.R., Garvey, J.F., et al. (2011). An Intact Canonical NF-κB Pathway Is Required for Inflammatory Gene Expression in Response to Hypoxia. J. Immunol. *186*, 1091–1096.

Forsythe, J.A., Jiang, B.H., Iyer, N.V., Agani, F., Leung, S.W., Koos, R.D., and Semenza, G.L. (1996). Activation of vascular endothelial growth factor gene transcription by hypoxia-inducible factor 1. Mol. Cell. Biol. *16*, 4604–4613.

Freedman, S.J., Sun, Z.-Y.J., Poy, F., Kung, A.L., Livingston, D.M., Wagner, G., and Eck, M.J. (2002). Structural basis for recruitment of CBP/p300 by hypoxia-inducible factor-1α. Proc. Natl. Acad. Sci. *99*, 5367–5372.

Gallagher, L.A., and Manoil, C. (2001). *Pseudomonas aeruginosa* PAO1 Kills *Caenorhabditis elegans* by Cyanide Poisoning. J. Bacteriol. *183*, 6207–6214.

Gerald, D., Berra, E., Frapart, Y.M., Chan, D.A., Giaccia, A.J., Mansuy, D., Pouysségur, J., Yaniv, M., and Mechta-Grigoriou, F. (2004). JunD Reduces Tumor Angiogenesis by Protecting Cells from Oxidative Stress. Cell *118*, 781–794.

German, N.J., Yoon, H., Yusuf, R.Z., Murphy, J.P., Finley, L.W.S., Laurent, G., Haas, W., Satterstrom, F.K., Guarnerio, J., Zaganjor, E., et al. (2016). PHD3 Loss in Cancer Enables Metabolic Reliance on Fatty Acid Oxidation via Deactivation of ACC2. Mol. Cell *63*, 1006–1020.

Gnarra, J.R., Zhou, S., Merrill, M.J., Wagner, J.R., Krumm, A., Papavassiliou, E., Oldfield, E.H., Klausner, R.D., and Linehan, W.M. (1996). Post-transcriptional regulation of vascular endothelial growth factor mRNA by the product of the VHL tumor suppressor gene. Proc. Natl. Acad. Sci. *93*, 10589–10594.

Goldberg, M.A., Glass, G.A., Cunningham, J.M., and Bunn, H.F. (1987). The regulated expression of erythropoietin by two human hepatoma cell lines. Proc. Natl. Acad. Sci. *84*, 7972–7976.

Gray, J.M., Karow, D.S., Lu, H., Chang, A.J., Chang, J.S., Ellis, R.E., Marletta, M.A., and Bargmann, C.I. (2004). Oxygen sensation and social feeding mediated by a *C. elegans* guanylate cyclase homologue. Nature *430*, 317–322.

Guo, J., Chakraborty, A.A., Liu, P., Gan, W., Zheng, X., Inuzuka, H., Wang, B., Zhang, J., Zhang, L., Yuan, M., et al. (2016). pVHL suppresses kinase activity of Akt in a proline-hydroxylation–dependent manner. Science *353*, 929–932.

Hagen, T., Taylor, C.T., Lam, F., and Moncada, S. (2003). Redistribution of Intracellular Oxygen in Hypoxia by Nitric Oxide: Effect on HIF1α. Science *302*, 1975–1978.

Hartmann, H., Eltzschig, H.K., Wurz, H., Hantke, K., Rakin, A., Yazdi, A.S., Matteoli, G., Bohn, E., Autenrieth, I.B., Karhausen, J., et al. (2008). Hypoxia-Independent Activation of HIF-1 by Enterobacteriaceae and Their Siderophores. Gastroenterology *134*, 756–767.e6.

Hergovich, A., Lisztwan, J., Barry, R., Ballschmieter, P., and Krek, W. (2003). Regulation of microtubule stability by the von Hippel-Lindau tumour suppressor protein pVHL. Nat. Cell Biol. *5*, 64.

Hoffman, M.A., Ohh, M., Yang, H., Klco, J.M., Ivan, M., Jr, K., and G, W. (2001). von Hippel-Lindau protein mutants linked to type 2C VHL disease preserve the ability to downregulate HIF. Hum. Mol. Genet. *10*, 1019–1027.

Hölscher, M., Schäfer, K., Krull, S., Farhat, K., Hesse, A., Silter, M., Lin, Y., Pichler, B.J., Thistlethwaite, P., El-Armouche, A., et al. (2012). Unfavourable consequences of chronic cardiac HIF-1α stabilization. Cardiovasc. Res. *94*, 77–86.

Hu, C.-J., Wang, L.-Y., Chodosh, L.A., Keith, B., and Simon, M.C. (2003). Differential Roles of Hypoxia-Inducible Factor 1α (HIF-1α) and HIF-2α in Hypoxic Gene Regulation. Mol. Cell. Biol. *23*, 9361–9374.

Hu, C.-J., Iyer, S., Sataur, A., Covello, K.L., Chodosh, L.A., and Simon, M.C. (2006). Differential Regulation of the Transcriptional Activities of Hypoxia-Inducible Factor 1 Alpha (HIF-1α) and HIF-2α in Stem Cells. Mol. Cell. Biol. *26*, 3514–3526.

Hu, C.-J., Sataur, A., Wang, L., Chen, H., and Simon, M.C. (2007). The N-Terminal Transactivation Domain Confers Target Gene Specificity of Hypoxia-inducible Factors HIF-1α and HIF-2α. Mol. Biol. Cell *18*, 4528–4542.

Huang, L.E., Arany, Z., Livingston, D.M., and Bunn, H.F. (1996). Activation of Hypoxia-inducible Transcription Factor Depends Primarily upon Redox-sensitive Stabilization of Its α Subunit. J. Biol. Chem. *271*, 32253–32259.

Huang, L.E., Gu, J., Schau, M., and Bunn, H.F. (1998). Regulation of hypoxia-inducible factor 1α is mediated by an O2-dependent degradation domain via the ubiquitin-proteasome pathway. Proc. Natl. Acad. Sci. *95*, 7987–7992.

Huang, Y., Hickey, R.P., Yeh, J.L., Liu, D., Dadak, A., Young, L.H., Johnson, R.S., and Giordano, F.J. (2004). Cardiac myocyte-specific HIF-1α deletion alters vascularization, energy availability, calcium flux, and contractility in the normoxic heart. FASEB J. *18*, 1138–1140.

Iliopoulos, O., Levy, A.P., Jiang, C., Kaelin, W.G., and Goldberg, M.A. (1996). Negative regulation of hypoxia-inducible genes by the von Hippel-Lindau protein. Proc. Natl. Acad. Sci. *93*, 10595–10599.

Intlekofer, A.M., Dematteo, R.G., Venneti, S., Finley, L.W.S., Lu, C., Judkins, A.R., Rustenburg, A.S., Grinaway, P.B., Chodera, J.D., Cross, J.R., et al. (2015). Hypoxia Induces Production of L-2-Hydroxyglutarate. Cell Metab. *22*, 304–311.

Intlekofer, A.M., Wang, B., Liu, H., Shah, H., Carmona-Fontaine, C., Rustenburg, A.S., Salah, S., Gunner, M.R., Chodera, J.D., Cross, J.R., et al. (2017). L-2-Hydroxyglutarate production arises from noncanonical enzyme function at acidic pH. Nat. Chem. Biol. *13*, 494.

Isaacs, J.S., Jung, Y.-J., Mimnaugh, E.G., Martinez, A., Cuttitta, F., and Neckers, L.M. (2002). Hsp90 Regulates a von Hippel Lindau-independent Hypoxia-inducible Factor-1α-degradative Pathway. J. Biol. Chem. *277*, 29936–29944.

Ivan, M., and Kaelin, W.G. (2017). The EGLN-HIF O_2-Sensing System: Multiple Inputs and Feedbacks. Mol. Cell *66*, 772–779.

Ivan, M., Kondo, K., Yang, H., Kim, W., Valiando, J., Ohh, M., Salic, A., Asara, J.M., Lane, W.S., and Jr, W.G.K. (2001). HIFα Targeted for VHL-mediated destruction by proline hydroxylation: Implications for O_2 sensing. Science *292*, 464–468.

Iyer, N.V., Kotch, L.E., Agani, F., Leung, S.W., Laughner, E., Wenger, R.H., Gassmann, M., Gearhart, J.D., Lawler, A.M., Yu, A.Y., et al. (1998). Cellular and developmental control of O_2 homeostasis by hypoxia-inducible factor 1α. Genes Dev. *12*, 149–162.

Jaakkola, P., Mole, D.R., Tian, Y.-M., Wilson, M.I., Gielbert, J., Gaskell, S.J., Kriegsheim, A. von, Hebestreit, H.F., Mukherji, M., Schofield, C.J., et al. (2001). Targeting of HIF-α to the von Hippel-Lindau ubiquitylation complex by O_2-regulated prolyl hydroxylation. Science *292*, 468–472.

Jelkmann, W. (1992). Erythropoietin: structure, control of production, and function. Physiol. Rev. *72*, 449–489.

Jiang, H., Guo, R., and Powell-Coffman, J.A. (2001). The *Caenorhabditis elegans hif-1* gene encodes a bHLH-PAS protein that is required for adaptation to hypoxia. Proc. Natl. Acad. Sci. *98*, 7916–7921.

Kaelin, W.G. (2007). von Hippel-Lindau Disease. Annu. Rev. Pathol. Mech. Dis. *2*, 145–173.

Kaelin, W.G., and Ratcliffe, P.J. (2008). Oxygen sensing by metazoans: The central role of the HIF hydroxylase pathway. Mol. Cell *30*, 393–402.

Kamura, T., Koepp, D.M., Conrad, M.N., Skowyra, D., Moreland, R.J., Iliopoulos, O., Lane, W.S., Kaelin, W.G., Elledge, S.J., Conaway, R.C., et al. (1999). Rbx1, a Component of the VHL Tumor Suppressor Complex and SCF Ubiquitin Ligase. Science *284*, 657–661.

Kelly, B.D., Hackett, S.F., Hirota, K., Oshima, Y., Cai, Z., Berg-Dixon, S., Rowan, A., Yan, Z., Campochiaro, P.A., and Semenza, G.L. (2003). Cell Type–Specific Regulation of Angiogenic Growth Factor Gene Expression and Induction of Angiogenesis in Nonischemic Tissue by a Constitutively Active Form of Hypoxia-Inducible Factor 1. Circ. Res. *93*, 1074–1081.

Kewley, R.J., Whitelaw, M.L., and Chapman-Smith, A. (2004). The mammalian basic helix–loop–helix/PAS family of transcriptional regulators. Int. J. Biochem. Cell Biol. *36*, 189–204.

Kim, J., Tchernyshyov, I., Semenza, G.L., and Dang, C.V. (2006). HIF-1-mediated expression of pyruvate dehydrogenase kinase: A metabolic switch required for cellular adaptation to hypoxia. Cell Metab. *3*, 177–185.

Knowles, H.J., Raval, R.R., Harris, A.L., and Ratcliffe, P.J. (2003). Effect of Ascorbate on the Activity of Hypoxia-inducible Factor in Cancer Cells. Cancer Res. *63*, 1764–1768.

Koivunen, P., Hirsilä, M., Günzler, V., Kivirikko, K.I., and Myllyharju, J. (2004). Catalytic Properties of the Asparaginyl Hydroxylase (FIH) in the Oxygen Sensing Pathway Are Distinct from Those of Its Prolyl 4-Hydroxylases. J. Biol. Chem. *279*, 9899–9904.

Koivunen, P., Tiainen, P., Hyvärinen, J., Williams, K.E., Sormunen, R., Klaus, S.J., Kivirikko, K.I., and Myllyharju, J. (2007a). An Endoplasmic Reticulum Transmembrane Prolyl 4-Hydroxylase Is Induced by Hypoxia and Acts on Hypoxia-inducible Factor α. J. Biol. Chem. *282*, 30544–30552.

Koivunen, P., Hirsilä, M., Remes, A.M., Hassinen, I.E., Kivirikko, K.I., and Myllyharju, J. (2007b). Inhibition of Hypoxia-inducible Factor (HIF) Hydroxylases by Citric Acid Cycle Intermediates. J. Biol. Chem. *282*, 4524–4532.

Kojima, H., Gu, H., Nomura, S., Caldwell, C.C., Kobata, T., Carmeliet, P., Semenza, G.L., and Sitkovsky, M.V. (2002). Abnormal B lymphocyte development and autoimmunity in hypoxia-inducible factor 1α-deficient chimeric mice. Proc. Natl. Acad. Sci. *99*, 2170–2174.

Kondo, K., Klco, J., Nakamura, E., Lechpammer, M., and Kaelin, W.G. (2002). Inhibition of HIF is necessary for tumor suppression by the von Hippel-Lindau protein. Cancer Cell *1*, 237–246.

Kondo, K., Kim, W.Y., Lechpammer, M., and Jr, W.G.K. (2003). Inhibition of HIF2α Is Sufficient to Suppress pVHL-Defective Tumor Growth. PLOS Biol. *1*, e83.

Kozak, K.R., Abbott, B., and Hankinson, O. (1997). ARNT-Deficient Mice and Placental Differentiation. Dev. Biol. *191*, 297–305.

Kurban, G., Hudon, V., Duplan, E., Ohh, M., and Pause, A. (2006). Characterization of a von Hippel Lindau Pathway Involved in Extracellular Matrix Remodeling, Cell Invasion, and Angiogenesis. Cancer Res. *66*, 1313–1319.

Kuznetsova, A.V., Meller, J., Schnell, P.O., Nash, J.A., Ignacak, M.L., Sanchez, Y., Conaway, J.W., Conaway, R.C., and Czyzyk-Krzeska, M.F. (2003). von Hippel–Lindau protein binds hyperphosphorylated large subunit of RNA polymerase II through a proline hydroxylation motif and targets it for ubiquitination. Proc. Natl. Acad. Sci. *100*, 2706–2711.

Laitala, A., Aro, E., Walkinshaw, G., Mäki, J.M., Rossi, M., Heikkilä, M., Savolainen, E.-R., Arend, M., Kivirikko, K.I., Koivunen, P., et al. (2012). Transmembrane prolyl 4-hydroxylase is a

fourth prolyl 4-hydroxylase regulating EPO production and erythropoiesis. Blood *120*, 3336–3344.

Lam, S.-Y., Tipoe, G.L., Liong, E.C., and Fung, M.-L. (2008). Differential expressions and roles of hypoxia-inducible factor-1a,-2a and-3a in the rat carotid body during chronic and intermittent hypoxia. Histol. Histopathol. *23*, 271.

Lando, D., Peet, D.J., Whelan, D.A., Gorman, J.J., and Whitelaw, M.L. (2002). Asparagine Hydroxylation of the HIF Transactivation Domain: A Hypoxic Switch. Science *295*, 858–861.

Lane, N., and Martin, W. (2010). The energetics of genome complexity. Nature *467*, 929–934.

Lang, K.J.D., Kappel, A., and Goodall, G.J. (2002). Hypoxia-inducible Factor-1α mRNA Contains an Internal Ribosome Entry Site That Allows Efficient Translation during Normoxia and Hypoxia. Mol. Biol. Cell *13*, 1792–1801.

Lee, D.C., Sohn, H.A., Park, Z.-Y., Oh, S., Kang, Y.K., Lee, K., Kang, M., Jang, Y.J., Yang, S.-J., Hong, Y.K., et al. (2015). A Lactate-Induced Response to Hypoxia. Cell *161*, 595–609.

Lee, S.-J., Hwang, A.B., and Kenyon, C. (2010). Inhibition of respiration extends *C. elegans* life span via reactive oxygen species that increase HIF-1 activity. Curr. Biol. CB *20*, 2131–2136.

Lee, Y.M., Jeong, C.-H., Koo, S.-Y., Son, M.J., Song, H.S., Bae, S.-K., Raleigh, J.A., Chung, H.-Y., Yoo, M.-A., and Kim, K.-W. (2001). Determination of hypoxic region by hypoxia marker in developing mouse embryos in vivo: A possible signal for vessel development. Dev. Dyn. *220*, 175–186.

Lee, Y.S., Kim, J., Osborne, O., Oh, D.Y., Sasik, R., Schenk, S., Chen, A., Chung, H., Murphy, A., Watkins, S.M., et al. (2014). Increased Adipocyte O_2 Consumption Triggers HIF-1α, Causing Inflammation and Insulin Resistance in Obesity. Cell *157*, 1339–1352.

Leiser, S.F., Begun, A., and Kaeberlein, M. (2011). HIF-1 modulates longevity and healthspan in a temperature-dependent manner. Aging Cell *10*, 318–326.

Leiser, S.F., Miller, H., Rossner, R., Fletcher, M., Leonard, A., Primitivo, M., Rintala, N., Ramos, F.J., Miller, D.L., and Kaeberlein, M. (2015). Cell nonautonomous activation of flavin-containing monooxygenase promotes longevity and health span. Science *350*, 1375–1378.

Li, Z., Wang, D., Messing, E.M., and Wu, G. (2005). VHL protein-interacting deubiquitinating enzyme 2 deubiquitinates and stabilizes HIF-1α. EMBO Rep. *6*, 373–378.

Lindau, A. (1926). Zur frage der angiomatosis retinae und ihrer hirnkomplikationen. Acta Ophthalmol. (Copenh.) *4*, 193–226.

Liu, L., Marti, G.P., Wei, X., Zhang, X., Zhang, H., Liu, Y.V., Nastai, M., Semenza, G.L., and Harmon, J.W. (2008). Age-dependent impairment of HIF-1α expression in diabetic mice: Correction with electroporation-facilitated gene therapy increases wound healing, angiogenesis, and circulating angiogenic cells. J. Cell. Physiol. *217*, 319–327.

Liu, Y.V., Baek, J.H., Zhang, H., Diez, R., Cole, R.N., and Semenza, G.L. (2007). RACK1 Competes with HSP90 for Binding to HIF-1α and Is Required for O_2-Independent and HSP90 Inhibitor-Induced Degradation of HIF-1α. Mol. Cell *25*, 207–217.

Loboda, A., Jozkowicz, A., and Dulak, J. (2010). HIF-1 and HIF-2 transcription factors — Similar but not identical. Mol. Cells *29*, 435–442.

Lopez-Barneo, J., Lopez-Lopez, J.R., Urena, J., and Gonzalez, C. (1988). Chemotransduction in the carotid body: K+ current modulated by PO2 in type I chemoreceptor cells. Science *241*, 580–582.

Lorenzo, F.R., Huff, C., Myllymäki, M., Olenchock, B., Swierczek, S., Tashi, T., Gordeuk, V., Wuren, T., Ri-Li, G., McClain, D.A., et al. (2014). A genetic mechanism for Tibetan high-altitude adaptation. Nat. Genet. *46*, 951.

Luhachack, L.G., Visvikis, O., Wollenberg, A.C., Lacy-Hulbert, A., Stuart, L.M., and Irazoqui, J.E. (2012). EGL-9 Controls *C. elegans* Host Defense Specificity through Prolyl Hydroxylation-Dependent and -Independent HIF-1 Pathways. PLoS Pathog *8*, e1002798.

Luo, W., Hu, H., Chang, R., Zhong, J., Knabel, M., O'Meally, R., Cole, R.N., Pandey, A., and Semenza, G.L. (2011). Pyruvate Kinase M2 Is a PHD3-Stimulated Coactivator for Hypoxia-Inducible Factor 1. Cell *145*, 732–744.

Ma, D.K., and Ringstad, N. (2012). The neurobiology of sensing respiratory gases for the control of animal behavior. Front. Biol. *7*, 246–253.

Ma, D.K., Vozdek, R., Bhatla, N., and Horvitz, H.R. (2012). CYSL-1 interacts with the O_2-sensing hydroxylase EGL-9 to promote H2S-modulated hypoxia-induced behavioral plasticity in *C. elegans*. Neuron *73*, 925–940.

Ma, D.K., Rothe, M., Zheng, S., Bhatla, N., Pender, C.L., Menzel, R., and Horvitz, H.R. (2013). Cytochrome P450 drives a HIF-regulated behavioral response to reoxygenation by *C. elegans*. Science *341*, 554–558.

MacKenzie, E.D., Selak, M.A., Tennant, D.A., Payne, L.J., Crosby, S., Frederiksen, C.M., Watson, D.G., and Gottlieb, E. (2007). Cell-Permeating α-Ketoglutarate Derivatives Alleviate Pseudohypoxia in Succinate Dehydrogenase-Deficient Cells. Mol. Cell. Biol. *27*, 3282–3289.

Maher, E.R., Yates, J.R., and Ferguson-Smith, M.A. (1990). Statistical analysis of the two stage mutation model in von Hippel-Lindau disease, and in sporadic cerebellar haemangioblastoma and renal cell carcinoma. J. Med. Genet. *27*, 311–314.

Makino, Y., Cao, R., Svensson, K., Bertilsson, G., Asman, M., Tanaka, H., Cao, Y., Berkenstam, A., and Poellinger, L. (2001). Inhibitory PAS domain protein is a negative regulator of hypoxia-inducible gene expression. Nature *414*, 550.

Makino, Y., Kanopka, A., Wilson, W.J., Tanaka, H., and Poellinger, L. (2002). Inhibitory PAS Domain Protein (IPAS) Is a Hypoxia-inducible Splicing Variant of the Hypoxia-inducible Factor-3α Locus. J. Biol. Chem. *277*, 32405–32408.

Maltepe, E., Schmidt, J.V., Baunoch, D., Bradfield, C.A., and Simon, M.C. (1997). Abnormal angiogenesis and responses to glucose and oxygen deprivation in mice lacking the protein ARNT. Nature *386*, 403.

Manalo, D.J., Rowan, A., Lavoie, T., Natarajan, L., Kelly, B.D., Ye, S.Q., Garcia, J.G.N., and Semenza, G.L. (2005). Transcriptional regulation of vascular endothelial cell responses to hypoxia by HIF-1. Blood *105*, 659–669.

Maranchie, J.K., and Zhan, Y. (2005). Nox4 Is Critical for Hypoxia-Inducible Factor 2-α Transcriptional Activity in von Hippel-Lindau–Deficient Renal Cell Carcinoma. Cancer Res. *65*, 9190–9193.

Masson, N., Willam, C., Maxwell, P.H., Pugh, C.W., and Ratcliffe, P.J. (2001). Independent function of two destruction domains in hypoxia-inducible factor-α chains activated by prolyl hydroxylation. EMBO J. *20*, 5197–5206.

Maxwell, P.H., Pugh, C.W., and Ratcliffe, P.J. (1993). Inducible operation of the erythropoietin 3' enhancer in multiple cell lines: evidence for a widespread oxygen-sensing mechanism. Proc. Natl. Acad. Sci. *90*, 2423–2427.

Maxwell, P.H., Wiesener, M.S., Chang, G.-W., Clifford, S.C., Vaux, E.C., Cockman, M.E., Wykoff, C.C., Pugh, C.W., Maher, E.R., and Ratcliffe, P.J. (1999). The tumour suppressor protein VHL targets hypoxia-inducible factors for oxygen-dependent proteolysis. Nature *399*, 271–275.

McDonough, M.A., Loenarz, C., Chowdhury, R., Clifton, I.J., and Schofield, C.J. (2010). Structural studies on human 2-oxoglutarate dependent oxygenases. Curr. Opin. Struct. Biol. *20*, 659–672.

McNeill, L.A., Hewitson, K.S., Gleadle, J.M., Horsfall, L.E., Oldham, N.J., Maxwell, P.H., Pugh, C.W., Ratcliffe, P.J., and Schofield, C.J. (2002). The use of dioxygen by HIF prolyl hydroxylase (PHD1). Bioorg. Med. Chem. Lett. *12*, 1547–1550.

Mehta, R., Steinkraus, K.A., Sutphin, G.L., Ramos, F.J., Shamieh, L.S., Huh, A., Davis, C., Chandler-Brown, D., and Kaeberlein, M. (2009). Proteasomal Regulation of the Hypoxic Response Modulates Aging in *C. elegans*. Science *324*, 1196–1198.

Metzen, E., Berchner-Pfannschmidt, U., Stengel, P., Marxsen, J.H., Stolze, I., Klinger, M., Huang, W.Q., Wotzlaw, C., Hellwig-Bürgel, T., Jelkmann, W., et al. (2003a). Intracellular localisation of human HIF-1α hydroxylases: implications for oxygen sensing. J. Cell Sci. *116*, 1319–1326.

Metzen, E., Zhou, J., Jelkmann, W., Fandrey, J., and Brüne, B. (2003b). Nitric Oxide Impairs Normoxic Degradation of HIF-1α by Inhibition of Prolyl Hydroxylases. Mol. Biol. Cell *14*, 3470–3481.

Miller, D.L., and Roth, M.B. (2009). *C. elegans* are protected from lethal hypoxia by an embryonic diapause. Curr. Biol. *19*, 1233–1237.

Minamishima, Y.A., and Kaelin, W.G. (2010). Reactivation of Hepatic EPO Synthesis in Mice After PHD Loss. Science *329*, 407–407.

Mole, D.R., Blancher, C., Copley, R.R., Pollard, P.J., Gleadle, J.M., Ragoussis, J., and Ratcliffe, P.J. (2009). Genome-wide association of hypoxia-inducible factor (HIF)-1α and HIF-2α DNA binding with expression profiling of hypoxia-inducible transcripts. J. Biol. Chem. *284*, 16767–16775.

Moslehi, J., Minamishima, Y.A., Shi, J., Neuberg, D., Charytan, D.M., Padera, R.F., Signoretti, S., Liao, R., and Kaelin, W.G. (2010). Loss of Hypoxia-Inducible Factor Prolyl Hydroxylase Activity in Cardiomyocytes Phenocopies Ischemic Cardiomyopathy. Circulation *122*, 1004–1016.

Mukhopadhyay, D., Knebelmann, B., Cohen, H.T., Ananth, S., and Sukhatme, V.P. (1997). The von Hippel-Lindau tumor suppressor gene product interacts with Sp1 to repress vascular endothelial growth factor promoter activity. Mol. Cell. Biol. *17*, 5629–5639.

Na, X., Duan, H.O., Messing, E.M., Schoen, S.R., Ryan, C.K., Sant'Agnese, P.A. di, Golemis, E.A., and Wu, G. (2003). Identification of the RNA polymerase II subunit hsRPB7 as a novel target of the von Hippel—Lindau protein. EMBO J. *22*, 4249–4259.

Nadtochiy, S.M., Schafer, X., Fu, D., Nehrke, K., Munger, J., and Brookes, P.S. (2016). Acidic pH Is a Metabolic Switch for 2-Hydroxyglutarate Generation and Signaling. J. Biol. Chem. *291*, 20188–20197.

Oldham, W.M., Clish, C.B., Yang, Y., and Loscalzo, J. (2015). Hypoxia-Mediated Increases in l-2-hydroxyglutarate Coordinate the Metabolic Response to Reductive Stress. Cell Metab. *22*, 291–303.

Olenchock, B.A., Moslehi, J., Baik, A.H., Davidson, S.M., Williams, J., Gibson, W.J., Chakraborty, A.A., Pierce, K.A., Miller, C.M., Hanse, E.A., et al. (2016). EGLN1 inhibition and rerouting of α-ketoglutarate suffice for remote ischemic protection. Cell *164*, 884–895.

Pan, Y., Mansfield, K.D., Bertozzi, C.C., Rudenko, V., Chan, D.A., Giaccia, A.J., and Simon, M.C. (2007). Multiple Factors Affecting Cellular Redox Status and Energy Metabolism Modulate Hypoxia-Inducible Factor Prolyl Hydroxylase Activity In Vivo and In Vitro. Mol. Cell. Biol. *27*, 912–925.

Papandreou, I., Cairns, R.A., Fontana, L., Lim, A.L., and Denko, N.C. (2006). HIF-1 mediates adaptation to hypoxia by actively downregulating mitochondrial oxygen consumption. Cell Metab. *3*, 187–197.

Park, E.C., Ghose, P., Shao, Z., Ye, Q., Kang, L., Xu, X.Z.S., Powell-Coffman, J.A., and Rongo, C. (2012). Hypoxia regulates glutamate receptor trafficking through an HIF-independent mechanism. EMBO J. *31*, 1379–1393.

Pasarica, M., Sereda, O.R., Redman, L.M., Albarado, D.C., Hymel, D.T., Roan, L.E., Rood, J.C., Burk, D.H., and Smith, S.R. (2009). Reduced Adipose Tissue Oxygenation in Human Obesity: Evidence for Rarefaction, Macrophage Chemotaxis, and Inflammation Without an Angiogenic Response. Diabetes *58*, 718–725.

Peng, J., Zhang, L., Drysdale, L., and Fong, G.-H. (2000). The transcription factor EPAS-1/hypoxia-inducible factor 2α plays an important role in vascular remodeling. Proc. Natl. Acad. Sci. *97*, 8386–8391.

Peyssonnaux, C., Datta, V., Cramer, T., Doedens, A., Theodorakis, E.A., Gallo, R.L., Hurtado-Ziola, N., Nizet, V., and Johnson, R.S. (2005). HIF-1α expression regulates the bactericidal capacity of phagocytes. J. Clin. Invest. *115*, 1806–1815.

Pocock, R., and Hobert, O. (2010). Hypoxia activates a latent circuit for processing gustatory information in *C. elegans*. Nat. Neurosci. *13*, 610–614.

Pollard, P., Wortham, N., and Tomlinson, I. (2003). The TCA cycle and tumorigenesis: the examples of fumarate hydratase and succinate dehydrogenase. Ann. Med. *35*, 634–635.

Powell, F.L., and Fu, Z. (2008). HIF-1 and ventilatory acclimatization to chronic hypoxia. Respir. Physiol. Neurobiol. *164*, 282–287.

Prabhakar, N.R., and Semenza, G.L. (2012). Adaptive and Maladaptive Cardiorespiratory Responses to Continuous and Intermittent Hypoxia Mediated by Hypoxia-Inducible Factors 1 and 2. Physiol. Rev. *92*, 967–1003.

Pugh, C.W., Tan, C.C., Jones, R.W., and Ratcliffe, P.J. (1991). Functional analysis of an oxygen-regulated transcriptional enhancer lying 3' to the mouse erythropoietin gene. Proc. Natl. Acad. Sci. *88*, 10553–10557.

Rankin, E.B., Biju, M.P., Liu, Q., Unger, T.L., Rha, J., Johnson, R.S., Simon, M.C., Keith, B., and Haase, V.H. (2007). Hypoxia-inducible factor–2 (HIF-2) regulates hepatic erythropoietin in vivo. J. Clin. Invest. *117*, 1068–1077.

Ratcliffe, P.J. (2013). Oxygen sensing and hypoxia signalling pathways in animals: the implications of physiology for cancer. J. Physiol. *591*, 2027–2042.

Richard, D.E., Berra, E., Gothié, E., Roux, D., and Pouysségur, J. (1999). p42/p44 Mitogen-activated Protein Kinases Phosphorylate Hypoxia-inducible Factor 1α (HIF-1α) and Enhance the Transcriptional Activity of HIF-1. J. Biol. Chem. *274*, 32631–32637.

Rius, J., Guma, M., Schachtrup, C., Akassoglou, K., Zinkernagel, A.S., Nizet, V., Johnson, R.S., Haddad, G.G., and Karin, M. (2008). NF-κB links innate immunity to the hypoxic response through transcriptional regulation of HIF-1α. Nature *453*, 807.

Rogers, C., Persson, A., Cheung, B., and Bono, M. de (2006). Behavioral Motifs and Neural Pathways Coordinating O2 Responses and Aggregation in *C. elegans*. Curr. Biol. *16*, 649–659.

Ryan, H.E., Lo, J., and Johnson, R.S. (1998). HIF-1α is required for solid tumor formation and embryonic vascularization. EMBO J. *17*, 3005–3015.

Salnikow, K., Donald, S.P., Bruick, R.K., Zhitkovich, A., Phang, J.M., and Kasprzak, K.S. (2004). Depletion of Intracellular Ascorbate by the Carcinogenic Metals Nickel and Cobalt Results in the Induction of Hypoxic Stress. J. Biol. Chem. *279*, 40337–40344.

Schipani, E., Ryan, H.E., Didrickson, S., Kobayashi, T., Knight, M., and Johnson, R.S. (2001). Hypoxia in cartilage: HIF-1α is essential for chondrocyte growth arrest and survival. Genes Dev. *15*, 2865–2876.

Schofield, C.J., and Ratcliffe, P.J. (2004). Oxygen sensing by HIF hydroxylases. Nat. Rev. Mol. Cell Biol. *5*, 343.

Scortegagna, M., Ding, K., Oktay, Y., Gaur, A., Thurmond, F., Yan, L.-J., Marck, B.T., Matsumoto, A.M., Shelton, J.M., Richardson, J.A., et al. (2003). Multiple organ pathology, metabolic abnormalities and impaired homeostasis of reactive oxygen species in *Epas1*$^{-/-}$ mice. Nat. Genet. *35*, 331.

Semenza, G.L. (2009). Defining the role of hypoxia-inducible factor 1 in cancer biology and therapeutics. Oncogene *29*, 625–634.

Semenza, G.L. (2010). Oxygen homeostasis. Wiley Interdiscip. Rev. Syst. Biol. Med. *2*, 336–361.

Semenza, G.L. (2012). Hypoxia-inducible factors in physiology and medicine. Cell *148*, 399–408.

Semenza, G.L., and Wang, G.L. (1992). A nuclear factor induced by hypoxia via *de novo* protein synthesis binds to the human erythropoietin gene enhancer at a site required for transcriptional activation. Mol. Cell. Biol. *12*, 5447–5454.

Semenza, G.L., Nejfelt, M.K., Chi, S.M., and Antonarakis, S.E. (1991). Hypoxia-inducible nuclear factors bind to an enhancer element located 3'to the human erythropoietin gene. Proc. Natl. Acad. Sci. *88*, 5680–5684.

Semenza, G.L., Roth, P.H., Fang, H.M., and Wang, G.L. (1994). Transcriptional regulation of genes encoding glycolytic enzymes by hypoxia-inducible factor 1. J. Biol. Chem. *269*, 23757–23763.

Semenza, G.L., Jiang, B.-H., Leung, S.W., Passantino, R., Concordet, J.-P., Maire, P., and Giallongo, A. (1996). Hypoxia response elements in the aldolase A, enolase 1, and lactate dehydrogenase A gene promoters contain essential binding sites for hypoxia-inducible factor 1. J. Biol. Chem. *271*, 32529–32537.

Sendoel, A., Kohler, I., Fellmann, C., Lowe, S.W., and Hengartner, M.O. (2010). HIF-1 antagonizes p53-mediated apoptosis through a secreted neuronal tyrosinase. Nature *465*, 577–583.

Seth, P., Krop, I., Porter, D., and Polyak, K. (2002). Novel estrogen and tamoxifen induced genes identified by SAGE (Serial Analysis of Gene Expression). Oncogene *21*, 836.

Shatrov, V.A. (2003). Oxidized low-density lipoprotein (oxLDL) triggers hypoxia-inducible factor-1 (HIF-1) accumulation via redox-dependent mechanisms. Blood *101*, 4847–4849.

Shen, C., and Kaelin, W.G. (2013). The VHL/HIF axis in clear cell renal carcinoma. Semin. Cancer Biol. *23*, 18–25.

Shohet, R.V., and Garcia, J.A. (2007). Keeping the engine primed: HIF factors as key regulators of cardiac metabolism and angiogenesis during ischemia. J. Mol. Med. *85*, 1309–1315.

Shore, D.E., and Ruvkun, G. (2013). A cytoprotective perspective on longevity regulation. Trends Cell Biol. *23*, 409–420.

Simonson, T.S., Yang, Y., Huff, C.D., Yun, H., Qin, G., Witherspoon, D.J., Bai, Z., Lorenzo, F.R., Xing, J., Jorde, L.B., et al. (2010). Genetic evidence for high-altitude adaptation in Tibet. Science *329*, 72–75.

Song, D., Li, L.-S., Heaton-Johnson, K.J., Arsenault, P.R., Master, S.R., and Lee, F.S. (2013). Prolyl Hydroxylase Domain Protein 2 (PHD2) Binds a Pro-Xaa-Leu-Glu Motif, Linking It to the Heat Shock Protein 90 Pathway. J. Biol. Chem. *288*, 9662–9674.

Stebbins, C.E., Kaelin, W.G., and Pavletich, N.P. (1999). Structure of the VHL-ElonginC-ElonginB Complex: Implications for VHL Tumor Suppressor Function. Science *284*, 455–461.

Sun, R.C., and Denko, N.C. (2014). Hypoxic Regulation of Glutamine Metabolism through HIF1 and SIAH2 Supports Lipid Synthesis that Is Necessary for Tumor Growth. Cell Metab. *19*, 285–292.

Takeda, K., Ho, V.C., Takeda, H., Duan, L.-J., Nagy, A., and Fong, G.-H. (2006). Placental but Not Heart Defects Are Associated with Elevated Hypoxia-Inducible Factor α Levels in Mice Lacking Prolyl Hydroxylase Domain Protein 2. Mol. Cell. Biol. *26*, 8336–8346.

Tan, M.-W., Rahme, L.G., Sternberg, J.A., Tompkins, R.G., and Ausubel, F.M. (1999). *Pseudomonas aeruginosa* killing of *Caenorhabditis elegans* used to identify *P. aeruginosa* virulence factors. Proc. Natl. Acad. Sci. *96*, 2408–2413.

Thompson, A.A.R., Elks, P.M., Marriott, H.M., Eamsamarng, S., Higgins, K.R., Lewis, A., Williams, L., Parmar, S., Shaw, G., McGrath, E.E., et al. (2014). Hypoxia-inducible factor 2α regulates key neutrophil functions in humans, mice, and zebrafish. Blood *123*, 366–376.

Tian, H., Hammer, R.E., Matsumoto, A.M., Russell, D.W., and McKnight, S.L. (1998). The hypoxia-responsive transcription factor EPAS1 is essential for catecholamine homeostasis and protection against heart failure during embryonic development. Genes Dev. *12*, 3320–3324.

Tomita, S., Ueno, M., Sakamoto, M., Kitahama, Y., Ueki, M., Maekawa, N., Sakamoto, H., Gassmann, M., Kageyama, R., Ueda, N., et al. (2003). Defective Brain Development in Mice Lacking the Hif-1α Gene in Neural Cells. Mol. Cell. Biol. *23*, 6739–6749.

Treinin, M., Shliar, J., Jiang, H., Powell-Coffman, J.A., Bromberg, Z., and Horowitz, M. (2003). HIF-1 is required for heat acclimation in the nematode *Caenorhabditis elegans*. Physiol. Genomics *14*, 17–24.

Trent, C., Tsung, N., and Horvitz, H.R. (1983). Egg-laying defective mutants of the nematode *Caenorhabditis elegans*. Genetics *104*, 619–647.

Ullah, M.S., Davies, A.J., and Halestrap, A.P. (2006). The Plasma Membrane Lactate Transporter MCT4, but Not MCT1, Is Up-regulated by Hypoxia through a HIF-1α-dependent Mechanism. J. Biol. Chem. *281*, 9030–9037.

Vo, N., and Goodman, R.H. (2001). CREB-binding Protein and p300 in Transcriptional Regulation. J. Biol. Chem. *276*, 13505–13508.

von Hippel, E. v (1904). Ueber eine sehr seltene Erkrankung der Netzhaut. Albrecht Von Graefes Arch. Für Ophthalmol. *59*, 83–106.

Walmsley, S.R., Print, C., Farahi, N., Peyssonnaux, C., Johnson, R.S., Cramer, T., Sobolewski, A., Condliffe, A.M., Cowburn, A.S., Johnson, N., et al. (2005). Hypoxia-induced neutrophil survival is mediated by HIF-1α–dependent NF-κB activity. J. Exp. Med. *201*, 105–115.

Wang, G.L., and Semenza, G.L. (1995). Purification and Characterization of Hypoxia-inducible Factor 1. J. Biol. Chem. *270*, 1230–1237.

Wang, G.L., Jiang, B.H., Rue, E.A., and Semenza, G.L. (1995). Hypoxia-inducible factor 1 is a basic-helix-loop-helix-PAS heterodimer regulated by cellular O_2 tension. Proc. Natl. Acad. Sci. *92*, 5510–5514.

Wang, Y., Wan, C., Deng, L., Liu, X., Cao, X., Gilbert, S.R., Bouxsein, M.L., Faugere, M.-C., Guldberg, R.E., Gerstenfeld, L.C., et al. (2007). The hypoxia-inducible factor α pathway couples angiogenesis to osteogenesis during skeletal development. J. Clin. Invest. *117*, 1616–1626.

Wang, Y., Reis, C., Applegate, R., Stier, G., Martin, R., and Zhang, J.H. (2015). Ischemic conditioning-induced endogenous brain protection: Applications pre-, per- or post-stroke. Exp. Neurol. *272*, 26–40.

Winter, S.C., Buffa, F.M., Silva, P., Miller, C., Valentine, H.R., Turley, H., Shah, K.A., Cox, G.J., Corbridge, R.J., Homer, J.J., et al. (2007). Relation of a Hypoxia Metagene Derived from Head and Neck Cancer to Prognosis of Multiple Cancers. Cancer Res. *67*, 3441–3449.

Wouters, B.G., and Koritzinsky, M. (2008). Hypoxia signalling through mTOR and the unfolded protein response in cancer. Nat. Rev. Cancer *8*, 851–864.

Wu, D., and Rastinejad, F. (2017). Structural characterization of mammalian bHLH-PAS transcription factors. Curr. Opin. Struct. Biol. *43*, 1–9.

Wu, D., Potluri, N., Lu, J., Kim, Y., and Rastinejad, F. (2015). Structural integration in hypoxia-inducible factors. Nature *524*, 303.

Xie, L., Xiao, K., Whalen, E.J., Forrester, M.T., Freeman, R.S., Fong, G., Gygi, S.P., Lefkowitz, R.J., and Stamler, J.S. (2009). Oxygen-Regulated β2-Adrenergic Receptor Hydroxylation by EGLN3 and Ubiquitylation by pVHL. Sci Signal *2*, ra33-ra33.

Xu, W., Yang, H., Liu, Y., Yang, Y., Wang, P., Kim, S.-H., Ito, S., Yang, C., Wang, P., Xiao, M.-T., et al. (2011). Oncometabolite 2-Hydroxyglutarate Is a Competitive Inhibitor of α-Ketoglutarate-Dependent Dioxygenases. Cancer Cell *19*, 17–30.

Yan, Q., Bartz, S., Mao, M., Li, L., and Kaelin, W.G. (2007). The Hypoxia-Inducible Factor 2α N-Terminal and C-Terminal Transactivation Domains Cooperate To Promote Renal Tumorigenesis In Vivo. Mol. Cell. Biol. *27*, 2092–2102.

Yi, X., Liang, Y., Huerta-Sanchez, E., Jin, X., Cuo, Z.X.P., Pool, J.E., Xu, X., Jiang, H., Vinckenbosch, N., Korneliussen, T.S., et al. (2010). Sequencing of 50 Human Exomes Reveals Adaptation to High Altitude. Science *329*, 75–78.

Yoon, D., Pastore, Y.D., Divoky, V., Liu, E., Mlodnicka, A.E., Rainey, K., Ponka, P., Semenza, G.L., Schumacher, A., and Prchal, J.T. (2006). Hypoxia-inducible Factor-1 Deficiency Results in Dysregulated Erythropoiesis Signaling and Iron Homeostasis in Mouse Development. J. Biol. Chem. *281*, 25703–25711.

Young, R.M., Wang, S.-J., Gordan, J.D., Ji, X., Liebhaber, S.A., and Simon, M.C. (2008). Hypoxia-mediated Selective mRNA Translation by an Internal Ribosome Entry Site-independent Mechanism. J. Biol. Chem. *283*, 16309–16319.

Zhang, H., Gao, P., Fukuda, R., Kumar, G., Krishnamachary, B., Zeller, K.I., Dang, C.V., and Semenza, G.L. (2007). HIF-1 Inhibits Mitochondrial Biogenesis and Cellular Respiration in VHL-Deficient Renal Cell Carcinoma by Repression of C-MYC Activity. Cancer Cell *11*, 407–420.

Zhang, H., Bosch-Marce, M., Shimoda, L.A., Tan, Y.S., Baek, J.H., Wesley, J.B., Gonzalez, F.J., and Semenza, G.L. (2008). Mitochondrial Autophagy Is an HIF-1-dependent Adaptive Metabolic Response to Hypoxia. J. Biol. Chem. *283*, 10892–10903.

Zhang, X., Liu, L., Wei, X., Tan, Y.S., Tong, L., Chang, B., Ryan, Ghanamah, M.S., Reinblatt, M., Marti, G.P., Harmon, J.W., et al. (2010). Impaired angiogenesis and mobilization of circulating angiogenic cells in HIF-1α heterozygous-null mice after burn wounding. Wound Repair Regen. *18*, 193–201.

Zhang, Y., Shao, Z., Zhai, Z., Shen, C., and Powell-Coffman, J.A. (2009). The HIF-1 hypoxia-inducible factor modulates lifespan in *C. elegans*. PLoS ONE *4*, e6348.

Zhang, Z., Ren, J., Harlos, K., McKinnon, C.H., Clifton, I.J., and Schofield, C.J. (2002). Crystal structure of a clavaminate synthase–Fe(II)–2-oxoglutarate–substrate–NO complex: evidence for metal centred rearrangements. FEBS Lett. *517*, 7–12.

Zheng, X., Zhai, B., Koivunen, P., Shin, S.J., Lu, G., Liu, J., Geisen, C., Chakraborty, A.A., Moslehi, J.J., Smalley, D.M., et al. (2014). Prolyl hydroxylation by EglN2 destabilizes FOXO3a by blocking its interaction with the USP9x deubiquitinase. Genes Dev. *28*, 1429–1444.

Zhou, M.I., Wang, H., Ross, J.J., Kuzmin, I., Xu, C., and Cohen, H.T. (2002). The von Hippel-Lindau Tumor Suppressor Stabilizes Novel Plant Homeodomain Protein Jade-1. J. Biol. Chem. *277*, 39887–39898.

Zimmer, M., Doucette, D., Siddiqui, N., and Iliopoulos, O. (2004). Inhibition of Hypoxia-Inducible Factor Is Sufficient for Growth Suppression of VHL−/− Tumors1 1 NIH grant R29CA78358-06 (O. I.), Bertucci Fund for Urologic Malignancies (O. I.), David P. Foss Fund (O. I.), and VHL Family Alliance 2003 award (M. Z.). Mol. Cancer Res. *2*, 89–95.

Chapter Two

The HIF hypoxia-response pathway drives hormonal signaling to modulate *C. elegans* stress resistance and behavior

Corinne L. Pender and H. Robert Horvitz

A modified version of this chapter has been submitted for publication

Summary

The HIF (hypoxia-inducible factor) transcription factor is the master regulator of the metazoan response to chronic hypoxia. In addition to promoting adaptations to low oxygen, HIF drives cytoprotective mechanisms in response to stresses and modulates neural circuit function. How most HIF targets act in the control of the diverse aspects of HIF-regulated biology remains unknown. We discovered that a HIF target, the *C. elegans* gene *cyp-36A1*, is required for numerous HIF-dependent processes, including modulation of gene expression, stress resistance, and behavior. *cyp-36A1* encodes a cytochrome P450 enzyme that controls expression of more than a third of HIF-induced genes. CYP-36A1 acts cell non-autonomously by regulating the activity of the nuclear hormone receptor NHR-46, suggesting that CYP-36A1 functions as a biosynthetic enzyme for the hormone ligand of this receptor. We propose that cell non-autonomous regulation of HIF effectors through activation of cytochrome P450 enzyme/nuclear receptor signaling pathways could similarly occur in humans.

Introduction

The capacity to sense and respond to oxygen deprivation, or hypoxia, is crucial to normal physiological function and survival of aerobic organisms, which require oxygen to perform respiration and generate energy in the form of ATP. The fundamental importance of a mechanism to detect and react to low oxygen is reflected in the presence of a conserved hypoxia-response pathway in all animal cells. This pathway consists of the transcription factor HIF, or hypoxia-inducible factor, and its negative regulator, the prolyl hydroxylase EGLN, which together mediate a diversity of metabolic and physiological adaptations to hypoxia. The three human EGLNs, which were identified as homologs of the *C. elegans* protein EGL-9, function as oxygen sensors. In the presence of oxygen, EGLN hydroxylates the HIF α-subunit (HIFα), allowing the von Hippel-Lindau (VHL) E3 ubiquitin ligase to promote HIFα degradation (Epstein et al., 2001; Ivan et al., 2001; Jaakkola et al., 2001; Maxwell et al., 1999). In conditions of low oxygen, HIFα is stabilized and acts with its partner HIFβ to drive adaptations to hypoxia through activation of its transcriptional targets (Kaelin and Ratcliffe, 2008; Semenza, 2011; Wang et al., 1995).

The canonical function of the EGLN/HIF pathway is to regulate genes that either increase oxygen availability, e.g. by promoting erythropoiesis and angiogenesis, or reduce the cellular requirement for oxygen, e.g. by driving a shift from oxidative phosphorylation to glycolytic metabolism. However, a growing body of work has found roles for the EGLN/HIF pathway in controlling other aspects of animal physiology and behavior. HIF promotes the response to numerous stressors, including infection, proteotoxicity, and oxidative stress (Nakazawa et al., 2016; Palazon et al., 2014; Powell-Coffman, 2010; Schito and Rey, 2018). HIF activation is associated with increased lifespan in *C. elegans* (Chen et al., 2009; Lee et al., 2010; Mehta et al.,

2009; Zhang et al., 2009); this longevity phenotype likely stems from the improved stress resistance associated with HIF activity, as is typically the case for pathways regulating longevity (Leiser et al., 2015; Shore and Ruvkun, 2013). The EGLN/HIF pathway also modulates several behaviors of *C. elegans* following prolonged hypoxia exposure, suggesting a role for this pathway in tuning neural circuit function (Chang and Bargmann, 2008; Ma et al., 2012; Pocock and Hobert, 2010). The mechanisms by which HIF mediates these non-canonical physiological and behavioral changes remain poorly defined.

Here we report the discovery of an endocrine signaling pathway that regulates multiple aspects of physiology and behavior downstream of HIF in *C. elegans*. From a genetic screen for suppressors of an *egl-9(lf)* mutant behavioral defect, we identified a cytochrome P450 gene, *cyp-36A1*, that is required for modulation of egg-laying behavior by the *egl-9*/*hif-1* pathway. *cyp-36A1* is transcriptionally upregulated in hypoxia or *egl-9(lf)* mutants, in which HIF-1 is constitutively active, and appears to be a direct HIF-1 target. *cyp-36A1* controls expression of more than a third of HIF-1-upregulated genes, demonstrating that *cyp-36A1* acts broadly downstream of *hif-1* to regulate gene expression; interestingly, regulation of gene expression and behavior by *cyp-36A1* occurs cell non-autonomously. We identified the downstream effector of *cyp-36A1* as the nuclear hormone receptor *nhr-46*, indicating that the likely function of CYP-36A1 is to generate an endocrine signal that regulates NHR-46. In addition to regulating behavior and gene expression, *cyp-36A1* and *nhr-46* mediate multiple forms of stress resistance associated with HIF activation. We conclude that CYP-36A1 and NHR-46 are important downstream effectors of the EGL-9/HIF pathway and function together to regulate a wide range of HIF-mediated physiology.

Results

A screen for suppressors of the *egl-9(lf)* egg-laying defect identifies the cytochrome P450 gene *cyp-36A1*

To identify novel, functionally important HIF effectors, we analyzed the modulation of *C. elegans* egg laying, the behavior that led our laboratory to discover the first EGLN gene, *egl-9*, and the first known functional role for any member of the EGLN/HIF pathway (Trent et al., 1983). *egl-9(lf)* mutants, in which HIF-1 is constitutively active, are defective in egg laying and become bloated with eggs as adults. Although the egg-laying defect of *egl-9(lf)* mutants is well-established, the downstream effectors of EGL-9 and HIF-1 in regulating egg-laying behavior remain unknown.

We performed a mutagenesis screen to identify genes that act in response to *egl-9* to control egg laying. Specifically, we screened for second-site mutations that suppressed the egg-laying defect of *egl-9(lf)* animals (Figure S1A). Two isolates from this screen were allelic to *hif-1* (Figures S1B and S1C), consistent with a previous observation that *hif-1(lf)* suppresses the *egl-9(lf)* egg-laying defect (Bishop et al., 2004) and validating the screen as a means of identifying components of the HIF-1 pathway. A third isolate, *n5666*, was not allelic to *hif-1* and had a G106R missense mutation in the gene *cyp-36A1*, which encodes a cytochrome P450 enzyme (Figure S1B and S1D). A transgene carrying a wild-type copy of *cyp-36A1* fully rescued the suppression by *n5666* of the *egl-9(lf)* egg-laying defect, demonstrating that the mutation in *cyp-36A1* is the causative mutation and suggesting that the suppression phenotype is caused by loss of *cyp-36A1* function (Figures 1A-1E). *cyp-36A1(n5666)* single mutants did not exhibit hyperactive egg-laying behavior (Figure 1F), indicating that suppression of the *egl-9(lf)* egg-laying defect by *cyp-36A1(n5666)* is not a consequence of a nonspecific increase in egg-laying

rate. We further showed that *cyp-36A1(lf)* suppressed the previously reported egg-laying defect of hypoxia-exposed worms (Miller and Roth, 2009), demonstrating a role for CYP-36A1 under physiological conditions of HIF-1 activation (Figure S2). We then analyzed the role of *cyp-36A1* in regulating other behaviors. We observed that *egl-9(lf)* mutants have reduced locomotion and defecation rates, both of which were suppressed by *hif-1(lf)* (Figures 1G and 1H). *cyp-36A1(lf)* partially suppressed slow locomotion and defecation rates of *egl-9(lf)* mutants, showing that CYP-36A1 is a downstream effector of HIF-1 in regulating not only egg-laying but also multiple other behaviors.

Next we observed that *cyp-36A1* expression is increased in *egl-9(lf)* mutants in a *hif-1*-dependent manner (Figure 1I), consistent with results from an earlier genome-wide microarray study that identified *cyp-36A1* as one of 63 genes regulated by *hif-1* in hypoxia-exposed worms (Shen et al., 2005). ChIP-seq of HIF-1 by the modERN project showed HIF-1 binding at two sites near the *cyp-36A1* coding region, one 5' to the start of the gene and one in the first intron (Dunham et al., 2012); both of the sites contain the HIF binding motif 5'RCGTG (Kaelin and Ratcliffe, 2008). Together these data indicate that *cyp-36A1* is a downstream effector of the hypoxia-response pathway that regulates multiple behaviors and strongly suggest that *cyp-36A1* is a direct transcriptional target of HIF-1.

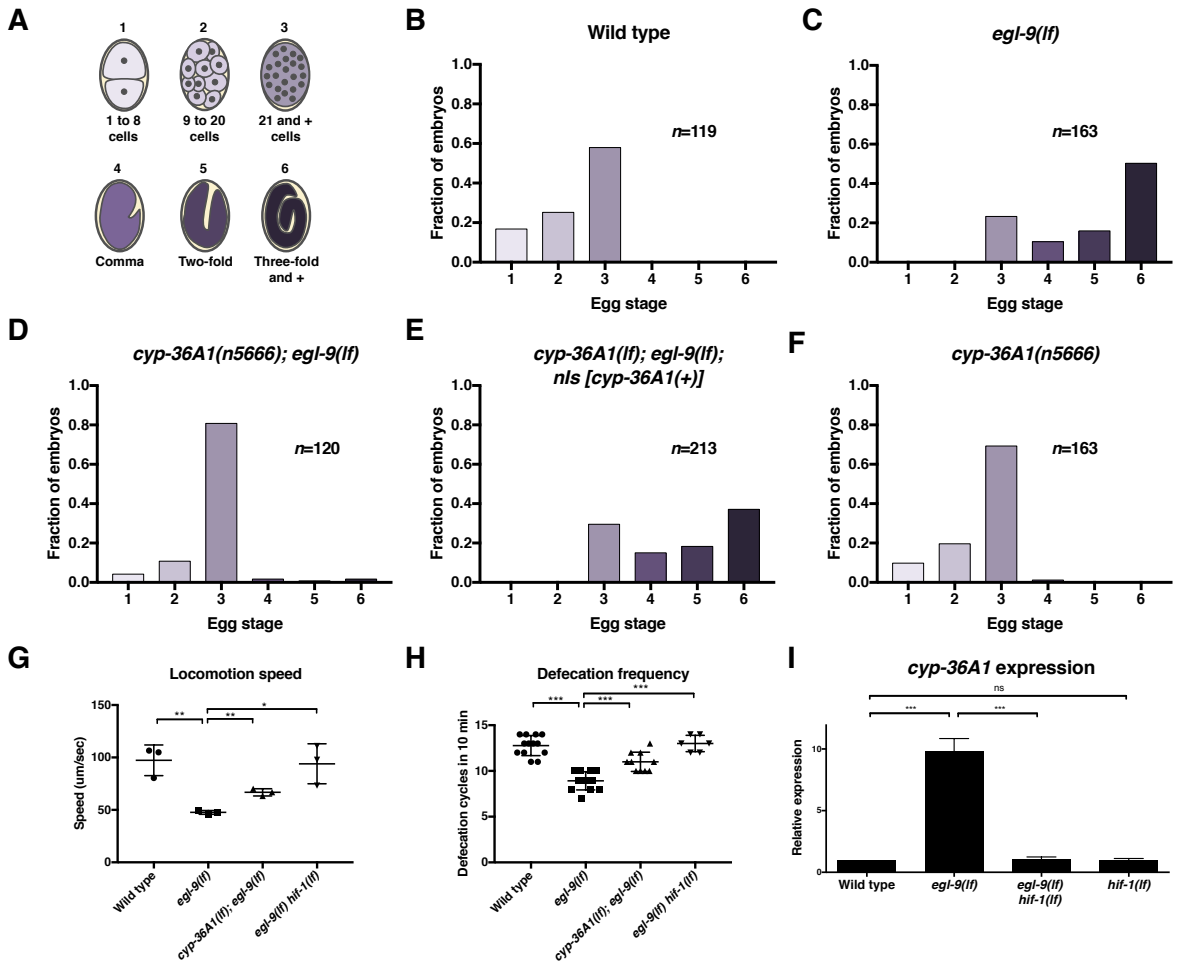

Figure 1. The cytochrome P450 gene *cyp-36A1* is an effector of the hypoxia-response pathway that regulates behavior. (A) Stages of embryonic development, adapted from Ringstad and Horvitz, 2008 and Paquin et al., 2016. (B-F) Distribution of stages of eggs newly laid by adult hermaphrodites, used as a proxy for egg retention time *in utero*, of animals the indicated genotypes. All genotypes contained the *nIs470* ($P_{cysl\text{-}2}$*::gfp*) transgene. (B) Stages of eggs laid by wild-type animals. (C) *egl-9* loss-of-function (*lf*) mutants laid later stage eggs than the wild type ($P < 0.001$, Chi-square test with Holm-Bonferroni correction). (D) *cyp-36A1(n5666)* suppressed the egg-laying defect of *egl-9(lf)* mutants ($P < 0.001$). Data from an additional *cyp-36A1(lf)* allele is shown in Figure S5C. (E) The *cyp-36A1(+)* transgene, which contains wild-type *cyp-36A1*, rescued the suppression of the egg-laying defect observed in *cyp-36A1(n5666); egl-9(lf)* mutants ($P < 0.001$). (F) *cyp-36A1(n5666)* mutants displayed wild-type egg laying ($P > 0.05$). (G) *egl-9(lf)* mutants were defective in locomotion rate, and this defect was suppressed by *hif-1(lf)* and *cyp-36A1(lf)* mutations. (H) *egl-9(lf)* mutants were defective in defecation rate, and this defect was suppressed by *hif-1(lf)* and *cyp-36A1(lf)*. Error bars for (G) and (H) denote SD of $n \geq 3$ experiments, *$P < 0.05$, **$P < 0.01$ and ***$P < 0.001$ considered significant. ns, not significant (Student's t-test with Holm-Bonferroni correction). (I) Relative

expression of *cyp-36A1* mRNA in the wild type, *egl-9(lf)*, *egl-9(lf) hif-1(lf)*, and *hif-1(lf)* mutants, measured by qRT-PCR and normalized to the expression of the large ribosomal subunit *rpl-32*. Error bars denote SD of n=3 experiments, ***P < 0.001 considered significant. ns, not significant (Student's t-test with Holm-Bonferroni correction). Alleles used for (B-F) were *cyp-36A1(n5666)*, *egl-9(n586)*, and *nIs674* (*nIs* [*cyp-36A1(+)*]). Alleles used for (G-I) were *egl-9(sa307), hif-1(ia4)*, and *cyp-36A1(gk824636)*. See also Figures S1 and S2.

CYP-36A1 regulates gene expression changes and stress resistance downstream of HIF-1

We sought to determine if CYP-36A1 regulates other HIF-1-dependent processes. CYP-36A1 is most closely related to the CYP2 family of cytochrome P450 enzymes, which function in both detoxification of xenobiotics and metabolism of endogenous molecules (Nebert et al., 2013). CYP2 family members and other CYPs can act on endogenous substrates to generate signaling molecules that regulate gene expression, such as eicosanoids and steroid hormones (Rendic and Guengerich, 2015; Dennis and Norris, 2015; Evans and Mangelsdorf, 2014). We hypothesized that CYP-36A1 might function in a transcriptional cascade to mediate aspects of HIF-1-dependent gene regulation. We performed an RNA-seq experiment comparing the wild type, *egl-9(lf)* mutants, *egl-9(lf) hif-1(lf)* double mutants, and *cyp-36A1(lf); egl-9(lf)* double mutants, and found that 36% of HIF-1-upregulated genes (i.e. genes that are upregulated in *egl-9(lf)* mutants and suppressed by *hif-1(lf)*) and 10% of HIF-1-downregulated genes were also regulated by *cyp-36A1* (Figures 2A and 2B). We focused on the HIF-1-upregulated genes, for which CYP-36A1 function appeared to be more broadly required. Gene ontology (GO) enrichment analysis of these HIF-1/CYP-36A1-upregulated genes suggested a possible role for *cyp-36A1* in regulating stress resistance downstream of *egl-9* and *hif-1* (Figure 2C). The EGL-9/HIF-1 pathway has previously been implicated in responses to numerous stressors in both nematodes and mammals, with crosstalk occurring between HIF and regulators of the immune

response, unfolded protein response, and other stress-response pathways (Palazon et al., 2014; Schito and Rey, 2018; Wouters and Koritzinsky, 2008; Nakazawa et al., 2016; Powell-Coffman, 2010). We tested whether CYP-36A1 is involved in the response to three stressors for which HIF-1 is known to mediate resistance in *C. elegans*: infection by the pathogenic bacteria *Pseudomonas aeruginosa* (Darby et al., 1999; Kirienko et al., 2013; Bellier et al., 2009), tunicamycin-induced ER stress (Leiser et al., 2015), and oxidative stress from tert-butyl hydroperoxide (Bellier et al., 2009). Animals in which HIF-1 is constitutively active because of mutation in *egl-9* or the *C. elegans* VHL homolog *vhl-1* are resistant to these stressors relative to wild-type animals: such mutants survive longer when grown on *Pseudomonas aeruginosa* strain PA14 (Bellier et al., 2009), display reduced tunicamycin-induced growth inhibition (Leiser et al., 2015), and survive exposure to tert-butyl hydroperoxide at a higher rate than the wild type (Bellier et al., 2009). We found that *cyp-36A1(lf); egl-9(lf)* double mutants are more sensitive than *egl-9(lf)* mutants to all three of these stressors (Figures 2D-2F and S6A), suggesting that CYP-36A1 mediates responses to these stressors downstream of HIF-1. Together the CYP-36A1-dependent changes in gene expression and stress resistance indicate that CYP-36A1 plays a major role in regulating HIF-1-mediated physiology.

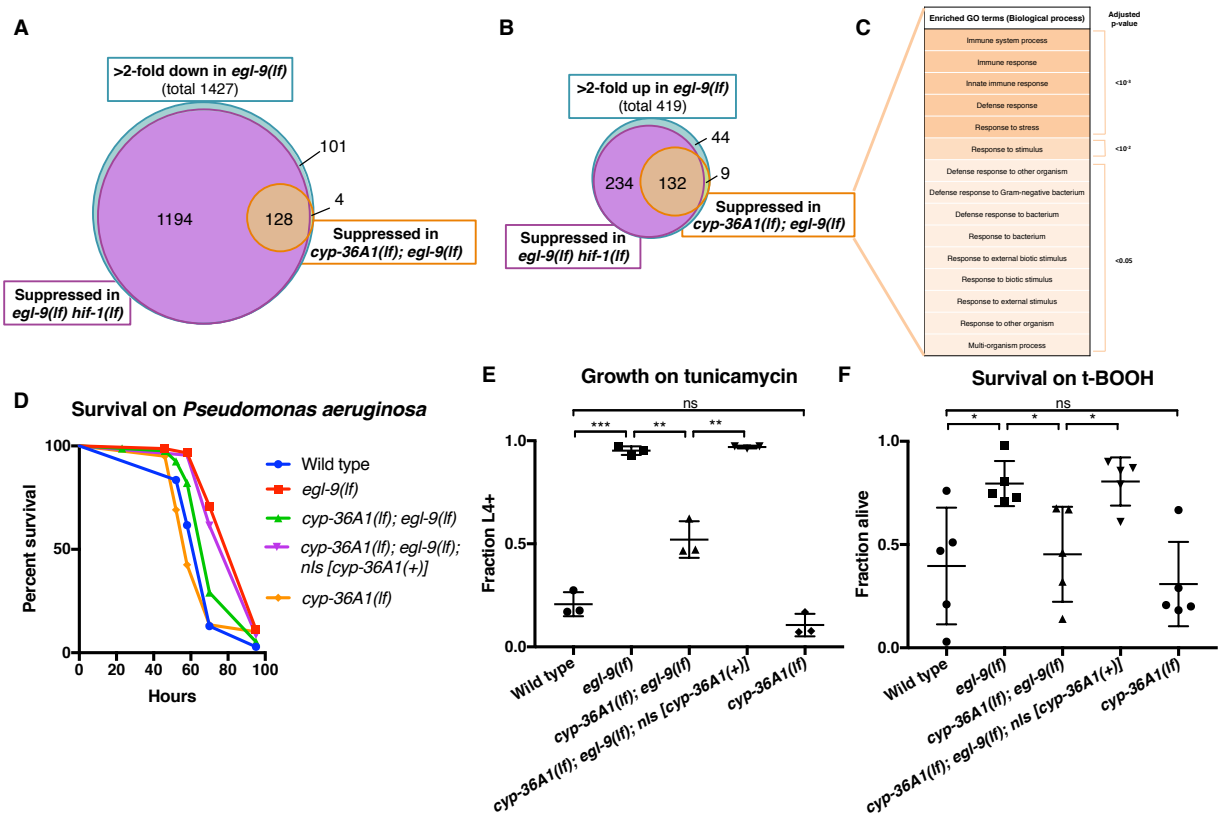

Figure 2. CYP-36A1 acts downstream of HIF-1 to regulate gene expression changes and stress responses. (A) Blue circle: Genes that were at least twofold downregulated in *egl-9(lf)* mutants. Purple and orange circles: Subset of *egl-9(lf)*-downregulated genes that were significantly upregulated in *egl-9(lf) hif-1(lf)* double mutants (purple) or *cyp-36A1(lf); egl-9(lf)* double mutants (orange) vs. *egl-9(lf)* single mutants. (B) Blue circle: Genes that were at least twofold upregulated in *egl-9(lf)* mutants. Purple and orange circles: Subset of *egl-9(lf)*-upregulated genes that were significantly downregulated in *egl-9(lf) hif-1(lf)* double mutants (purple) or *cyp-36A1(lf); egl-9(lf)* double mutants (orange) vs. *egl-9(lf)* single mutants. Significance for all comparisons in (A) and (B) was determined by the Benjamini-Hochberg procedure with a false-discovery rate of 0.05. (C) GO enrichment analysis terms for genes more than two-fold upregulated in *egl-9* mutants and significantly suppressed by *hif-1(lf)* and *cyp-36A1(lf)*. (D) Survival of animals grown from the L4 larval stage on the pathogen *Pseudomonas aeruginosa*. Wild type vs. *egl-9(lf)*, P<0.001; *egl-9(lf)* vs. *cyp-36A1(lf); egl-9(lf)*, P<0.001; *cyp-36A1(lf); egl-9(lf)* vs. *cyp-36A1(lf); egl-9(lf); cyp-36A1(+)*, P<0.001, as determined by the log-rank (Mantel-Cox) test, correcting for multiple comparisons with the Holm-Bonferroni method. *n*>60 animals per strain. (E) Survival of animals to the L4 larval stage or later after growth for three days from the L1 larval stage on plates containing 5 µg/ml tunicamycin. (F) Survival of animals exposed to tert-butyl hydroperoxide for 10 hrs as young adults. Error bars for (E) and (F) denote SD of *n*≥3 replicates. *P<0.05, **P<0.01, and ***P<0.001 considered significant. ns, not

significant (Student's t-test with Holm-Bonferroni correction). Alleles used for (A) and (B) were *egl-9(sa307), hif-1(ia4),* and *cyp-36A1(gk824636)*. Alleles used for (D-F) were *egl-9(n586)*, *cyp-36A1(n5666)*, and *nIs674* (*nIs* [*cyp-36A1(+)*]). See also Figure S6A.

CYP-36A1 functions cell non-autonomously to regulate gene expression

We next sought to identify the site of action of CYP-36A1. We hypothesized that CYP-36A1 might function cell non-autonomously, as is the case for other cytochrome P450 enzymes that generate signaling molecules (Nebert et al., 2013; Evans and Mangelsdorf, 2014; Gerisch and Antebi, 2004). We observed *cyp-36A1* expression in many tissues, including neurons, intestine, hypoderm, and muscle (Figure S3). To test the hypothesis of cell non-autonomous CYP-36A1 function, we focused on a *cyp-36A1*-mediated abnormality of *egl-9(lf)* mutants for which the site of dysfunction is well defined. Specifically, we examined expression of a GFP transcriptional reporter for the gene *T24B8.5* (Shivers et al., 2009), which is expressed in only the intestine and is upregulated in *egl-9(lf)* mutants in a *cyp-36A1*-dependent manner, based on our RNA-seq data. Interestingly, *T24B8.5* expression is also upregulated in response to infection, ER stress, and oxidative stress (Shivers et al., 2009; Lim et al., 2014; Park et al., 2009). Expression of the reporter recapitulated the *T24B8.5* expression changes observed by RNA-seq: increased expression of GFP was observed in *egl-9(lf)* mutants, which was suppressed by a second mutation in either *hif-1* or *cyp-36A1* (Figures 3A and 3B). To determine the site of action of *cyp-36A1* for regulation of intestinal *T24B8.5* expression, we expressed wild-type *cyp-36A1* cDNA using tissue-specific promoters. We found that the low $P_{T24B8.5}$*::gfp* expression of *cyp-36A1(lf); egl-9(lf)* double mutants was rescued by expressing *cyp-36A1(+)* either cell autonomously in the intestine or cell non-autonomously in neurons, hypoderm or body-wall muscle (Figure 3C). *cyp-36A1(+)* expression in all four tissues also rescued the suppression of

the egg-laying defect of *cyp-36A1(lf); egl-9(lf)* mutants (Figure S4). Next we found that expressing a nondegradable constitutively active HIF-1 mutant (P621A) transgene (Pocock and Hobert, 2008) in any of the same four tissues also promoted intestinal expression of the GFP reporter and that this HIF-1-mediated increase in expression required *cyp-36A1* (Figure 3D). Thus, CYP-36A1 functions downstream of HIF-1 to cell non-autonomously regulate gene expression.

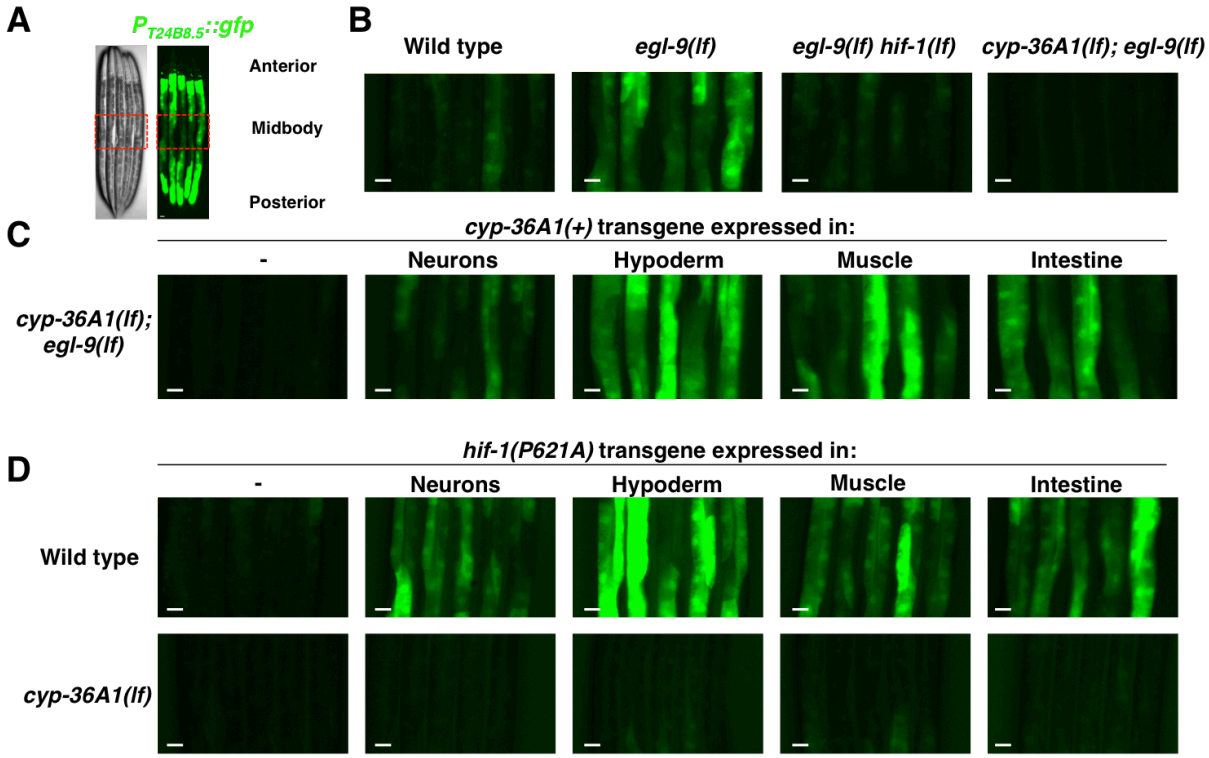

Figure 3. HIF-1 and CYP-36A1 cell non-autonomously regulate expression of a stress-responsive gene. (A) Transmission light (left) and epifluorescence (right) images showing intestinal expression of the $P_{T24B8.5}$*::gfp* reporter (from *egl-9(lf)* in panel B). Region pictured in subsequent images outlined by red box; differences among strains were most prominent in midbody. (B) $P_{T24B8.5}$*::gfp* expression of the indicated genotypes. (C) Expression of *cyp-36A1(+)* specifically in neurons, hypoderm, muscle, or intestine of *cyp-36A1(lf); egl-9(lf)* animals increased expression of $P_{T24B8.5}$*::gfp* in intestine (*n*=5 animals per image). (D) Expression of *hif-1(P621A)*, which encodes a stable variant of HIF-1 (Pocock and Hobert, 2008), specifically in neurons, hypoderm, muscle, or intestine increased expression of $P_{T24B8.5}$*::gfp* in intestine; increased expression was suppressed by *cyp-36A1(lf)* (*n*=5 animals per image). Alleles used were

egl-9(sa307), hif-1(ia4), and *cyp-36A1(gk824636).* All strains contained *agIs219* ($P_{T24B8.5}$*::gfp*). Scale bars, 20 um. See also Figures S3 and S4.

A screen for suppressors of *cyp-36A1(lf)* identifies the nuclear receptor gene *nhr-46*

We performed a mutagenesis screen to identify CYP-36A1 effectors that mediate egg-laying behavior, stress responses, and non-autonomous regulation of gene expression. We screened for mutations that suppressed both the low $P_{T24B8.5}$*::gfp* expression and normal egg laying of *cyp-36A1(lf); egl-9(lf)* double mutants, looking for triple mutants that, like *egl-9(lf)* single mutants, had high GFP expression and were egg-laying defective. By screening for suppressors of the two abnormalities simultaneously, we were able to focus on effectors of CYP-36A1 rather than finding mutations that affect only egg laying or only expression of *T24B8.5* independently of the EGL-9/HIF-1/CYP-36A1 pathway. From this screen we identified two putative loss-of-function alleles of the nuclear receptor gene *nhr-46* (Figures 4A-4C), both of which caused an egg-laying defect and high expression of the $P_{T24B8.5}$*::GFP* reporter. We tested whether *nhr-46* also functions in regulating stress responses downstream of *cyp-36A1* and found that *cyp-36A1(lf); nhr-46(lf); egl-9(lf)* triple mutants were more resistant to *Pseudomonas* infection, ER stress, and oxidative stress than *cyp-36A1(lf); egl-9(lf)* double mutants (Figures 4D-4F and S6B). Thus, NHR-46 is a downstream effector of CYP-36A1 in regulation of stress resistance as well as of behavior and gene expression.

Because cytochrome P450 enzyme-generated nuclear receptor ligands are typically steroid hormones, we hypothesized that CYP-36A1 might generate a steroid hormone that acts on NHR-46. To test this hypothesis, we grew animals on medium without cholesterol, the precursor for all steroid hormones; because worms are cholesterol auxotrophs, removing cholesterol from their growth medium eliminates the necessary precursor for steroid hormone

synthesis. Intriguingly, we found that growing *egl-9(lf)* mutants on cholesterol-free medium phenocopied *cyp-36A1(lf)* mutation: whereas egg laying of wild-type animals was unaffected by cholesterol deprivation, growing *egl-9(lf)* mutants off of cholesterol suppressed their egg-laying defect (Figure S5). We thus hypothesize that a cholesterol derivative could be the substrate for CYP-36A1, and that the molecular function of CYP-36A1 is to generate a steroid hormone.

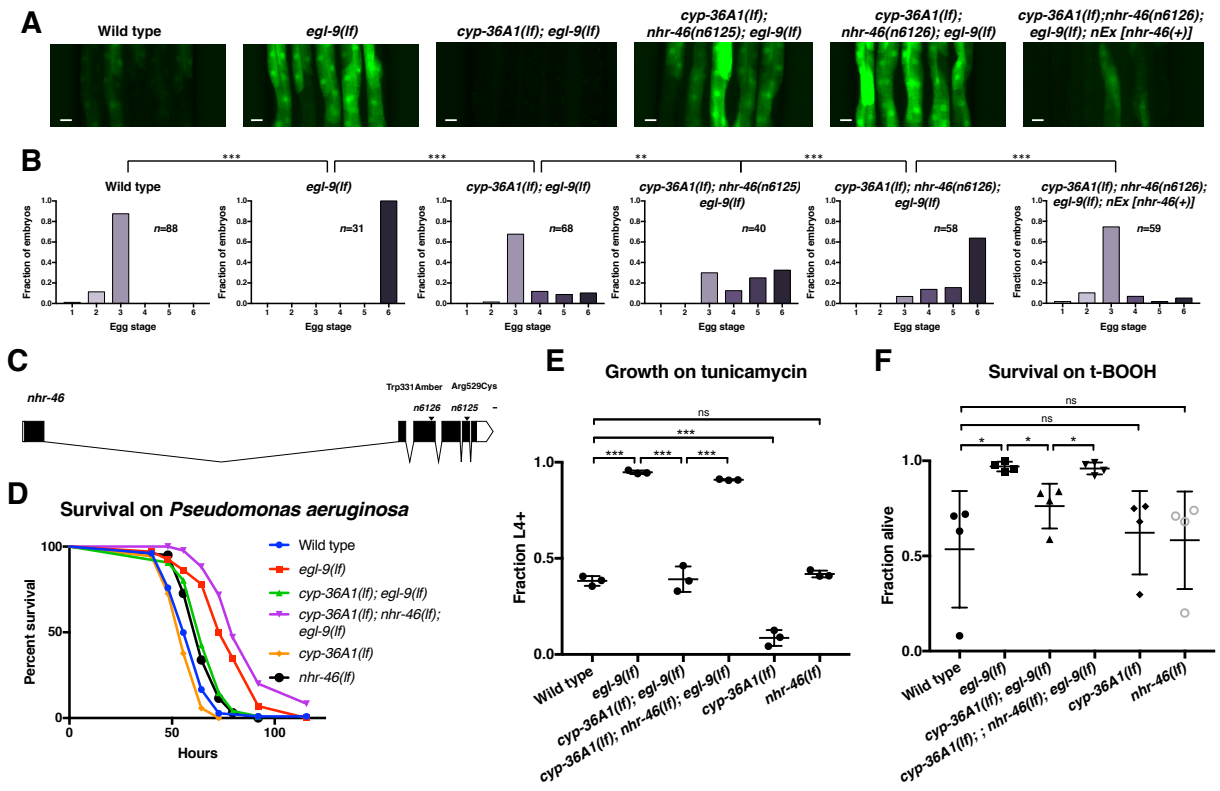

Figure 4. The nuclear hormone receptor NHR-46 acts downstream of CYP-36A1. (A) $P_{T24B8.5}$*::gfp* fluorescence of the indicated genotypes. Scale bars, 20 um. (B) Distribution of stages of eggs newly laid by adult hermaphrodites of the indicated genotypes. **P<0.01 and ***P<0.001 considered significant, Chi-square test with Holm-Bonferroni correction. (C) *nhr-46* gene diagram; isoform *C45E5.6b* is shown. (D) Survival of animals grown from the L4 larval stage on the pathogen *Pseudomonas aeruginosa*. Wild type vs. *egl-9(lf)*, P<0.001; *egl-9(lf)* vs. *cyp-36A1(lf); egl-9(lf)*, P<0.001; *cyp-36A1(lf); egl-9(lf)* vs. *cyp-36A1(lf); nhr-46(lf); egl-9(lf)*, P<0.001, as determined by the log-rank (Mantel-Cox) test, correcting for multiple comparisons with the Holm-Bonferroni method. *n*>65 animals per strain. *egl-9(lf)* allele was *egl-9(n586)*. (E) Survival of animals to the L4 larval stage or later after growth for three days from the L1 larval

stage on plates containing 5 μg/ml tunicamycin. (F) Survival of animals exposed to tert-butyl hydroperoxide for 10 hrs as young adults. Error bars for (E) and (F) denote SD of $n \geq 3$ replicates. *P<0.05, **P<0.01, and ***P<0.001 considered significant. ns, not significant (Student's t-test with Holm-Bonferroni correction). Alleles used for (A-F) were *egl-9(sa307), cyp-36A1(gk824636)*, *nhr-46(n6126)*, and *nEx2586* (*nEx [nhr-46(+)*) except where otherwise noted. All strains in (A), (B), (E), and (F) contained *agIs219* ($P_{T24B8.5}$*::gfp*). See also Figure S6B.

nhr-46 functions tissue-specifically to regulate gene expression and behavior

nhr-46 is expressed in many tissues, including neurons, hypoderm, muscle, intestine, and the spermatheca (Feng et al., 2012). Tissue-specific expression of *nhr-46* in the intestine, but not in neurons or muscle, rescued the high GFP expression caused by *nhr-46(lf)*, indicating that *nhr-46*, unlike *cyp-36A1*, acts cell autonomously in the intestine to control intestinal expression of *T24B8.5* (Figure 5A). *nhr-46* expression in neurons fully rescued the egg-laying defect of *cyp-36A1(lf); nhr-46(lf); egl-9(lf)* triple mutants (Figure 5B), demonstrating that *nhr-46* function in neurons is sufficient to regulate egg-laying behavior. *nhr-46* expression in intestine also partially rescued the egg-laying defect of *cyp-36A1(lf); nhr-46(lf); egl-9(lf)* triple mutants. In combination with the tissue-specific CYP-36A1 experiments described above, these results suggest that a CYP-36A1-generated cell non-autonomous signal from any tissue can act on NHR-46 in the intestine to drive intestinal *T24B8.5* expression and in either the nervous system or the intestine to regulate egg-laying behavior.

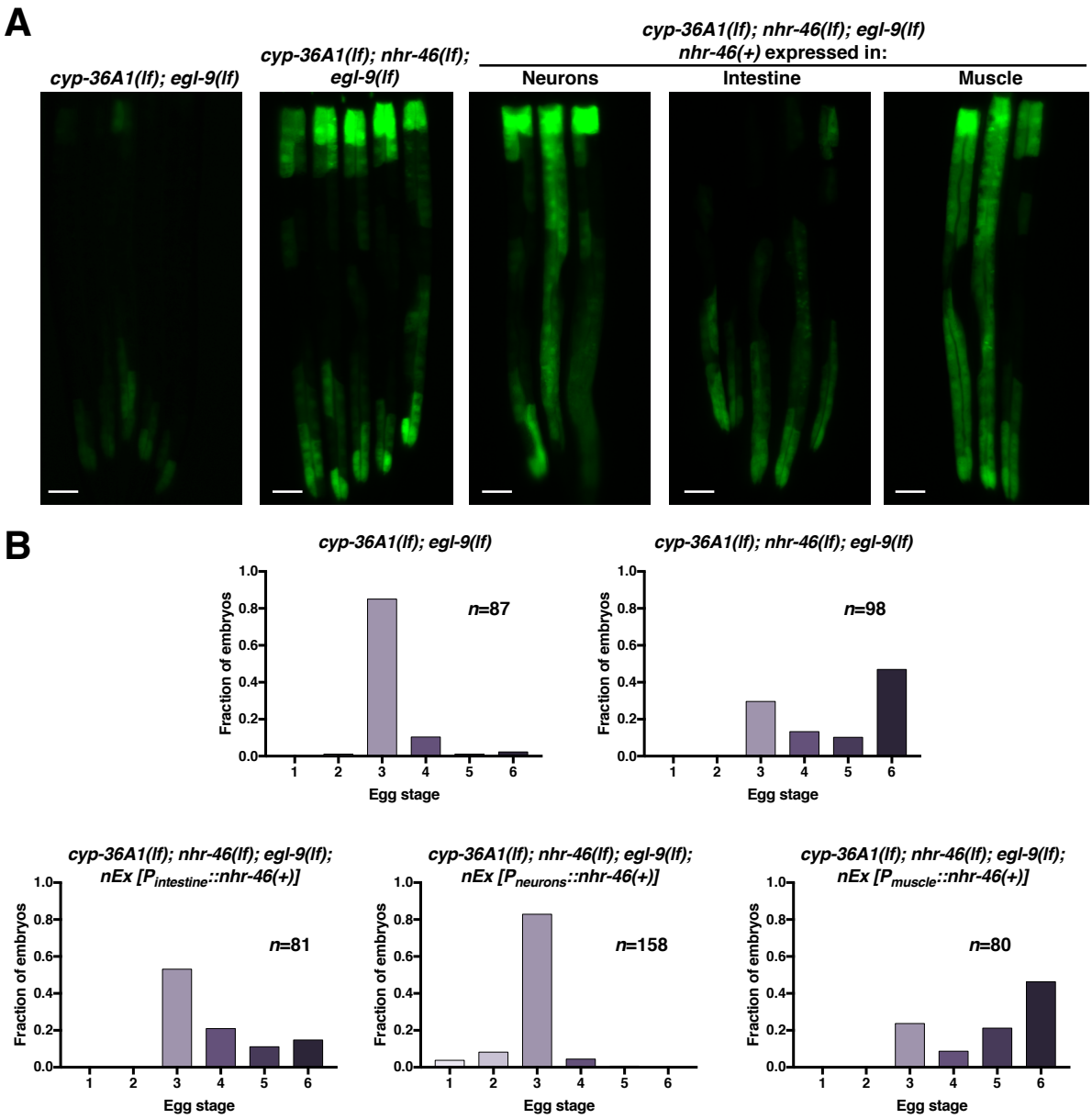

Figure 5. ***nhr-46*** **acts in different tissues to regulate** ***T24B8.5*** **expression and egg laying.** (A) Expression of *nhr-46(+)* in the intestine but not in neurons or muscle rescued the high $P_{T24B8.5}$*::gfp* expression in the intestine of *cyp-36A1(lf); nhr-46(lf); egl-9(lf)* mutants. GFP fluorescence micrographs of worms lined up side-by-side are shown; from left to right, *n*=5, 5, 3, 5, and 3 worms. Scale bar, 20 μm. (B) Distribution of stages of eggs laid by adult hermaphrodites. Expression of *nhr-46(+)* in the intestine partially rescued the egg-laying defect of *cyp-36A1(lf); nhr-46(lf); egl-9(lf)* mutants (P<0.001, Chi-square test with Holm-Bonferroni correction); neuronal *nhr-46(+)* expression fully rescued the egg-laying defect (P<0.001). Expression of *nhr-46(+)* in muscle did not rescue the egg-laying defect of *cyp-36A1(lf); nhr-46(lf); egl-9(lf)* mutants (P>0.05).

Discussion

These studies define a novel molecular genetic pathway that mediates cell non-autonomous regulation of gene expression by the HIF-1 transcription factor. Our genetic analysis indicates that *hif-1* activates the cytochrome P450 *cyp-36A1*, which in turn inhibits the nuclear receptor *nhr-46* (Figure 6A). We speculate that the molecular function of CYP-36A1 is to synthesize a steroid hormone that binds and regulates NHR-46, similar to other cytochrome P450 enzymes that function upstream of nuclear receptors (Evans and Mangelsdorf, 2014) and consistent with our observed cell non-autonomous function of CYP-36A1. We propose the following model (Figure 6B): In wild-type animals, EGL-9 inhibits HIF-1 activity, such that the HIF-1 target *cyp-36A1* is not transcribed. The unliganded NHR-46 represses expression of genes that promote stress resistance and inhibit egg laying. In *egl-9(lf)* mutants, as in hypoxia-exposed worms, HIF-1 is stabilized and drives increased *cyp-36A1* expression. A CYP-36A1-generated hormone then binds NHR-46 and antagonizes the repressive function of NHR-46, accounting for the observed negative regulatory relationship between *cyp-36A1* and *nhr-46*. Ligand-bound NHR-46 is likely activated to promote the expression of target genes, by analogy to a well-established mechanism of nuclear receptor regulation in which ligand binding mediates a switch from repressive to activating nuclear receptor function (Evans and Mangelsdorf, 2014).

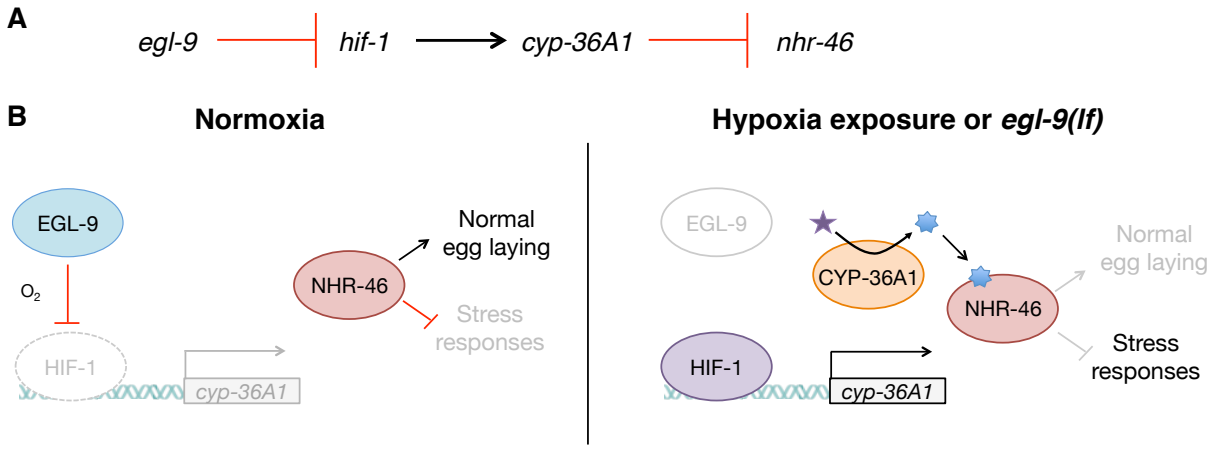

Figure 6. Model for the regulation of physiology and behavior by NHR-46 and CYP-36A1
(A) The genetic pathway in which *egl-9* inhibits *hif-1*, which activates *cyp-36A1*, which in turn inhibits *nhr-46*. (B) Model for how CYP-36A1 and NHR-46 function downstream of HIF-1. We suggest that CYP-36A1, which is transcriptionally upregulated by HIF-1, generates a hormone that binds NHR-46, thereby promoting transcriptional and physiological changes. See text for details.

Cell non-autonomous regulation of stress resistance by HIF involves multiple pathways

Numerous studies have reported that *egl-9(lf)*, *vhl-1(lf)*, and *hif-1(gf)* mutants, all of which have constitutively active HIF, show increased lifespan and enhanced stress resistance relative to wild-type animals (Darby et al., 1999; Kirienko et al., 2013; Bellier et al., 2009; Mehta et al., 2009; Zhang et al., 2009; Chen et al., 2009; Lee et al., 2010). However, despite substantial interest in the role of this pathway in stress biology, few relevant HIF effectors have been identified. Interestingly, a recent study reported that HIF-dependent serotonin signaling from the nervous system cell non-autonomously drives expression of a xenobiotic detoxification enzyme in the intestine, resulting in increased stress resistance and consequent extension of lifespan (Leiser et al., 2015). Here we report that a different signal, likely a steroid hormone, acts cell non-autonomously downstream of HIF to regulate gene expression and stress resistance.

Consistent with the findings of Leiser et al. (2015), our RNA-seq data showed that in *egl-9(lf)* mutants there is a strong induction of *fmo-2* expression and that this induction is suppressed by *hif-1* mutation, i.e. HIF-1 upregulates *fmo-2* expression. Notably, this HIF-dependent expression of *fmo-2* does not require *cyp-36A1*: the high *fmo-2* expression of *egl-9(lf)* mutants is not suppressed by *cyp-36A1(lf)*. We therefore suggest that serotonin-mediated *fmo-2* expression and *cyp-36A1/nhr-46*-mediated gene expression are parallel pathways downstream of HIF that regulate stress resistance. Recent work by others has highlighted the importance of coordinated regulation of stress response pathways, including the heat shock response, unfolded protein response, and mitochondrial unfolded protein response, by cell non-autonomous mechanisms (Taylor et al., 2014); our work and that of Leiser et al. show that the hypoxia-response pathway is also an important player in the cell non-autonomous control of stress resistance.

Human cytochrome P450 enzymes might act as mediators of HIF-dependent gene expression

Regulation of many HIF effectors in humans presumably occurs indirectly through transcriptional cascades, as suggested by the observation that most HIF-regulated genes in humans do not have clear HIF binding sites in their promoters (Mole et al., 2009; Schodel et al., 2011). We speculate that some human CYPs might serve as mediators of HIF-dependent gene expression changes by regulating nuclear receptor activity. In support of this hypothesis, previous studies have identified several human cytochrome P450 enzymes that are putative direct HIF targets based on whole-genome ChIP-chip and ChIP-seq analysis (Mole et al., 2009;Schodel et al., 2011). We note that the humoral nature of a CYP-generated molecule would make it a candidate mediator of non-autonomous regulation of hypoxia response by the EGLN/HIF

pathway, such as is observed in remote ischemic preconditioning (Cai et al., 2013; Olenchock et al., 2016).

Cytochrome P450 enzymes are major players in the hypoxia-response pathway

We previously identified another cytochrome P450 gene, *cyp-13A12*, as acting downstream of *egl-9* in a locomotory behavior (Ma et al., 2013). In contrast to CYP-36A1, which is upregulated by HIF-1, CYP-13A12 is downregulated upon hypoxia exposure or in *egl-9(lf)* mutants. The downstream effectors of CYP-36A1 and CYP-13A12 are also distinct, as we show here that CYP-36A1 regulates a nuclear receptor that controls transcription, whereas CYP-13A12 generates eicosanoids that act on a seconds-to-minutes timescale unlikely to require gene expression changes. Thus, different cytochrome P450 enzymes can act broadly, through multiple mechanisms, downstream of the EGL-9/HIF-1 hypoxia-response pathway in *C. elegans.* We propose that cytochrome P450 enzymes might similarly be important HIF effectors in mammals. Polymorphisms in numerous human cytochrome P450 genes have been associated with cardiovascular disease (Elbekai and El-Kadi, 2006; Rowland and Mangoni, 2014), for which HIF plays a protective role (Semenza, 2012), and with cancers (Agundez, 2004), for which HIF contributes to pathogenesis (Semenza, 2012). Furthermore, a study of genetic adaptations in the human genome to the environmentally hypoxic Tibetan plateau identified well-established members of the HIF pathway and, intriguingly, also noted positive selection at two cytochrome P450 loci (Simonson et al., 2010). Together these observations suggest that the cytochrome P450 family of enzymes is important in a wide range of hypoxia-associated contexts in humans. We suggest the presence of a mechanistic link between the canonical HIF pathway and the function

of cytochrome P450 enzymes in humans and posit that an understanding of how these highly druggable enzymes (Schuster and Bernhardt, 2007) control processes downstream of HIF might reveal new therapeutic avenues for treating a broad array of disorders.

Methods

C. elegans strains and transgenes

All *C. elegans* strains were cultured as described previously (Brenner, 1974). We used the N2 Bristol strain as the reference wild-type strain, and the polymorphic Hawaiian strain CB4856 (Davis et al., 2005) for genetic mapping and SNP analysis. We used the following mutations and transgenes:

LGI: *cyp-36A1(n5666, gk824636)*

LGIII: *agIs219[$P_{T24B8.5}$::gfp::unc-54 3'UTR, P_{ttx-3}::gfp::unc-54 3'UTR]*

LGIV: *nhr-46(n6125, n6126), nIs470[P_{cysl-2}::gfp, P_{myo-2}::mCherry]*, *him-8(e1489)*

LGV: *egl-9(n586, sa307)*, *hif-1(ia4)*

LGX: *nIs682[$P_{cyp-36A1}$::gfp::unc-54 3'UTR, P_{myo-3}::mCherry::unc-54 3'UTR]*

Unknown linkage: *nIs674[$P_{cyp-36A1}$::cyp-36A1(+) gDNA::cyp-36A1 3'UTR, P_{myo-3}::mCherry::unc-54 3'UTR]*

Extrachromosomal arrays: *otEx3156[P_{dpy-7}::hif-1(P621A), ttx-3::rfp]*, *otEx3165[$P_{unc-120}$::hif-1(P621A), ttx-3::rfp]*, *nEx2699[P_{rab-3}::hif-1(P621A)::F2A::mCherry::tbb-2 3'UTR, P_{ttx-3}::mCherry]*, *nEx2700[P_{ges-1}::hif-1(P621A)::F2A::mCherry::tbb-2 3'UTR, P_{ttx-3}::mCherry]*, *nEx2704 [P_{ges-1}::cyp-36A1 cDNA::unc-54 3'UTR, P_{myo-3}::mCherry::unc-54 3'UTR], nEx2594[P_{dpy-7}::cyp-36A1 cDNA::unc-54 3'UTR, P_{myo-3}::mCherry::unc-54 3'UTR], nEx2731 [P_{myo-3}::cyp-36A1 cDNA::unc-54 3'UTR, P_{myo-3}::mCherry::unc-54 3'UTR], nEx2732 [P_{rab-3}::cyp-36A1 cDNA::unc-54 3'UTR, P_{myo-3}::mCherry::unc-54 3'UTR], nEx2586[P_{nhr-46}::nhr-46(+) gDNA::nhr-46 3'UTR, P_{myo-3}::mCherry::unc-54 3'UTR], nEx2715[P_{unc-54}::nhr-46*

cDNA::F2A::mCherry::tbb-2 3'UTR], *nEx2713 [P_{rab-3}::nhr-46 cDNA::F2A::mCherry::tbb-2 3'UTR]*, *nEx2730 [P_{ges-1}::nhr-46 cDNA::F2A::mCherry::tbb-2 3'UTR]*

Note on allele usage: For *egl-9*, the weaker *n586* allele was used for the screen and in the initial phenotypic characterization of screen mutants (Figures 1B-1F and Figures 2D-2F). The stronger *sa307* allele was used for all other experiments, except for in the slow killing assay, for which the *sa307* allele is less protective than weaker alleles, as previously reported (Bellier et al., 2009). For *cyp-36A1*, the allele identified from the screen, *n5666*, was used in the initial phenotypic characterization (Figures 1D-1F, and 2D-2F); the putative null allele *gk824636* was used for all other experiments. Alleles for other genes were used as indicated in the figure legends.

Molecular biology and transgenic strain construction

The *$P_{cyp-36A1}$::gfp::unc-54 3'UTR* construct (transgene *nIs682)* was generated by using PCR fusion (Oliver Hobert, 2002) to fuse a PCR product containing the *cyp-36A1* promoter fragment (4.4 kb of upstream sequence) to a PCR product containing *gfp::unc-54 3'UTR.* The *cyp-36A1* rescuing construct (transgene *nIs674*) was generated by amplifying a PCR product from gDNA containing 4.4 kb upstream, the *cyp-36A1* locus, and 1.6 kb downstream. The *nhr-46* rescuing construct (transgene *nEx2586*) was generated by amplifying a PCR product from gDNA containing 1.9 kb upstream, the *nhr-46* locus, and 0.9 kb downstream. All remaining constructs were generated using the Infusion cloning technique (Clontech). The *dpy-7* (hypoderm), *ges-1* (intestine), *myo-3* (muscle), *rab-3* (neurons) and *unc-54* (muscle) promoter fragments contain 1.3, 2.9, 2.6, 1.4, and 1.9 kb, respectively, of sequence upstream of the start codons of each of

these genes. *C45E5.6b* was used for *nhr-46* cDNA. *F38A6.3a* with a P621A stabilizing mutation was used for *hif-1* cDNA (Pocock and Hobert, 2008). Where present, the F2A sequence served as a ribosomal skip sequence to cause separation of the two peptides encoded before and after the F2A (Ahier and Jarriault, 2014). Transgenic strains were generated by germline transformation as described (Mello et al., 1991). All transgenic constructs were injected at 2.5 – 50 ng/µl.

Mutagenesis screen for suppressors of *egl-9*

To screen for suppressors of the *egl-9* egg-laying defect, we mutagenized *egl-9(n586)* mutants with ethyl methanesulfonate (EMS) as described previously (Brenner, 1974). The starting strain contained the $P_{cysl\text{-}2}$*::gfp (nIs470)* transgene, which is highly expressed in *egl-9(lf)* mutants and served as a reporter for HIF-1 activity (Ma et al., 2012). We used a dissecting microscope to screen the F2 progeny for suppression of the egg-laying defect (i.e. the Egl phenotype), picking (1) adults that appeared less Egl than *egl-9(n586)* mutants, and (2) eggs laid by the F2 animals that were at an earlier developmental stage than those laid by *egl-9(n586)* mutants. Screen isolates were backcrossed to determine dominant vs. recessive and single-gene inheritance pattern and crossed to *him-8(e1489); egl-9(sa307) hif-1(ia4)* to test complementation with *hif-1(lf)*. The screen allele *n5666*, which conferred a recessive phenotype and was not allelic to *hif-1*, mapped between SNPs *pkP1052* and *rs3139013* on LGI with SNP mapping (Davis et al., 2005) using a strain containing *egl-9(n586)* introgressed into the Hawaiian strain CB4856 (Ma et al., 2013). Whole-genome sequencing identified a mutation in *cyp-36A1* in the *n5666* interval, and transgenic rescue demonstrated that this *cyp-36A1* mutation is the causative mutation, as described in the text.

Mutagenesis screen for suppressors of *cyp-36A1*

To screen for downstream effectors of *cyp-36A1*, we mutagenized *cyp-36A1(gk824636); egl-9(sa307)* with ethyl methanesulfonate (EMS). The starting strain contained the $P_{T24B8.5}$*::gfp (agIs219)* transgene, which has low expression in *cyp-36A1(gk824636); egl-9(sa307)* mutants and served as a reporter for CYP-36A1 activity. We used a dissecting microscope equipped to examine GFP fluorescence to screen for F2 progeny with high GFP fluorescence and an Egl appearance. The only two isolates failed to complement and were found to be alleles of *nhr-46* by whole-genome sequencing and transgenic rescue. The mutant phenotypes of *cyp-36A1(lf); n6126; egl-9(lf)* were rescued by an *nhr-46(+)* transgene, demonstrating that the mutation in *nhr-46* is the causative mutation and suggesting that *n6126* is a loss-of-function allele.

Behavioral assays

To quantify egg-laying behavior, we scored the developmental stages of eggs laid by young adult hermaphrodites as described previously (Ringstad and Horvitz, 2008). Egg-laying defective mutants retain eggs longer in the uterus, thus laying them at later developmental stages. To examine egg-laying behavior after exposure to hypoxia, young adult animals were placed in a hypoxia chamber (Coy Laboratory) at 1% O_2 balanced by N_2 for 24 hrs after which the egg-laying assay was performed in normoxia. Locomotion assays were performed on bacterial food and quantified using a custom worm tracker, as described previously (Paquin et al., 2016). Defecation assays were performed as described previously (Thomas, 1990), counting the number of defecation cycles in ten minutes.

Pseudomonas aeruginosa killing assay

Sensitivity to the *Pseudomonas aeruginosa* strain PA14 was assayed using the big lawn killing assay as described previously (Reddy et al., 2009). The big lawn killing assay was used to remove any influence of avoidance behavior on survival, as wild-type PA14 avoidance is dependent on normal aerotaxis behavior (Reddy et al., 2009), and *egl-9(lf)* mutants have previously been shown to display abnormal aerotaxis (Chang and Bargmann, 2008).

Tunicamycin survival assay

Sensitivity to tunicamycin was assayed by placing at least 100 starvation-synchronized L1 animals on NGM plates containing 5 μg/ml tunicamycin (Sigma), made using 10 mg/ml tunicamycin stock in DMSO and seeded with *E. coli* OP50 bacteria. Survival to the L4 larval stage or later was determined after three days.

t-BOOH survival assay

Sensitivity to tert-butyl hydroperoxide (t-BOOH) was assayed by placing ~60 young adult worms on NGM plates containing 7.5 mM t-BOOH, made using 70% t-BOOH solution (Sigma) and seeded with *E. coli* OP50 bacteria. Survival was evaluated after 10 hrs.

Microscopy

Epifluorescence images of $P_{T4B8.5}$*::gfp* expression were obtained using a SteREO Discovery V.8 stereomicroscope (Zeiss) and ZEN software (Zeiss). Confocal images of *Pcyp-36A1::gfp* expression were obtained using an LSM 800 instrument (Zeiss) and ZEN software.

RNA isolation for qRT-PCR and RNA-seq

Very young adults were picked into M9 buffer and allowed to settle. Excess M9 was aspirated, and the pellet was frozen in liquid nitrogen. RLT buffer (QIAGEN) was added to the pellet, and worms were lysed using a BeadBug microtube homogenizer (Sigma) and 0.5 mm zirconium beads (Sigma). RNA was extracted using the RNeasy Mini kit (QIAGEN) according to the manufacturer's instructions.

***cyp-36A1* mRNA expression analysis by qRT-PCR**

Reverse transcription was performed using SuperScript III (Invitrogen). Quantitative PCR was performed using Applied Biosystems Real-Time PCR Instruments. Expression levels were normalized to the expression of the ribosomal subunit gene *rpl-32*.

Primers for qRT-PCR

cyp-36A1 F: ACCAGCTTGTCCAACACCAA

cyp-36A1 R: CACGCTTTGGCTCCCATTTC

rpl-32 F: GGCTACACGACGGTATCTGT

rpl-32 R: CAAGGTCGTCAAGAAGAAGC

RNA-seq library preparation

RNA integrity and concentration were checked on a Fragment Analyzer (Advanced Analytical). The mRNA was purified by polyA-tail enrichment, fragmented, and reverse transcribed into cDNA (Illumina TruSeq). cDNA samples were then end-repaired and adaptor-ligated using the SPRI-works Fragment Library System I (Beckman Coulter Genomics) and indexed during

amplification. Libraries were quantified using the Fragment Analyzer (Advanced Analytical) and qPCR before being loaded for single-end sequencing using the Illumina HiSeq 2000.

RNA-seq data analysis

Reads were aligned against the *C. elegans* ce10 genome assembly using bwa 0.7.5a (Li and Durbin, 2009) and samtools/0.1.19 (Li et al., 2009) (bwa aln/ bwa samse), and mapping rates, fraction of multiply-mapping reads, number of unique 20-mers at the 5' end of the reads, insert size distributions and fraction of ribosomal RNAs were calculated using dedicated perl scripts and bedtools v. 2.17.0 (Quinlan and Hall, 2010). For expression analysis, reads were aligned against the *C. elegans* ce10 genome / ENSEMBL 65 annotation using RSEM 1.2.15 (Li and Dewey, 2011) and bowtie 1.0.1 (Langmead et al., 2009), with the following parameters: -p 6 --bowtie-chunkmbs 1024 --output-genome-bam. Raw expected read counts were retrieved and used for differential expression analysis with Bioconductor's edgeR package in the R 3.2.3 statistical environment (Robinson et al., 2010). First, common, trended, and gene-specific read dispersion across sequencing libraries and genes was estimated using the estimateDisp function. Given the small number of replicates, a gene-wise negative binomial generalized linear model (GLM) with quasi-likelihood tests (as implemented in the glmQLFit function) was used to test for differential expression between conditions (Lun et al., 2016). Briefly, this statistical framework works by first fitting the observed and expected distributions of read counts for each gene across conditions using a GLM, which is based on the negative binomial distribution and the observed read dispersion. The significance of biases in read counts is then tested using the quasi-likelihood F-test (implemented in glmQLFTest). This test provides more robust and reliable error rate control at low number of replicates, because it reflects the uncertainty in read

distribution better than the likelihood ratio test. Models were fitted across all conditions and relevant differential expression testing was performed using glmQLFTest between pairs of conditions of interest. P-values were adjusted for multiple comparisons using the Benjamini-Hochberg procedure (Benjamini and Hochberg, 1995). Gene ontology enrichment analysis was performed using GOrilla (Eden et al., 2009), examining genes that were significantly downregulated in *cyp-36A1(lf); egl-9(lf)* double mutants vs. *egl-9(lf)* single mutants (i.e. orange circle in Figure 2B) as compared to genes that were at least twofold upregulated in *egl-9(lf)* mutants vs. wild type (adjusted P-value < 0.05) and significantly downregulated in *egl-9(lf) hif-1(lf)* vs. *egl-9(lf)* (adjusted P-value < 0.05) (i.e. purple circle in Figure 2B).

Statistical Analysis

Chi-square tests were used to compare the distribution of stages of eggs laid by wild-type and mutant animals. Unpaired t-tests were used to compare *cyp-36A1* mRNA expression between strains, survival on tunicamycin between strains, and survival on t-BOOH between strains. Log-rank (Mantel-Cox) tests were used to compare survival of different strains on *Pseudomonas aeruginosa.* In cases of multiple comparisons, a Holm-Bonferroni correction was applied.

Accession numbers

The GEO accession number for the RNA-seq dataset in this chapter is GSE108283.

Supplemental Figures

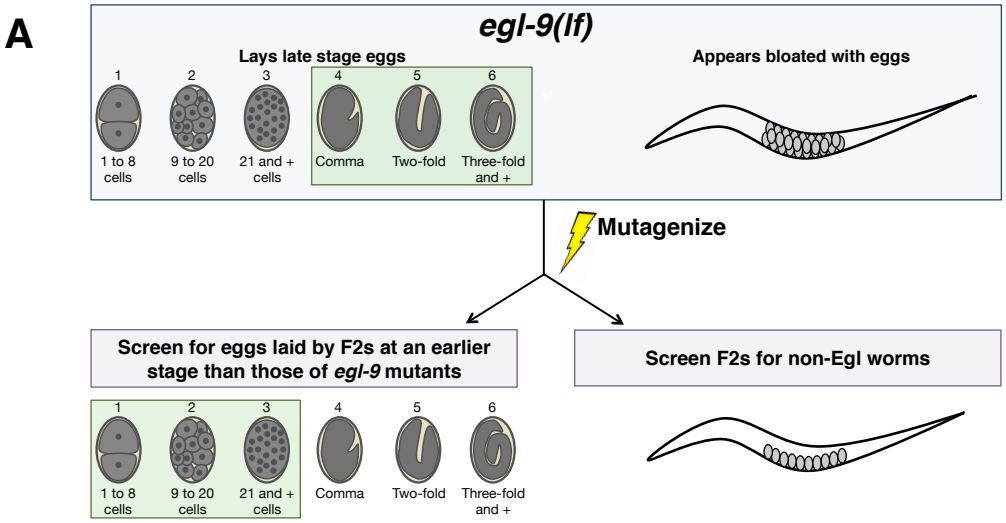

B

Allele	Cloning method	Gene	Mutation
n5666	Mapping and whole-genome sequencing	*cyp-36A1*	GGA->AGA[Gly->Arg]
n5668	Failure to complement *hif-1(ia4)*	*hif-1*	agGAG->aaGAG [Splice acceptor]
n5678	Failure to complement *hif-1(ia4)*	*hif-1*	CGA->TGA[Arg->STOP]

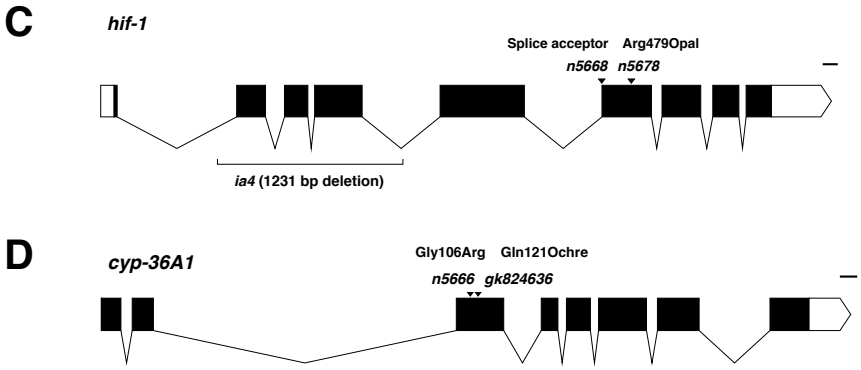

Figure S1. A screen for suppressors of the *egl-9(lf)* egg-laying defect. Related to Figure 1.

(A) Schematic of the screen design. (B) Summary of three cloned alleles from a suppressor screen of the *egl-9(lf)* egg-defect. (C) Gene diagram of *hif-1*; isoform *F38A6.3b* is shown. The *ia4* deletion allele was generated by deletion screening (Jiang et al., 2001). (D) Gene diagram of *cyp-36A1*. The *gk824636* allele is from the Million Mutation Project (Thompson et al., 2013).

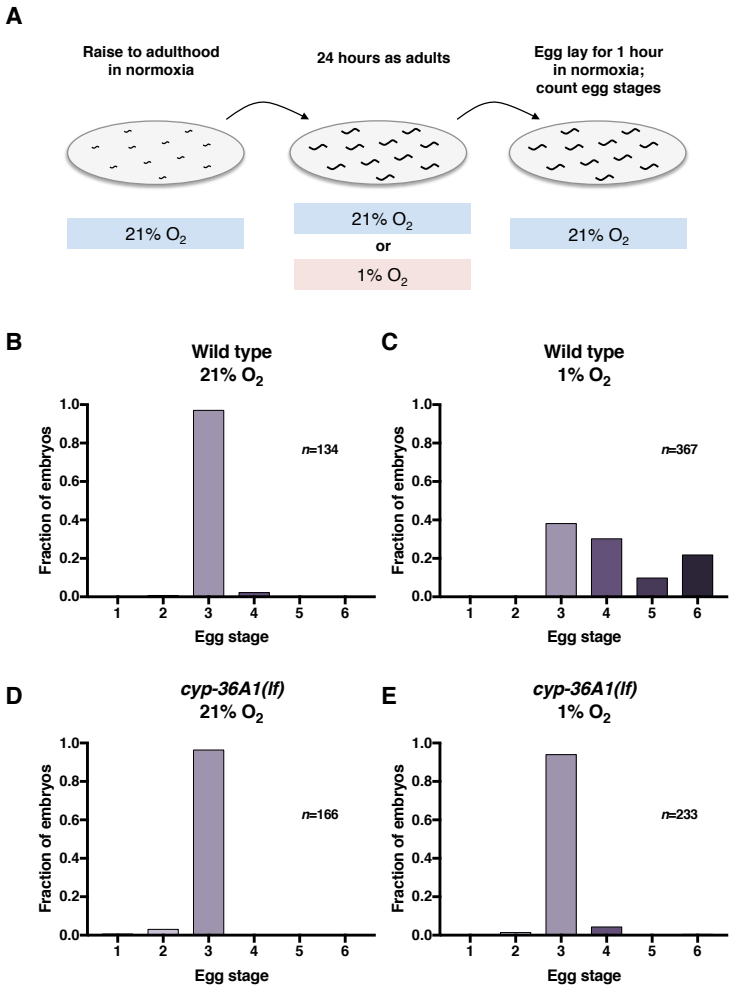

Figure S2. *cyp-36A1(lf)* suppresses the egg-laying defect of hypoxia-exposed animals.

Related to Figure 1. (A) Schematic depicting experimental design. (B-E) Distribution of stages of eggs laid by adult hermaphrodites. (B) Stages of eggs laid by wild-type animals grown in normoxia (21% O_2). (C) Animals exposed to hypoxia (1% O_2) for 24 hrs as adults laid later stage eggs than those in normoxia ($P<0.001$, Chi-square test with Holm-Bonferroni correction). (D) *cyp-36A1(gk824636)* mutants grown in normoxia displayed wild-type egg laying ($P>0.05$). (E) *cyp-36A1(gk824636)* mutants exposed to 1% O_2 laid eggs at earlier stages than wild-type animals in the same condition ($P<0.001$).

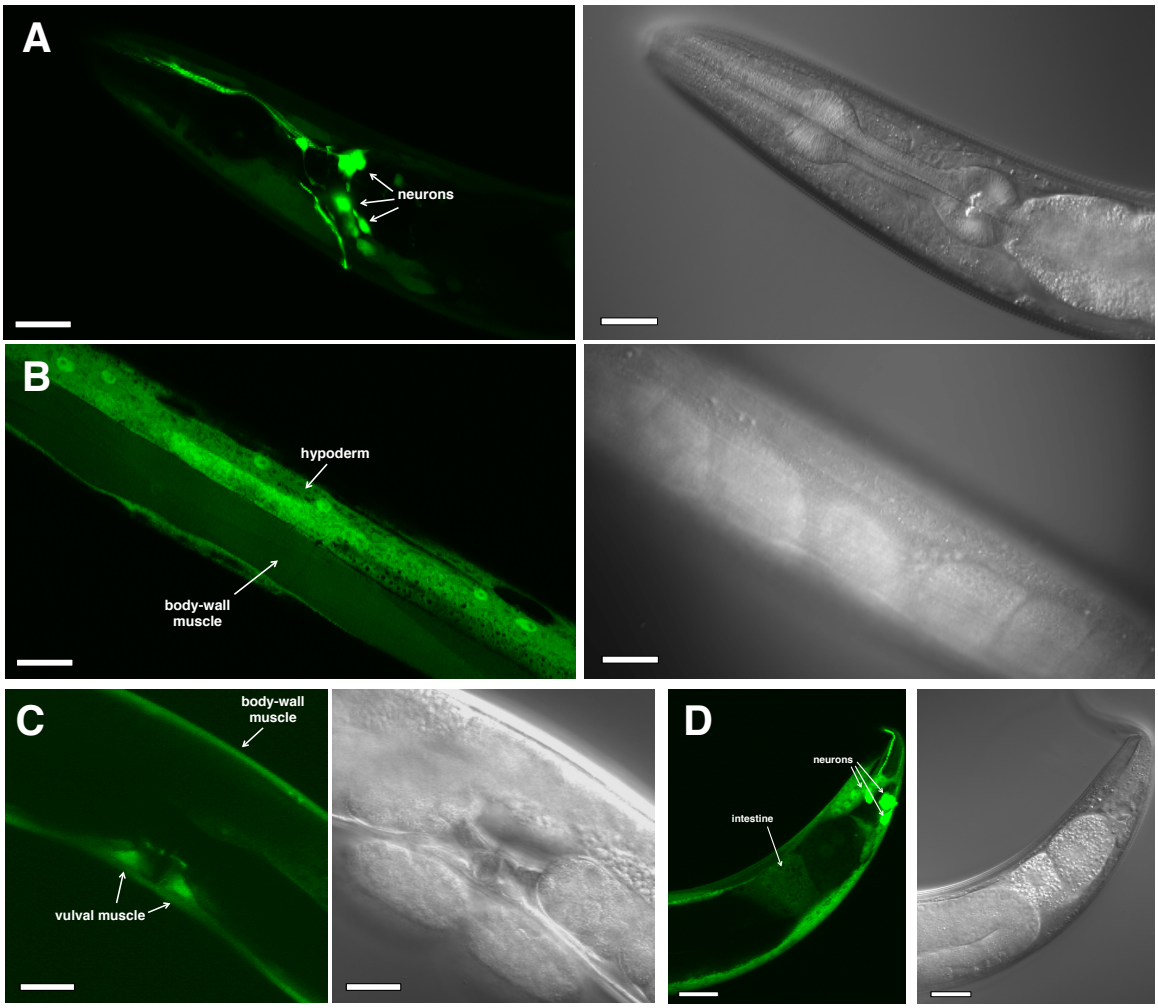

Figure S3. *cyp-36A1* is expressed in many tissues. Related to Figure 3. (A-D) Paired fluorescent (left in each panel) and Nomarski (right in each panel) micrographs showing expression of a transcriptional $P_{cyp\text{-}36A1}$*::gfp* reporter (*nIs682*) in an adult worm. Expression was observed in the head (A), midbody (B and C), and tail (D), including in neurons, body-wall muscle, vulval muscle, intestine, and hypoderm, as indicated. Scale bars, 20 um.

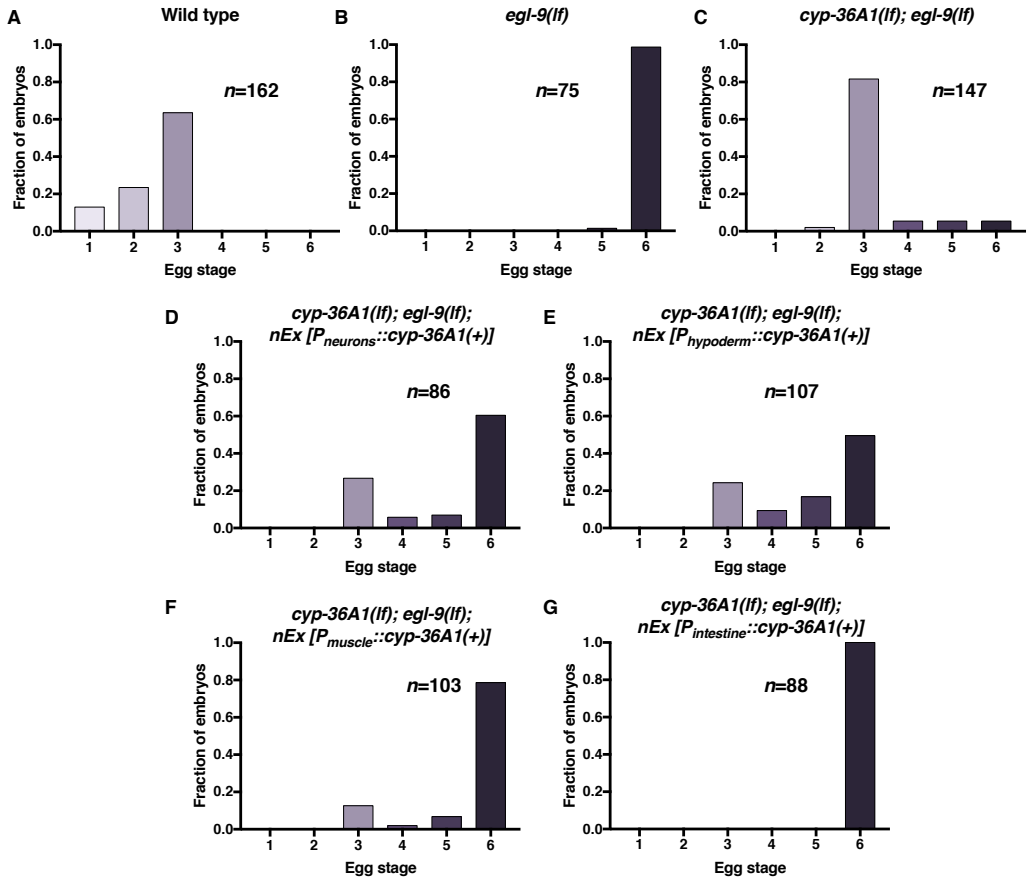

Figure S4. *cyp-36A1* expression in multiple tissues rescues the egg-laying phenotype of *cyp-36A1(lf); egl-9(lf)*. Related to Figure 3. (A-G) Distribution of stages of eggs laid by adult hermaphrodites of the indicated genotypes. All genotypes contained the *agIs219* ($P_{T24B8.5}$*::gfp*) transgene. (A) Stages of eggs laid by wild-type animals. (B) *egl-9(sa307)* animals laid later stage eggs than wild type ($P < 0.001$, Chi-square test with Holm-Bonferroni correction). (C) *cyp-36A1(gk824636)* suppressed the egg-laying defect of *egl-9(sa307)* mutants ($P < 0.001$). (D-G) Expression of *cyp-36A1(+)* specifically in neurons, hypoderm, muscle, or intestine of *cyp-36A1(gk824636); egl-9(sa307)* animals all rescued the suppression by *cyp-36A1(lf)* of the egg-laying defect of *egl-9(lf)* ($P < 0.001$).

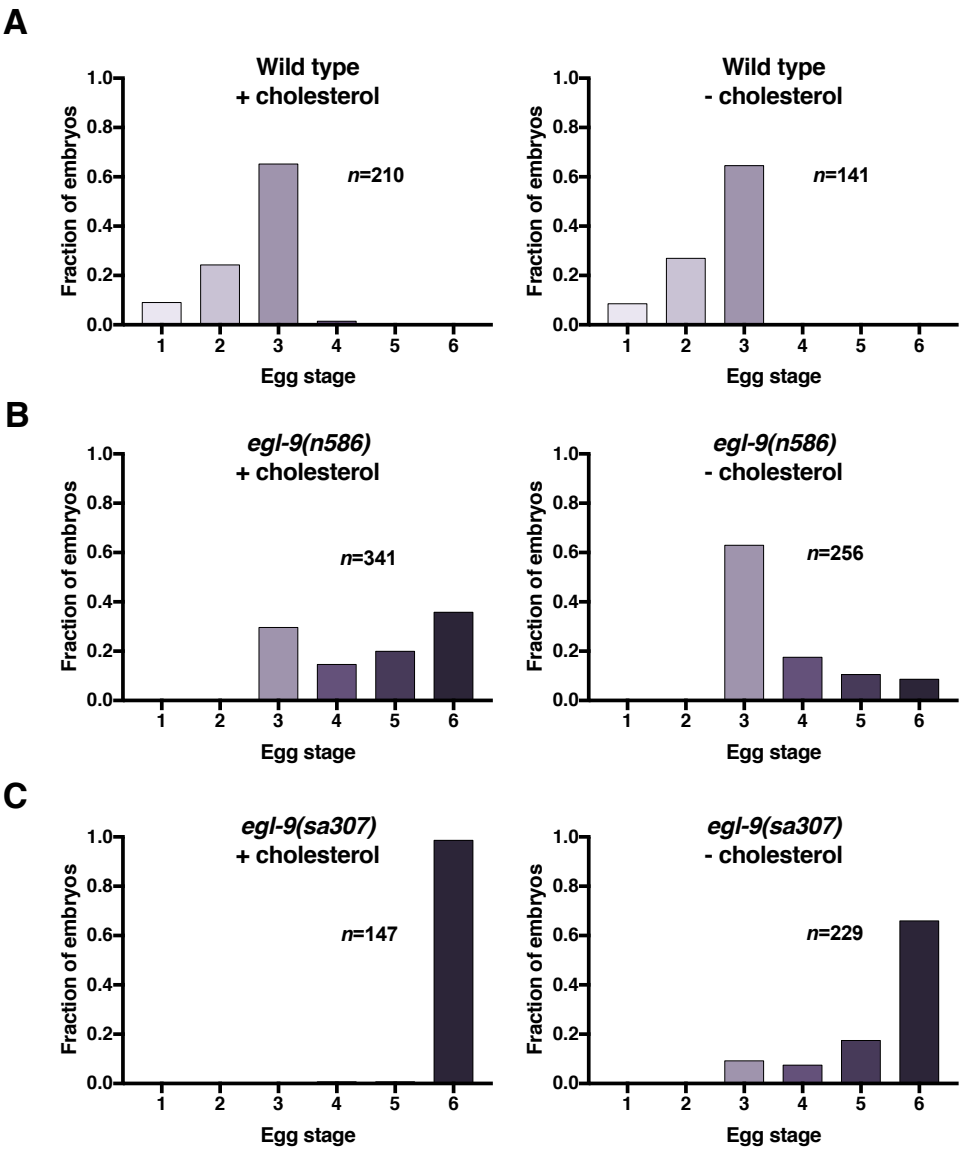

Figure S5. Cholesterol deprivation suppresses the *egl-9(lf)* egg-laying defect. (A-C) Distribution of stages of eggs laid by adult hermaphrodites. (A) The distribution of eggs laid by wild-type animals grown off of cholesterol was indistinguishable from that of wild-type animals grown under standard conditions ($P>0.05$; Chi-square test with Holm-Bonferroni correction). (B) *egl-9(n586)* (nonsense allele) mutants laid significantly earlier stage eggs when grown off cholesterol versus standard conditions ($P<0.001$). (C) *egl-9(sa307)* (deletion allele) mutants laid significantly earlier stage eggs when grown off cholesterol versus standard conditions ($P<0.001$).

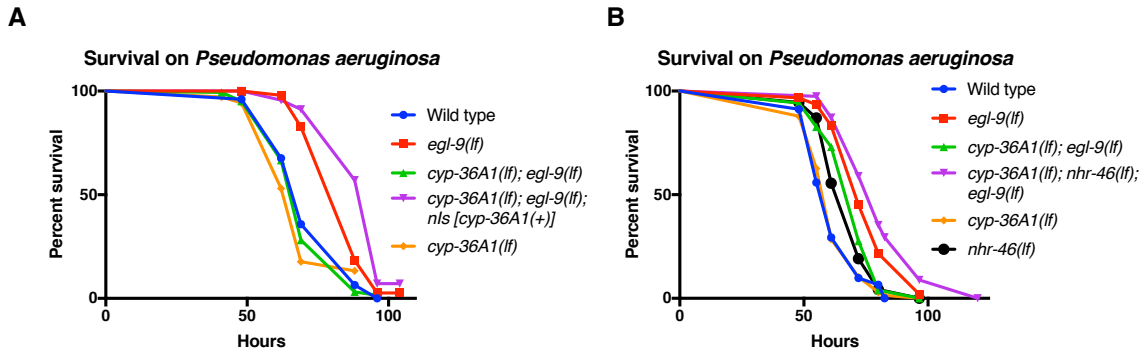

Figure S6. Replicate data for survival on *Pseudomonas aeruginosa.* Related to Figures 2 and 4. (A) Replicate data for Figure 2D. Wild type vs. *egl-9(lf)*, P<0.001; *egl-9(lf)* vs. *cyp-36A1(lf); egl-9(lf)*, P<0.001; *cyp-36A1(lf); egl-9(lf)* vs. *cyp-36A1(lf); egl-9(lf); cyp-36A1(+)*, P<0.001, as determined by the log-rank (Mantel-Cox) test, correcting for multiple comparisons with the Holm-Bonferroni method. *n*>30 animals per strain. (B) Replicate data for Figure 4D. Wild type vs. *egl-9(n586)*, P<0.001; *egl-9(lf)* vs. *cyp-36A1(lf); egl-9(lf)*, P<0.05; *cyp-36A1(lf); egl-9(lf)* vs. *cyp-36A1(lf); nhr-46(lf); egl-9(lf)*, P<0.001, as determined by the log-rank (Mantel-Cox) test, correcting for multiple comparisons with the Holm-Bonferroni method. *n*>30 animals per strain.

Author Contributions

H.R.H. supervised the project. C.P. designed and performed all experiments. Both authors analyzed the data, interpreted results, and wrote the manuscript.

Acknowledgments

We thank K. Burkhart, A. Doi, V. Dwivedi, S. Sando, J. Saul, E. Lee, J.N. Kong, and D. Ghosh for helpful discussion. Strains were provided by the *Caenorhabditis* Genetics Center. H.R.H. is an Investigator of the Howard Hughes Medical Institute. This work was also supported by the NIH grant 6936438. C.P. was supported by the NIH pre-doctoral training grant T32GM007287.

References

Agundez, J.A.G. (2004). Cytochrome P450 gene polymorphism and cancer. Curr. Drug Metab. *5*, 211–224.

Ahier, A., and Jarriault, S. (2014). Simultaneous expression of multiple proteins under a single promoter in *Caenorhabditis elegans* via a versatile 2A-based toolkit. Genetics *196*, 605–613.

Bellier, A., Chen, C.-S., Kao, C.-Y., Cinar, H.N., and Aroian, R.V. (2009). Hypoxia and the hypoxic response pathway protect against pore-forming toxins in *C. elegans*. PLoS Pathog *5*, e1000689.

Benjamini, Y., and Hochberg, Y. (1995). Controlling the false discovery rate: A practical and powerful approach to multiple testing. J. R. Stat. Soc. Ser. B Methodol. *57*, 289–300.

Bishop, T., Lau, K.W., Epstein, A.C.R., Kim, S.K., Jiang, M., O'Rourke, D., Pugh, C.W., Gleadle, J.M., Taylor, M.S., Hodgkin, J., et al. (2004). Genetic analysis of pathways regulated by the von Hippel-Lindau tumor suppressor in *Caenorhabditis elegans*. PLoS Biol *2*, e289.

Brenner, S. (1974). The genetics of *Caenorhabditis elegans*. Genetics *77*, 71–94.

Cai, Z., Luo, W., Zhan, H., and Semenza, G.L. (2013). Hypoxia-inducible factor 1 is required for remote ischemic preconditioning of the heart. Proc. Natl. Acad. Sci. U. S. A. *110*, 17462–17467.

Chang, A.J., and Bargmann, C.I. (2008). Hypoxia and the HIF-1 transcriptional pathway reorganize a neuronal circuit for oxygen-dependent behavior in *Caenorhabditis elegans*. Proc. Natl. Acad. Sci. *105*, 7321–7326.

Chen, D., Thomas, E.L., and Kapahi, P. (2009). HIF-1 Modulates Dietary Restriction-Mediated Lifespan Extension via IRE-1 in *Caenorhabditis elegans*. PLoS Genet *5*, e1000486.

Darby, C., Cosma, C.L., Thomas, J.H., and Manoil, C. (1999). Lethal paralysis of *Caenorhabditis elegans* by *Pseudomonas aeruginosa*. Proc. Natl. Acad. Sci. U. S. A. *96*, 15202–15207.

Davis, M.W., Hammarlund, M., Harrach, T., Hullett, P., Olsen, S., and Jorgensen, E.M. (2005). Rapid single nucleotide polymorphism mapping in *C. elegans*. BMC Genomics *6*, 118.

Dennis, E.A., and Norris, P.C. (2015). Eicosanoid storm in infection and inflammation. Nat. Rev. Immunol. *15*, 511–523.

Dunham, I., Kundaje, A., Aldred, S.F., Collins, P.J., Davis, C.A., Doyle, F., Epstein, C.B., Frietze, S., Harrow, J., Kaul, R., et al. (2012). An integrated encyclopedia of DNA elements in the human genome. Nature *489*, 57–74.

Eden, E., Navon, R., Steinfeld, I., Lipson, D., and Yakhini, Z. (2009). GOrilla: a tool for discovery and visualization of enriched GO terms in ranked gene lists. BMC Bioinformatics *10*, 48.

Elbekai, R.H., and El-Kadi, A.O.S. (2006). Cytochrome P450 enzymes: Central players in cardiovascular health and disease. Pharmacol. Ther. *112*, 564–587.

Epstein, A.C.R., Gleadle, J.M., McNeill, L.A., Hewitson, K.S., O'Rourke, J., Mole, D.R., Mukherji, M., Metzen, E., Wilson, M.I., Dhanda, A., et al. (2001). *C. elegans* EGL-9 and mammalian homologs define a family of dioxygenases that regulate HIF by prolyl hydroxylation. Cell *107*, 43–54.

Evans, R.M., and Mangelsdorf, D.J. (2014). Nuclear receptors, RXR, and the Big Bang. Cell *157*, 255–266.

Feng, H., Craig, H., and Hope, I. (2012). Expression Pattern Analysis of Regulatory Transcription Factors in *Caenorhabditis elegans*. In Gene Regulatory Networks, B. Deplancke, and N. Gheldof, eds. (Humana Press), pp. 21–50.

Gerisch, B., and Antebi, A. (2004). Hormonal signals produced by DAF-9/cytochrome P450 regulate *C. elegans* dauer diapause in response to environmental cues. Development *131*, 1765–1776.

Ivan, M., Kondo, K., Yang, H., Kim, W., Valiando, J., Ohh, M., Salic, A., Asara, J.M., Lane, W.S., and Jr, W.G.K. (2001). HIFα Targeted for VHL-mediated destruction by proline hydroxylation: Implications for O_2 sensing. Science *292*, 464–468.

Jaakkola, P., Mole, D.R., Tian, Y.-M., Wilson, M.I., Gielbert, J., Gaskell, S.J., Kriegsheim, A. von, Hebestreit, H.F., Mukherji, M., Schofield, C.J., et al. (2001). Targeting of HIF-α to the von Hippel-Lindau ubiquitylation complex by O_2-regulated prolyl hydroxylation. Science *292*, 468–472.

Jiang, H., Guo, R., and Powell-Coffman, J.A. (2001). The *Caenorhabditis elegans hif-1* gene encodes a bHLH-PAS protein that is required for adaptation to hypoxia. Proc. Natl. Acad. Sci. *98*, 7916–7921.

Kaelin, W.G., and Ratcliffe, P.J. (2008). Oxygen sensing by metazoans: The central role of the HIF hydroxylase pathway. Mol. Cell *30*, 393–402.

Kirienko, N.V., Kirienko, D.R., Larkins-Ford, J., Wählby, C., Ruvkun, G., and Ausubel, F.M. (2013). *Pseudomonas aeruginosa* disrupts *Caenorhabditis elegans* iron homeostasis, causing a hypoxic response and death. Cell Host Microbe *13*, 406–416.

Langmead, B., Trapnell, C., Pop, M., and Salzberg, S.L. (2009). Ultrafast and memory-efficient alignment of short DNA sequences to the human genome. Genome Biol. *10*, R25.

Lee, S.-J., Hwang, A.B., and Kenyon, C. (2010). Inhibition of Respiration Extends *C. elegans* Life Span via Reactive Oxygen Species that Increase HIF-1 Activity. Curr. Biol. *20*, 2131–2136.

Leiser, S.F., Miller, H., Rossner, R., Fletcher, M., Leonard, A., Primitivo, M., Rintala, N., Ramos, F.J., Miller, D.L., and Kaeberlein, M. (2015). Cell nonautonomous activation of flavin-containing monooxygenase promotes longevity and health span. Science *350*, 1375–1378.

Li, B., and Dewey, C.N. (2011). RSEM: accurate transcript quantification from RNA-Seq data with or without a reference genome. BMC Bioinformatics *12*, 323.

Li, H., and Durbin, R. (2009). Fast and accurate short read alignment with Burrows–Wheeler transform. Bioinformatics *25*, 1754–1760.

Li, H., Handsaker, B., Wysoker, A., Fennell, T., Ruan, J., Homer, N., Marth, G., Abecasis, G., and Durbin, R. (2009). The Sequence Alignment/Map format and SAMtools. Bioinformatics *25*, 2078–2079.

Lim, Y., Lee, D., Kalichamy, K., Hong, S.-E., Michalak, M., Ahnn, J., Kim, D.H., and Lee, S.-K. (2014). Sumoylation regulates ER stress response by modulating calreticulin gene expression in XBP-1-dependent mode in *Caenorhabditis elegans*. Int. J. Biochem. Cell Biol. *53*, 399–408.

Lun, A.T.L., Chen, Y., and Smyth, G.K. (2016). It's DE-licious: A Recipe for Differential Expression Analyses of RNA-seq Experiments Using Quasi-Likelihood Methods in edgeR. In Statistical Genomics, (Humana Press, New York, NY), pp. 391–416.

Ma, D.K., Vozdek, R., Bhatla, N., and Horvitz, H.R. (2012). CYSL-1 interacts with the O_2-sensing hydroxylase EGL-9 to promote H2S-modulated hypoxia-induced behavioral plasticity in *C. elegans*. Neuron *73*, 925–940.

Ma, D.K., Rothe, M., Zheng, S., Bhatla, N., Pender, C.L., Menzel, R., and Horvitz, H.R. (2013). Cytochrome P450 drives a HIF-regulated behavioral response to reoxygenation by *C. elegans*. Science *341*, 554–558.

Maxwell, P.H., Wiesener, M.S., Chang, G.-W., Clifford, S.C., Vaux, E.C., Cockman, M.E., Wykoff, C.C., Pugh, C.W., Maher, E.R., and Ratcliffe, P.J. (1999). The tumour suppressor protein VHL targets hypoxia-inducible factors for oxygen-dependent proteolysis. Nature *399*, 271–275.

Mehta, R., Steinkraus, K.A., Sutphin, G.L., Ramos, F.J., Shamieh, L.S., Huh, A., Davis, C., Chandler-Brown, D., and Kaeberlein, M. (2009). Proteasomal Regulation of the Hypoxic Response Modulates Aging in *C. elegans*. Science *324*, 1196–1198.

Mello, C.C., Kramer, J.M., Stinchcomb, D., and Ambros, V. (1991). Efficient gene transfer in *C. elegans*: extrachromosomal maintenance and integration of transforming sequences. EMBO J. *10*, 3959.

Miller, D.L., and Roth, M.B. (2009). *C. elegans* are protected from lethal hypoxia by an embryonic diapause. Curr. Biol. *19*, 1233–1237.

Mole, D.R., Blancher, C., Copley, R.R., Pollard, P.J., Gleadle, J.M., Ragoussis, J., and Ratcliffe, P.J. (2009). Genome-wide association of hypoxia-inducible factor (HIF)-1α and HIF-2α DNA binding with expression profiling of hypoxia-inducible transcripts. J. Biol. Chem. *284*, 16767–16775.

Nakazawa, M.S., Keith, B., and Simon, M.C. (2016). Oxygen availability and metabolic adaptations. Nat. Rev. Cancer *16*, 663–673.

Nebert, D.W., Wikvall, K., and Miller, W.L. (2013). Human cytochromes P450 in health and disease. Philos. Trans. R. Soc. B Biol. Sci. *368*, 20120431–20120431.

Olenchock, B.A., Moslehi, J., Baik, A.H., Davidson, S.M., Williams, J., Gibson, W.J., Chakraborty, A.A., Pierce, K.A., Miller, C.M., Hanse, E.A., et al. (2016). EGLN1 inhibition and rerouting of α-ketoglutarate suffice for remote ischemic protection. Cell *164*, 884–895.

Oliver Hobert (2002). PCR fusion method. BioTechniques *32*, 728–730.

Palazon, A., Goldrath, A.W., Nizet, V., and Johnson, R.S. (2014). HIF transcription factors, inflammation, and immunity. Immunity *41*, 518–528.

Paquin, N., Murata, Y., Froehlich, A., Omura, D.T., Ailion, M., Pender, C.L., Constantine-Paton, M., and Horvitz, H.R. (2016). The conserved VPS-50 protein functions in dense-core vesicle maturation and acidification and controls animal behavior. Curr. Biol. *26*, 862–871.

Park, S.-K., Tedesco, P.M., and Johnson, T.E. (2009). Oxidative stress and longevity in *Caenorhabditis elegans* as mediated by SKN-1: SKN-1 response to oxidative stress. Aging Cell *8*, 258–269.

Pocock, R., and Hobert, O. (2008). Oxygen levels affect axon guidance and neuronal migration in *Caenorhabditis elegans*. Nat. Neurosci. *11*, 894–900.

Pocock, R., and Hobert, O. (2010). Hypoxia activates a latent circuit for processing gustatory information in *C. elegans*. Nat. Neurosci. *13*, 610–614.

Powell-Coffman, J.A. (2010). Hypoxia signaling and resistance in *C. elegans*. Trends Endocrinol. Metab. *21*, 435–440.

Quinlan, A.R., and Hall, I.M. (2010). BEDTools: a flexible suite of utilities for comparing genomic features. Bioinformatics *26*, 841–842.

Reddy, K.C., Andersen, E.C., Kruglyak, L., and Kim, D.H. (2009). A polymorphism in *npr-1* Is a behavioral determinant of pathogen susceptibility in *C. elegans*. Science *323*, 382–384.

Rendic, S., and Guengerich, F.P. (2015). Survey of human oxidoreductases and cytochrome P450 enzymes involved in the metabolism of xenobiotic and natural chemicals. Chem. Res. Toxicol. *28*, 38–42.

Ringstad, N., and Horvitz, H.R. (2008). FMRFamide neuropeptides and acetylcholine synergistically inhibit egg-laying by *C. elegans*. Nat. Neurosci. *11*, 1168–1176.

Robinson, M.D., McCarthy, D.J., and Smyth, G.K. (2010). edgeR: a Bioconductor package for differential expression analysis of digital gene expression data. Bioinformatics *26*, 139–140.

Rowland, A., and Mangoni, A.A. (2014). Cytochrome P450 and ischemic heart disease: current concepts and future directions. Expert Opin. Drug Metab. Toxicol. *10*, 191–213.

Schito, L., and Rey, S. (2018). Cell-Autonomous Metabolic Reprogramming in Hypoxia. Trends Cell Biol. *28*, 128-142.

Schodel, J., Oikonomopoulos, S., Ragoussis, J., Pugh, C.W., Ratcliffe, P.J., and Mole, D.R. (2011). High-resolution genome-wide mapping of HIF-binding sites by ChIP-seq. Blood *117*, e207–e217.

Schuster, I., and Bernhardt, R. (2007). Inhibition of cytochromes P450: Existing and new promising therapeutic targets. Drug Metab. Rev. *39*, 481–499.

Semenza, G.L. (2011). Oxygen sensing, homeostasis, and disease. N. Engl. J. Med. *365*, 537–547.

Semenza, G.L. (2012). Hypoxia-inducible factors in physiology and medicine. Cell *148*, 399–408.

Shen, C., Nettleton, D., Jiang, M., Kim, S.K., and Powell-Coffman, J.A. (2005). Roles of the HIF-1 hypoxia-inducible factor during hypoxia response in *Caenorhabditis elegans*. J. Biol. Chem. *280*, 20580–20588.

Shivers, R.P., Kooistra, T., Chu, S.W., Pagano, D.J., and Kim, D.H. (2009). Tissue-specific activities of an immune signaling module regulate physiological responses to pathogenic and nutritional bacteria in *C. elegans*. Cell Host Microbe *6*, 321–330.

Shore, D.E., and Ruvkun, G. (2013). A cytoprotective perspective on longevity regulation. Trends Cell Biol. *23*, 409–420.

Simonson, T.S., Yang, Y., Huff, C.D., Yun, H., Qin, G., Witherspoon, D.J., Bai, Z., Lorenzo, F.R., Xing, J., Jorde, L.B., et al. (2010). Genetic evidence for high-altitude adaptation in Tibet. Science *329*, 72–75.

Taylor, R.C., Berendzen, K.M., and Dillin, A. (2014). Systemic stress signalling: understanding the cell non-autonomous control of proteostasis. Nat. Rev. Mol. Cell Biol. *15*, nrm3752.

Thomas, J.H. (1990). Genetic analysis of defecation in *Caenorhabditis elegans*. Genetics *124*, 855–872.

Thompson, O., Edgley, M., Strasbourger, P., Flibotte, S., Ewing, B., Adair, R., Au, V., Chaudhry, I., Fernando, L., Hutter, H., et al. (2013). The million mutation project: A new approach to genetics in *Caenorhabditis elegans*. Genome Res. *23*, 1749–1762.

Trent, C., Tsung, N., and Horvitz, H.R. (1983). Egg-laying defective mutants of the nematode *Caenorhabditis elegans*. Genetics *104*, 619–647.

Wang, G.L., Jiang, B.H., Rue, E.A., and Semenza, G.L. (1995). Hypoxia-inducible factor 1 is a basic-helix-loop-helix-PAS heterodimer regulated by cellular O_2 tension. Proc. Natl. Acad. Sci. *92*, 5510–5514.

Wouters, B.G., and Koritzinsky, M. (2008). Hypoxia signalling through mTOR and the unfolded protein response in cancer. Nat. Rev. Cancer *8*, 851–864.

Zhang, Y., Shao, Z., Zhai, Z., Shen, C., and Powell-Coffman, J.A. (2009). The HIF-1 hypoxia-inducible factor modulates lifespan in *C. elegans*. PLoS ONE *4*, e6348.

Chapter Three

Additional pathways act in parallel to CYP-36A1/NHR-46 to regulate egg laying downstream of EGL-9/HIF-1

Calista Diehl performed egg-laying assays for Figure 1; I conducted all other experiments and analyses

Summary

The EGL-9/HIF-1 hypoxia-response pathway controls *C. elegans* egg-laying behavior; *egl-9(lf)* mutants have an egg-laying defect that is suppressed by a second mutation in *hif-1.* We previously showed that the cytochrome P450 enzyme CYP-36A1 and nuclear hormone receptor NHR-46 regulate egg laying downstream of EGL-9 and HIF-1. Here we provide evidence that an additional pathway functions in parallel to the *cyp-36A1/nhr-46* pathway downstream of *egl-9/hif-1* to regulate egg laying. We also describe additional mutants from the *egl-9(lf)* suppressor screen that identified *cyp-36A1*, one or several of which might function in the putative parallel pathway. Future studies of the parallel pathway(s) and additional *egl-9(lf)* suppressors will likely reveal new insights into the function of the hypoxia-response pathway.

Introduction

C. elegans hermaphrodites mutant for the prolyl hydroxylase *egl-9* are egg-laying defective (Trent et al., 1983), and loss-of-function alleles of the hypoxia-inducible factor *hif-1* and the cytochrome P450 gene *cyp-36A1* were identified from a genetic screen for suppressors of the *egl-9(lf)* defect. As described in Chapter 2, additional work led to the following model for regulation of egg laying by *egl-9*: inactivation of *egl-9*, due to either a loss-of-function mutation or a hypoxic environment, results in stabilization of the transcription factor HIF-1, which promotes transcription of *cyp-36A1*. The CYP-36A1 enzyme synthesizes a putative hormone that acts on the nuclear hormone receptor NHR-46 to regulate egg laying and mediate other physiological changes. However, other genes with no clear connection to this hormone signaling pathway were also identified from the *egl-9(lf)* suppressor screen, indicating that additional players likely act downstream of or in parallel to *egl-9/hif-1/cyp-36A1/nhr-46* to regulate egg laying. The molecular nature of the CYP-36A1/NHR-46 pathway suggests the presence of downstream effectors in the regulation of egg laying: NHR-46 regulates transcription, and as such we hypothesize that at least one transcriptional target of NHR-46 is likely to regulate egg-laying behavior. In addition, several lines of evidence indicate that there are pathways parallel to *cyp-36A1/nhr-46* downstream of *egl-9* and *hif-1.* In this chapter we present evidence for these parallel pathways and will describe additional mutants from the screen for suppressors of the *egl-9(lf)* egg-laying defect, which might act either in parallel to or downstream of *cyp-36A1*.

Results

Genetic evidence for parallel pathways downstream of *egl-9*

cyp-36A1(lf) only partially suppresses the *egl-9(lf)* egg-laying defect (Chapter 2, Figure 1 B-D and Figure S4, A-C), as some late stage eggs (stage 4 or later) are laid by *cyp-36A1(lf); egl-9(lf)* mutants, whereas no late stage eggs are laid by wild-type animals when grown at 22°C, as in these assays. The incomplete suppression is even more apparent in animals grown at 25°C: most eggs laid by *cyp-36A1(lf); egl-9(lf)* mutants are stage 4 or later (Figure 1A - D). We note that the *gk824636* allele used in this analysis is a nonsense allele in the cytochrome P450 domain and thus a putative null, suggesting that incomplete suppression results from the presence of a parallel pathway rather than incomplete loss of *cyp-36A1* function in this mutant. By contrast, loss-of-function of *hif-1* fully suppresses the egg-laying defect of *egl-9(lf)* (Figure 1E), indicating that constitutive activation of HIF-1 fully accounts for the egg-laying defect of *egl-9(lf)* mutants and suggesting that the putative parallel pathway is downstream of *hif-1*.

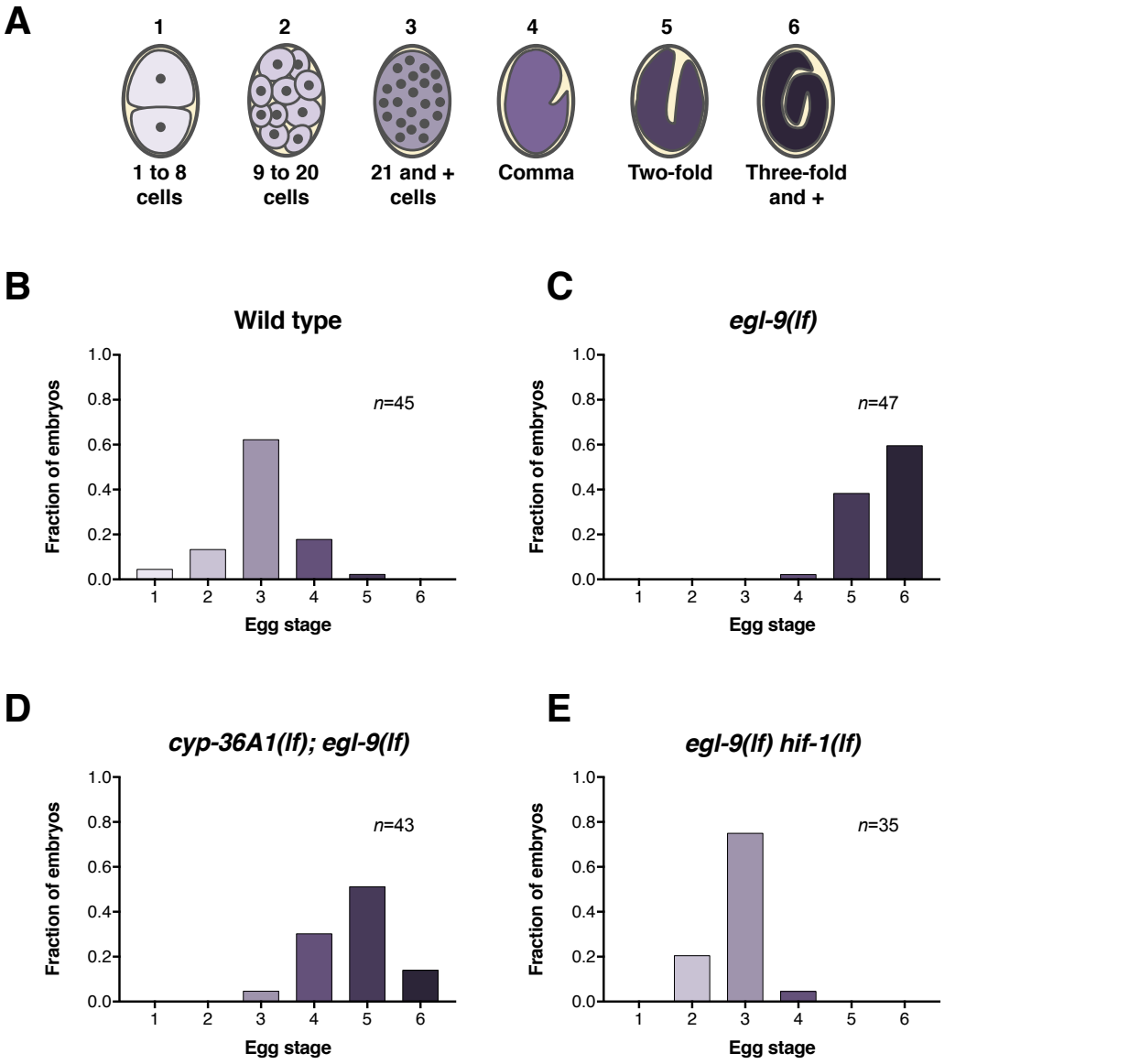

Figure 1. *cyp-36A1(lf)* partially suppresses the *egl-9(lf)* egg-laying defect at 25°C. (A) Stages of embryonic development, adapted from Ringstad and Horvitz, 2008 and Paquin et al., 2016. (B-E) Distribution of stages of eggs newly laid by adult hermaphrodites, used as a proxy for egg retention time *in utero*, of animals the indicated genotypes. All animals were raised at 25°C. (B) Stages of eggs laid by wild-type animals. (C) *egl-9* loss-of-function (*lf*) mutants laid later stage eggs than the wild type ($P < 0.001$, Chi-square test with Holm-Bonferroni correction). (D) *cyp-36A1(lf)* suppressed the egg-laying defect of *egl-9(lf)* mutants ($P < 0.001$), but laid significantly older eggs relative to wild-type animals ($P < 0.001$). (E) *hif-1(lf)* suppressed the egg-laying defect of *egl-9(lf)* mutants ($P < 0.001$); stages of eggs were indistinguishable from those laid by wild-type animals ($P > 0.05$). Alleles used were *cyp-36A1(gk824636), hif-1(ia4)*, and *egl-9(sa307)*.

cyp-36A1 gain-of-function and *nhr-46* loss-of-function experiments also provide evidence for a parallel pathway regulating egg laying. A transgene overexpressing wild-type *cyp-36A1* rescues the *cyp-36A1(lf); egl-9(lf)* mutant phenotype (Chapter 2, Figure 1E). We examined animals carrying this transgene in a wild-type background and found that they have a wild-type egg-laying phenotype (Figure 2A and B). This finding suggests that high *cyp-36A1* expression from a transgene is not sufficient to drive inhibition of egg laying, consistent with a model in which a second pathway downstream of *egl-9* must also be activated for egg-laying inhibition to occur. We also examined egg-laying behavior of *nhr-46(n6126)* single mutants and found that they display wild-type egg laying (Figure 2C and D), in contrast to *cyp-36A1(gk824636); nhr-46(n6126); egl-9(sa307)* triple mutants, which are egg-laying defective (Chapter 2, Figure 4B). If egg-laying regulation downstream of *egl-9* occurred by a simple linear pathway of *egl-9* --| *cyp-36A1* --| *nhr-46*, *nhr-46(lf)* should phenocopy *egl-9(lf)*; the observation that *egl-9(lf)* is egg-laying defective while *nhr-46(lf)* is normal for egg laying indicates that there must be a pathway functioning in parallel to *nhr-46* to regulate egg laying downstream of *egl-9*. Interestingly, *nhr-46(lf)* is sufficient for increased expression of $P_{T24B8.5}$*::gfp* expression, similar to *egl-9(lf)* (Figure S1), suggesting that some aspects of *egl-9/cyp-36A1/nhr-46*-regulated biology might not require multiple parallel pathways.

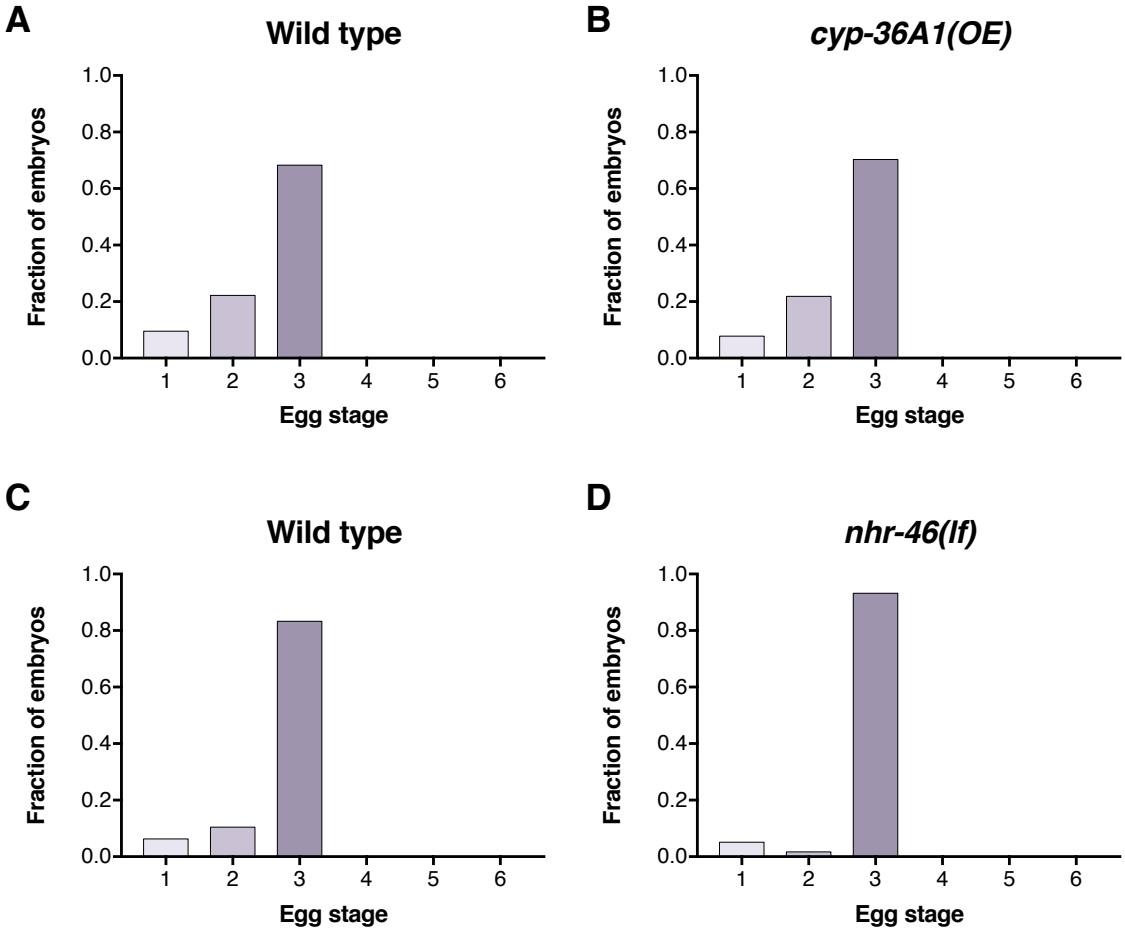

Figure 2. *cyp-36A1(OE)* and *nhr-46(lf)* do not have an egg-laying defect. (A-D) Distribution of stages of eggs newly laid by adult hermaphrodites, used as a proxy for egg retention time *in utero*, of animals the indicated genotypes. Animals were raised at 20°C for A and B, and 22°C for C and D. (A, B) Animals with a *cyp-36A1* overexpressing transgene display wild-type egg laying ($P > 0.05$, Chi-square test). (C, D) *nhr-46(lf)* mutants display wild-type egg laying ($P > 0.05$, Chi-square test). Alleles used were *nhr-46(n6126)* and *nIs674* (*cyp-36A1(OE)*).

Cellular evidence for parallel pathways downstream of *egl-9*

Site-of-action studies for *hif-1* and *cyp-36A1* have also provided evidence for multiple parallel pathways downstream of HIF-1 that regulate egg laying. We examined site of action for *hif-1* by expressing *hif-1(+)* under tissue-specific promoters in an *egl-9(lf) hif-1(lf)* background, and found that *hif-1* rescues the *egl-9(lf) hif-1(lf)* egg-laying phenotype (i.e. has an egg-laying defect, similar to *egl-9(lf)* mutants) when expressed in neurons but not in muscle, hypoderm, or intestine (Figure 3A-G), suggesting that *hif-1* functions in neurons to control egg laying. These site-of-action findings contrast with the tissue-specific rescue experiments described for *cyp-36A1* in Chapter 2 (Figure S4), which showed that *cyp-36A1(+)* expressed in any of neurons, hypoderm, muscle, or intestine can rescue the egg-laying phenotype of *cyp-36A1(lf); egl-9(lf)* mutants. Thus, while HIF-1 acts in the nervous system, CYP-36A1 can act in many tissue types to regulate egg laying. This is inconsistent with a model for CYP-36A1 as the sole effector of HIF-1 in the regulation of egg laying, which would predict that HIF-1 and CYP-36A1 function in the same tissue. We thus propose that multiple pathways function downstream of HIF-1 to regulate egg laying, one of which acts specifically in neurons and the second of which, the CYP-36A1 pathway, can act in several tissues. Interestingly, *nhr-46* also functions, at least in part, in neurons, suggesting that neurons are a possible site of convergence for the proposed parallel pathways; for example, an unidentified HIF-1 target and an NHR-46 target could act together in neurons to drive egg-laying inhibition.

A previous report examining site of action for *egl-9* in regulating aerotaxis behavior also noted that an *egl-9(+)*-expressing transgene rescues the egg-laying defect when expressed in neurons plus the uv1 neuroendocrine cell, indicating that *egl-9* functions in these tissues to regulate egg laying (Chang and Bargmann, 2008). The sites of action for *egl-9* and *hif-1* are thus

slightly different, i.e. *hif-1* acts in neurons while *egl-9* acts in neurons plus additional neuroendocrine cells. One possible model explaining this difference is that HIF-1 activity is sufficient in either uv1 or neurons to inhibit egg laying in the *egl-9(lf)* background. According to this model, *egl-9*, as the negative regulator of HIF-1, must be expressed in both neurons and uv1 to adequately inhibit HIF-1 and thus restore normal egg laying in an *egl-9(lf)* background, whereas HIF-1 activation in neurons alone is adequate to promote egg-laying inhibition in an *egl-9(lf) hif-1(lf)* background. These data are consistent with our model that HIF-1 is the only direct effector of EGL-9 in the regulation of egg-laying behavior.

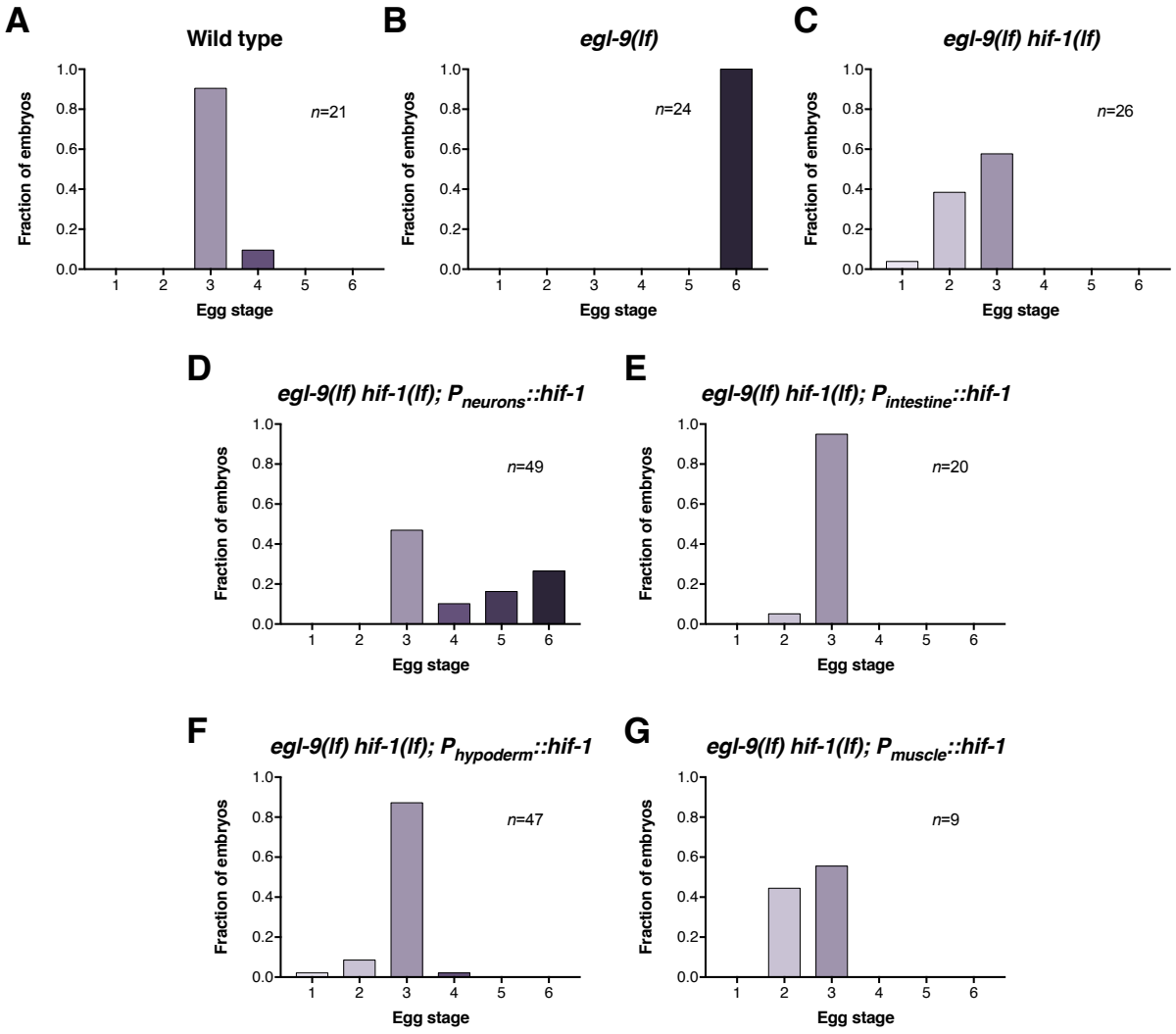

Figure 3. *hif-1* expression in neurons but not other tissues rescues the egg-laying phenotype of *hif-1(lf) egl-9(lf)*. (A-G) Distribution of stages of eggs laid by adult hermaphrodites of the indicated genotypes. All genotypes contained the *agIs219* ($P_{T24B8.5}$*::gfp*) transgene. (A) Stages of eggs laid by wild-type animals. (B) *egl-9(sa307)* animals laid later stage eggs than wild type ($P < 0.001$, Chi-square test). (C) *hif-1(ia4)* suppressed the egg-laying defect of *egl-9(sa307)* mutants ($P < 0.001$). (D) Expression of *hif-1* specifically in neurons rescued the suppression by *hif-1(lf)* of the *egl-9(lf)* egg-laying defect ($P < 0.001$, Chi-square test with Bonferroni correction). (E-G) Expression of *hif-1* in intestine (E), hypoderm (F), or muscle (G) did not rescue the suppression by *hif-1(lf)* of the *egl-9(lf)* egg-laying defect ($P > 0.05$).

Additional mutants that suppress *egl-9(lf)* egg-laying defect

To identify downstream effectors of *egl-9* that function in regulating egg-laying behavior, we performed a forward mutagenesis screen for suppressors of the *egl-9(lf)* egg-laying defect. Specifically, we mutagenized *nIs470; egl-9(n586)* animals and screened the F2 generation for animals that appear less egg-laying defective (i.e. are less bloated with eggs) than *egl-9(n586)* mutants, and screened eggs laid by the F2 generation for eggs that are at an earlier stage than those laid by *egl-9(n586)* mutants (see Chapter 2, Figure S1A for schematic). The *n586* allele used for the screen is a temperature-sensitive nonsense allele (Q131Ochre). The *nIs470* transgene is a transcriptional reporter for the HIF-1 target *cysl-2* ($P_{cysl\text{-}2}$*::gfp*); we used this reporter to categorize mutations with respect to how broadly they affect downstream effectors of the *egl-9/hif-1* pathway. *egl-9(lf)* mutants and animals mutant for upstream positive regulators of *egl-9*, e.g. the Regulator of HYpoxia-inducible factor *rhy-1*, are egg-laying defective and have high expression of $P_{cysl\text{-}2}$*::gfp* due to constitutive activation of HIF-1; loss-of-function mutation in *hif-1* suppresses the *egl-9(lf)* and *rhy-1(lf)* mutant egg-laying and *cysl-2* gene expression abnormalities (Ma et al., 2012). We predicted that some mutants might specifically affect egg-laying behavior downstream of *egl-9* and thus suppress only the *egl-9(lf)* egg-laying defect, while others might more broadly affect function of the *egl-9*/*hif-1* pathway and thus suppress both the egg-laying defect and high $P_{cysl\text{-}2}$*::gfp* of *egl-9(lf)* mutants.

We screened approximately 100,000 haploid genomes and identified 20 mutants, summarized in Table 1. These mutants represent at least 16 independent isolates; we used a pooled screen design, such that mutants in the same pool are potentially progeny of the same F1 animal with suppressing alleles arising from the same initial mutation. Two alleles suppressed both the egg-laying defect and high $P_{cysl\text{-}2}$*::gfp* expression of *egl-9(lf)* mutants; both failed to

complement *hif-1(lf),* and sequencing of the *hif-1* locus identified a splice acceptor and nonsense mutation in the two strains (see Chapter 2, Figure S1C). The remaining alleles retained high GFP expression and, for the alleles conferring recessive phenotypes, complemented *hif-1(lf)*. One of these alleles, *cyp-36A1(lf)*, is described in Chapter 2. We have identified two additional genes that regulate egg laying based on cloning mutants from this screen: *F09F9.4* and *mel-26*, both of which are described below.

Strain	Sup allele	Pool	Penetrance	Dominance	GFP?	*hif-1* allele?*	Map position	Gene	Mutation
MT21376	*n5607*	2	>90%	Recessive	Yes	No	LG X, -17 to -4	*F09F9.4*	V470D
MT21377	*n5608*	3	90%	Recessive	Yes	No			
MT21801	*n5664*	9	50%	Recessive	Yes	No			
MT21802	*n5665*	9	50%	Recessive	Yes	No			
MT21803	*n5666*	12	>90%	Recessive	Yes	No	LG I, -6 to +5	*cyp-36A1***	G106R
MT21804	*n5667*	13	90%	Recessive	Yes	No			
MT21805	*n5668*	13	100%	Recessive	NO	YES		*hif-1***	Splice acceptor
MT21806	*n5669*	15	70%	Recessive	Yes	No			
MT21807	*n5670*	17	>90%	Recessive	Yes	No			
MT21808	*n5671*	21	~50%	Recessive	Yes	No			
MT21810	*n5673*	28	100%	Recessive	Yes	No			
MT21811	*n5674*	29	50%	Recessive	Yes	No			
MT21812	*n5675*	30	100%	Recessive	Yes	No			
MT21813	*n5676*	32	>90%	Recessive	Yes	No			
MT21814	*n5677*	32	75%	Recessive	Yes	No			
MT21815	*n5678*	44	100%	Recessive	NO	YES		*hif-1***	R479Opal
MT21816	*n5679*	45	100%	Dominant	Yes	N/A	LG I, -1 to +5	*mel-26*	G84E
MT21817	*n5680*	48	100%	Dominant	Yes	N/A	LG I, -1 to +13	*mel-26*	R127C
MT21818	*n5681*	48	100%	Dominant	Yes	N/A			
MT21819	*n5682*	48	100%	Dominant	Yes	N/A			

*Determined based on failure to complement *hif-1(ia4)*, as described in Methods. Complementation tests are not possible for alleles conferring a dominant phenotype.
**Discussed in Chapter 2.

Table 1. Summary of mutants from *egl-9(lf)* egg-laying defect suppressor screen. 16 independent alleles were isolated from 50 screened pools. See text for details.

F09F9.4(n5607) suppresses the egg-laying defect of *egl-9(lf)* mutants

To identify causative mutation associated with the suppressor allele *n5607*, we performed genetic mapping using a SNP mapping strategy (Davis et al., 2005) and found that *n5607* maps between the SNPs pkP6143 and uCE6-981 on chromosome X (Figure 4A). We performed whole-genome sequencing of this strain and found four coding sequence mutations in the mapped region (Figure 4B). The *tm5190* deletion allele of one of these genes, *F09F9.4*, also suppressed the egg-laying defect of *egl-9(n586)*. We generated *trans* heterozygotes of *tm5190* and *n5607* (i.e. genotype *n5607/tm5190; nIs470; egl-9(n586)*) and found that the two alleles failed to complement, indicating that *n5607* is also an allele of *F09F9.4* (Figure 4C).

A

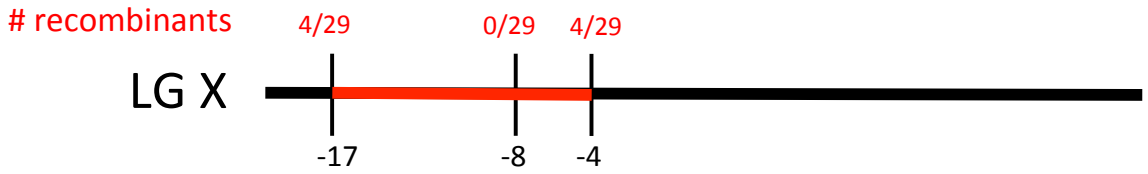

B

Chromosome	Start	Class	Description	Gene
X	2192525	missense	TGT->CGT[Cys->Arg]	*gap-1*
X	3765902	missense	CCT->TCT[Pro->Ser]	*F47B7.4*
X	4123843	missense	GTC->GAC[Val->Asp]	*F09F9.4*
X	5526944	missense	TGT->GGT[Cys->Gly]	*lgx-1*

C

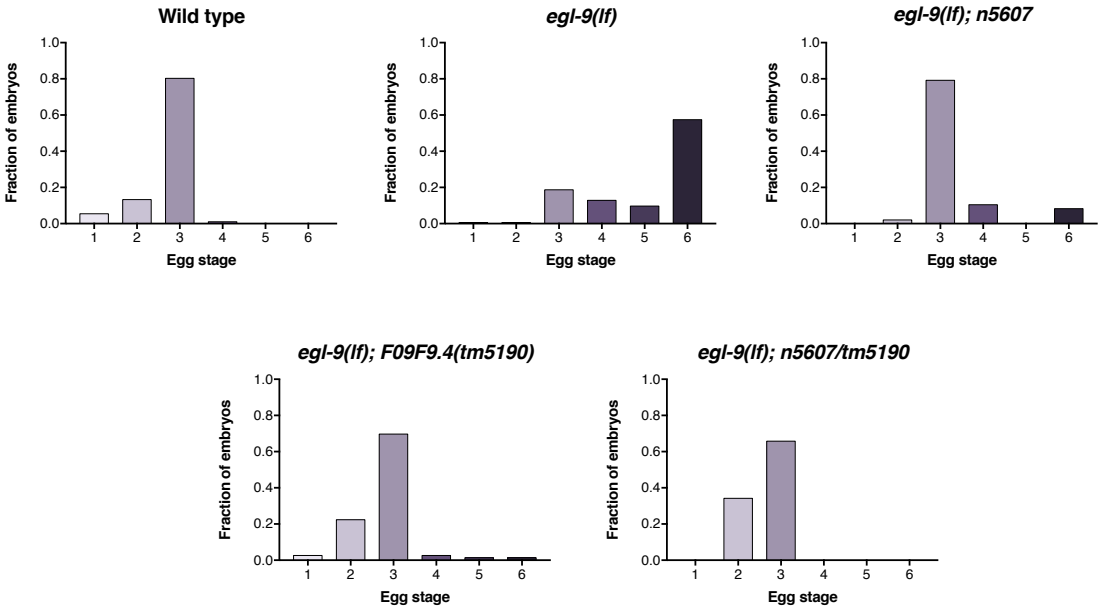

Figure 4. *F09F9.4(lf)* suppresses the *egl-9(lf)* egg-laying defect. (A) Mapping summary for *n5607.* (B) Mutations in coding sequences in the mapping interval in the strain MT21376 containing *n5607.* (C) Distribution of stages of eggs laid by adult hermaphrodites of the indicated genotypes. *n5607* significantly suppressed the egg-laying defect of *egl-9(n586)* mutants (P<0.001, Chi-square test). The 649 base-pair deletion allele *F09F9.4(tm5190)* and the *n5607/tm5190 trans* heterozygote also suppressed the *egl-9(n586)* egg-laying defect (P<0.001), indicating that *n5607* is an allele of *F09F9.4.*

The molecular function of *F09F9.4* has not been characterized. The fly homolog of *F09F9.4*, *gogo* (golden goal), regulates axon pathfinding (Hakeda-Suzuki et al., 2011; Tomasi et al., 2008) and dendrite formation (Hakeda and Suzuki, 2013). Consistent with the hypothesis of a neuronal function for *F09F9.4*, multiple studies have shown that *F09F9.4* is enriched in neurons (Kaletsky et al., 2016; Spencer et al., 2011; Von Stetina et al., 2007). Several genes that regulate axon guidance in *C. elegans* have an egg-laying constitutive (Egl-c) phenotype, i.e. lay eggs at a higher rate than wild-type animals or under conditions that would normally cause worms to inhibit egg laying. Specifically, abnormal axon pathfinding of the VC neurons, which play an inhibitory role in egg-laying behavior, leads to an Egl-c phenotype; for example, animals mutant for the netrin receptor, which has conserved and well-characterized roles in axon pathfinding, are Egl-c (Bany et al., 2003). We hypothesized that *F09F9.4(lf)* might similarly cause a nonspecific increase in egg laying.

Wild-type animals inhibit egg laying when they are not on their bacterial food source (Horvitz et al., 1982), whereas some Egl-c mutants lay eggs off of food. We tested egg-laying behavior on or off food by counting the number of eggs laid in two hours under each of these conditions (Figure 5). Wild-type animals and *egl-9(lf)* mutants laid eggs on food but not off of food; fewer eggs were laid on food by *egl-9(lf)* mutants, consistent with the observation that they are egg-laying defective. We tested several mutants identified from our *egl-9(lf)* suppressor screen in this assay and found that all mutants tested had a higher rate of egg laying than *egl-9(lf)* single mutants on food, consistent with the suppression of *egl-9(lf)* egg-laying defect observed by other assays for egg-laying behavior (e.g. stages of eggs laid by adults). Off food, most of the suppressors laid very few eggs, similar to wild-type animals and *egl-9(lf)* single mutants off food. However, *egl-9(n586); F09F9.4(n5607)* animals laid an average of ~5 eggs in 2 hours off

food, significantly more than wild-type animals or *egl-9(lf)* single mutant animals and consistent with an Egl-c phenotype of *F09F9.4(lf)*.

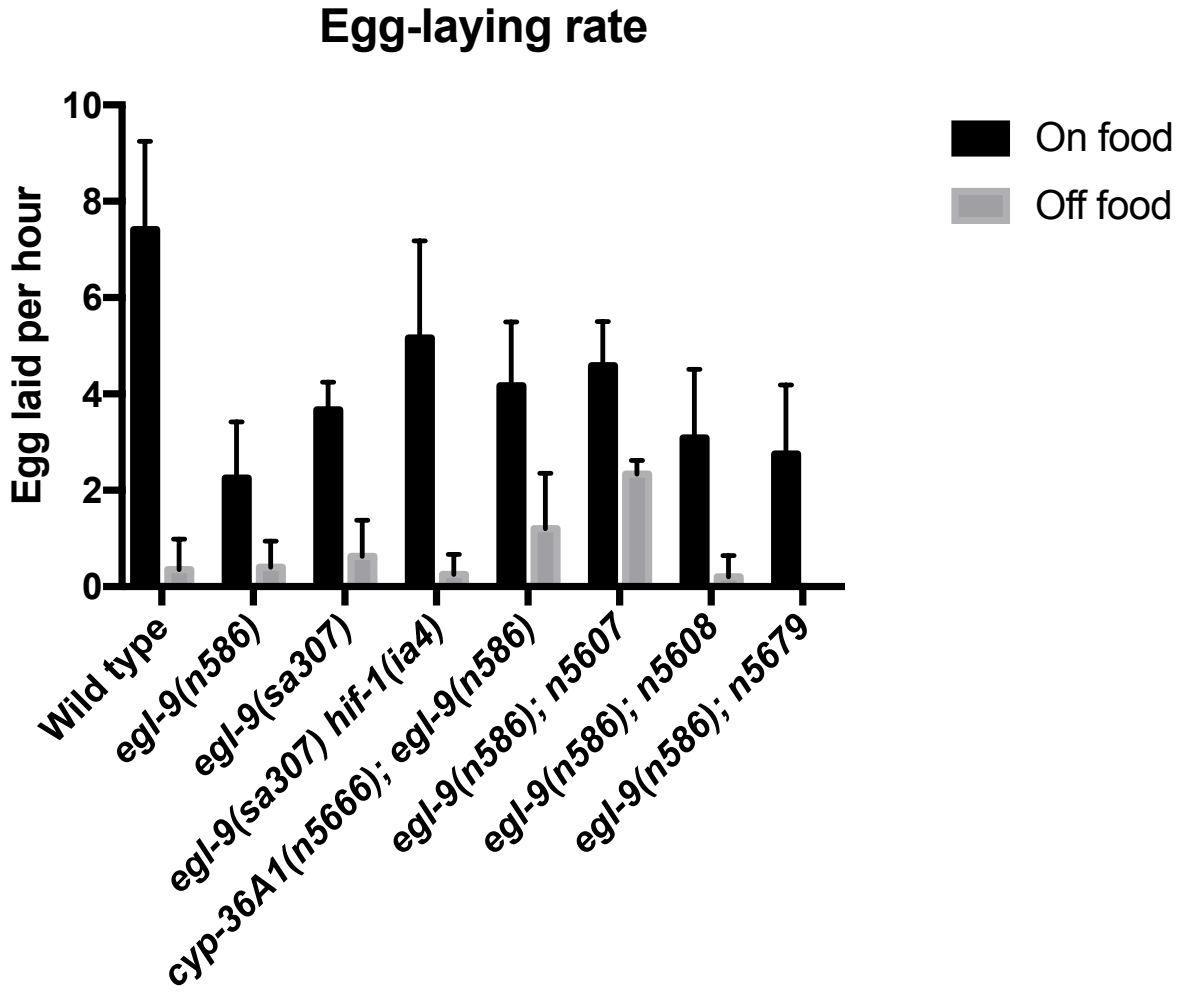

Figure 5. *F09F9.4(n5607)* promotes elevated egg-laying rate off of food. Animals were placed for two hours either on or off of bacterial food, and egg-laying rate was calculated. *egl-9(n586); n5607* mutants laid significantly more eggs off of food relative to *egl-9(n586)* animals ($P < 0.01$, Student's t-test with Bonferroni correction; other comparisons of double mutants vs. *egl-9(lf)* $P > 0.05$).

We also examined stages of eggs laid by *F09F9.4(lf)* single mutants to determine if these mutants are Egl-c. Some Egl-c mutant animals retain eggs in the uterus only briefly before laying them, and consequently lay eggs at earlier stages than wild-type animals. We performed an egg-laying assay comparing wild-type animals to *F09F9.4(tm5190)* animals and found that *F09F9.4(tm5190)* animals laid eggs at significantly earlier stages than the wild type (Figure 6). Together with the "off food" egg-laying assay, these data indicate that *F09F9.4(lf)* confers an egg-laying constitutive phenotype, in which eggs are laid after a shorter retention time in the uterus and without the same negative regulatory input from food deprivation. We suggest that the suppression of the *egl-9(lf)* egg laying defect is thus due to a nonspecific increase in egg-laying rate, rather than a specific function downstream of the *egl-9/hif-1* pathway. Further analysis will be required to understand the exact nature of the *F09F9.4(lf)* Egl-c phenotype. We speculate based on homology to *gogo* and by analogy to other Egl-c mutants that axonal pathfinding is disrupted in the VC neurons of *F09F9.4(lf)* mutants, resulting in a loss of inhibitory input into the egg-laying circuit and constitutive activation of egg-laying behavior.

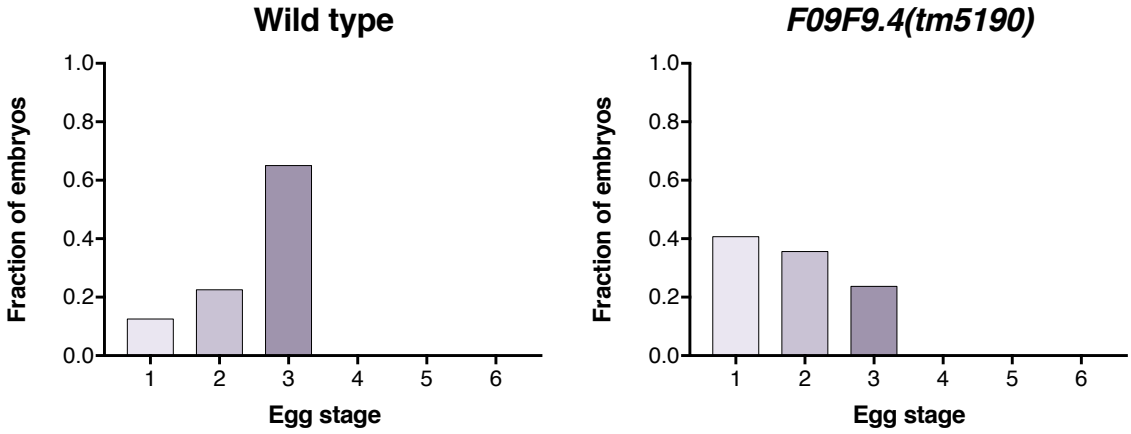

Figure 6. *F09F9.4(tm5190)* animals lay earlier-stage eggs than wild-type animals. Distribution of stages of eggs laid by adult hermaphrodites of the indicated genotypes. *F09F9.4(tm5190)* animals laid significantly earlier eggs than wild-type animals ($P < 0.001$, Chi-square test).

Mutations in *mel-26* suppress the egg-laying defect of *egl-9(lf)* mutants

We mapped the alleles *n5679* and *n5680* and found that both map to similar regions of chromosome I (Figure 7A and B). Both alleles confer a dominant phenotype and are similarly strong suppressors of the *egl-9(lf)* egg-laying defect (Table 1); we hypothesized that they might be alleles of the same gene. We performed whole-genome sequencing of both strains and found only one gene mutated in both strains in the mapped region, the maternal-effect lethal gene *mel-26* (Figure 7C). Because *n5679* and *n5680* dominantly suppress *egl-9(lf)*, we performed a modified rescue experiment to demonstrate that mutation in *mel-26* suppresses the *egl-9(lf)* egg-laying defect. Specifically, we amplified a 7 kb fragment containing *mel-26* from the *nIs470; egl-9(n586); n5679* strain (*nEx[mel-26(n5679)]*) and generated transgenic animals containing this fragment in an *nIs470; egl-9(n586)* background. We found that this mutant transgene dominantly suppressed *egl-9(n586)* egg-laying defect, indicating that the *mel-26* mutation is the causative mutation for *egl-9(lf)* suppression in the *nIs470; egl-9(n586); n5679* strain (Figure 7D).

A

***n5679* mapping**

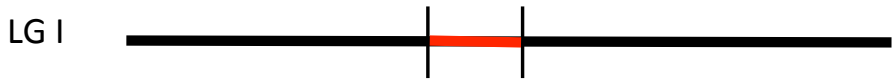

B

***n5680* mapping**

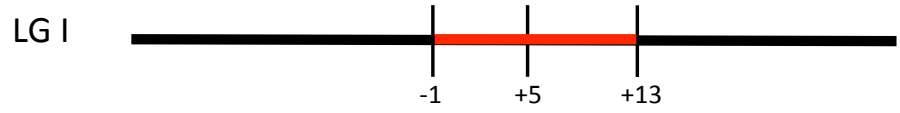

C

Allele	Chromosome	Start	Class	Description	Gene
n5679	I	9132785	missense	GGA->GAA[Gly->Glu]	*mel-26*
n5680	I	9132961	missense	CGT->TGT[Arg->Cys]	*mel-26*

D

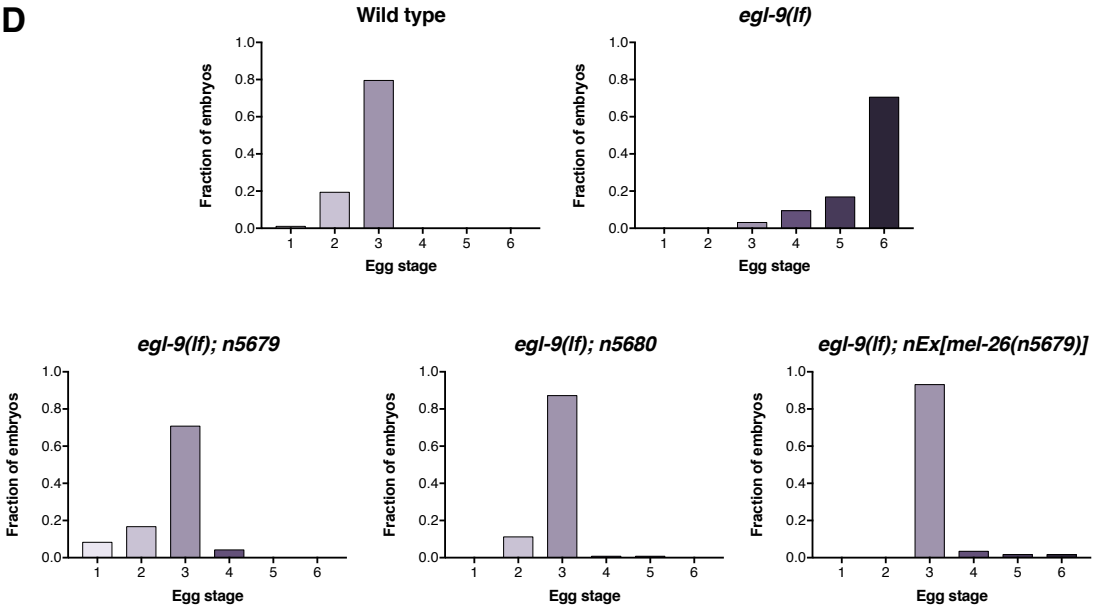

Figure 7. Mutation in *mel-26* suppresses the *egl-9(lf)* egg-laying defect. (A, B) Mapping summary for *n5679* and *n5680.* See Methods for details of mapping. (C) Strain MT21816 containing *n5679* and strain MT21817 containing *n5680* both have mutations in the coding sequence of *mel-26.* (D) Distribution of stages of eggs laid by adult hermaphrodites of the indicated genotypes. *egl-9(n586)* laid later-stage eggs than wild-type animals (P<0.001, Chi-square test). *n5679* and *n5680* both suppressed the *egl-9(lf)* egg-laying defect (P<0.001). A transgene containing *mel-26* amplified from strain MT21816 also dominantly suppressed the *egl-9(lf)* egg-laying defect (P<0.001).

mel-26 encodes an adaptor protein with multiple functions. MEL-26 interacts as a specificity factor for a CUL-3-based E3 ubiquitin ligase complex, and in this role promotes degradation of multiple proteins including the AAA-ATPases MEI-1 (katanin) and FIGL-1(Fidgetin-like 1) to control progression through meiosis and mitosis, respectively (Luke-Glaser et al., 2007; Pintard et al., 2003). MEL-26 also has CUL-3-independent functions; for example, it promotes localization of the actin-binding protein POD-1 to the cleavage furrow at cytokinesis (Luke-Glaser et al., 2005). A BTB domain in MEL-26 mediates the interaction with CUL-3, whereas interaction with other proteins, including MEI-1, FIGL-1, and POD-1, occurs through a MATH domain (Luke-Glaser et al., 2005, 2007; Pintard et al., 2003); the *n5679* and *n5680* mutations are both in this domain. Previously-identified *mel-26* alleles with mutations in the MATH domain dominantly confer maternal effect lethality by disrupting interaction with these binding partners (Luke-Glaser et al., 2005, 2007; Pintard et al., 2003). Because *mel-26* has an established role in embryonic development, we tested if *mel-26(n5679)* affects embryonic development rate, which would affect the stages of eggs laid in our assay for egg-laying defects. In parallel, we tested developmental rate for several other mutants from the suppressor screen. We found that *mel-26(n5679)* and other mutants tested developed at the same rate embryonically as wild-type animals and *egl-9(lf)* mutants (Figure S2).

We propose that *mel-26(n5679)* and *mel-26(n5680)* mutations disrupt an interaction between MEL-26 and another protein, resulting in suppression of the *egl-9(lf)* egg-laying defect rather than causing maternal effect lethality. The mechanisms by which *egl-9* and *hif-1* interact with *mel-26*, and through which *mel-26* regulates egg laying, remain unknown.

Methods

C. elegans strains and transgenes

All *C. elegans* strains were cultured as described previously (Brenner, 1974). We used the N2 Bristol strain as the reference wild-type strain, and the polymorphic Hawaiian strain CB4856 (Davis et al., 2005) for genetic mapping and SNP analysis. We used the following mutations and transgenes:

LGI: *mel-26(n5679, n5680)*

LGIII: *agIs219[$P_{T24B8.5}$::gfp::unc-54 3'UTR, P_{ttx-3}::gfp::unc-54 3'UTR]*

LGIV: *nhr-46(n6126), nIs470[P_{cysl-2}::gfp, P_{myo-2}::mCherry]*, *him-8(e1489)*

LGV: *egl-9(n586, sa307)*, *hif-1(ia4)*

LGX: *F09F9.4(n5607, tm5190)*

Unknown linkage: *nIs674[$P_{cyp-36A1}$::cyp-36A1(+) gDNA::cyp-36A1 3'UTR, P_{myo-3}::mCherry::unc-54 3'UTR]*

Extrachromosomal arrays: *otEx3156[P_{dpy-7}::hif-1(P621A), ttx-3::rfp]*, *otEx3165[$P_{unc-120}$::hif-1(P621A), ttx-3::rfp]*, *nEx2699[P_{rab-3}::hif-1(P621A)::F2A::mCherry::tbb-2 3'UTR, P_{ttx-3}::mCherry]*, *nEx2700[P_{ges-1}::hif-1(P621A)::F2A::mCherry::tbb-2 3'UTR, P_{ttx-3}::mCherry]*, *nEx2569[P_{mel-26}::mel-26(n5679) gDNA::mel-26 3'UTR, P_{myo-3}::mCherry::unc-54 3'UTR]*

Molecular biology and transgenic strain construction

The *nEx[mel-26(n5679)]* rescuing construct (transgene *nEx2569*) was generated by amplifying a PCR product from gDNA containing 3.9 kb upstream, the *cyp-36A1* locus,

and 0.6 kb downstream. All remaining constructs were generated using the Infusion cloning technique (Clontech). The *ges-1* (intestine) and *rab-3* (neurons) promoter fragments contain 2.9 and 1.4 kb, respectively, of sequence upstream of the start codons of each of these genes. *F38A6.3a* with a P621A stabilizing mutation was used for *hif-1* cDNA (Pocock and Hobert, 2008). The F2A sequence served as a ribosomal skip sequence to cause separation of the two peptides encoded before and after the F2A (Ahier and Jarriault, 2014). Transgenic strains were generated by germline transformation as described (Mello et al., 1991). All transgenic constructs were injected at 2.5 – 50 ng/µl.

Mutagenesis screen for suppressors of *egl-9*

To screen for suppressors of the *egl-9* egg-laying defect, we mutagenized *egl-9(n586)* mutants with ethyl methanesulfonate (EMS) as described previously (Brenner, 1974). The starting strain contained the $P_{cysl\text{-}2}$*::gfp (nIs470)* transgene, which is highly expressed in *egl-9(lf)* mutants and served as a reporter for HIF-1 activity (Ma et al., 2012). We used a dissecting microscope to screen the F2 progeny for suppression of the egg-laying defect (i.e. the Egl phenotype), picking (1) adults that appeared less Egl than *egl-9(n586)* mutants, and (2) eggs laid by the F2 animals that were at an earlier developmental stage than those laid by *egl-9(n586)* mutants. Screen isolates were backcrossed to determine dominant vs. recessive and single-gene inheritance pattern and, for alleles conferring a recessive phenotype, crossed with *him-8(e1489); egl-9(sa307) hif-1(ia4)* males to test complementation with *hif-1(lf)*. *n5607, n5679,* and *n5680* were genetically mapped by SNP mapping (Davis et al., 2005) using a strain containing *egl-9(n586)* introgressed into the Hawaiian strain CB4856 (Ma et al., 2013). SNP typing was performed on 8 SNPs per

chromosome to identify where recombination occurred. Due to the dominant nature of *n5679* and *n5680*, recombinants for mapping were selected based on the wild-type phenotype. Whole-genome sequencing identified mutations in the mapped intervals, and transgenic rescue identified the causal mutations for *n5607* and *n5679*, as described in the text.

Egg-laying behavioral assays

To quantify egg-laying behavior, we scored the developmental stages of eggs laid by young adult hermaphrodites as described previously (Ringstad and Horvitz, 2008). Egg-laying defective mutants retain eggs longer in the uterus, thus laying them at later developmental stages. To score egg-laying rate, one young adult animal per plate was placed for two hours either on or off of bacterial food (*E. coli* strain OP50), and egg-laying rate (eggs per hour) was calculated.

Developmental rate of suppressor mutants

Embryos were dissected from young adult hermaphrodites. 1 or 2-cell embryos were selected for observation throughout embryonic development, and developmental stage was recorded every hour.

Statistical Analysis

Chi-square tests were used to compare the distribution of stages of eggs laid by wild-type and mutant animals. Unpaired t-tests were used to compare egg-laying rates between strains. In cases of multiple comparisons, a Bonferroni correction was applied.

Supplemental Figures

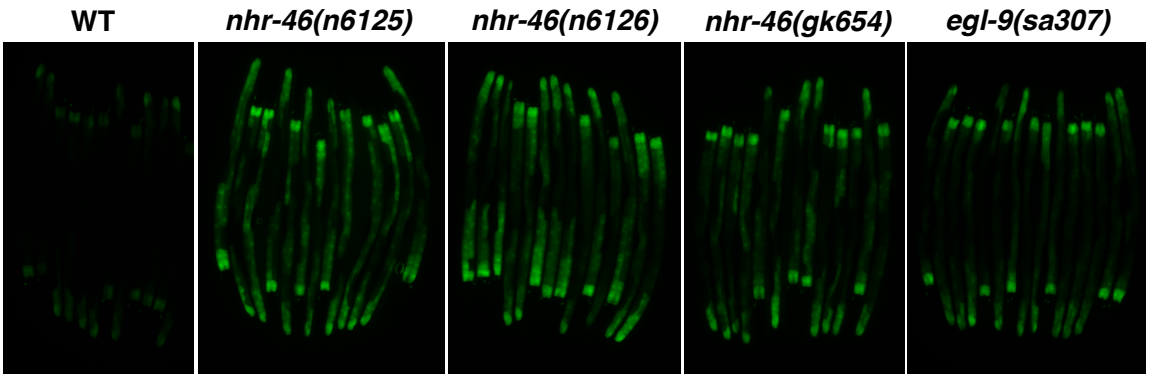

Figure S1. *nhr-46(lf)* single mutants have increased expression of $P_{T24B8.5}$*::gfp.*

nhr-46(n6125), *nhr-46(n6126)*, and *nhr-46(gk654)* animals have increased expression of the $P_{T24B8.5}$*::gfp* transcriptional reporter relative to wild-type animals, similar to *egl-9(sa307)* single mutants or *cyp-36A1(lf); nhr-46(lf); egl-9(lf)* triple mutants (see Chapter 2). GFP fluorescence micrographs of worms lined up side-by-side are shown; from left to right, *n*=12, 13, 14, 13, and 15 worms.

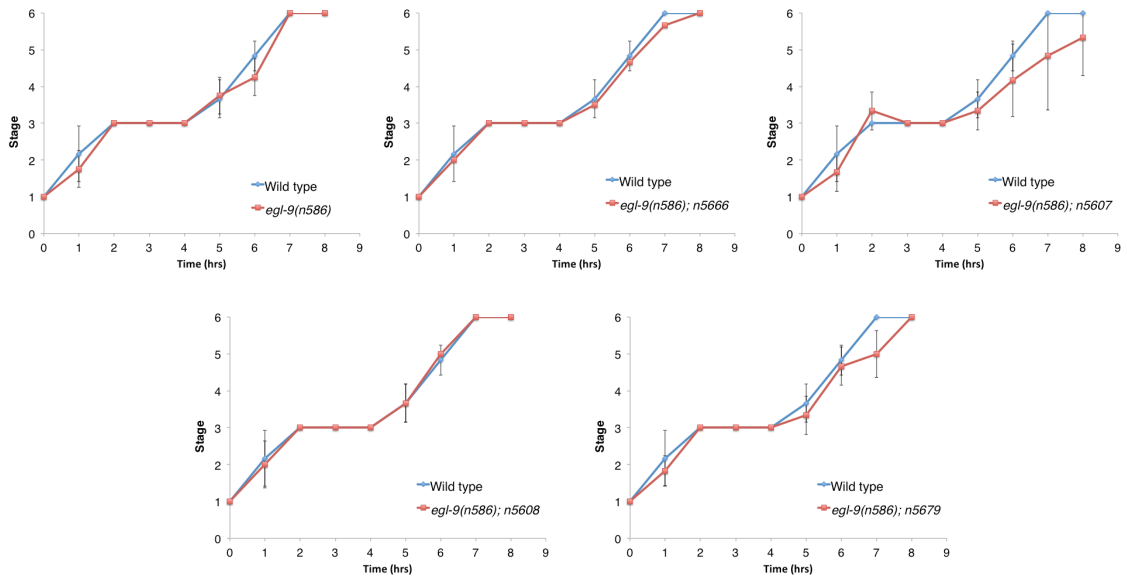

Figure S2. Developmental rates of suppressor mutants. Embryos were dissected from young adult hermaphrodites. 1 or 2-cell embryos were selected for observation throughout embryonic development, and developmental stage was recorded every hour. See Fig. 1A for embryonic stages. Developmental rate was similar for all mutants as compared to wild-type animals.

Acknowledgments

We thank Steve Sando and Vivek Dwivedi for helpful comments concerning this chapter.

References

Ahier, A., and Jarriault, S. (2014). Simultaneous expression of multiple proteins under a single promoter in *Caenorhabditis elegans* via a versatile 2A-based toolkit. Genetics *196*, 605–613.

Bany, I.A., Dong, M.-Q., and Koelle, M.R. (2003). Genetic and Cellular Basis for Acetylcholine Inhibition of *Caenorhabditis elegans* Egg-Laying Behavior. J. Neurosci. *23*, 8060–8069.

Brenner, S. (1974). The genetics of *Caenorhabditis elegans*. Genetics *77*, 71–94.

Chang, A.J., and Bargmann, C.I. (2008). Hypoxia and the HIF-1 transcriptional pathway reorganize a neuronal circuit for oxygen-dependent behavior in *Caenorhabditis elegans*. Proc. Natl. Acad. Sci. *105*, 7321–7326.

Davis, M.W., Hammarlund, M., Harrach, T., Hullett, P., Olsen, S., and Jorgensen, E.M. (2005). Rapid single nucleotide polymorphism mapping in *C. elegans*. BMC Genomics *6*, 118.

Hakeda, S., and Suzuki, T. (2013). Golden goal controls dendrite elongation and branching of multidendritic arborization neurons in Drosophila. Genes Cells *18*, 960–973.

Hakeda-Suzuki, S., Berger-Müller, S., Tomasi, T., Usui, T., Horiuchi, S., Uemura, T., and Suzuki, T. (2011). Golden Goal collaborates with Flamingo in conferring synaptic-layer specificity in the visual system. Nat. Neurosci. *14*, 314–323.

Horvitz, H.R., Chalfie, M., Trent, C., Sulston, J.E., and Evans, P.D. (1982). Serotonin and octopamine in the nematode *Caenorhabditis elegans*. Science *216*, 1012–1014.

Kaletsky, R., Lakhina, V., Arey, R., Williams, A., Landis, J., Ashraf, J., and Murphy, C.T. (2016). The *C. elegans* adult neuronal IIS/FOXO transcriptome reveals adult phenotype regulators. Nature *529*, 92–96.

Luke-Glaser, S., Pintard, L., Lu, C., Mains, P.E., and Peter, M. (2005). The BTB Protein MEL-26 Promotes Cytokinesis in *C. elegans* by a CUL-3-Independent Mechanism. Curr. Biol. *15*, 1605–1615.

Luke-Glaser, S., Pintard, L., Tyers, M., and Peter, M. (2007). The AAA-ATPase FIGL-1 controls mitotic progression, and its levels are regulated by the CUL-3MEL-26 E3 ligase in the *C. elegans* germ line. J. Cell Sci. *120*, 3179–3187.

Ma, D.K., Vozdek, R., Bhatla, N., and Horvitz, H.R. (2012). CYSL-1 interacts with the O_2-sensing hydroxylase EGL-9 to promote H2S-modulated hypoxia-induced behavioral plasticity in *C. elegans*. Neuron *73*, 925–940.

Ma, D.K., Rothe, M., Zheng, S., Bhatla, N., Pender, C.L., Menzel, R., and Horvitz, H.R. (2013). Cytochrome P450 drives a HIF-regulated behavioral response to reoxygenation by *C. elegans*. Science *341*, 554–558.

Mello, C.C., Kramer, J.M., Stinchcomb, D., and Ambros, V. (1991). Efficient gene transfer in *C. elegans*: extrachromosomal maintenance and integration of transforming sequences. EMBO J. *10*, 3959.

Pintard, L., Willis, J.H., Willems, A., Johnson, J.-L.F., Srayko, M., Kurz, T., Glaser, S., Mains, P.E., Tyers, M., Bowerman, B., et al. (2003). The BTB protein MEL-26 is a substrate-specific adaptor of the CUL-3 ubiquitin-ligase. Nature *425*, 311–316.

Pocock, R., and Hobert, O. (2008). Oxygen levels affect axon guidance and neuronal migration in *Caenorhabditis elegans*. Nat. Neurosci. *11*, 894–900.

Ringstad, N., and Horvitz, H.R. (2008). FMRFamide neuropeptides and acetylcholine synergistically inhibit egg-laying by *C. elegans*. Nat. Neurosci. *11*, 1168–1176.

Spencer, W.C., Zeller, G., Watson, J.D., Henz, S.R., Watkins, K.L., McWhirter, R.D., Petersen, S., Sreedharan, V.T., Widmer, C., Jo, J., et al. (2011). A spatial and temporal map of *C. elegans* gene expression. Genome Res. *21*, 325–341.

Tomasi, T., Hakeda-Suzuki, S., Ohler, S., Schleiffer, A., and Suzuki, T. (2008). The Transmembrane Protein Golden Goal Regulates R8 Photoreceptor Axon-Axon and Axon-Target Interactions. Neuron *57*, 691–704.

Trent, C., Tsung, N., and Horvitz, H.R. (1983). Egg-laying defective mutants of the nematode *Caenorhabditis elegans*. Genetics *104*, 619–647.

Von Stetina, S.E., Watson, J.D., Fox, R.M., Olszewski, K.L., Spencer, W.C., Roy, P.J., and Miller, D.M. (2007). Cell-specific microarray profiling experiments reveal a comprehensive picture of gene expression in the *C. elegans* nervous system. Genome Biol. *8*, R135.

Chapter Four

Future Directions

Analysis of CYP-36A1 and NHR-46-dependent hormone signaling

The identification of the CYP-36A1/NHR-46 hormone-signaling pathway downstream of HIF-1 suggests a number of additional studies that might further illuminate the mechanisms by which HIF-1 regulates behavior and physiology. First, additional characterization of CYP-36A1 and NHR-46 will likely provide insight into their molecular functions. In particular, it would be of great interest to identify the putative NHR-46 ligand(s) that we propose to be synthesized by CYP-36A1.

The approaches used to identify ligands of another *C. elegans* nuclear hormone receptor, DAF-12, suggest strategies for identification of the NHR-46 ligand(s). Entry of *C. elegans* larvae into a stress-resistant larval stage, called dauer, is regulated by a cytochrome P450 enzyme, DAF-9, which synthesizes cholesterol-derived ligands of the downstream nuclear hormone receptor DAF-12 (Antebi et al., 1998, 2000; Gerisch and Antebi, 2004; Gerisch et al., 2001, 2007; Motola et al., 2006). Recently, endogenous ligands of the nuclear hormone receptor DAF-12 were identified using an approach that combined activity-guided fractionation with comparative metabolomics (Mahanti et al., 2014). In that study, a heterologous reporter assay for DAF-12 activity and *daf-9(lf)* mutant rescue assays were used to identify metabolome fractions involved in DAF-12 activation; 2D-NMR and gas chromatography-mass spectrometry (GC-MS) were then used to identify ligand candidates in the active fractions; and candidates were assayed for binding to DAF-12 and biological activity. A similar approach might be useful in the determination of NHR-46 ligands, which we propose are also synthesized by a cytochrome P450 enzyme and require cholesterol as a precursor, as detailed in Chapter 2. The first step in using such an approach would involve the development of an assay for activity of the putative NHR-46 ligand. Rescue of the *cyp-36A1(lf); egl-9(lf)* mutant phenotype might represent such an assay.

Preliminary attempts to rescue *cyp-36A1(lf); egl-9(lf)* with *egl-9(lf)* worm extracts, or to suppress the *egl-9(lf)* mutant phenotype with *cyp-36A1(lf); egl-9(lf)* extracts, were unsuccessful; further optimization is likely required to see rescue, e.g. higher concentrations of the extract. Development of a heterologous reporter assay for NHR-46 activity might also prove useful, e.g. expression of luciferase or another reporter under the promoter of a direct NHR-46 transcriptional target in cell culture. Currently no NHR-46 direct targets have been identified, but *T24B8.5* and other *cyp-36A1*-regulated genes are candidate targets; chIP-seq of NHR-46 might identify such targets.

Continued genetic analysis might also further elaborate the pathway involved in hormonal signaling downstream of HIF-1. If the function of CYP-36A1 is to synthesize the ligand of NHR-46, there are likely other enzymes involved in the biosynthesis of this hormone; genetic screens might identify the genes encoding these putative biosynthetic enzymes. A screen for mutants that phenocopy *cyp-36A1(lf)*, i.e. suppress both the egg-laying defect and high *T24B8.5* expression of *egl-9(sa307)* mutants, identified two independent suppressors; both mutations (*n6276* and *n6277*) failed to complement *cyp-36A1(gk824636)* and are thus presumably alleles of *cyp-36A1*. However, this screen might not be saturated, and was conducted using the stronger *sa307* allele of *egl-9*. Additional *egl-9(lf)* suppressor screens with more animals, the weaker *egl-9(n586)* allele, or different reporters for *cyp-36A1*-dependent gene expression might identify genes other than *cyp-36A1* involved in the synthesis of the putative NHR-46 ligand.

Identification of parallel and downstream pathways mediating HIF-1 regulation of egg laying

As described in Chapter 3, multiple lines of evidence indicate that there are additional pathways regulating egg-laying behavior downstream of *egl-9/hif-1* in addition to the *cyp-36A1/nhr-46* pathway. I propose several screens that might identify parallel and/or downstream pathways involved in egg-laying inhibition.

Screen 1: First, a screen similar to the original *egl-9(lf)* suppressor screen might identify downstream or parallel pathways regulating egg laying. I propose a slight modification to the original screen: rather than using the $P_{cysl\text{-}2}$*::gfp* reporter, which reflects expression of the putative HIF-1 direct target *cysl-2*, using the $P_{T24B8.5}$*::gfp* reporter would provide a more informative readout for classifying suppressor mutants. *T24B8.5* expression is low in *cyp-36A1(lf); egl-9(lf)* mutants, intermediate in wild-type animals or *egl-9(lf) hif-1(lf)* mutants, and high in *egl-9(lf)* mutants; thus suppressors of the *egl-9(lf)* egg-laying defect can be immediately classified based on expression of this reporter as (A) *cyp-36A1(lf)*-like, (B) *hif-1(lf)*-like, or (C) other (affects only egg-laying, not reporter expression), and might define genes that (A) act with *cyp-36A1* and, as described above, could affect synthesis of the putative NHR-46 ligand; (B) affect *hif-1* function broadly; or (C) represent pathways that regulate egg laying without affecting expression of all *cyp-36A1*-regulated genes. I further suggest the use of off-food egg-laying behavior as a preliminary means of categorizing mutants based on whether they have an Egl-c (egg-laying constitutive) phenotype and thus might represent nonspecific regulators of egg-laying behavior, similar to *F09F9.4(lf)*, rather than functioning specifically downstream of HIF-

1. This analysis is also applicable to other screens described here for which the mutant phenotype is suppression of an egg-laying defect (Screens 2 and 3 below).

Screen 2: A variation on Screen 1 involves screening for suppressors of the *cyp-36A1(lf); nhr-46(lf); egl-9(lf)* egg-laying defect, again using the $P_{T24B8.5}$*::gfp* reporter to classify suppressor mutants. As with Screen 1, this screen could identify pathways acting downstream of or in parallel to the *cyp-36A1*/*nhr-46* pathway. Unlike Screen 1, I do not expect this screen to identify upstream regulators of NHR-46 function, thus making it more suitable for specifically identifying downstream or parallel pathways. However, the triple mutant starting strain makes post-screen mapping and analysis more challenging.

Screen 3: As noted in Chapter 3, *cyp-36A1(lf); egl-9(lf)* mutants are still noticeably egg-laying defective when grown at 25°C. Presumably, the residual egg-laying defect is caused by continued activity of a pathway acting in parallel to the *cyp-36A1*/*nhr-46* pathway. A screen for enhancers of the *cyp-36A1(lf)* mutant phenotype might identify this pathway, i.e. third-site mutations that are less egg-laying defective than *cyp-36A1(lf); egl-9(lf)* animals grown at 25°C. I propose using the P_{cysl-2}*::gfp* reporter for this screen. Expression of this reporter is high in *cyp-36A1(lf); egl-9(lf)* double mutants, similar to *egl-9(lf)* single mutants. Mutations that suppress both *cyp-36A1(lf); egl-9(lf)* egg-laying defect and reporter expression likely would define genes that function broadly in HIF-1 pathway function, whereas those that suppress only the egg-laying defect presumably would represent genes that function more specifically in the regulation of egg laying. The $P_{T24B8.5}$*::gfp* reporter would likely not be as useful of a tool in this screen, as its

expression is already very low in *cyp-36A1(lf); egl-9(lf)* double mutants and as such enhancement of low reporter expression would be more difficult to assess.

Screen 4: As discussed in Chapter 3, *cyp-36A1(OE)* animals or *nhr-46(lf)* mutants are not egg-laying defective, presumably because a parallel pathway downstream of HIF-1 is not engaged in the absence of *egl-9(lf)* mutation. As a complementary approach to screen 3, I propose that this parallel pathway could be identified by searching for mutations that cause a synthetic egg-laying defect in combination with *cyp-36A1(OE)* or *nhr-46(lf)*. A caveat of this screen is that it would also identify mutants that are egg-laying defective (Egl) on their own and would thus require additional analysis to determine whether the egg-laying defect is synthetic. As such, I would suggest that this screen should be lower priority than the other screens described above. Nonetheless, there are strategies available to determine whether the defect is synthetic. For example, for mutants with an Egl phenotype in an *nhr-46(lf)* background, an *nhr-46(+)* rescuing transgene would rescue the egg-laying defect only if the defect is synthetic between *nhr-46(lf)* and the second-site mutation.

Tissue-specific analysis of NHR-46-mediated transcriptional changes

One or more of the screens described above might reveal an NHR-46 transcriptional target that regulates egg-laying behavior, and as such, genes identified from these screens should be analyzed for *nhr-46*-dependent expression changes. As a complementary approach, *nhr-46*-mediated transcriptional changes could be used to search for candidate regulators of egg-laying behavior. Although clear candidates for genes regulating egg laying downstream of *egl-9* and

cyp-36A1 were not identified from the RNA-seq experiment described in Chapter 2, this experiment looked at only transcriptional changes of the entire worm. Because we showed that *nhr-46(+)* best rescues the *nhr-46(lf)* egg-laying phenotype when expressed in neurons, I propose performing tissue-specific RNA-seq of neurons from the wild type, *egl-9(lf)* mutants, *cyp-36A1(lf); egl-9(lf)* double mutants, and *cyp-36A1(lf); nhr-46(lf); egl-9(lf)* triple mutants to identify candidate NHR-46 effectors that control egg laying. Specifically, this analysis should search for genes exhibiting differential expression in *egl-9(lf)* mutants relative to wild-type animals and for which the differential expression is suppressed in *cyp-36A1(lf); egl-9(lf)* double mutants. The double-mutant expression phenotype should in turn be suppressed in *cyp-36A1(lf); nhr-46(lf); egl-9(lf)* triple mutants. Priority should be given to genes previously shown to have roles in the regulation of egg-laying behavior, and loss-of-function or gain-of-function (e.g. overexpression) alleles should be tested, as appropriate, for ability to suppress the egg-laying defects of *egl-9(lf)* and *cyp-36A1(lf); nhr-46(lf); egl-9(lf)* mutants.

Using chIP-seq and RNA-seq data to identify candidate HIF-1 direct targets

As described in Chapter 2, we identified 366 genes that are upregulated in *egl-9(lf)* mutants in a *hif-1*-dependent manner. Some of these genes presumably represent direct transcriptional targets of HIF-1. We also found 1,322 genes that are downregulated in *egl-9(lf)* mutants in a *hif-1*-dependent manner; however, previous work has found roles for HIF functioning only as a transcriptional activator, suggesting that the HIF-mediated transcriptional repression we observed occurs indirectly (Semenza, 2010). In addition to the RNA-seq datasets generated in our studies, two chIP-seq datasets of *C. elegans* HIF binding sites are available:

HIF-1 (HIFα) binding and AHA-1 (HIFβ) binding. Several genes thought to be direct HIF-1 targets, such as *cysl-2*, *nhr-57*, and *cyp-36A1*, have peaks in their regulatory regions in one or both of these datasets. I propose to generate a list of candidate *C. elegans* HIF targets based on the overlap of the HIF-1-upregulated genes (from RNA-seq) and HIF binding (from one or both chIP-seq experiments). Worms mutant for these candidates can then be tested for functional roles in HIF-1-regulated behavior or stress responses, such as (1) survival in hypoxia (Jiang et al., 2001); (2) egg-laying in hypoxia (Miller and Roth, 2009); (3) resistance to *Pseudomonas aeruginosa* infection in the slow killing assay (Bellier et al., 2009), fast killing assay (Darby et al., 1999), or liquid killing assay (Kirienko et al., 2013); (4) resistance to tunicamycin (Leiser et al., 2015); (5) resistance to oxidative stress (Bellier et al., 2009); (6) O2-ON response (Ma et al., 2012); or others (see Chapter 1, section IV). In some cases (e.g. (1), (2), or the *Pseudomonas* liquid killing assay), *hif-1(lf)* has an effect on its own and thus candidates can be directly tested in the assay; for other phenotypes, candidate mutants will need to be evaluated for their ability to suppress *egl-9(lf)*. To facilitate this analysis, *egl-9(RNAi)* might be useful to the extent that it can recapitulate the *egl-9(lf)* phenotype, such that candidate mutants can be paired with *egl-9(RNAi)* to observe genetic interactions.

Screens for novel upstream regulators of HIF-1 activity

Here we show that HIF-1 activation by *egl-9(lf)* drives an egg-laying defect. Interestingly, *vhl-1(lf)* mutants, which fail to degrade HIF-1, or animals with a nondegradable HIF-1 variant transgene display wild-type egg-laying behavior, indicating that HIF-1 stabilization is not sufficient to drive egg-laying inhibition downstream of *egl-9*. Previous work has demonstrated that both HIF-1 stability and transcriptional activity are regulated by EGL-9

and represent *vhl-1*-dependent and independent pathways, respectively (Shao et al., 2009; Shen et al., 2006). Several *egl-9/hif-1*-regulated phenotypes, including pathogen resistance (Shao et al., 2010) and regulation of a locomotory response to ischemia-reperfusion (Ma et al., 2012), are observed only upon HIF-1 activation by both *vhl-1*-dependent and independent pathways. That *vhl-1(lf)* and *hif-1(gf)* mutants are not egg-laying defective suggests that inhibition of egg laying by *egl-9* and *hif-1* similarly requires both of these pathways. The WD-repeat protein SWAN-1 appears to function in parallel to VHL-1 to regulate several EGL-9-dependent phenotypes, including modulation of egg laying (Shao et al., 2010); however, SWAN-1 function does not fully explain the VHL-independent effects of EGL-9, and the mechanism by which SWAN-1 affects HIF-1 transcriptional activity is not well understood. I propose that the difference between *egl-9(lf)* and *vhl-1(lf)* mutants with respect to egg laying could be used as the basis for a screen to identify genes that act in the *vhl-1*-independent pathway downstream of *egl-9*. Specifically, I propose performing a screen of *vhl-1(lf)* mutants for second-site mutations that cause synthetic egg-laying defects; such mutations might define genes in the *vhl-1*-independent pathway. This screen would ideally be conducted using the $P_{cysl\text{-}2}$*::gfp* transgene as a second readout for HIF-1 activity; expression of *cysl-2* is much higher in *egl-9(lf)* mutants than in *vhl-1(lf)* mutants, indicating that *cysl-2* expression downstream of HIF-1 is regulated by the *vhl-1*-independent pathway (Shao et al., 2009). Mutation of a gene required for the *vhl-1*-independent regulation of HIF-1 should induce both an egg-laying defect and increased expression of $P_{cysl\text{-}2}$*::gfp* in a *vhl-1(lf)* mutant background. Use of the transgene would increase the specificity of the screen and reduce the likelihood of recovering mutants that are egg-laying defective independent of the *egl-9/hif-1* pathway.

Characterization of other *egl-9/hif-1/cyp-36A1*-regulated behaviors

Multiple behaviors other than egg laying are regulated by *egl-9*, *hif-1*, and *cyp-36A1.* As described in Chapter 2, both locomotion and defecation occur at a slower rate in *egl-9(lf)* mutants than in wild-type animals; both defects are fully suppressed by *hif-1(lf)* and partially suppressed by *cyp-36A1(lf)*. In addition, I have identified two other behaviors that are regulated by *egl-9*, *hif-1* and *cyp-36A1*, described below: (1) burst pumping behavior and (2) behavioral avoidance of pathogen. It would be interesting to identify the mechanisms by which *egl-9*, *hif-1*, and *cyp-36A1* regulate each of these other behaviors, and to determine the extent to which those mechanisms overlap with the mechanisms controlling egg-laying behavior by this pathway.

(1) In collaboration with Steve Sando, I found that *egl-9(lf)* mutants are defective in an aspect of pharyngeal behavior called "burst pumping" (Figure 1). When exposed to 365 nm ultraviolet light, wild-type worms initially reduce their rate of feeding (i.e. rate of contraction, or pumping, of the pharynx), followed by a brief increase in pumping rate (burst pumping) prior to a sustained pumping rate inhibition (Bhatla and Horvitz, 2015; Bhatla et al., 2015). Although feeding behavior under standard conditions appears essentially normal in *egl-9(lf)* mutants, the rate of burst pumping is dramatically reduced in *egl-9(lf)* animals exposed to 365 nm light (Figures 1A and 1E, black vs. red lines). As with defecation and locomotion, this behavioral defect is fully suppressed by *hif-1(lf)* and partially suppressed by *cyp-36A1(lf)* (Figures 1A to 1G). Interestingly, the pumping response to light is thought to result from the generation of reactive oxygen species by the light (Bhatla and Horvitz, 2015). As described in Chapters 1 and 2, HIF activity can protect against ROS; thus changes in resistance to ROS in *egl-9(lf)* mutants might contribute to the *egl-9(lf)* abnormality in burst pumping.

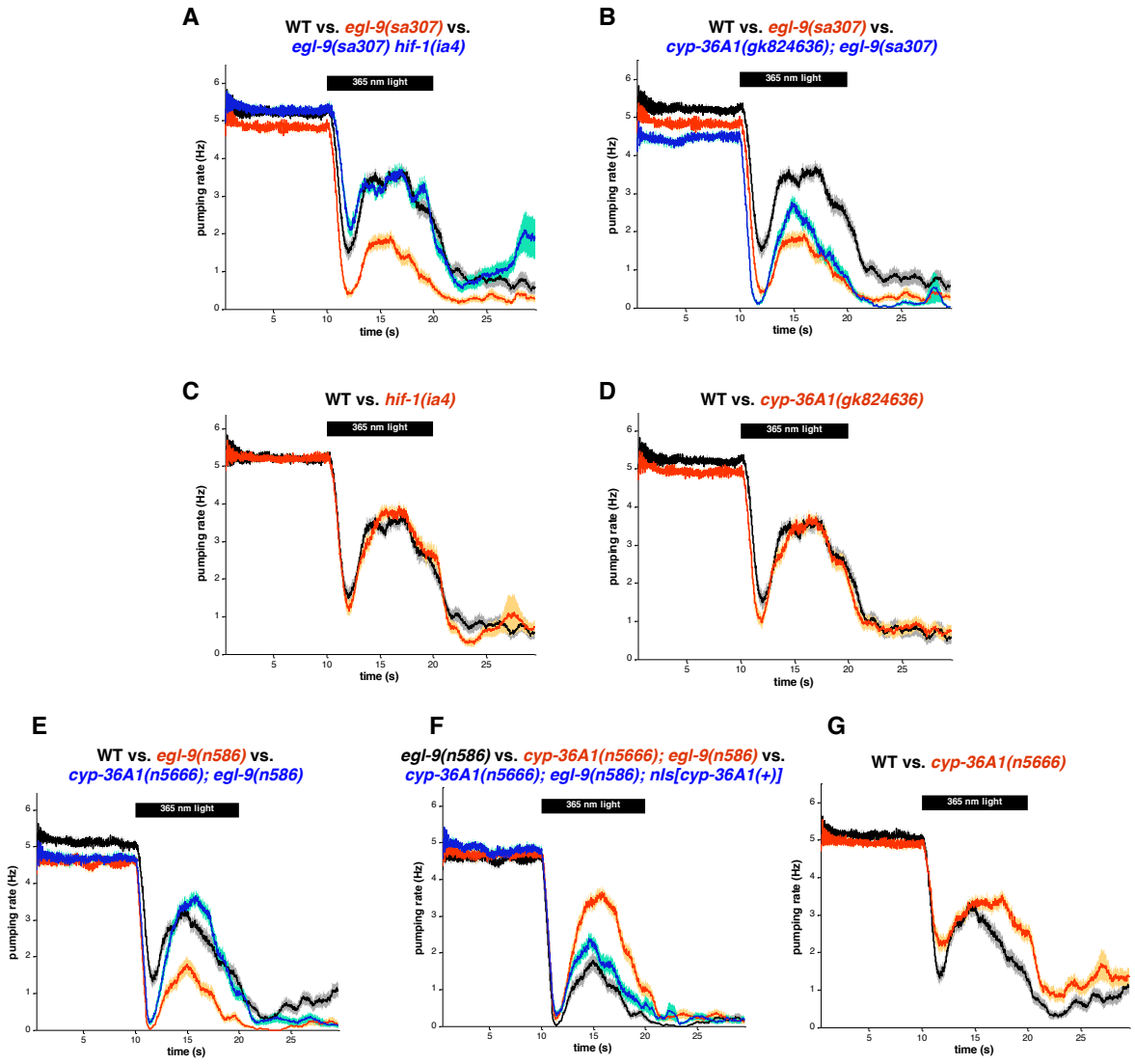

Figure 1. *egl-9(lf)* mutants have a defect in burst pumping that requires *hif-1* and *cyp-36A1*. (A) *egl-9(sa307)* mutants had a lower rate of burst pumping relative to wild-type animals (red vs. black line). This defect was suppressed by a second mutation in *hif-1* (blue vs. red line). (B) *cyp-36A1(lf)* partially suppressed the burst-pumping defect of *egl-9(sa307)* mutants (blue vs. red line). (C, D) *hif-1(ia4)* and *cyp-36A1(gk824636)* single mutants displayed wild-type burst-pumping behavior. (E) *egl-9(n586)* mutants also displayed a reduction in burst-pumping rate (red vs. black line), which was suppressed by *cyp-36A1(n5666)* (blue vs. red line). (F) The *nIs[cyp-36A1(+)]* transgene (*nIs674)*, which contains wild-type *cyp-36A1*, rescued the suppression of the burst-pumping defect observed in *cyp-36A1(n5666); egl-9(n586)* mutants (blue vs. red line). (G) *cyp-36A1(n5666)* single mutants displayed wild-type burst-pumping behavior. Strains in (E-G) contained the $P_{cysl\text{-}2}$*::gfp* transgene *nIs470.* Assay for pumping rate in response to light was performed as described previously (Bhatla and Horvitz, 2015).

(2) In the course of characterizing the survival of *egl-9(lf)* mutants on the pathogen *Pseudomonas aeruginosa*, I also found that *egl-9(lf)* mutants are defective in behavioral avoidance of the *P. aeruginosa* strain PA14, i.e. lawn-leaving behavior (Figure 2A). Such avoidance is normally observed within a day of exposure to *Pseudomonas* (Meisel and Kim, 2014). This defect is fully suppressed by *hif-1(lf)* and partially suppressed by *cyp-36A1(lf)* (Figure 2A), indicating that the *egl-9/hif-1/cyp-36A1* pathway regulates the behavioral response to pathogen exposure. Wild-type PA14 avoidance is dependent on normal aerotaxis behavior (Reddy et al., 2009), and *egl-9(lf)* mutants have previously been shown to display abnormal aerotaxis (Chang and Bargmann, 2008). We found that normal avoidance behavior was restored in *egl-9(lf)* when the avoidance assay was performed at 4% oxygen (Figure 2B), which eliminates the influence of abnormal aerotaxis on avoidance behavior (Meisel et al., 2014; Reddy et al., 2009). We thus suggest that the *egl-9(lf)* defect in avoidance is caused by abnormalities in aerotaxis behavior; the molecular mechanism by which *egl-9* regulates aerotaxis is not well understood (Chang and Bargmann, 2008).

New mutants that define genes mediating egg-laying inhibition downstream of *egl-9*, such as those that might be identified in the screens described in the sections above, should also be tested for their locomotion, defecation, burst pumping, and pathogen avoidance behaviors. Dedicated screens could also be conducted to specifically identify regulators of each of these behaviors.

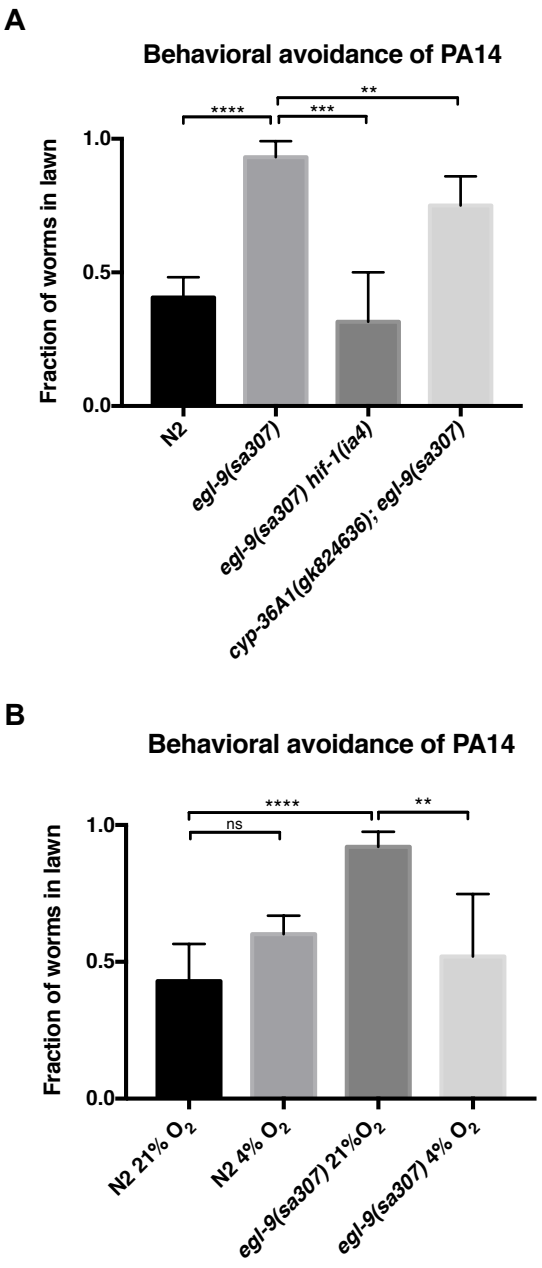

Figure 2. *egl-9(lf)* mutants have a defect in pathogen avoidance behavior that requires *hif-1* and *cyp-36A1*. (A) *egl-9(sa307)* mutants had a reduction in lawn-leaving behavior after exposure to the pathogenic *P. aeruginosa* strain PA14. This defect was suppressed by *hif-1(ia4)* and partially suppressed by *cyp-36A1(gk824636)*. **P < 0.01, ***P < 0.001, and ****P < 0.0001 considered significant (Student's t-test with Holm-Bonferroni correction). (B) Performing the avoidance assay in 4% oxygen suppressed the avoidance defect of *egl-9(sa307)* mutants. **P < 0.01 and ****P < 0.0001 considered significant. ns, not significant (P > 0.05) (Student's t-test with Holm-Bonferroni correction). Avoidance assays were performed as described previously (Meisel et al., 2014), scoring avoidance after 18 hours (A) or 20 hours (B) of exposure to PA14.

Acknowledgments

I thank Josh Saul and Calista Diehl for helpful comments concerning this chapter. I thank Steve Sando for performing the experiments shown in Figure 1, and for helpful discussion and comments.

References

Antebi, A., Culotti, J.G., and Hedgecock, E.M. (1998). *daf-12* regulates developmental age and the dauer alternative in *Caenorhabditis elegans*. Development *125*, 1191–1205.

Antebi, A., Yeh, W.-H., Tait, D., Hedgecock, E.M., and Riddle, D.L. (2000). *daf-12* encodes a nuclear receptor that regulates the dauer diapause and developmental age in *C. elegans*. Genes Dev. *14*, 1512–1527.

Bellier, A., Chen, C.-S., Kao, C.-Y., Cinar, H.N., and Aroian, R.V. (2009). Hypoxia and the hypoxic response pathway protect against pore-forming toxins in *C. elegans*. PLoS Pathog *5*, e1000689.

Bhatla, N., and Horvitz, H.R. (2015). Light and Hydrogen Peroxide Inhibit *C. elegans* Feeding through Gustatory Receptor Orthologs and Pharyngeal Neurons. Neuron *85*, 804–818.

Bhatla, N., Droste, R., Sando, S.R., Huang, A., and Horvitz, H.R. (2015). Distinct Neural Circuits Control Rhythm Inhibition and Spitting by the Myogenic Pharynx of *C. elegans*. Curr. Biol. *25*, 2075–2089.

Chang, A.J., and Bargmann, C.I. (2008). Hypoxia and the HIF-1 transcriptional pathway reorganize a neuronal circuit for oxygen-dependent behavior in *Caenorhabditis elegans*. Proc. Natl. Acad. Sci. *105*, 7321–7326.

Darby, C., Cosma, C.L., Thomas, J.H., and Manoil, C. (1999). Lethal paralysis of *Caenorhabditis elegans* by *Pseudomonas aeruginosa*. Proc. Natl. Acad. Sci. U. S. A. *96*, 15202–15207.

Gerisch, B., and Antebi, A. (2004). Hormonal signals produced by DAF-9/cytochrome P450 regulate *C. elegans* dauer diapause in response to environmental cues. Development *131*, 1765–1776.

Gerisch, B., Weitzel, C., Kober-Eisermann, C., Rottiers, V., and Antebi, A. (2001). A Hormonal Signaling Pathway Influencing *C. elegans* Metabolism, Reproductive Development, and Life Span. Dev. Cell *1*, 841–851.

Gerisch, B., Rottiers, V., Li, D., Motola, D.L., Cummins, C.L., Lehrach, H., Mangelsdorf, D.J., and Antebi, A. (2007). A bile acid-like steroid modulates *Caenorhabditis elegans* lifespan through nuclear receptor signaling. Proc. Natl. Acad. Sci. *104*, 5014–5019.

Jiang, H., Guo, R., and Powell-Coffman, J.A. (2001). The *Caenorhabditis elegans hif-1* gene encodes a bHLH-PAS protein that is required for adaptation to hypoxia. Proc. Natl. Acad. Sci. *98*, 7916–7921.

Kirienko, N.V., Kirienko, D.R., Larkins-Ford, J., Wählby, C., Ruvkun, G., and Ausubel, F.M. (2013). *Pseudomonas aeruginosa* disrupts *Caenorhabditis elegans* iron homeostasis, causing a hypoxic response and death. Cell Host Microbe *13*, 406–416.

Leiser, S.F., Miller, H., Rossner, R., Fletcher, M., Leonard, A., Primitivo, M., Rintala, N., Ramos, F.J., Miller, D.L., and Kaeberlein, M. (2015). Cell nonautonomous activation of flavin-containing monooxygenase promotes longevity and health span. Science *350*, 1375–1378.

Ma, D.K., Vozdek, R., Bhatla, N., and Horvitz, H.R. (2012). CYSL-1 interacts with the O_2-sensing hydroxylase EGL-9 to promote H_2S-modulated hypoxia-induced behavioral plasticity in *C. elegans*. Neuron *73*, 925–940.

Mahanti, P., Bose, N., Bethke, A., Judkins, J.C., Wollam, J., Dumas, K.J., Zimmerman, A.M., Campbell, S.L., Hu, P.J., Antebi, A., et al. (2014). Comparative Metabolomics Reveals Endogenous Ligands of DAF-12, a Nuclear Hormone Receptor, Regulating *C. elegans* Development and Lifespan. Cell Metab. *19*, 73–83.

Meisel, J.D., and Kim, D.H. (2014). Behavioral avoidance of pathogenic bacteria by *Caenorhabditis elegans*. Trends Immunol. *35*, 465–470.

Meisel, J.D., Panda, O., Mahanti, P., Schroeder, F.C., and Kim, D.H. (2014). Chemosensation of Bacterial Secondary Metabolites Modulates Neuroendocrine Signaling and Behavior of *C. elegans*. Cell *159*, 267–280.

Miller, D.L., and Roth, M.B. (2009). *C. elegans* are protected from lethal hypoxia by an embryonic diapause. Curr. Biol. *19*, 1233–1237.

Motola, D.L., Cummins, C.L., Rottiers, V., Sharma, K.K., Li, T., Li, Y., Suino-Powell, K., Xu, H.E., Auchus, R.J., Antebi, A., et al. (2006). Identification of Ligands for DAF-12 that Govern Dauer Formation and Reproduction in *C. elegans*. Cell *124*, 1209–1223.

Reddy, K.C., Andersen, E.C., Kruglyak, L., and Kim, D.H. (2009). A polymorphism in *npr-1* Is a behavioral determinant of pathogen susceptibility in *C. elegans*. Science *323*, 382–384.

Semenza, G.L. (2010). Oxygen homeostasis. Wiley Interdiscip. Rev. Syst. Biol. Med. *2*, 336–361.

Shao, Z., Zhang, Y., and Powell-Coffman, J.A. (2009). Two distinct roles for EGL-9 in the regulation of HIF-1-mediated gene expression in *Caenorhabditis elegans*. Genetics *183*, 821–829.

Shao, Z., Zhang, Y., Ye, Q., Saldanha, J.N., and Powell-Coffman, J.A. (2010). *C. elegans* SWAN-1 binds to EGL-9 and regulates HIF-1-mediated resistance to the bacterial pathogen *Pseudomonas aeruginosa* PAO1. PLoS Pathog *6*, e1001075.

Shen, C., Shao, Z., and Powell-Coffman, J.A. (2006). The *Caenorhabditis elegans rhy-1* Gene Inhibits HIF-1 Hypoxia-Inducible Factor Activity in a Negative Feedback Loop That Does Not Include vhl-1. Genetics *174*, 1205–1214.

Appendix A

Cytochrome P450 drives a HIF-regulated behavioral response to reoxygenation by *C. elegans*

Dengke K. Ma[1], Michael Rothe[2], Shu Zheng[1], Nikhil Bhatla[1], Corinne L. Pender[1], Ralph Menzel[3] and H. Robert Horvitz[1,*]

Affiliations:

[1] Howard Hughes Medical Institute, Department of Biology, McGovern Institute for Brain Research, Koch Institute for Integrative Cancer Research, MIT, Cambridge, MA 02139, USA.

[2] Lipidomix GmbH, Robert-Roessle-Str. 10, 13125 Berlin, Germany

[3] Humboldt-Universität zu Berlin, Department of Biology, Freshwater and Stress Ecology, Spaethstr. 80/81, 12437 Berlin, Germany.

Published as: Ma, D.K., Rothe, M., Zheng, S., Bhatla, N., Pender, C.L., Menzel, R., and Horvitz, H.R. (2013). Cytochrome P450 drives a HIF-regulated behavioral response to reoxygenation by *C. elegans*. Science *341*, 554–558. Reprinted with permission from AAAS.

Contribution: Identification of non-Egl mutants, described in Figure S1B

Abstract:

Oxygen deprivation followed by reoxygenation causes pathological responses in many disorders, including ischemic stroke, heart attacks and reperfusion injury. Key aspects of ischemia-reperfusion can be modeled by a *C. elegans* behavior, the O2-ON response, which is suppressed by hypoxic preconditioning or inactivation of the O_2-sensing HIF (hypoxia-inducible-factor) hydroxylase EGL-9. From a genetic screen, we found that the cytochrome P450 oxygenase CYP-13A12 acts in response to the EGL-9/HIF-1 pathway to facilitate the O2-ON response. CYP-13A12 promotes oxidation of polyunsaturated fatty acids into eicosanoids, signaling molecules that can strongly affect inflammatory pain and ischemia-reperfusion injury responses in mammals. We propose that roles of the EGL-9/HIF-1 pathway and cytochrome P450 in controlling responses to anoxia-reoxygenation are evolutionarily conserved.

One Sentence Summary:

A genetic screen using a *C. elegans* behavioral model of ischemia-reperfusion injury identifies a gene that drives response to anoxia-reoxygenation and encodes a cytochrome P450.

Main Text:

Ischemia-reperfusion-related disorders, such as strokes and heart attacks, are the most common causes of adult deaths worldwide (*1*). Blood delivers O_2 and nutrients to target tissues, and ischemia results when the blood supply is interrupted. The restoration of O_2 from blood flow after ischemia, known as reperfusion, can exacerbate tissue damage (*2*). How organisms prevent ischemia-reperfusion injury is poorly understood. Studies of the nematode *C. elegans* led to

discovery of an evolutionarily conserved family of O_2-dependent enzymes (EGL-9 in *C. elegans* and EGLN2 in mammals) that hydroxylate the HIF transcription factor and link hypoxia to HIF-mediated physiological responses (*3-7*). Exposure to chronic low concentrations of O_2 (hypoxic preconditioning) or direct inhibition of EGLN2 strongly protects mammals from stroke and ischemia-reperfusion injury (*2, 8, 9*). Similarly, EGL-9 inactivation in *C. elegans* blocks a behavioral response to reoxygenation, the O2-ON response (characterized by a rapidly increased locomotion speed triggered by reoxygenation after anoxia) (*10, 11*), which is similar to mammalian tissue responses to ischemia-reperfusion: (i) reoxygenation drives the O2-ON response and is the major pathological driver of reperfusion injury, (ii) hypoxic preconditioning can suppress both processes, and (iii) the central regulators (EGL-9/HIF) of both processes are evolutionarily conserved. How the EGL-9/HIF-1 and EGLN2/HIF pathways control the O2-ON response and ischemia-reperfusion injury, respectively, is largely unknown.

To seek EGL-9/HIF-1 effectors important in the O2-ON response, we performed an *egl-9* suppressor screen for mutations that can restore the defective O2-ON response in *egl-9* mutants (fig. S1A). We identified new alleles of *hif*-1 in this screen; because EGL-9 inhibits HIF-1, *hif-1* mutations suppress the effects of *egl-9* mutations (*10*). We also identified mutations that are not alleles of *hif-1* (Figs. 1A-1C and fig. S1B). *hif-1* mutations recessively suppressed three defects of *egl-9* mutants: the defective O2-ON response, defects in egg-laying and the ectopic expression of the HIF-1 target gene *cysl-2* (previously called *K10H10.2*) (fig. S1C) (*10, 12*). By contrast, one mutation, *n5590*, dominantly suppressed the O2-ON defect but did not suppress the egg-laying defect or the ectopic expression of *cysl-2::GFP* (Figs. 1D, 1E and fig. S2). *n5590* restored the sustained phase (starting at 30s post-reoxygenation) better than it did the initial phase (within 30s post-reoxygenation) (Figs. 1A-1C). *egl-9*; *hif-1*; *n5590* triple mutants displayed a normal O2-

ON response, just like the wild type and *egl-9*; *hif-1* double mutants (fig. S1D). Thus, *n5590* specifically suppresses the *egl-9* defect in the sustained phase of the O2-ON response.

We genetically mapped *n5590* and identified an M46I missense mutation in the gene *cyp-13A12* by whole-genome sequencing (Fig. 2A, fig. S3A and Table S1A). Decreased wild-type *cyp-13A12* gene dosage in animals heterozygous for a wild-type allele and the splice acceptor null mutation *gk733685*, which truncates the majority of the protein, did not recapitulate the dominant effect of *n5590* (Fig. 2B). *gk733685* homozygous mutants similarly did not recapitulate the effect of *n5590* (Fig. 2C). Thus, *n5590* does not cause a loss of gene function. By contrast, increasing wild-type *cyp-13A12* gene dosage by overexpression restored the sustained phase of the O2-ON response (Fig. 2D), and RNAi against *cyp-13A12* abolished the effect of *n5590* (Fig. 2E). We conclude that *n5590* is a gain-of-function allele of *cyp-13A12*.

cyp-13A12 encodes a cytochrome P450 oxygenase (CYP). CYPs can oxidize diverse substrates (*13-15*). The *C. elegans* genome contains 82 CYP genes, at least two of which are polyunsaturated fatty acid (PUFA) oxygenases that generate eicosanoid signaling molecules (fig. S3B) (*16, 17*). The closest human homolog of CYP-13A12 based on BLASTP scores is CYP3A4 (fig. S4). We aligned the protein sequences of CYP-13A12 and CYP3A4 and found that *n5590* converts methionine 46 to an isoleucine, the residue in the corresponding position of normal human CYP3A4 (fig. S4). Methionines can be oxidized by free radicals, which are produced in the CYP enzymatic cycle, rendering CYPs prone to degradation (*18, 19*). Using transcriptional and translational GFP-based reporters, we identified the pharyngeal marginal cells as the major site of expression of *cyp-13A12* (fig. S5) and observed that the abundance of CYP-13A12::GFP protein was decreased by prolonged hypoxic preconditioning and also decreased in *egl-9* but not in *egl-9; hif-1* mutants (Fig. 2F and fig. S5). The *n5590* mutation prevented the decrease in CYP-

13A12::GFP abundance by hypoxia or *egl-9*. Thus, *n5590* acts, at least in part, by restoring the normal abundance of CYP-13A12, which then promotes the O2-ON response in *egl-9* mutants.

We tested whether CYP-13A12 was normally required for the O2-ON response in wild-type animals. The *cyp-13A12* null allele *gk733685* abolished the sustained phase of the O2-ON response; the initial phase of the O2-ON response was unaffected (Fig. 3A). A wild-type *cyp-13A12* transgene fully rescued this defect (Fig. 3B). A primary role of CYP-13A12 in the sustained phase of the O2-ON response explains the incomplete rescue of the defective O2-ON response of *egl-9* mutants by *n5590* during the initial phase (Fig. 1C). The activity of most and possibly all *C. elegans* CYPs requires EMB-8, a CYP reductase that transfers electrons to CYPs (*20*). No non-CYP EMB-8 targets are known. *emb-8(hc69)* causes a temperature-sensitive embryonic lethal phenotype. We grew *emb-8(hc69)* mutants at the permissive temperature to the young-adult stage. A shift to the non-permissive temperature simultaneously with *E. coli*-feeding RNAi against *emb-8* nearly abolished the O2-ON response (Figs. 3C and 3D) (Both the *hc69* mutation and RNAi against *emb-8* were required to substantially reduce the level of EMB-8 (*17*).) CYP-13A12 is thus required for the sustained phase of the O2-ON response, and one or more other CYPs likely act with CYP-13A12 to control both phases of the O2-ON response.

CYP oxygenases define one of three enzyme families that can convert PUFAs to eicosanoids, signaling molecules that affect inflammatory pain and ischemia-reperfusion responses of mammals (*15, 21-23*); the other two families, cyclooxygenases and lipoxygenases, do not appear to be present in *C. elegans* (*17, 24*). To test whether eicosanoids are regulated by EGL-9 and CYP-13A12, we used high-performance liquid chromatography (HPLC) coupled with mass spectrometry (MS) to profile steady-state amounts of 21 endogenous eicosanoid species from cell extracts of wild-type, *egl-9(n586)* and *egl-9(n586)*; *cyp-13A12*(*n5590*) strains.

Only free eicosanoids have potential signaling roles (*21, 22, 24*), so we focused on free eicosanoids. The *egl-9* mutation caused a markedly decreased overall amount of free eicosanoids, while the total amount of eicosanoid, including both free and membrane-bound fractions, was unaltered (Fig. 4A and fig. S6). Among the eicosanoids profiled, 17,18-DiHEQ (17,18-diolhydroxyeicosatetraenoic acid) was the most abundant species (fig. S6B). 17,18-DiHEQ is the catabolic hydrolase product of 17,18-EEQ (17,18-epoxyeicosatetraenoic acid), an epoxide active in eicosanoid signaling (*25*). Free cytosolic 17,18-EEQ and 19-hydroxyeicosatetraenoic acid (19-HETE) were present in the wild type but undetectable in *egl-9* mutants (Figs. 4C-4F). *egl-9(n586)*; *cyp-13A12*(*n5590*) mutants exhibited partially restored free overall eicosanoid levels as well as restored levels of 17,18-EEQ and 19-HETE (Figs. 4A-4F and fig. S6B). Thus, both EGL-9 and CYP-13A12 regulate amounts of free cytosolic eicosanoids.

We tested whether the O2-ON response requires PUFAs, which are CYP substrates and eicosanoid precursors. PUFA-deficient *fat-2* and *fat-3* mutants (*26*) exhibited a complete lack of the O2-ON response, although the acceleration in response to anoxia preceding the O2-ON response was normal (Fig. 4G and figs. S7A-S7C). The defective O2-ON response of *fat-2* mutants was restored by feeding animals the C20 PUFA arachidonic acid (Fig. 4H) but not oleate, a C18 monounsaturated fatty acid that is processed by FAT-2 to generate C20 PUFAs (fig. S7D). These results demonstrate an essential role of PUFAs for the O2-ON response.

We suggest a model in which CYPs, which are strictly O_2-dependent (*27, 28*), generate eicosanoids to drive the O2-ON response (Figs. 4I and fig. S8). In this model, EGL-9 acts as a chronic O_2-sensor, so that during hypoxic preconditioning, the O_2-dependent activity of EGL-9 is inhibited, HIF-1 is activated and unknown HIF-1 up-regulated targets decrease CYP protein abundance. The low abundance of CYPs defines the hypoxic preconditioned state. Without

hypoxic preconditioning, CYPs generate eicosanoids, which drive the O2-ON response. By contrast, with hypoxic preconditioning or in *egl-9* mutants, the CYP amounts are insufficient to generate eicosanoids and the O2-ON response is not triggered. Neither C20 PUFAs nor overexpression of CYP-29A3 restored the defective O2-ON response of *egl-9* mutants (figs. S9 and S10), indicating that this defect is unlikely caused by a general deficiency in C20 PUFAs or CYPs. Since the O2-ON response requires EMB-8, a general CYP reductase, but only the sustained phase requires CYP-13A12, we propose that CYP-13A12 and other CYPs act as acute O_2 sensors and produce eicosanoids, which are short-lived and act locally (*22*) during reoxygenation to signal nearby sensory circuits that drive the O2-ON response.

In humans, a low uptake of PUFAs or an imbalanced ratio of ω3/ω6 PUFAs is associated with elevated risk of stroke, cardiovascular disease and cancer (*21, 23, 29, 30*). Cytochrome P450s and eicosanoid production also have been implicated in mammalian ischemia-reperfusion (*15, 21*). Nonetheless, the causal relationships among and mechanisms relating O_2 and PUFA homeostasis, CYP and PUFA-mediated cell signaling and organismal susceptibility to oxidative disorders are poorly understood. We identify a novel pathway in which EGL-9/HIF-1 regulates CYP-eicosanoid signaling, demonstrate that PUFAs confer a rapid response to reoxygenation via CYP-generated eicosanoids and provide direct causal links among CYPs, PUFA-derived eicosanoids, and an animal behavioral response to reoxygenation. As molecular mechanisms of O_2 and PUFA homeostasis are fundamentally similar and evolutionarily conserved between nematodes and mammals (*7, 11, 26*), we suggest that the *C. elegans* O2-ON response is analogous to the mammalian tissue/cellular response to ischemia-reperfusion injury and that the principle of CYP-mediated regulation and the molecular pathway including EGL-9/HIF-1 and CYPs in controlling responses to anoxia-reoxygenation are evolutionarily conserved.

References and Notes:

1. A. S. Go *et al.*, *Circulation*, (Dec 12, 2012).
2. H. K. Eltzschig, T. Eckle, *Nat Med* **17**, 1391 (2011).
3. A. C. Epstein *et al.*, *Cell* **107**, 43 (Oct 5, 2001).
4. W. G. Kaelin, Jr., P. J. Ratcliffe, *Mol Cell* **30**, 393 (May 23, 2008).
5. C. Trent, N. Tsung, H. R. Horvitz, *Genetics* **104**, 619 (Aug, 1983).
6. G. L. Semenza, *Cell* **148**, 399 (Feb 3, 2012).
7. J. A. Powell-Coffman, *Trends Endocrinol Metab* **21**, 435 (Jul, 2010).
8. G. L. Semenza, *Biochim Biophys Acta* **1813**, 1263 (Jul, 2011).
9. J. Aragones *et al.*, *Nat Genet* **40**, 170 (Feb, 2008).
10. D. K. Ma, R. Vozdek, N. Bhatla, H. R. Horvitz, *Neuron* **73**, 925 (Mar 8, 2012).
11. D. K. Ma, N. Ringstad, *Front Biol* **7**, 246 (Jun, 2012).
12. M. W. Budde, M. B. Roth, *Genetics* **189**, 521 (Oct, 2011).
13. D. R. Nelson *et al.*, *Pharmacogenetics* **6**, 1 (Feb, 1996).
14. O. Gotoh, *Mol Biol Evol* **15**, 1447 (Nov, 1998).
15. R. A. Gottlieb, *Arch Biochem Biophys* **420**, 262 (Dec 15, 2003).
16. M. Kosel *et al.*, *Biochem J* **435**, 689 (May 1, 2011).
17. J. Kulas, C. Schmidt, M. Rothe, W. H. Schunck, R. Menzel, *Arch Biochem Biophys* **472**, 65 (Apr 1, 2008).
18. B. S. Berlett, E. R. Stadtman, *J Biol Chem* **272**, 20313 (Aug 15, 1997).
19. R. C. Zangar, D. R. Davydov, S. Verma, *Toxicol Appl Pharmacol* **199**, 316 (Sep 15, 2004).
20. C. A. Rappleye, A. Tagawa, N. Le Bot, J. Ahringer, R. V. Aroian, *BMC developmental biology* **3**, 3 (Oct 3, 2003).
21. J. Szefel *et al.*, *Curr Mol Med* **11**, 13 (Feb, 2011).
22. M. P. Wymann, R. Schneiter, *Nat Rev Mol Cell Biol* **9**, 162 (Feb, 2008).
23. R. S. Chapkin, W. Kim, J. R. Lupton, D. N. McMurray, *Prostaglandins Leukot Essent Fatty Acids* **81**, 187 (Aug-Sep, 2009).
24. D. Panigrahy, A. Kaipainen, E. R. Greene, S. Huang, *Cancer Metastasis Rev* **29**, 723 (Dec, 2010).
25. C. Arnold *et al.*, *J Biol Chem* **285**, 32720 (Oct 22, 2010).
26. J. L. Watts, *Trends Endocrinol Metab* **20**, 58 (Mar, 2009).
27. D. R. Harder *et al.*, *Circ Res* **79**, 54 (Jul, 1996).

28. J. P. Ward, *Biochim Biophys Acta* **1777**, 1 (Jan, 2008).
29. M. Gerber, *Br J Nutr* **107 Suppl 2**, S228 (Jun, 2012).
30. D. Mozaffarian, J. H. Wu, *J Am Coll Cardiol* **58**, 2047 (Nov 8, 2011).

Acknowledgments: We thank C. Bargmann, A. Fire, A. Hart, Y. Iino, J. Powell-Coffman and C. Rongo for reagents; the *Caenorhabditis* Genetics Center and the Million Mutation Project for strains. H.R.H. is an Investigator of the Howard Hughes Medical Institute and the David H. Koch Professor of Biology at MIT. Supported by NIH grant GM24663 (H.R.H), German Research Foundation grant ME2056/3-1 (R.M.), NSF Graduate Research Fellowship (N.B.), MIT Undergraduate Research Opportunities Program (S.Z.) and a Helen Hay Whitney Foundation postdoctoral fellowship (D.K.M.).

Fig. 1. ***n5590* suppresses the defect of *egl-9* mutants in the O2-ON response.** (A) Speed graph of wild-type animals, showing a normal O2-ON response. Average speed values ± 2 SEMs (blue) of animals (n > 50) are shown with step changes of O_2 between 20% and 0% at the indicated times. The mean speed within 0-120 s after O_2 restoration is increased compared with that before O_2 restoration ($p < 0.01$, one-sided unpaired t-test). The dashed green line indicates the approximate boundary (30s post-reoxygenation) between the initial and sustained phases of the O2-ON response. (B) Speed graph of *egl-9*(*n586*) mutants, showing a defective O2-ON response. (C) Speed graph of *egl-9*(*n586*); *cyp-13A12(n5590)* mutants, showing a restored O2-ON response mainly in the sustained phase (right of the dashed green line). The mean speed within 30-120 s after O_2 restoration was significantly higher than that of *egl-9*(*n586*) mutants ($p <0.01$). (D) Speed graph of *egl-9*(*n586*); *cyp-13A12(n5590)*/+ mutants, showing a restored O2-ON response in the sustained phase. (E) *hif-1* but not *cyp-13A12(n5590)* suppressed the expression of *cysl-2::GFP* by *egl-9*(*n586*) mutants. GFP fluorescence micrographs of 5-7 worms aligned side by side carrying the transgene *nIs470 [P_{cysl-2}::GFP]* are shown. Scale bar, 50 µm.

Fig. 2. *n5590* is a gain-of-function allele of *cyp-13A12*. (A) Genetic mapping positioned *n5590* between the SNPs *pkP3075* and *uCE3-1426*. Solid grey lines indicate genomic regions for which recombinants exhibited a defective O2-ON response, thus excluding *n5590* from those regions. The locations of *n5590* and *gk733685* are indicated in the gene diagram of *cyp-13A12*. (B) Speed graph of *egl-9*(*n586*); *cyp-13A12(gk733685)*/+ animals, showing a defective O2-ON response. (C) Speed graph of *egl-9(n586); cyp-13A12(gk733685)* mutants, showing a defective O2-ON response. (D) Speed graph of *egl-9*(*n586*); *nEx [cyp-13A12(+)]* animals, showing a restored O2-ON response in the sustained phase (right of the dashed green line). (E) Speed graph of *egl-9*(*n586*); *cyp-13A12(n5590); cyp-13A12(RNAi)* animals, showing a suppressed O2-ON response. (F) Fractions of animals expressing CYP-13A12::GFP or CYP-13A12(*n5590*)::GFP (* $p<0.01$, two-way ANOVA with Bonferroni's test, n=4).

Fig. 3. Requirement of CYP-13A12 for a normal O2-ON response. (A) Speed graph of *cyp-13A12(gk733685)* loss-of-function mutants, showing an O2-ON response with a normal initial phase but a diminished sustained phase (left and right, respectively, of the dashed green line). (B) Speed graph of *cyp-13A12(gk733685)* mutants with a rescuing wild-type *cyp-13A12* transgene, showing the O2-ON response with a normal initial phase and sustained phase. The mean speed within 30-120 s after O_2 restoration was higher than that of *cyp-13A12(gk733685)* mutants ($p <0.01$, one-sided unpaired t-test, n >50). (C) Speed graph of *emb-8(hc69)* mutants growing at the permissive temperature of 15°C with simultaneous *E. coli* feeding RNAi against *emb-8*, showing a normal O2-ON response. (D) Speed graph of *emb-8(hc69)* mutants growing post-embryonically at the restrictive temperature of 25°C with simultaneous *E. coli* feeding-RNAi against *emb-8*, showing a reduced O2-ON response.

Fig. 4. Modulation of eicosanoid concentrations by EGL-9 and CYP-13A12. (A) Overall levels of free eicosanoids, calculated by adding the values of the profiled 21 eicosanoids in the wild type and *egl-9(n586)* and *egl-9(n586); cyp-13A12(n5590)* strains. (B) Schematic illustrating the conversion of arachidonic acid (AA, 20:4n-6) to 19-HETE and of EPA (20:5n-3) to 17,18-EEQ by CYPs. (C) Quantification of 19-HETE and 17,18-EEQ concentrations in the wild type and *egl-9(n586); cyp-13A12(n5590)* and *egl-9(n586)* mutant strains. Amounts of free (membrane unbound) forms of 17,18-EEQ and 19-HETE from extracts of age-synchronized young adult hermaphrodites are shown. $p < 0.01$, one-way ANOVA post hoc test, $n = 3$. Error bars are SEMs. (D-F) Representative HPLC-MS traces indicating free 17,18-EEQ levels based on the spectrograms of three MS samples: (D) wild type, (E) *egl-9(n586),* and (F) *egl-9(n586) ; cyp-13A12(n5590)*. Peaks of 17,18-EEQ at its transition m/z (mass-to-charge ratio) were measured and extracted (MassHunter). The x-axis shows the retention time (minutes); the y-axis shows the abundance (counts), with specific integral values over individual peaks indicated above each peak. (G) Speed graph of *fat-2* mutants, showing a defective O2-ON response. Animals were supplemented with the solvents used in (H) as a control. (H) Speed graph of *fat-2* mutants, showing the O2-ON response rescued by C20 PUFA (AA) supplementation. (I-J) Model of how EGL-9 and CYPs control the O2-ON response under (I) normoxic conditions and (J) conditions of hypoxic preconditioning or in *egl-9* mutants (see text for details). The light blue indicates low protein activity, low amounts of eicosanoids or a defective O2-ON response.

Fig. 1

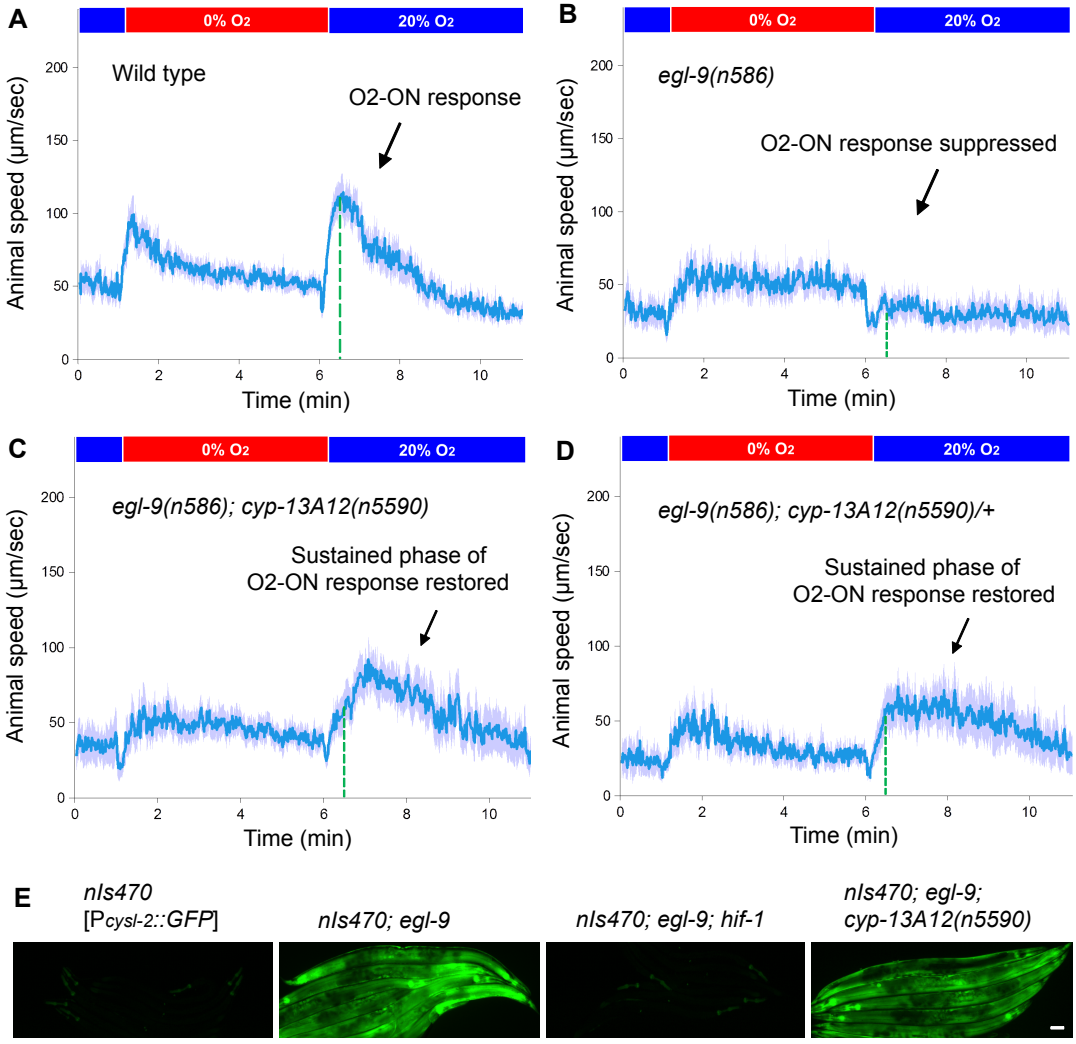
A
0% O2
20% O2
Wild type
O2-ON response
Animal speed (µm/sec)
Time (min)
B
0% O2
20% O2
egl-9(n586)
O2-ON response suppressed
Animal speed (µm/sec)
Time (min)
C
0% O2
20% O2
egl-9(n586); cyp-13A12(n5590)
Sustained phase of
O2-ON response restored
Animal speed (µm/sec)
Time (min)
D
0% O2
20% O2
egl-9(n586); cyp-13A12(n5590)/+
Sustained phase of
O2-ON response restored
Animal speed (µm/sec)
Time (min)
E
nIs470
[Pcysl-2::GFP]
nIs470; egl-9
nIs470; egl-9; hif-1
nIs470; egl-9;
cyp-13A12(n5590)

Fig. 2

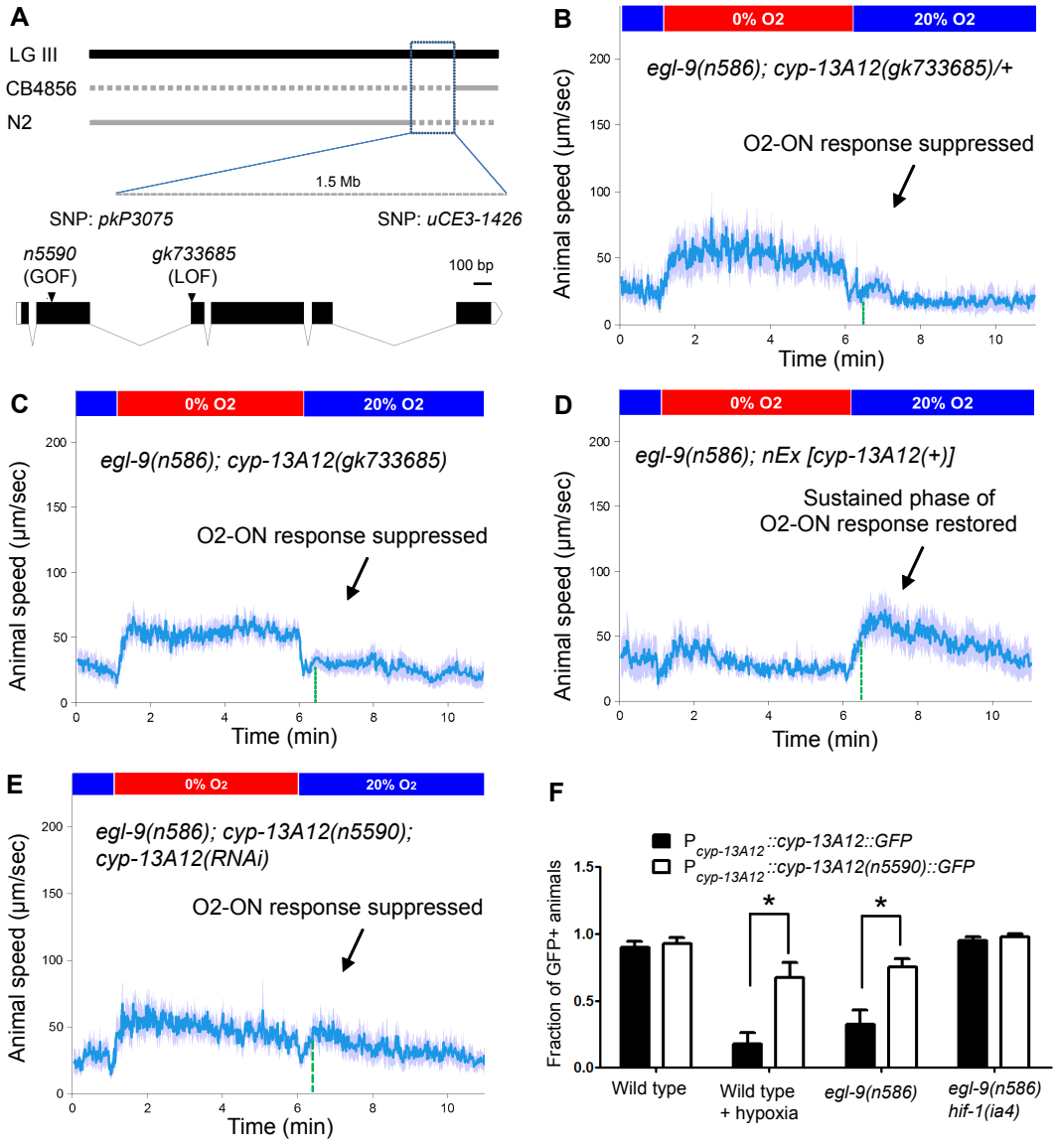
A
LG III
CB4856
N2
1.5 Mb
SNP: pkP3075
SNP: uCE3-1426
n5590
(GOF)
gk733685
(LOF)
100 bp
B
0% O2
20% O2
egl-9(n586); cyp-13A12(gk733685)/+
O2-ON response suppressed
Animal speed (µm/sec)
Time (min)
C
egl-9(n586); cyp-13A12(gk733685)
O2-ON response suppressed
D
egl-9(n586); nEx [cyp-13A12(+)]
Sustained phase of
O2-ON response restored
E
egl-9(n586); cyp-13A12(n5590);
cyp-13A12(RNAi)
F
P cyp-13A12 ::cyp-13A12::GFP
P cyp-13A12 ::cyp-13A12(n5590)::GFP
Fraction of GFP+ animals
Wild type
Wild type
+ hypoxia
egl-9(n586)
egl-9(n586)
hif-1(ia4)

Fig. 3

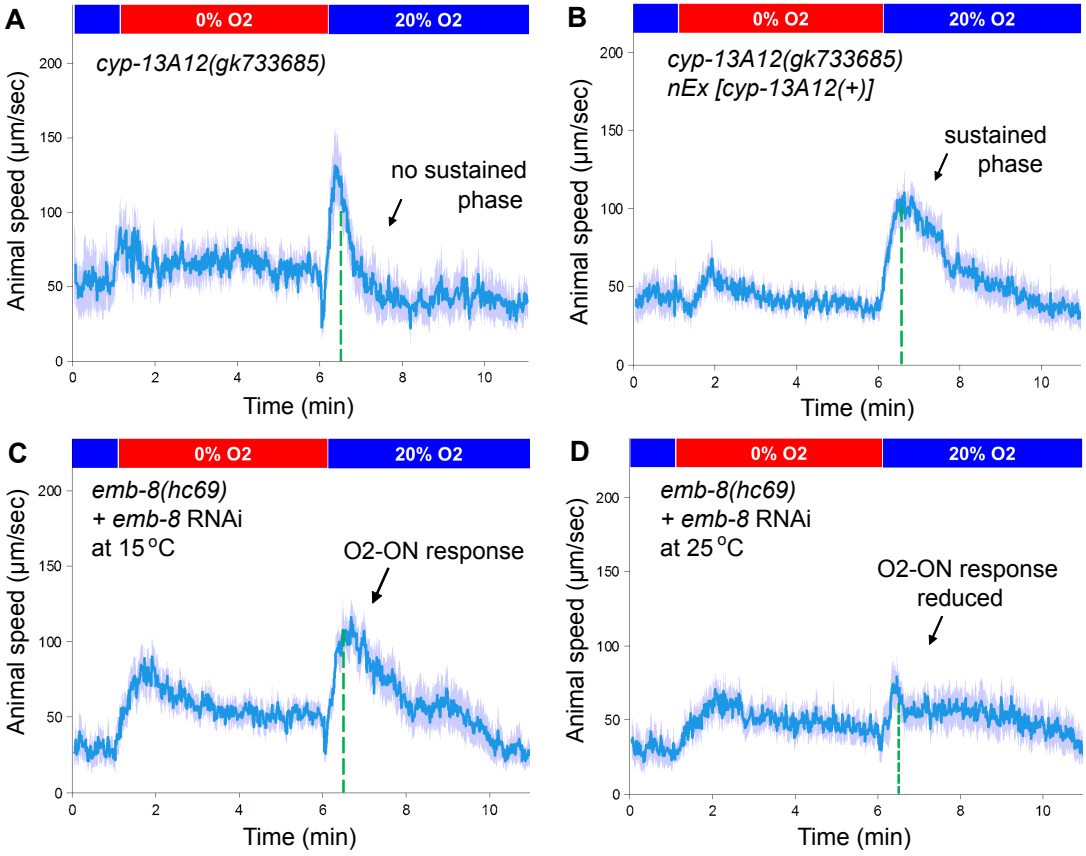
A
0% O2
20% O2
cyp-13A12(gk733685)
no sustained phase
Animal speed (µm/sec)
Time (min)
B
0% O2
20% O2
cyp-13A12(gk733685)
nEx [cyp-13A12(+)]
sustained phase
Animal speed (µm/sec)
Time (min)
C
0% O2
20% O2
emb-8(hc69)
+ emb-8 RNAi
at 15 °C
O2-ON response
Animal speed (µm/sec)
Time (min)
D
0% O2
20% O2
emb-8(hc69)
+ emb-8 RNAi
at 25 °C
O2-ON response reduced
Animal speed (µm/sec)
Time (min)

Fig. 4

A

	Wild type	*egl-9(n586)*	*egl-9(n586); cyp-13A12(n5590)*
21 eicosanoids overall (ng/mg)	17.2±1.4	1.8±0.6	4.4±0.1

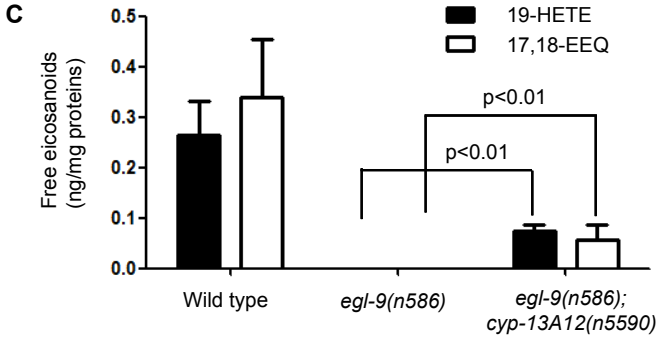

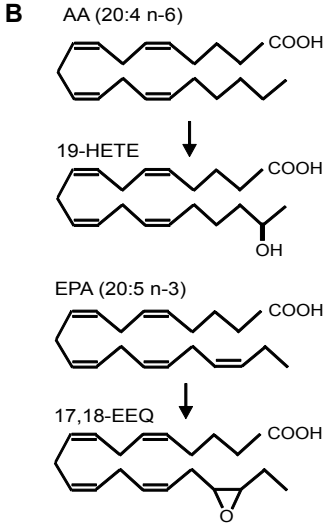

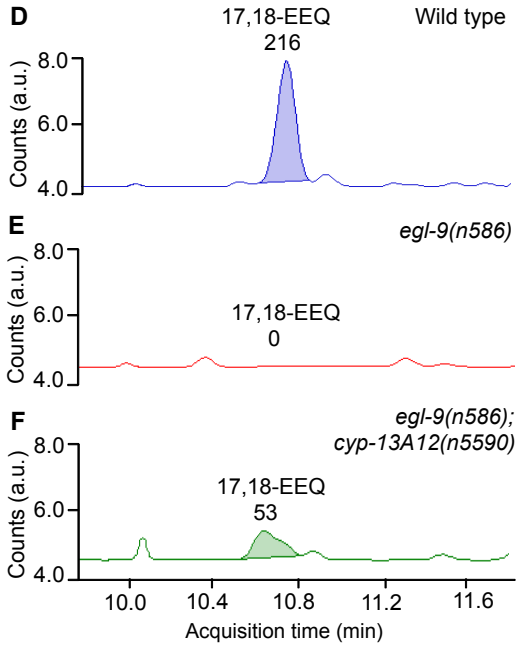

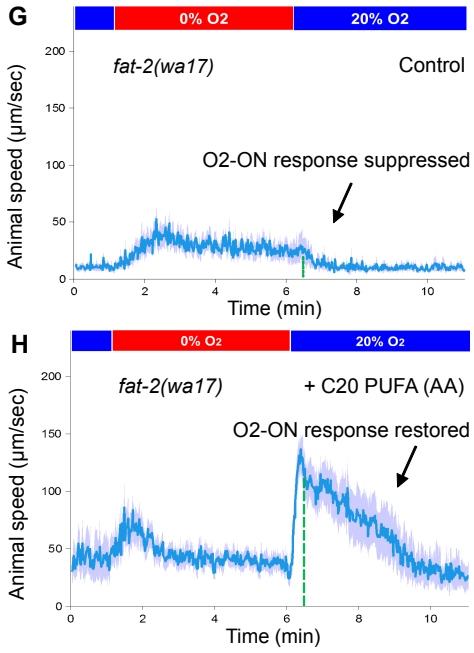

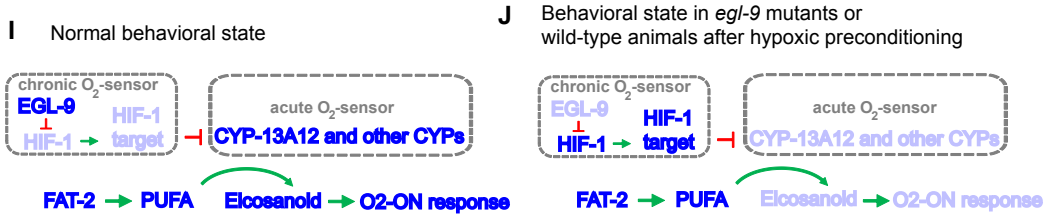

Supplementary Materials

Materials and Methods

Supplementary Text

Supplementary Figs. S1 to S11

Supplementary Table S1

Full Reference List

Materials and Methods

EMS Mutagenesis, Genetic Screens, Mapping and Whole-genome Sequencing

To screen for *egl-9* suppressors, we mutagenized *egl-9(n586)* mutants carrying the *cysl-2::GFP* transgene *nIs470* with ethyl methanesulfonate (EMS) and observed the F2 progeny in one of three ways using: (1) a dissecting microscope and GFP fluorescence to isolate suppressors of *cysl-2::GFP* overexpression, (2) a dissecting microscope to isolate suppressors of the defective egg-laying behavior, and (3) a compound microscope and a nitrogen gas-flow chamber to isolate suppressors of the defective O2-ON response.

We refer to mutations that cause diminished *cysl-2::GFP* fluorescence or restored egg-laying behavior under conditions of normoxia (21% O_2) as GFP or Egl suppressors, respectively. To isolate suppressors of the defective O2-ON response of *egl-9* mutants, we used a nitrogen gas-flow chamber system with a 100% nitrogen gas source, flow-meters, and a lid with gas tubing inlets and outlets mounted on a Petri plate freshly seeded with *E. coli* OP50 (*10*). Animals with restored rapid acceleration immediately (0 - 60s) after reoxygenation (by removal of the plate lid) were identified as suppressors of the defective O2-ON response. False positives were eliminated by retesting animals in the next generation using a population assay (>50 animals) (*10*).

To map the *egl-9* suppressor mutation *n5590*, we first generated a polymorphic Hawaiian *egl-9*(*n586)* strain by repeatedly crossing *egl-9*(*n586)* with the Hawaiian wild-type strain CB4856. *nIs470*; *egl-9*(*n586*); *n5590* mutants were then crossed with the Hawaiian *egl-9*(*n586*) strain for genetic mapping. F2 animals were isolated, and clonal F3 populations were assayed for

the O2-ON response. Mapping using SNP analysis (*50*) positioned *n5590* between the SNPs *pkP3075* and *uCE3-1426* on chromosome III (Fig. 2A).

Whole-genome sequencing and data analyses were performed as described (*51*). Two protein-coding mutations were identified in the *n5590* interval defined above: a T-to-G mutation in the gene *Y39E4A.2* and a G-to-A mutation in the gene *cyp-13A12*. As described in the text, we showed that the *egl-9* suppressor *n5590* is a gain-of-function mutation of *cyp-13A12*.

Behavioral Analyses

The O2-ON response was measured using a multi-worm tracker with a gas-flow chamber system and quantified by customized MatLab algorithms as previously described (*10*). For experiments using the C20 PUFA arachidonic acid as a food supplement, arachidonic acid salts (Cayman Chemical) were dissolved in ethanol at 1 mg/ml, and 50 µL was spread evenly onto NGM plates before drying briefly and cultivating OP50 *E. coli* on the plates. *C. elegans* was then transferred to the PUFA-supplemented plates.

To quantify egg-laying behavior, we scored the developmental stages of newly laid eggs of young adult hermaphrodites that had been transferred to fresh NGM plates with OP50 (*52*).

Determination of eicosanoid levels

Endogenous CYP-derived eicosanoids were assayed for the N2 wild-type strain as well as for *egl-9(n586)* and *egl-9(n586); cyp-13A12(n5590)* mutant strains. For each experiment (three independent cultures per strain), 12,000 stage-synchronized larvae were allocated to four fresh Petri plates (diameter = 94 mm) and further cultivated at 22.5°C until the young adult stage (24

hrs post-L4). To generate a synchronous culture of first-stage (L1) larvae, a population of well-fed animals was collected from Petri plates by rinsing and then filtered through a 10 μm membrane (SM 16510/11, Sartorius, Goettingen, Germany), a pore size that retains all but L1 larvae. These larvae were allowed to grow to be young adults and then were filtered again to eliminate L1 larvae of the next generation and so retain exclusively young adults. Subsequently, animals were prepared for LC-MS/MS analysis essentially as described previously (*17*). Briefly, aliquots corresponding to 30 mg wet weight were mixed with internal standard compounds (10 ng each of 20-HETE-d6, 14,15-EET-d8 and 14,15-DHET-d11; from Cayman Chemicals, Ann Arbor, MI, USA) and either subjected to alkaline hydrolysis (total eicosanoids) or directly extracted with methanol/water (free eicosanoids) followed by solid-phase extraction of the metabolites. Sample preparation, HPLC and MS conditions as well as the monitoring of multiple reactions for the analysis of the CYP-eicosanoid profile were as described previously (*25*). The protein concentration of each sample was measured after hydrolysis (*53*).

Mutations and Strains

C. elegans strains were cultured as described previously (*54*). The N2 Bristol strain (*54*) was used as the reference wild-type strain, and the polymorphic Hawaiian strain CB4856 (*55*) was used for genetic mapping and SNP analysis. Mutations used were as follows: LG III, *cyp-13A12(n5590 and gk733685) (gk733685* was obtained from the Million Mutation Project (*56*)*), emb-8(hc69)* (*20*), *cdk-5(ok626)* (*41*); LG IV, *fat-2(wa17), fat-3(wa22, ok1126) (57)*; LG V, *egl-9(sa307, n586)* (*5, 58*)*, hif-1(ia4, n5513, n5527)* (*59, 60*).

Transgenic strains were generated by germline transformation as described (*61*). Transgenic constructs were co-injected (at 20 - 50 ng/μl) with mCherry reporters, and lines of

mCherry-positive animals were established. Gamma irradiation was used to generate integrated transgenes. Transgenic strains used were as follows: *nEx2015 [$P_{cyp\text{-}13A12}$::GFP; $P_{unc\text{-}54}$::mCherry]*; *nEx2016 [$P_{cyp\text{-}13A12}$::cyp-13A12::GFP; $P_{unc\text{-}54}$::mCherry]*; *nEx2017 [cyp-13A12(+)]*; *nEx2018 [cyp-13A12(n5590)]*; *nIs587 [$P_{cyp\text{-}13A12}$::GFP; $P_{unc\text{-}54}$::mCherry]; nIs588 [$P_{cyp\text{-}13A12}$::cyp-13A12::GFP; $P_{unc\text{-}54}$::mCherry]*; *nIs589 [$P_{cyp\text{-}13A12}$::cyp-13A12(n5590)::GFP; $P_{unc\text{-}54}$::mCherry]; nIs470 [$P_{cysl\text{-}2}$::GFP; $P_{myo\text{-}2}$::mCherry]*.

Molecular biology

Constructs were generated using the PCR-fusion technique (*62*), the Gateway system (Invitrogen) and the Infusion cloning (Clontech) technique (*63*). Primer sequences are shown in Table S1.

Statistical analyses

One-sided unpaired t-tests were used to compare the mean speeds of all animals within 60 or 120 seconds before or after O_2 restoration (*10*). $p<0.01$ indicates speed differences that are significant, as noted in each figure. Fisher's exact tests were used after egg-laying behavioral assays to compare the distributions of the six categories of embryos from the wild type and various mutants. Two-way ANOVA was used to calculate p values to test for significance of the effects of genotypes and different conditions in the O2-ON response.

Bioinformatics

The BLASTP program from NCBI was used to search for proteins homologous to CYP-13A12 (*64*). Multiple sequence alignments were generated and analyzed using ClusterW2 (*65*), and the results were displayed and annotated using JalView (*66*). Schematic gene structures and annotations were generated using the Exon-Intron Graphic Maker (http://wormweb.org/exonintron).

Supplementary Text

Transcriptional and translational GFP reporters with the *cyp-13A12* promoter or with the promoter and coding sequence were both most strongly expressed in the pharynx (fig. S5). The GFP-stained pharyngeal cells extended processes along the anterior pharyngeal bulb and exhibited finger-like protrusions, and we identified these cells as the pharyngeal marginal cells (MCs). MCs intercalate with pharyngeal muscles and might structurally reinforce these muscles (*31*). However, MCs contain abundant mitochondria, suggesting that these cells might perform active non-structural roles (*32*). The O2-ON response involves rapid reoxygenation and occurs independently of known aerotaxic neural O_2 sensors (*10, 11, 33-35*); we hypothesize that MCs actively signal reoxygenation by converting PUFAs to membrane-diffusible eicosanoids, which are sensed by nearby sensory neurons and trigger the O2-ON response via neural circuits that control forward/backward locomotion (*36, 37*).

In *egl-9* mutants or animals with prolonged (24 hrs) hypoxic preconditioning (*10*), the O2-ON response is suppressed because CYP-13A12 is decreased through the EGL-9/HIF-1

pathway (Figs. 2F and 4J). Our GFP reporter experiments indicate that regulation of CYP-13A12 by EGL-9/HIF-1 occurs primarily by regulation of the abundance of CYP proteins (Fig. 2F and fig. S5). HIF-1 activation can facilitate protein ubiquitination and homeostasis and pro-survival effects of hypoxic preconditioning likely require suppression of protein translation in *C. elegans* (*38-40*). We suggest that one or more transcriptional targets of HIF-1 regulate the abundance of CYP-13A12 and likely that of other CYPs, since CYP-13A12 does not control the initial phase but EMB-8, a general CYP reductase, affects both the initial and sustained phases (Fig. 3). *egl-9(n685); cyp-13A12(n5590)* mutants might have been restored for the sustained phase of the O2-ON response because they have restored the abundance of CYP-13A12 and thus partially restored the ability to produce eicosanoids from PUFAs. Because *cdk-5* mutations suppress the defective LIN-10 trafficking in *egl-9* mutants (*41*), we also tested *cdk-5* mutants and found that *cdk-5* mutations did not suppress *cysl-2::GFP* expression, the defective egg-laying behavior, or the defective O2-ON response or of *egl-9* mutants (figs. S11A-S11B), indicating that EGL-9 regulates the O2-ON response independently of CDK-5.

Our conclusions are consistent with findings that mammalian CYP proteins closely related to *C. elegans* CYP13A12 are expressed in tissues that display ischemia-reperfusion injury and are involved in eicosanoid signaling. For example, CYP3A4 is the most closely related human homolog of *C. elegans* CYP13A12 (162/501 or 32% amino acid identity with CYP13A12) and is mainly expressed in the liver but is also highly expressed in the brain (*42-44*), consistent with our hypothesis that CYP3A4 modulates ischemic processes in these organs. We note that members of particular CYP protein families share high similarity in general, and CYP13A12 is also homologous to other mammalian CYPs, including the CYP5A1 thromboxane synthase (148/481 or 31% amino acid identity with CYP13A12), which generates the eicosanoid

thromboxane and is widely expressed in the vasculature (*45*), suggesting that CYP5A1-generated eicosanoids function in the vasculature. Increased production of HETE-type eicosanoids is also associated with ischemia-reperfusion processes (*46, 47*). The modulation of ischemia-reperfusion by CYPs in mammals is thus unlikely mediated by a single CYP, such as CYP3A4, just as the O2-ON response of *C. elegans* is likely mediated by one or more other CYPs in addition to CYP-13A12. Rather, we suggest that the principle of CYP-mediated regulation and the novel molecular pathway including EGL-9/HIF-1 and CYPs in regulating responses to anoxia-reoxygenation are conserved; different mammalian CYPs might act in different tissues and organs. The observation that potent inhibitors of CYPs, such as sulfaphenazole, cause strong protection against ischemia-reperfusion injury (*15, 48, 49*) is consistent with our model. Using *C. elegans* genetics and a behavioral model of ischemia/reperfusion, we demonstrate a direct causal role of CYPs in the response to anoxia-reoxygenation and therefore suggest a similarly causal role of CYPs in modulating mammalian ischemia-reperfusion processes.

Supplementary Figures

fig. S1

A

nls470 IV; egl-9(n586) V

(*cysl-2::GFP*+, Egl and defective O2-ON response)

↓ EMS

F1

↓

F2 single animals examined

Three classes of suppressor mutants:

i, CYSL-2::GFP: GFP-

ii, Egg laying: non-Egl

iii, Locomotion: O2-ON defect restored

B

Class	*nls470; egl-9* suppressor	GFP	Egg-laying	O2-ON
	none	GFP+	Egl	Defective
i	*n5601* *n5602* *n5603* *n5604* *n5605* *n5606*	GFP-	Egl	Defective
ii	*n5454* *n5607* *n5608*	GFP+	Non-Egl	Defective
iii	*n5460* *n5609* *n5590*	GFP+	Egl	Normal

C

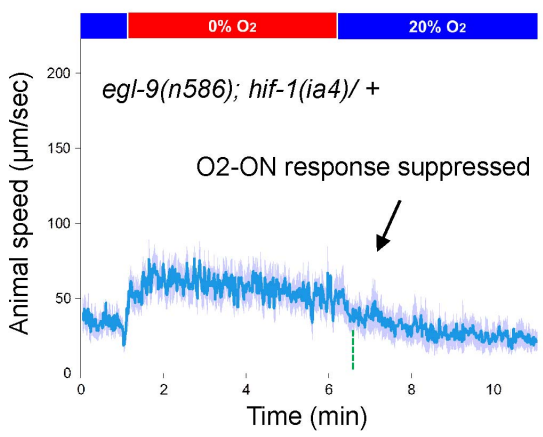

D

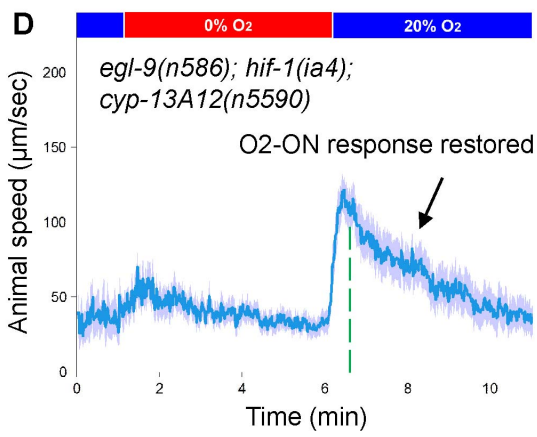

fig. S1. Genetic screens for *egl-9* suppressors

(A) Schematic of the screens for *egl-9* suppressors. Approximately 15,000 haploid genomes were screened. (B) Summary of the non-*hif-1* suppressor mutant isolates, showing that each of the three aspects of the *egl-9* mutant phenotype was separately suppressed. (C) Speed graph of *egl-9; hif-1*/+ mutants with a defective O2-ON response, showing the recessive suppression of *egl-9* by *hif-1*. Cross progeny of *egl-9; hif-1* and *egl-9* mutants were assayed for the O2-ON response. (D) Speed graph of *egl-9(n586); hif-1(ia4); cyp-13A12(n5590)* triple mutants, showing a normal O2-ON response. Canonical alleles of *egl-9* and *hif-1* were used.

fig. S2

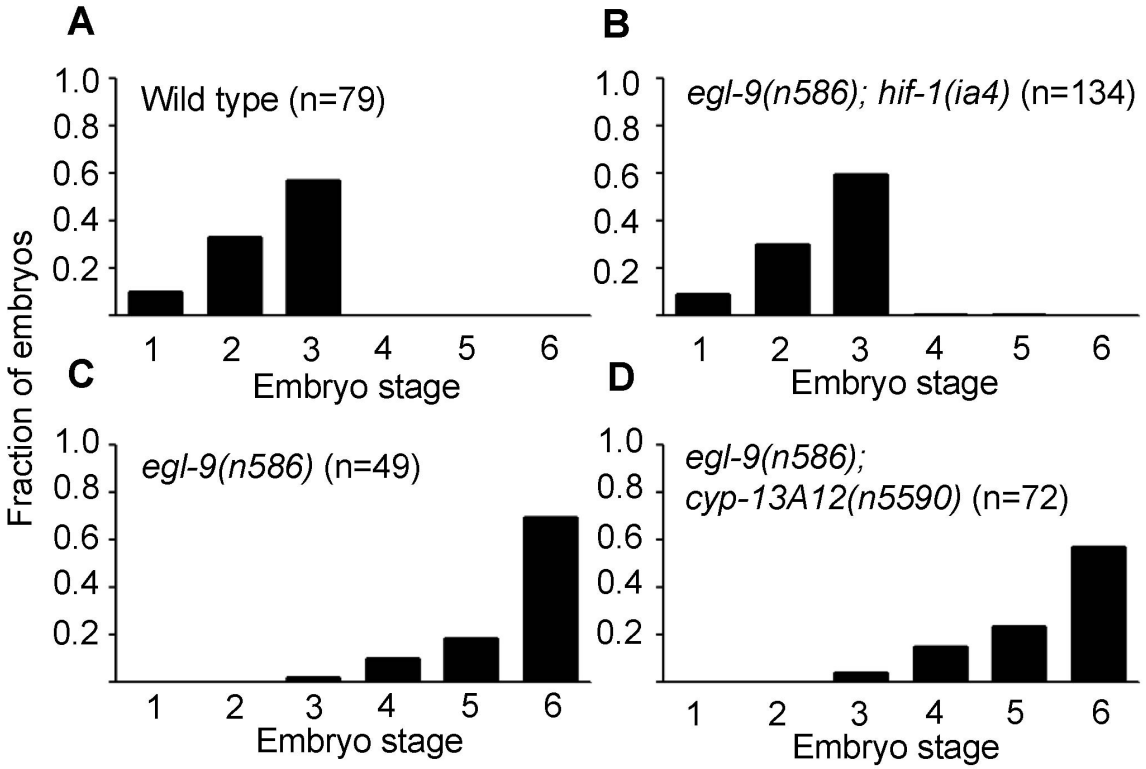

fig. S2. *n5590* did not suppress the defective egg-laying of *egl-9* mutants

(A-D) *hif-1* but not *cyp-13A12(n5590)* suppressed the egg-laying defect of *egl-9*(*n586*) mutants ($p < 0.001$, Fisher's exact test). Fractions of the developmental stages of eggs laid by animals carrying various mutations are shown.

fig. S3

A

transmembrane domain [cytochrome P450 catalytic domain...

MAIIFLAILTSIIGVLSFYLWTWSYWKRRGIAGPSGYPILGSALEMLSSENPPYLQLKE
WTKQYGKVYGITEGLSRTLVISDPDLVQEVFVKQYDNFFGRKLNPIQGDPNKDKRVNLFSSQGHR
WKRLRTISSPTFSNNSLRKLKTTVEECAVELLRHIEQHTDGGQPIDLLDFYQEFTLDVIGRIAMGQT
DSQMFKNPLLPYVRAVFGEPRKGLFLSGSLAPWIGPILRMVMFSLPNIVKNPAVHVIRHTSNAVEQ
RVKLRMADEKAGIDPGEPQDFIDLFLDAKSDDVELENNEDFTKAGVKVTRQLTTEEIVGQCFVFLI
AGFDTTALSLSYSSFLLATHPKVQKKLQEEIDRECADPEVTFDQLSKLKYMECVIKETLRMYPLGA
LANSRCCMRATKIGNYEIDEGTNILCDTWTLHSDKSIWGEDAEEFKPERWESGDEHFYQKGGYIP
FGLGPRQCIGMRLAYMEEKLLLSHILRKYTLEVCNKTQIPLKLIGSRTTQPESVWLNLTPRDDN

...cytochrome P450 catalytic domain]

B

Human CYP gene family	*C. elegans* CYPs	Known *C. elegans* functions
CYP1 and CYP2	CYP-14A1 to A5	PCB hydroxylase?
	CYP-22A1 (DAF-9)	steroidogenic or fatty acid hydroxylase
	CYP-23A1	
	CYP-33A1	
	CYP-33B1	
	CYP-33C1 to C12	
	CYP-33D1 to D3	
	CYP-33E1	
	CYP-33E2	PUFA hydroxylase
	CYP-33E3	
	CYP-34A1 to A10	PCB hydroxylase?
	CYP-35A1 to A5	
	CYP-35B1 to B3	
	CYP-35C1	
	CYP-35D1	
	CYP-35E1 to E3	
	CYP-36A1	
CYP3	CYP-13A1 to A12	
	CYP-13B1 to B2	
	CYP-25A1 to A5	
	CYP-43A1	
CYP4	CYP-29A1 to A2	
	CYP-29A3	PUFA hydroxylase
	CYP-31A2 to A3	
	CYP-32A1-B1	
	CYP-37A1-B1	
	CYP-42A1	
CYP11, CYP24 and CYP27	CYP-44A1	

fig. S3. The predicted catalytic CYP domain of CYP-13A12 and its protein family homology

(A) Primary structure of CYP-13A12, which is predicted by SOSUI (*67*) to be membrane-spanning with the C-terminal end in the cytoplasm. The membrane-spanning segment is indicated with red, the predicted CYP domain is indicated with blue and the methionine residue mutated in *cyp-13A12(n5590)* is indicated with green. (B) Four categories of

predicted *C. elegans* CYP genes based on their amino acid sequence similarities to human counterparts. Known biochemical functions for CYP-22A1 (a.k.a. DAF-9), CYP-33E2 and CYP-29A3 as lipid hydroxylases are noted (*16, 17, 68, 69*).

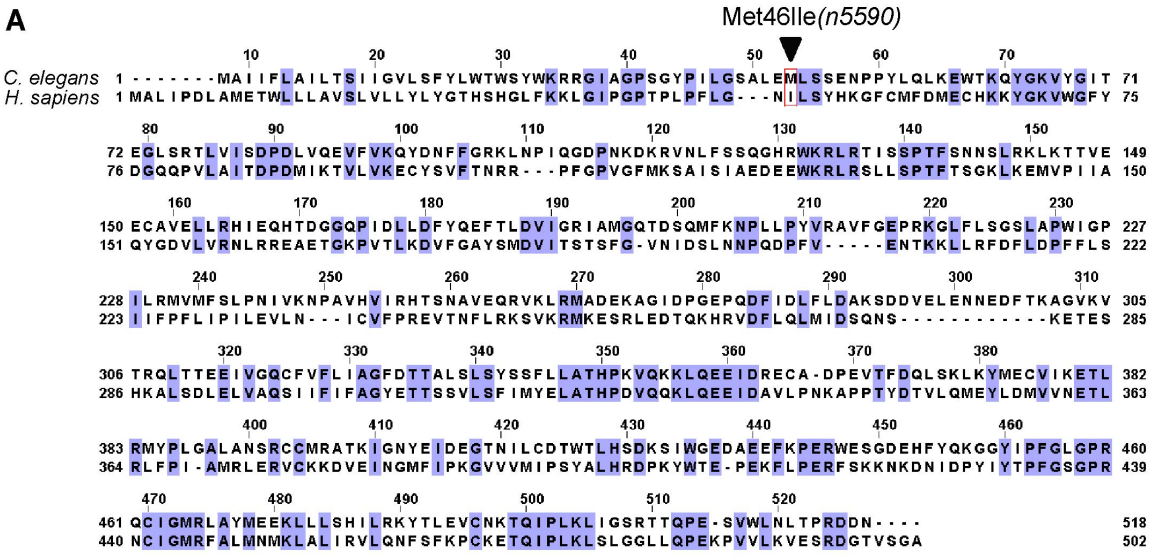

fig. S4. Similarity between *C. elegans* CYP-13A12 and human CYP3A4 proteins

(A) Protein sequence alignment showing homology between CYP-13A12 and human CYP3A4. The arrowhead indicates the *n5590* Met46Ile mutation.

fig. S5

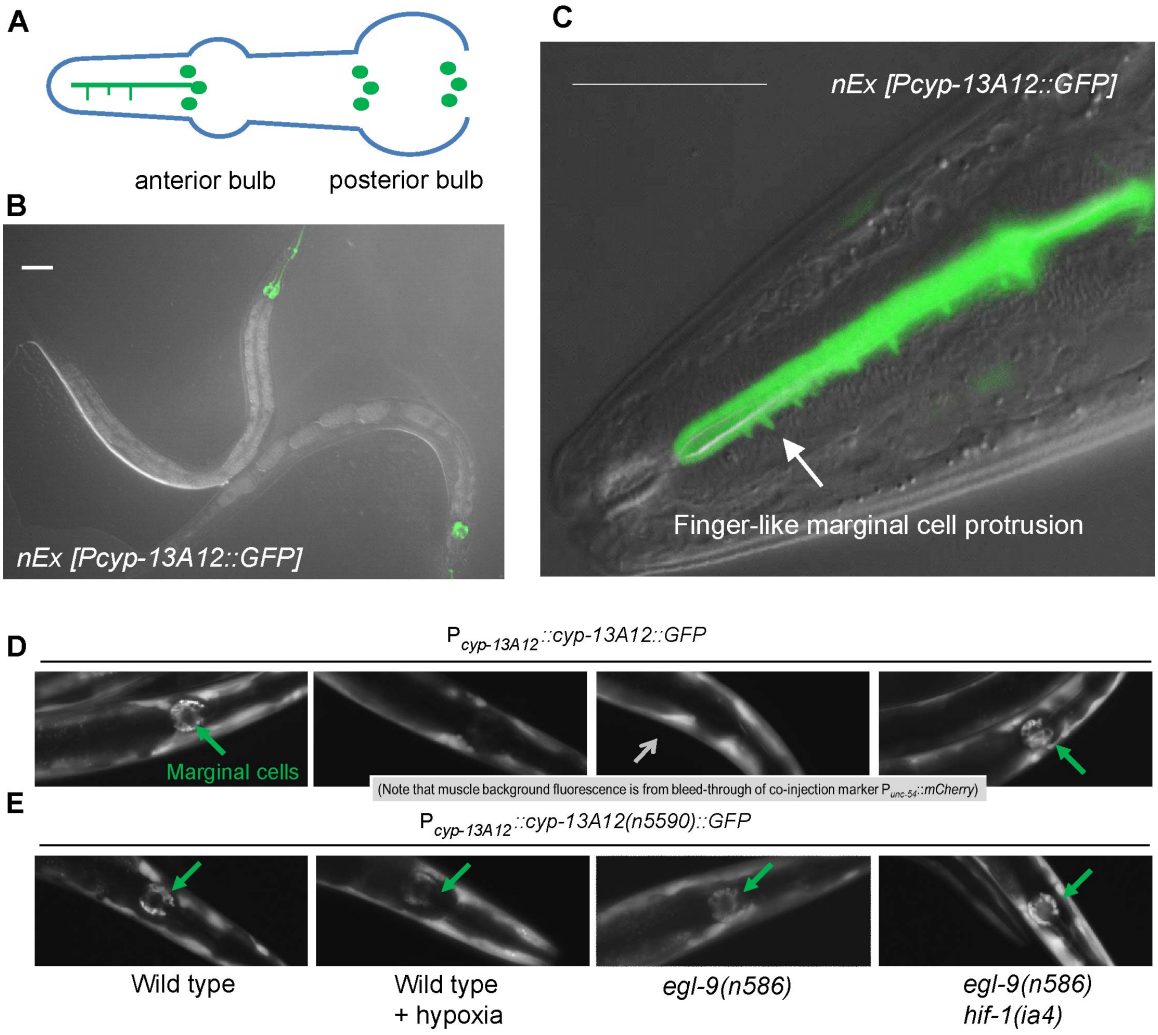

fig. S5. Expression pattern of *cyp-13A12* and effects of hypoxia, *cyp-13A12(n5590)* and *egl-9* mutations on CYP-13A12

(A) A diagram of the *C. elegans* pharynx, showing the locations of the nuclei of the nine marginal cells (green). The process of one anterior marginal cell is shown with tiny protrusions that intercalate with pharyngeal muscles. (B) Merged image of Nomarski and GFP fluorescence micrographs showing expression of *cyp-13A12* in the pharynx. Scale bar, 50 µm. The transcriptional reporter used was an extrachromosomal array of genotype *nEx [$P_{cyp\text{-}13A12}$::GFP]*.

(C) Merged image of high-magnification Nomarski and GFP fluorescence micrographs showing expression of *cyp-13A12* in a marginal cell with finger-like protrusions, one of which is indicated by the arrow. Unlike translational reporters (see below), patterns or levels of GFP expression in such *cyp-13A12* transcriptional reporters are not significantly altered by hypoxic preconditioning or *egl-9* mutations. (D) Representative fluorescence micrographs indicating expression of a $P_{cyp\text{-}13A12}$*::cyp-13A12::GFP* transgene of translational fusion protein in various strains or after 24 hrs hypoxic preconditioning (*10*). The reporter contains the promoter and genomic coding regions of *cyp-13A12* fused with GFP. Note that CYP-13A12::GFP proteins, which were present in marginal cells (green arrows), were down-regulated by hypoxia and in *egl-9* mutants, compared with in wild-type animals. (E) Representative fluorescence micrographs indicating expression of a $P_{cyp\text{-}13A12}$*::cyp-13A12(n5590)::GFP* transgene of translational fusion protein in various strains or after 24 hrs hypoxic preconditioning. CYP-13A12(M46I)::GFP proteins were not down-regulated by hypoxia or in *egl-9* mutants. Equal exposure times were used. Also note that the background fluorescence from body wall muscles (grey arrow) corresponds to fluorescence emission bleed-through from the co-injection marker $P_{unc\text{-}54}$*::mCherry*. The background fluorescence is not present in the transcriptional reporter because the transcriptional GFP reporter is at least one magnitude brighter than the translational GFP reporter.

fig. S6

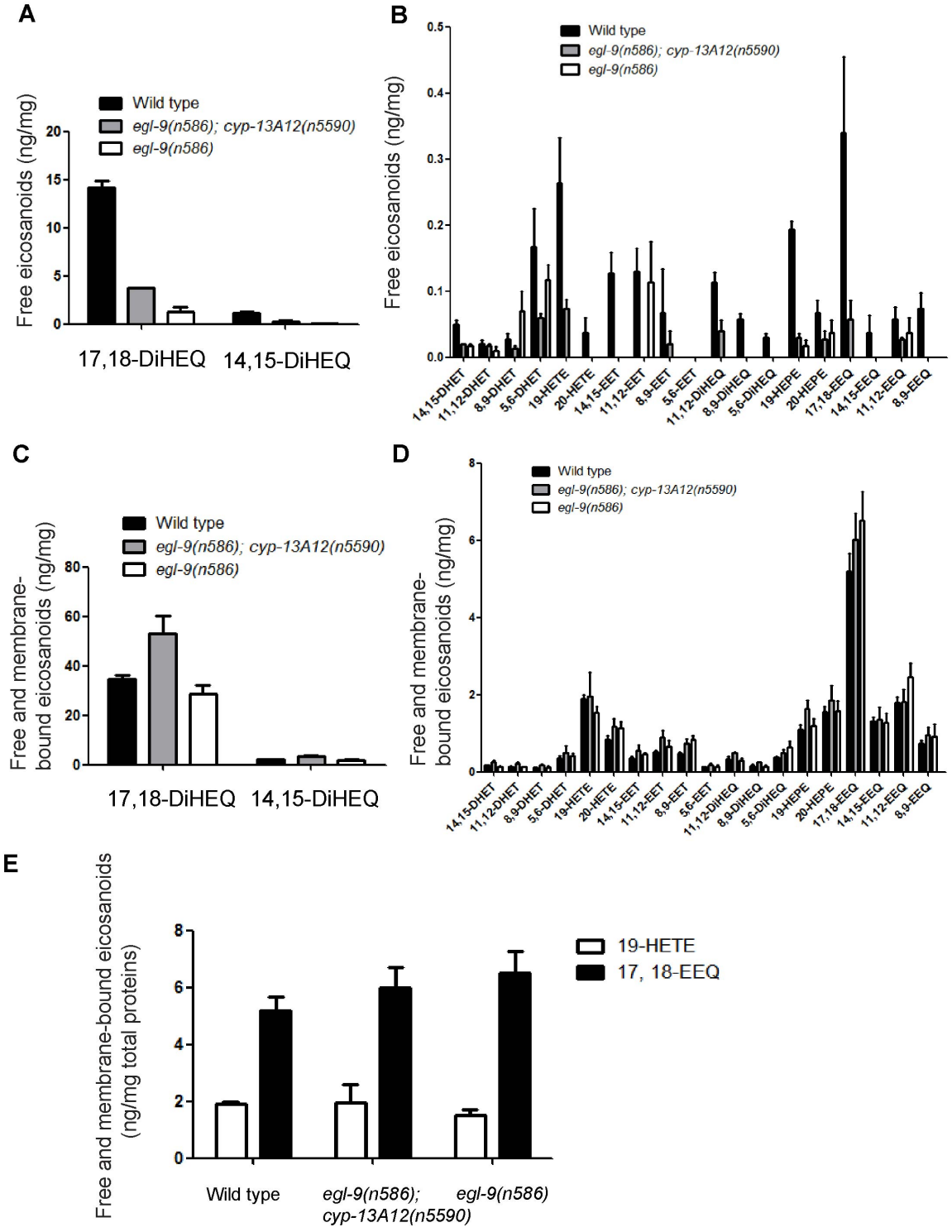
A
Free eicosanoids (ng/mg)
Wild type
egl-9(n586); cyp-13A12(n5590)
egl-9(n586)
17,18-DiHEQ
14,15-DiHEQ
B
Free eicosanoids (ng/mg)
Wild type
egl-9(n586); cyp-13A12(n5590)
egl-9(n586)
14,15-DHET
11,12-DHET
8,9-DHET
5,6-DHET
19-HETE
20-HETE
14,15-EET
11,12-EET
8,9-EET
5,6-EET
11,12-DiHEQ
8,9-DiHEQ
5,6-DiHEQ
19-HEPE
20-HEPE
17,18-EEQ
14,15-EEQ
11,12-EEQ
8,9-EEQ
C
Free and membrane-bound eicosanoids (ng/mg)
Wild type
egl-9(n586); cyp-13A12(n5590)
egl-9(n586)
17,18-DiHEQ
14,15-DiHEQ
D
Free and membrane-bound eicosanoids (ng/mg)
Wild type
egl-9(n586); cyp-13A12(n5590)
egl-9(n586)
14,15-DHET
11,12-DHET
8,9-DHET
5,6-DHET
19-HETE
20-HETE
14,15-EET
11,12-EET
8,9-EET
5,6-EET
11,12-DiHEQ
8,9-DiHEQ
5,6-DiHEQ
19-HEPE
20-HEPE
17,18-EEQ
14,15-EEQ
11,12-EEQ
8,9-EEQ
E
Free and membrane-bound eicosanoids (ng/mg total proteins)
19-HETE
17, 18-EEQ
Wild type
egl-9(n586); cyp-13A12(n5590)
egl-9(n586)

fig. S6. EGL-9 and CYP-13A12-regulated eicosanoids

(A) Levels of free (membrane-unbound) 17,18-DiHEQ and 14,15-DiHEQ profiled by HPLC/MS. (B) Levels of free (membrane-unbound) 14,15-DHET, 11,12-DHET, 8,9-DHET, 5,6-DHET, 19-HETE, 20-HETE, 14,15-EET, 11,12-EET, 8,9-EET, 5,6-EET, 11,12-DiHEQ, 8,9-DiHEQ, 5,6-DiHEQ, 19-HEPE, 20-HEPE, 17,18-EEQ, 14,15-EEQ, 11,12-EEQ, and 8,9-EEQ profiled by HPLC/MS. (C) Levels of total (both free and membrane-bound) 17,18-DiHEQ and 14,15-DiHEQ profiled by HPLC/MS. (D) Levels of total (both free and membrane-bound) 14,15-DHET, 11,12-DHET, 8,9-DHET, 5,6-DHET, 19-HETE, 20-HETE, 14,15-EET, 11,12-EET, 8,9-EET, 5,6-EET, 11,12-DiHEQ, 8,9-DiHEQ, 5,6-DiHEQ, 19-HEPE, 20-HEPE, 17,18-EEQ, 14,15-EEQ, 11,12-EEQ, and 8,9-EEQ profiled by HPLC/MS. (E) Levels of total 17,18-EEQ and 19-HETE profiled by HPLC/MS. Error bars, SEMs, n = 3.

fig. S7

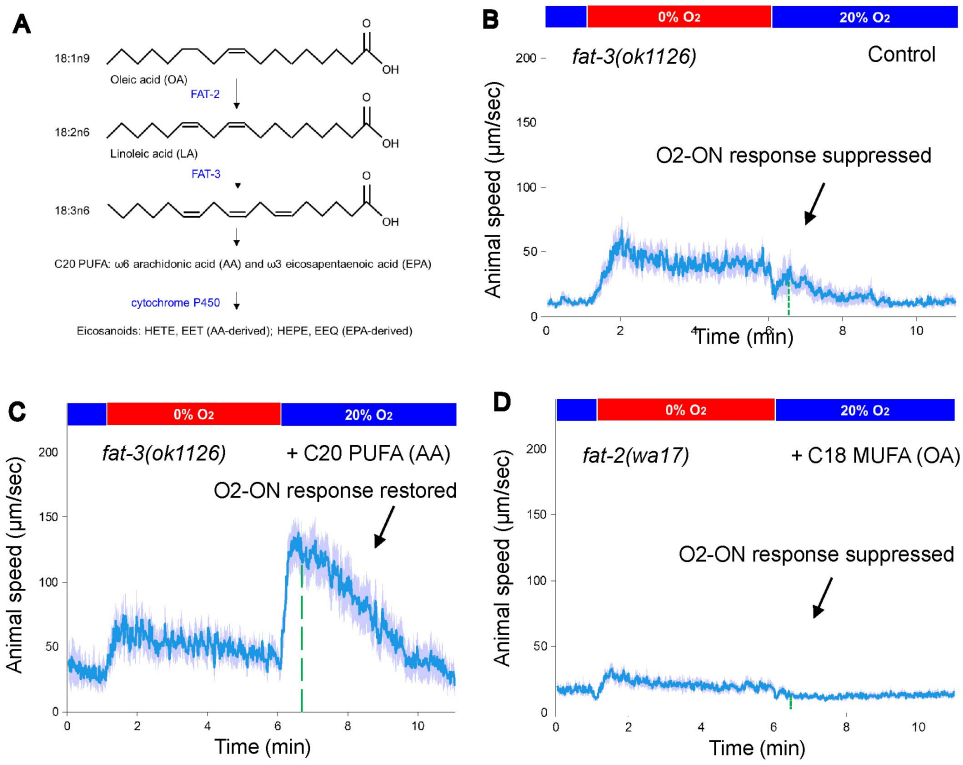

fig. S7. The O2-ON response requires C20 PUFA biosynthesis

(A) A schematic of a PUFA biosynthetic pathway showing biochemical functions of FAT-2 and FAT-3. Note that *fat-2* and *fat-3* mutants completely lack C20 PUFAs. (B) Speed graph of *fat-3* null mutants, showing a defective O2-ON response. Animals were supplemented with PUFA solvents used in (C) as a control. (C) Speed graph of *fat-3* mutants, showing the O2-ON response was rescued by C20 PUFA (arachidonic acid) supplementation. (D) Speed graph *fat-2* mutants, showing the O2-ON response was not rescued by supplementation with the C18 MUFA oleate.

fig. S8

A Normal behavioral state in wild type

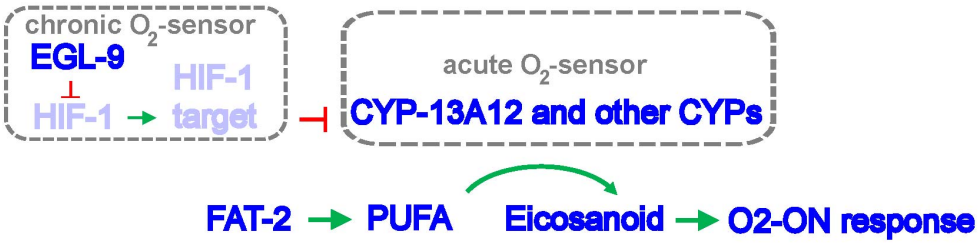

B Behavioral state in *egl-9* mutants or wild-type animals after hypoxic preconditioning

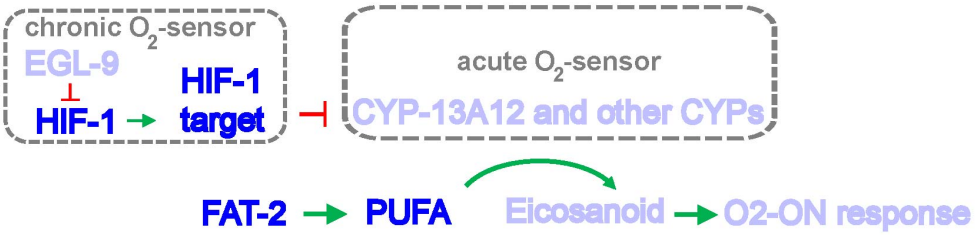

C Behavioral state in *egl-9; cyp-13A12(n5590)* mutants

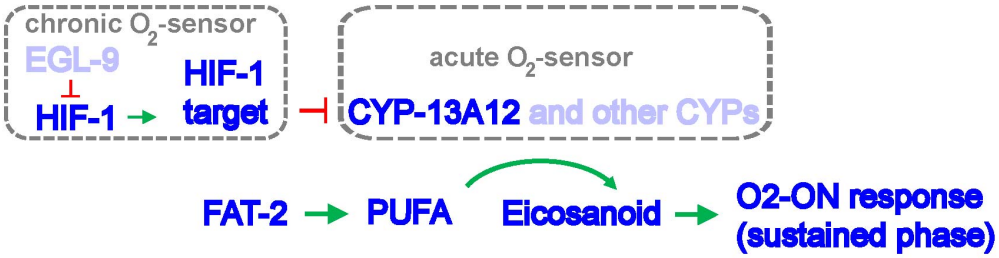

D Behavioral state in *cyp-13A12* loss-of-function mutants

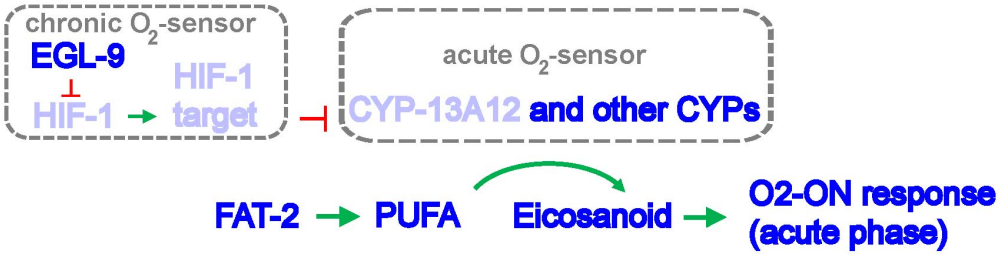

fig. S8. Model for the control of the O2-ON response by EGL-9, CYPs and PUFAs.

(A) Model for the molecular pathway by which EGL-9, CYP, PUFA-eicosanoids coordinately control the O2-ON response under normal conditions. CYP enzymes, including the PUFA oxygenase CYP-13A12, act as acute molecular O_2-sensors during reoxygenation to promote the O2-ON response. The HIF hydroxylase EGL-9, by contrast, acts as a chronic O_2 sensor to suppress the O2-ON response by hypoxic preconditioning (*10*) via regulation of CYPs. The regulation of CYP-13A12 by HIF-1 occurs primarily at the protein level, likely via an unidentified HIF-1 transcriptional target that decreases CYP-13A12 protein levels. The biosynthesis of PUFAs, known physiological substrates of CYP enzymes, is mediated by the FAT-2 and FAT-3 lipid desaturases in a parallel pathway. The defective O2-ON response of *egl-9* mutants is not caused by a reduced activity of the FAT-2/FAT-3/PUFA pathway (fig. S9A); furthermore, HIF-1 activation might enhance but not reduce PUFA biosynthesis (*70*). In panels (A) - (D), the light blue indicates low levels of protein activity, eicosanoids, or a failure of the O2-ON response. (B) *egl-9* mutation causes HIF-1 activation and down-regulation of CYP-13A12 and other CYPs, resulting in a down-regulation of eicosanoids and suppression of the O2-ON response. (C) The gain-of-function mutation *cyp-13A12(n5590)* restores eicosanoid levels, leading to restoration of the sustained phase of the defective O2-ON response of *egl-9* mutants. In contrast to *cyp-13A12,* over-expression of another CYP gene *cyp-29A3* did not restore the defective O2-ON response in *egl-9* mutants (figs. S10A-S10B), indicating that restoration of the O2-ON response in *egl-9* mutants by *cyp-13A12(n5590)* is not caused by a general increased function of PUFA oxygenases. (D) The loss-of-function mutation *cyp-13A12(gk733685)* causes a specific defect in the sustained phase of the O2-ON response.

fig. S9

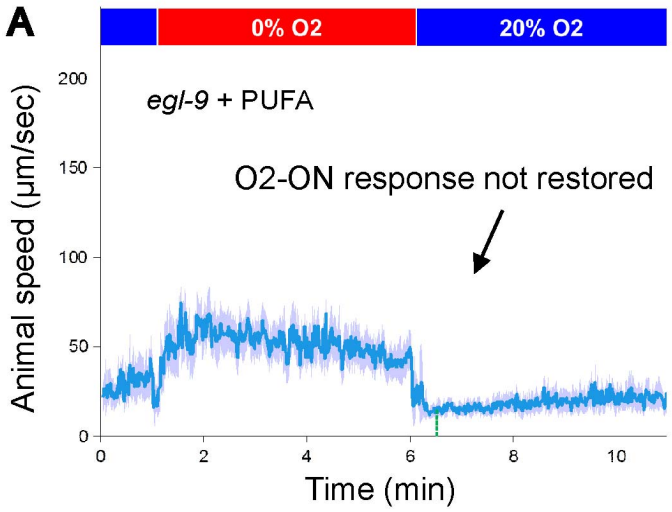

fig. S9. The defective O2-ON response of *egl-9* mutants is not caused by a constitutive deficiency in PUFAs.

(A) Speed graph of *egl-9* mutants, showing the defective O2-ON response was not rescued by exogenous C20 PUFA (arachidonic acid) as a dietary supplement.

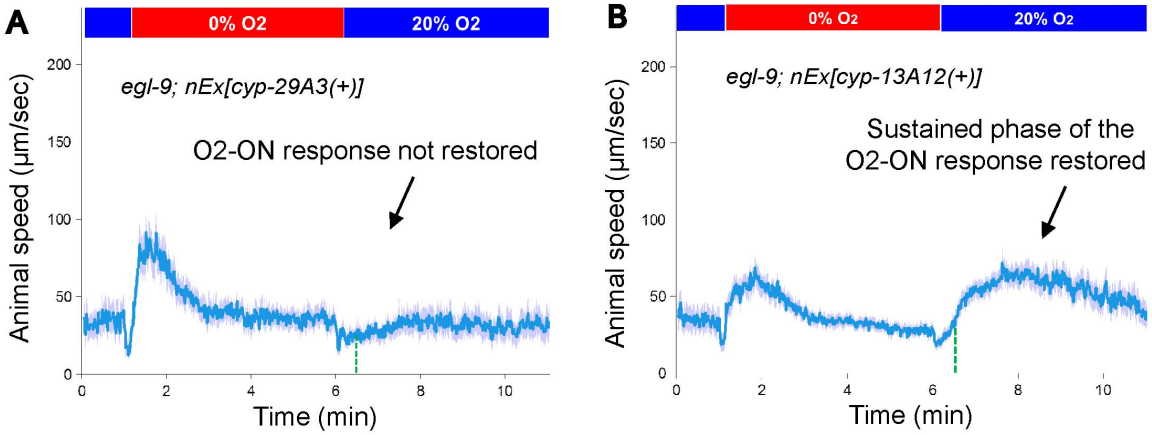

fig. S10. Specificity of CYP-13A12 in rescuing the O2-ON response by *egl-9* mutants.

(A) Speed graph of *egl-9* mutants, showing the defective O2-ON response was not rescued by overexpression of *cyp-29A3(+)*. (B) Speed graph of *egl-9* mutants, showing the defective O2-ON response was rescued by overexpression of *cyp-13A12(+)* in the sustained but not the initial phase. The mean speed within 30-120 s after O_2 restoration is significantly higher than that of *egl-9*(*n586*) mutants ($p < 0.01$).

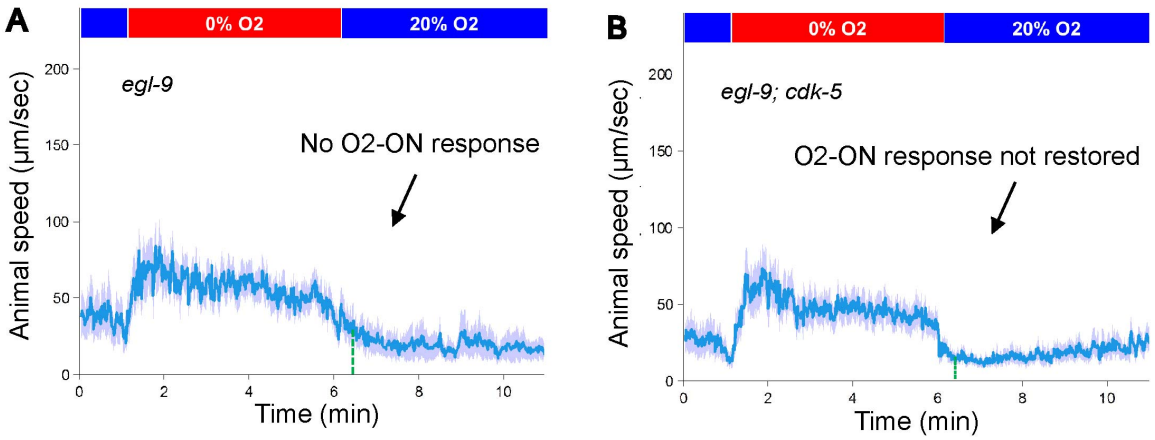

fig. S11. EGL-9 and CYPs regulate the O2-ON response independently of CDK-5.

(A) Speed graph of *egl-9* mutants, showing a defective O2-ON response. (B) Speed graph of *egl-9;cdk-5* mutants, showing the defective O2-ON response was not rescued by loss of *cdk-5*.

Supplementary Table S1

(A) Protein-coding mutations within the genetically mapped interval identified by whole-genome sequencing of the *n5590* mutant. These mutations seen after EMS mutagenesis were not present in the parental mutagenized strain.

LG	Position	Ref. base	Sample base	Coverage	Mutation type	Codon change	Affected gene
III	12953211	T	G	6X	missense	AAT->ACT [Asn->Thr]	*Y39E4A.2*
III	13024707	G	A	10X	missense	ATG->ATA [Met->Ile]	*F14F7.3 (cyp-13A12)*
III	13050495	G	A	8X	silent	AAC->AAT [Asn->Asn]	*F54F12.1*
III	13303608	G	A	13X	silent	CGC->CGT [Arg->Arg]	*Y43F4B.6*

(B) Primers used for molecular cloning and the construction of transgenes

Primer name	Primer sequence
DM1377_cyp-13A12 g5p	TGCTTCTTAAAAGTCTGTAGAACCAAT
DM1378_cyp-13A12 g3p	GGTTTGCTGATTTGCCATTT
DM1391_cyp-13A12 nested c5p	tcaaaaattaaagccagcgtct
DM1392_cyp-13A12Pro to GFP c3p	CGACCTGCAGGCATGCAAGCTtttttaaactcaaaact

	tgaatggtc
DM1393_cyp-13A12Procod to GFP c3p	CAGTGAAAAGTTCTTCTCCTTTACTCATATT ATCATCCCTCGGCGTCA
DM1503_cyp-13A12codutr Nested3p	GCTGATTTGCCATTTTGAAATT

References and Notes:

1. A. S. Go *et al.*, *Circulation*, (Dec 12, 2012).
2. H. K. Eltzschig, T. Eckle, *Nat Med* **17**, 1391 (2011).
3. A. C. Epstein *et al.*, *Cell* **107**, 43 (Oct 5, 2001).
4. W. G. Kaelin, Jr., P. J. Ratcliffe, *Mol Cell* **30**, 393 (May 23, 2008).
5. C. Trent, N. Tsung, H. R. Horvitz, *Genetics* **104**, 619 (Aug, 1983).
6. G. L. Semenza, *Cell* **148**, 399 (Feb 3, 2012).
7. J. A. Powell-Coffman, *Trends Endocrinol Metab* **21**, 435 (Jul, 2010).
8. G. L. Semenza, *Biochim Biophys Acta* **1813**, 1263 (Jul, 2011).
9. J. Aragones *et al.*, *Nat Genet* **40**, 170 (Feb, 2008).
10. D. K. Ma, R. Vozdek, N. Bhatla, H. R. Horvitz, *Neuron* **73**, 925 (Mar 8, 2012).
11. D. K. Ma, N. Ringstad, *Front Biol* **7**, 246 (Jun, 2012).
12. M. W. Budde, M. B. Roth, *Genetics* **189**, 521 (Oct, 2011).
13. D. R. Nelson *et al.*, *Pharmacogenetics* **6**, 1 (Feb, 1996).
14. O. Gotoh, *Mol Biol Evol* **15**, 1447 (Nov, 1998).
15. R. A. Gottlieb, *Arch Biochem Biophys* **420**, 262 (Dec 15, 2003).
16. M. Kosel *et al.*, *Biochem J* **435**, 689 (May 1, 2011).
17. J. Kulas, C. Schmidt, M. Rothe, W. H. Schunck, R. Menzel, *Arch Biochem Biophys* **472**, 65 (Apr 1, 2008).
18. B. S. Berlett, E. R. Stadtman, *J Biol Chem* **272**, 20313 (Aug 15, 1997).
19. R. C. Zangar, D. R. Davydov, S. Verma, *Toxicol Appl Pharmacol* **199**, 316 (Sep 15, 2004).
20. C. A. Rappleye, A. Tagawa, N. Le Bot, J. Ahringer, R. V. Aroian, *BMC developmental biology* **3**, 3 (Oct 3, 2003).
21. J. Szefel *et al.*, *Curr Mol Med* **11**, 13 (Feb, 2011).

22. M. P. Wymann, R. Schneiter, *Nat Rev Mol Cell Biol* **9**, 162 (Feb, 2008).
23. R. S. Chapkin, W. Kim, J. R. Lupton, D. N. McMurray, *Prostaglandins Leukot Essent Fatty Acids* **81**, 187 (Aug-Sep, 2009).
24. D. Panigrahy, A. Kaipainen, E. R. Greene, S. Huang, *Cancer Metastasis Rev* **29**, 723 (Dec, 2010).
25. C. Arnold *et al.*, *J Biol Chem* **285**, 32720 (Oct 22, 2010).
26. J. L. Watts, *Trends Endocrinol Metab* **20**, 58 (Mar, 2009).
27. D. R. Harder *et al.*, *Circ Res* **79**, 54 (Jul, 1996).
28. J. P. Ward, *Biochim Biophys Acta* **1777**, 1 (Jan, 2008).
29. M. Gerber, *Br J Nutr* **107 Suppl 2**, S228 (Jun, 2012).
30. D. Mozaffarian, J. H. Wu, *J Am Coll Cardiol* **58**, 2047 (Nov 8, 2011).
31. L. Avery, J. H. Thomas, Eds., *C. elegans II: Feeding and Defecation*, (2011).
32. Z. F. Altun, D. H. Hall, in *WormAtlas,* L. A. Herndon, Ed. (2009).
33. K. E. Busch *et al.*, *Nat Neurosci* **15**, 581 (Apr, 2012).
34. M. Zimmer *et al.*, *Neuron* **61**, 865 (Mar 26, 2009).
35. J. M. Gray *et al.*, *Nature* **430**, 317 (Jul 15, 2004).
36. M. de Bono, A. V. Maricq, *Annu Rev Neurosci* **28**, 451 (2005).
37. B. J. Piggott, J. Liu, Z. Feng, S. A. Wescott, X. Z. Xu, *Cell* **147**, 922 (Nov 11, 2011).
38. R. Mehta *et al.*, *Science* **324**, 1196 (May 29, 2009).
39. X. R. Mao, C. M. Crowder, *Mol Cell Biol* **30**, 5033 (Nov, 2010).
40. D. L. Miller, M. W. Budde, M. B. Roth, *PLoS One* **6**, e25476 (2011).
41. E. C. Park *et al.*, *EMBO J* **31**, 1379 (Mar 21, 2012).
42. I. M. Booth Depaz, F. Toselli, P. A. Wilce, E. M. Gillam, *Drug Metab Dispos*, (Mar 14, 2013).
43. C. Ghosh *et al.*, *Epilepsia* **52**, 562 (Mar, 2011).
44. V. Agarwal *et al.*, *PLoS One* **3**, e2337 (2008).
45. A. Gabrielsen *et al.*, *J Mol Med (Berl)* **88**, 795 (Aug, 2010).
46. T. Kawasaki *et al.*, *J Cereb Blood Flow Metab* **32**, 1737 (Sep, 2012).
47. K. M. Dunn *et al.*, *Am J Physiol Heart Circ Physiol* **295**, H2455 (Dec, 2008).
48. Y. Ishihara, M. Sekine, M. Nakazawa, N. Shimamoto, *Eur J Pharmacol* **611**, 64 (Jun 2, 2009).
49. M. Khan, I. K. Mohan, V. K. Kutala, D. Kumbala, P. Kuppusamy, *J Pharmacol Exp Ther* **323**, 813 (Dec, 2007).
50. M. W. Davis *et al.*, *BMC Genomics* **6**, 10.1186/1471 (2005).

51. S. Sarin, S. Prabhu, M. M. O'Meara, I. Pe'er, O. Hobert, *Nat Methods* **5**, 865 (Oct, 2008).

52. N. Ringstad, H. R. Horvitz, *Nat Neurosci* **11**, 1168 (Oct, 2008).

53. O. H. Lowry, N. J. Rosebrough, A. L. Farr, R. J. Randall, *J Biol Chem* **193**, 265 (Nov, 1951).

54. S. Brenner, *Genetics* **77**, 71 (May, 1974).

55. S. R. Wicks, R. T. Yeh, W. R. Gish, R. H. Waterston, R. H. Plasterk, *Nat Genet* **28**, 160 (Jun, 2001).

56. S. Flibotte *et al.*, *Genetics* **185**, 431 (Jun, 2010).

57. J. L. Watts, J. Browse, *Proc Natl Acad Sci U S A* **99**, 5854 (Apr 30, 2002).

58. C. Darby, C. L. Cosma, J. H. Thomas, C. Manoil, *Proc Natl Acad Sci U S A* **96**, 15202 (Dec 21, 1999).

59. C. Shen, D. Nettleton, M. Jiang, S. K. Kim, J. A. Powell-Coffman, *J Biol Chem* **280**, 20580 (May 27, 2005).

60. H. Jiang, R. Guo, J. A. Powell-Coffman, *Proc Natl Acad Sci U S A* **98**, 7916 (Jul 3, 2001).

61. C. C. Mello, J. M. Kramer, D. Stinchcomb, V. Ambros, *EMBO J* **10**, 3959 (Dec, 1991).

62. T. Boulin, J. F. Etchberger, O. Hobert, *WormBook: WormMethods: Gene expression*, 1 (2006).

63. J. L. Hartley, G. F. Temple, M. A. Brasch, *Genome Res* **10**, 1788 (Nov, 2000).

64. S. F. Altschul, W. Gish, W. Miller, E. W. Myers, D. J. Lipman, *J Mol Biol* **215**, 403 (Oct 5, 1990).

65. M. A. Larkin *et al.*, *Bioinformatics* **23**, 2947 (Nov 1, 2007).

66. A. M. Waterhouse, J. B. Procter, D. M. Martin, M. Clamp, G. J. Barton, *Bioinformatics* **25**, 1189 (May 1, 2009).

67. T. Hirokawa, S. Boon-Chieng, S. Mitaku, *Bioinformatics* **14**, 378 (1998).

68. H. Y. Mak, G. Ruvkun, *Development* **131**, 1777 (Apr, 2004).

69. D. L. Motola *et al.*, *Cell* **124**, 1209 (Mar 24, 2006).

70. M. Xie, R. Roy, *Cell Metab* **16**, 322 (Sep 5, 2012).

Appendix B

The conserved VPS-50 protein functions in dense-core vesicle maturation and acidification and controls animal behavior

Nicolas Paquin[1,2], Yasunobu Murata[1,2,3], Allan Froehlich[1,2,4], Daniel T. Omura[1,2,4], Michael Ailion[5], Corinne L. Pender[1,2], Martha Constantine-Paton[1,2,3] and H. Robert Horvitz[1,2,4]

Affiliations:

1. Department of Biology, Massachusetts Institute of Technology, 77 Massachusetts Avenue, Cambridge, MA 02139, USA.
2. McGovern Institute for Brain Research, Massachusetts Institute of Technology, 77 Massachusetts Avenue, Cambridge, MA 02139, USA.
3. Department of Brain and Cognitive Science, Massachusetts Institute of Technology, 77 Massachusetts Avenue, Cambridge, MA 02139, USA.
4. Howard Hughes Medical Institute, Massachusetts Institute of Technology, 77 Massachusetts Avenue, Cambridge, MA 02139, USA.
5. Department of Biochemistry, University of Washington, 1705 NE Pacific Street, Seattle, WA 98195, USA.

Published as: Paquin, N., Murata, Y., Froehlich, A., Omura, D.T., Ailion, M., Pender, C.L., Constantine-Paton, M., and Horvitz, H.R. (2016). The conserved VPS-50 protein functions in dense-core vesicle maturation and acidification and controls animal behavior. Curr. Biol. *26*, 862–871. Reprinted with permission from Elsevier.

Contribution: Analysis of locomotion behavior for mutants defective in biogenic amine synthesis, described in Figure 5b

Summary

The modification of behavior in response to experience is crucial for animals to adapt to environmental changes. Although factors such as neuropeptides and hormones are known to function in the switch between alternative behavioral states, the mechanisms by which these factors transduce, store, retrieve and integrate environmental signals to regulate behavior are poorly understood. The rate of locomotion of the nematode *Caenorhabditis elegans* depends on both current and past food availability. Specifically, *C. elegans* slows its locomotion when it encounters food, and animals in a food-deprived state slow even more than animals in a well-fed state. The slowing responses of well-fed and food-deprived animals in the presence of food represent distinct behavioral states, as they are controlled by different sets of genes, neurotransmitters and neurons. Here we describe an evolutionarily conserved *C. elegans* protein, VPS-50, that is required for animals to assume the well-fed behavioral state. Both VPS-50 and its murine homolog mVPS50 are expressed in neurons, are associated with synaptic and dense-core vesicles and control vesicle acidification and hence synaptic function, likely through regulation of the assembly of the V-ATPase complex. We propose that dense-core vesicle acidification controlled by the evolutionarily conserved protein VPS-50/mVPS50 affects behavioral state by modulating neuropeptide levels and presynaptic neuronal function in both *C. elegans* and mammals.

Introduction

Like other animals, *C. elegans* modulates its behavior in response to both environmental signals and past experience [1, 2]. For example, both well-fed and food-deprived worms slow their locomotion after encountering food, and well-fed worms slow less than food-deprived worms (Fig. 1A), presumably because food-deprived animals have a greater need to be in the proximity of food. The responses of well-fed and food-deprived worms upon encountering food require different sets of genes, neurotransmitters and neurons, indicating that these responses reflect two distinct behavioral states [1, 2]. The mechanisms by which animals integrate information about their current environment and their past experience to modulate behavior are poorly understood.

Mutations that impair the maturation of dense-core vesicles and neuropeptide signaling alter the locomotion behavior of *C. elegans* [3]. Whereas synaptic vesicles transport and release neurotransmitters, such as acetylcholine, GABA and glutamate, dense-core vesicles transport and release neuromulators, such as biogenic amines and neuropeptides. In mammals, specific neuropeptides have been associated with the assumption of one of two alternative behavioral states, including hunger-satiety and sleep-wakefulness [4, 5].

From genetic screens, we isolated mutants of *C. elegans* that behave similarly whether they have been well-fed or food-deprived. We have characterized one gene defined by these mutations, *vps-50*, and show that while *vps-50* mutants behave as if they have been food-deprived, they are not malnourished but rather failing to switch behavioral states: they behave as if food-deprived even when well-fed. We describe below the characterization of both *C. elegans*

VPS-50 and its murine homolog, mVPS50 and show that both function in dense-core vesicle maturation and acidification.

Results

vps-50 regulates *C. elegans* behavior

To understand the mechanisms that control the behavioral states of *C. elegans* in response to food availability and past feeding experience, we have characterized three allelic mutations, *ox476*, *n3925* and *n4022*, that cause well-fed animals to behave as if they had been food-deprived (Fig. 1A). *ox476*, *n3925* and *n4022* are alleles of an evolutionarily conserved gene, *C44B9.1*, which we have named *vps-50* (see below) (Fig. S1A-C). *vps-50* mutants have normal rates of pharyngeal pumping and do not display the slow growth and abnormal pigmentation of starved wild-type animals (Fig. 1B-C), indicating that *vps-50* mutants are not malnourished but rather are in the behavioral state normally induced by acute food deprivation. *vps-50* mutants are abnormal not only in locomotion but also in egg laying, as they retain eggs for an abnormally long period of time and lay eggs at substantially later developmental stages than do wild-type worms (Fig. 1D). Food-deprived wild-type worms are similarly abnormal in egg laying, further indicating that *vps-50* mutants are in a food-deprived state when not food-deprived.

vps-50 acts in neurons to control *C. elegans* behavior

We examined the expression pattern of a transgene that expresses a VPS-50::GFP fusion under the control of the *vps-50* promoter and observed that *vps-50* is expressed broadly in the nervous system and possibly in all neurons (Fig. 2 and data not shown). These observations suggest that *vps-50* plays a specific role in neuronal function. To determine where *vps-50*

functions, we used transgenes that express *vps-50* in a tissue-specific manner and attempted to rescue the mutant phenotype of *vps-50* mutants. Expression of *vps-50* using the *rab-3* pan-neuronal promoter significantly rescued both the locomotion and egg-laying defects of *vps-50(n4022)* mutants, while expression in body-wall muscles using the *myo-3* promoter failed to rescue the locomotion and egg-laying defects of *vps-50* mutants (Fig. 1D & 2B). We conclude that *vps-50* functions in neurons.

To analyze further the cellular sites of function of VPS-50 in the nervous system, we expressed *vps-50* in subsets of neurons. VPS-50 expression in cholinergic neurons in *vps-50* mutants using the *unc-17* promoter rescued the locomotion defect of well-fed *vps-50* mutant worms in the presence of food, while *vps-50* expression in GABAergic neurons using the *unc-47* promoter did not improve the locomotion of well-fed *vps-50* mutants in the presence of food (Fig. 2C). These observations suggest that *vps-50* functions in cholinergic neurons to control locomotion. Expression of *vps-50* using the *tax-2* promoter, which drives expression in the main sensory neurons that control olfaction, gustation and thermotaxis, did not rescue the locomotion defect of *vps-50* mutant worms, suggesting that this behavioral defect of *vps-50* mutants is not a consequence of altered food sensing (Fig. 2C).

VPS-50 is highly conserved from worms to mammals (Fig. S1B), and pan-neuronal expression in *vps-50* mutant worms of its murine homolog mCCDC132, which we refer to as mVPS50, rescued the locomotion defect of *vps-50* mutants (Fig. 2B). Thus, *C. elegans* VPS-50 and murine mVPS50 not only are similar in sequence but also are functionally similar and likely act in similar molecular processes.

VPS-50 and its murine homolog associate with synaptic vesicles

Using an anti-GFP antibody to visualize a VPS-50::GFP fusion protein in *C. elegans* whole mounts, we observed VPS-50::GFP in neuronal cell bodies and also at synapse-rich regions such as the nerve ring (Fig. 2D). In *C. elegans*, both synaptic and dense-core vesicles as well as their associated proteins are transported to synapses by the kinesin-like protein UNC-104/KIF1A [6, 7]. Like the transport of the vesicular SNARE protein synaptobrevin (SNB-1), the transport of VPS-50 to the nerve ring required UNC-104/KIF1A, suggesting that VPS-50 associates with synaptic or dense-core vesicles (Fig. 2D).

The mammalian *Vps50* gene (also known as *CCDC132* or *Syndetin*) has been reported to be highly expressed in many regions of both the mouse and the human brains [8]. Using an antibody against VPS50, we determined that the mVPS50 protein is widely expressed in the mouse brain throughout development (Fig. 3A-C) and in most and possibly all excitatory and inhibitory neurons (Fig. 3D). We examined the distribution of mVPS50 in mouse cultured primary cortical and hippocampal neurons. mVPS50 did not colocalize with the *cis*-Golgi apparatus marker GM130 (Fig. 4A) but did substantially colocalize with the *trans*-Golgi markers Golgin-97 and TGN38 (Fig. 4B & S3A). These observations suggest that mVPS50 is at least partially localized to the *trans*-Golgi. The *trans*-Golgi apparatus has been proposed to be the final sorting compartment for both synaptic and dense-core vesicles [10]. Based on this information and our observation that *C. elegans* VPS-50 associates with synaptic or dense-core vesicles, we analyzed the colocalization of mVPS50 with dense-core vesicles in mouse cultured primary neurons. mVPS50 colocalized with dense-core vesicles that contained Chromogranin C or neuropeptide Y (Fig. 4C-D). The mVPS50 signal did not extend as far in the neuronal

processes as did the neuropeptide signals, so it is possible that the colocalization observed between mVPS50 and neuropeptides is limited to the *trans*-Golgi apparatus and to early vesicles budding from it.

We fractionated extracts of adult mouse cortex and showed that mVPS50 was enriched in a fraction that contained synaptic and dense-core vesicles (LP2), suggesting that like *C. elegans* VPS-50 the murine protein is associated with synaptic or dense-core vesicles (Fig. 4E). The LP2 fraction, which is the pellet obtained after centrifugation of fraction LS1, also contained neuropeptides, as indicated by the detection of Chromogranin C. We further fractionated the synaptic vesicle and cytosol LS1 fraction using a sucrose density gradient. The distribution of mVPS50 is like that of the clathrin heavy chain, which assembles onto vesicle membranes, and not like that of the membrane-bound synaptophysin or that of the neuropeptide Chromogranin C (Fig. 4F). We concluded that mVPS50 likely associates with synaptic vesicles as a soluble protein and is not in the lumen of vesicles or integrated into synaptic and dense-core vesicle membranes. We have not observed VPS-50 or mVPS50 at synapses in *C. elegans* or in mouse cultured primary neurons, respectively, indicating that these proteins likely associate with immature synaptic and dense-core vesicles budding from the *trans*-Golgi but do not traffic all the way to mature synapses (data not shown).

vps-50 **mutant animal have a defect in dense-core vesicle maturation**

The behavioral defects of *vps-50* mutant worms are strikingly similar to those of mutants in *unc-31* (the worm homolog of mammalian CADPS2/CAPS), *rab-2* (the homolog of RAB2, which is also known as *unc-67* and *unc-108* in *C. elegans*) and *rund-1* (the ortholog of

RUNDC1), genes involved in the release and maturation of dense-core vesicles, but not like those of animals mutant for *egl-3*, which encodes a proprotein convertase that cleaves neuropeptides (Fig. 5A & Fig. S4) [3, 11–14]. *unc-31* affects the release of dense-core but not of synaptic vesicles [12], suggesting that VPS-50 functionally affects dense-core vesicles. Dense-core vesicles release biogenic amines and neuropeptides. *cat-2* and *tph-1* mutants, which are deficient in the synthesis of dopamine and serotonin, respectively, and *cat-2 tph-1 tdc-1* triple mutant animals, which are defective for the synthesis of all known biogenic amines in *C. elegans* [15–17], did not display the *vps-50* mutant phenotype (Fig. 5B), suggesting that VPS-50 functions in neuropeptide signaling.

To determine if *vps-50* affects neuropeptides, we used a FLP-3::Venus neuropeptide fusion protein to analyze neuropeptide levels, localization, release and processing [13]. *unc-31* (CADPS2/CAPS) mutants, which are impaired in the release of dense-core vesicles [12], and *egl-3* (PC2) mutants, which are impaired in the processing of neuropeptides [18], accumulated elevated levels of FLP-3::Venus at synapses in the dorsal nerve cord. By contrast, *rab-2* mutants, which are defective in dense-core vesicle maturation, have been reported to have decreased levels of neuropeptides at synapses [13]. *vps-50* mutants, like *rab-2* mutants, had decreased levels of FLP-3::Venus at synapses, revealing that *vps-50* function is necessary for normal levels of synaptic neuropeptides (Fig. 5C). The FLP-3::Venus fusion did not significantly accumulate in cell bodies of *vps-50* mutants, indicating that their low levels of neuropeptides at synapses were not the result of a transport defect (Fig. 5D).

Synaptic levels of neuropeptides could be low in *vps-50* mutants either because of defects in producing neuropeptides or because these mutants degrade or release neuropeptides faster than wild-type animals. To assess the rate of neuropeptide release, we quantified FLP-3::Venus levels in coelomocytes, scavenger cells that take up secreted proteins from the worm's body cavity [19]. Neuropeptide levels in coelomocytes correlate with the neuropeptide levels released from neurons [12, 20]. Coelomocytes in *vps-50* mutants exhibited abnormally low levels of FLP-3::Venus (Fig. 5E), indicating that *vps-50* mutants are not secreting neuropeptides faster than do wild-type animals. Taken together, these results suggest that *vps-50* mutants, like *rab-2* mutants, produce low levels of neuropeptides. The effect of *vps-50* on neuropeptide levels at synapses is not limited to FLP-3, as an NLP-21::Venus reporter also showed low levels at synapses in *vps-50* mutants as compared to wild-type animals (Fig. 5I). We postulate that mutation of *vps-50* has a broad impact on neuropeptides and that the behavioral defects of *vps-50* mutants is the result of the perturbation of one or of multiple neuropeptides.

We further compared *vps-50* and *rab-2* mutants using a transgene that expresses the dense-core vesicle marker IDA-1::GFP [13]. As previously reported, *rab-2* mutants have increased levels of IDA-1::GFP in cell bodies and lower levels of IDA-1::GFP at synapses, reflecting their defect in dense-core vesicle maturation. By contrast, *vps-50* mutants had elevated levels of IDA-1::GFP in both cell bodies and at synapses (Fig. 5F-G), indicating that *vps-50* and *rab-2* both affect dense-core vesicle maturation and do so with some differences.

Neuropeptides are produced from proproteins, which in *C. elegans* are cleaved into peptides by the proprotein convertase 2 enzyme EGL-3 [18]. We asked if *vps-50* mutants are

defective in neuropeptide processing. We examined FLP-3::Venus from protein extracts using immunoblotting and observed that *vps-50* mutants had reduced levels of FLP-3 and that the ratio of processed to unprocessed FLP-3 was significantly lower than in the wild type (Fig. 5H).

In short, our results suggest that the behavioral defects of *vps-50, unc-31* and *rab-2* mutants are similar because all three are low in neuropeptide release. However, *vps-50* mutants are distinct, because unlike *unc-31* mutants they did not accumulate neuropeptides at synapses and unlike *rab-2* mutants they had elevated levels of the dense-core vesicle protein IDA-1::GFP at synapses.

VPS-50 and its murine homolog affect synaptic and dense-core vesicle acidification

To identify physical partners of VPS-50, we purified recombinant VPS-50 sections fused to glutathione-S-transferase (GST-VPS-50) and probed a protein extract from wild-type *C. elegans* in a pull-down experiment. Using mass spectrometry, we identified VHA-15, a homolog of the H subunit of the V-ATPase complex [21], as a possible VPS-50 interactor (data not shown). We confirmed the interaction between VPS-50 and VHA-15, which might be direct or indirect, using the yeast two-hybrid system (Fig. 6A). The V-ATPase complex is a proton pump that acidifies cellular compartments, including synaptic and dense-core vesicles, the lysosome and the *trans*-Golgi apparatus [21, 22]. In neurons, V-ATPase activity is required for loading neurotransmitters into synaptic vesicles [23], and its disruption can impair neuropeptide processing because of a failure in acidifying vesicles to the pH optimum of processing enzymes [24]. Given the interaction between VPS-50 and VHA-15, we postulated that VPS-50 regulates

or responds to the activity of the V-ATPase complex responsible for the acidification of synaptic and dense-core vesicles.

To investigate the effect of impaired V-ATPase function in neurons, we examined mutants defective in the V-ATPase subunit UNC-32, which is required for synaptic vesicle acidification [25, 26], using the FLP-3::Venus and IDA-1::GFP reporters described above. *unc-32* mutants had low neuropeptide levels and high IDA-1::GFP levels at synapses, molecular defects similar to those of *vps-50* mutants (Fig. S5A-D). (*unc-32* mutants are small, sickly, and severely impaired in locomotion (Fig. S5E). For this reason *unc-32* mutants cannot be assessed for locomotory responses to external cues for comparison with *vps-50* mutants.) We then analyzed the acidification of synaptic and dense-core vesicles in intact worms by expressing synaptopHluorin (SpH) using the *unc-17* promoter. SpH is a fusion of the synaptic-vesicle protein synaptobrevin with the pH-sensitive GFP reporter pHluorin, and the pHluorin moiety is localized to the vesicular lumen, where it can be used to assay vesicle pH [27, 28]. SpH has been used to study the effects of mutations in the V-ATPase complex on *C. elegans* GABAergic neurons [25]. *vps-50* mutants, like *unc-32* mutants, showed increased SpH fluorescence, indicating that *vps-50* mutants are defective in vesicle acidification (Fig. 6B-C). *unc-32* mutants share several aspects of the *vps-50* mutant phenotype. However, whereas *unc-32* mutants have low levels of synaptobrevin (SNB-1) at synapses, *vps-50* mutants have normal levels (Fig. 6C). Since SpH is a SNB-1::pHluorin fusion, *unc-32* likely has a greater effect than *vps-50* on V-ATPase complex activity. The increased SpH fluorescence in *vps-50* mutant animals is unlikely to be the result of SpH missorting in these mutants, as SpH colocalizes with the vesicular acetylcholine transporter UNC-17 in both wild-type and *vps-50* mutant animals (Fig. S5F) and

SpH localization to dorsal cord synapses in *vps-50* mutants is dependent on UNC-104/KIF1A, as in the wild type (Fig. S5G). Impaired endocytosis at synapses could also lead to increased SpH fluorescence by causing an accumulation of SpH at the plasma membrane. To ask whether *vps-50* mutants fail to recycle SpH, we compared them to mutants for *unc-11,* the AP180 homolog; *unc-11* mutants fail to recycle synaptic vesicle-associated proteins like SpH and show a diffusion of SpH (and SNB-1) all along the plasma membrane [29]. The diffusion of synaptic vesicle-associated proteins in *unc-11* mutants is independent of UNC-104/KIF1A function, as *unc-11; unc-104* double mutants similarly show diffusion of SNB-1 along the plasma membrane in neuronal processes [29]. By contrast, we observed no such diffusion of SpH in *unc-104; vps-50* double mutants (Fig. S5G). We conclude that *vps-50* controls the acidification of vesicles rather than affect the levels of surface SpH.

To test if the role of VPS-50 in vesicle acidification is evolutionarily conserved, we used shRNAs to knock down *mVps50* levels in mouse primary cultured cortical neurons transfected with a synaptophysin-pHluorin fusion (SypHy) [30]. We observed that neurons reduced in mVPS50 levels had higher SypHy fluorescence levels than wild-type neurons (Fig. 6D). Most SypHy signal, like the SpH signal observed in *C. elegans*, is from synaptic vesicles, which are more abundant than dense-core vesicles. Thus, disruption of *mVps50* led to an acidification defect of synaptic vesicles in murine neurons. This observation further establishes the evolutionarily conserved functions of VPS-50 and mVPS50. Increasing the intravesicular pH to 7.4 using NH_4Cl (see Experimental Procedures) increased the SypHy fluorescence of wild-type and *mVps50* knockdown neurons to similar levels. Thus, the high SypHy fluorescence observed in neurons depleted for *mVps50* resulted from a defect in vesicle acidification and not from a

difference in SypHy expression, since neutralizing the pH of the vesicular lumen resulted in comparable SypHy fluorescence levels for wild-type and *mVps50* knocked-down neurons.

Since the signals from the SpH and SypHy reporters are predominantly from synaptic vesicles, we developed a new reporter to assess the acidification of dense-core vesicles specifically. We fused both mCherry and pHluorin to the C-terminal end of a neuropeptide reporter encoding the first five neuropeptides of the *flp-3* gene (FLP-3_{1-5}::mCherry::pHluorin); neuropeptides are found in dense-core vesicles but not in synaptic vesicles. mCherry, which is largely pH-insensitive, provides an internal control. We expressed this reporter in cholinergic neurons and used the ratio of the pHluorin/mCherry fluorescence intensities as a measure of pH. (A previous study showed that such a pHluorin/mCherry ratio indicates pH [31]). The intramolecular ratiometric nature of our reporter is important, because we use this neuropeptide reporter in mutants that have altered neuropeptide levels; this reporter allows us to normalize for these different neuropeptide levels. That the FLP-3_{1-5}::mCherry::pHluorin reporter is indeed vesicle-associated is confirmed by the observation that its transport to the dorsal nerve cord is UNC-104/KIF1A-dependent (data not shown); UNC-104/KIF1A transports dense-core and synaptic vesicles. Furthermore, the FLP-3_{1-5}::mCherry::pHluorin reporter can be observed in coelomocytes, indicating its release (see above) and establishing that it accurately reflects neuropeptide trafficking. Since FLP-3 is a soluble peptide, the FLP-3_{1-5}::mCherry::pHluorin reporter should be localized to the lumen of dense-core vesicles, unlike the SpH reporter (a fusion between pHluorin and the membrane protein synaptobrevin), which is localized to both synaptic vesicles and the plasma membrane. Thus, the FLP-3_{1-5}::mCherry::pHluorin reporter yields a more specific signal for intravesicular acidity than does SpH. Mutants for *vps-50* and the

V-ATPase subunit gene *unc-32* showed impaired dense-core vesicle acidification as their pHluorin/mCherry fluorescence intensity ratios were higher than that of wild-type animals (Fig. 6E).

mVPS50 functions in the assembly of the V-ATPase complex

Taken together, our results demonstrate that *C. elegans vps-50* functions in the maturation and acidification of dense-core vesicles and through the acidification process affects neuropeptide signaling. Given that VPS-50 interacts with VHA-15, the H subunit responsible for the assembly of the soluble and membrane-bound moieties of the complex, we hypothesized that through its interaction with VHA-15, VPS-50 might function in the assembly of the V-ATPase complex onto synaptic and dense-core vesicles, thus regulating vesicle acidification. To test this hypothesis, we analyzed the presence of two of the soluble subunits of the V-ATPase complex, V1 subunits A and B, on synaptic vesicles in control mouse cultured primary neurons and in neurons knocked down for *mVps50*. The rationale for this experiment was that these soluble A and B subunits would be present on the membrane of synaptic vesicles only when the V-ATPase complex is fully assembled. We purified the synaptosomal fraction and analyzed the amounts of V-ATPase V1 A and B subunits by immunoblotting. We found that knockdown of *mVps50* decreased the levels of synaptosomal V-ATPase subunits A and B as compared to control fractions (Fig. 6F). The total levels of these subunits were not affected in a whole-cell lysate, indicating that the decreased synaptosomal levels observed in the *mVps50* knockdown were not caused by generally lower V-ATPase V1 A and B subunit levels (Fig. 6F). Taken together, our results suggest that *C. elegans* VPS-50 and its mammalian homologs are required for the proper assembly of the V-ATPase subunits into a functional holoenzyme, a process necessary for

vesicle acidification. Alternatively, it is possible that VPS-50 acts in the sorting of the V-ATPase subunits to their site of assembly, which could lead to the formation of abnormal vesicles that are impaired in acidification.

Discussion

We propose that VPS-50 regulates the behavioral state of *C. elegans* by controlling dense-core vesicle maturation and acidification and thereby modulating neuropeptide signaling. VPS-50 and its mammalian homologs likely share an evolutionarily conserved function in V-ATPase complex assembly or sorting, leading to the generation of immature or otherwise abnormal dense-core vesicles impaired in vesicular acidification. The V-ATPase complex functions broadly to acidify cellular compartments, and the differential expression of subunit isoforms can confer cellular specificity to the localization and function of the complex [21]. It is possible that VPS-50 and its homologs regulate the V-ATPase complex specifically in neurons. VPS-50 might function in vesicle acidification as early as the *trans*-Golgi, from which dense-core vesicles are generated. Interestingly, recent studies have shown that fly and human VPS50 can associate with components of the Golgi-Associated Retrograde Protein (GARP) complex, which functions in retrograde transport from endosomes to the *trans*-Golgi, suggesting that *vps-50* might act in protein sorting [32–35]. GARP consists of four proteins: VPS51, VPS52, VPS53 and VPS54. VPS50 replaces VPS54 in an alternative complex, the Endosome-Associated Recycling Protein (EARP) complex, which shares the VPS51, VPS52, and VPS53 subunits with GARP. Based in those interactions, the murine and human proteins have been names VPS50. (We note that VPS50 is referred to as Syndetin [34] or VPS54L [35] in two of these studies.) These reports further suggest that VPS50 localizes in part to recycling endosomes and that knockdown of

VPS50 leads to impaired recycling of proteins to the plasma membrane. These observations are consistent with our findings that *vps-50* mutants show altered neuropeptide and dense-core vesicle protein levels at synapses and that *mVps50*-depleted neurons show impaired assembly or sorting of V-ATPase complex subunits. We suggest that the EARP complex could function in the maturation of dense-core vesicles.

unc-31 functions in dense-core vesicle release [12]. Mutations in *vps-50* and *unc-31* both lead to low levels of neuropeptide secretion as well as to similar behavioral phenotypes. Disruption of CADPS2, the mammalian homolog of *unc-31*, in both mouse and humans has been linked to autism spectrum disorders [36, 37]. In addition, a deletion spanning only *hVPS50* (the human homolog of *vps-50*) and a second gene, *CALCR* (calcitonin receptor), has been reported in an autistic patient [38]. We suggest that VPS-50 plays a fundamental role in synaptic function and in the modulation of behavior and that an understanding of *vps-50* and its mammalian homologs might shed light on mechanisms relevant to human behavior and possibly to neuropsychiatric disorders, including autism spectrum disorders.

Experimental Procedures

Behavioral analysis: For locomotion analyses, young adult worms were washed off a plate with S Basal medium and allowed to sediment in a 1.5 mL tube. Liquid was removed by aspiration, and worms in about 100 µL of S Basal were transferred to the center of an assay plate seeded with an *E. coli* OP50 lawn covering the entire surface. For tracking in the absence of bacteria, worms were washed an extra time in S Basal before transfer to an unseeded plate. After 30 minutes in the absence of bacteria, worms were washed off with S Basal and transferred to a new

seeded plate. We used a worm tracker [39] to record 10 min videos. The average speed of the population between minutes 3 and 4 of the recording is reported. The developmental stages of laid eggs were scored as described [40]. For pharyngeal pumping rates, animals were recorded at 25 fps using a Nikon SMZ18 microscope with a DS-Ri2 camera and the videos were scored for pumping events during a 10 second window.

Microscopy and immunohistochemistry: For analysis of coelomocyte fluorescence, worms were immobilized in 30 mM NaN_3 on NGM pads, and z-stacks of images were acquired using a Zeiss LSM510 confocal microscope. Maximal intensity projections of the coelomocytes were analyzed using ImageJ. Worms expressing other fluorescent reporters were immobilized with polystyrene beads on pads made of 10% agarose in M9 and imaged using a Zeiss Axioskop II microscope and a Hamamatsu ORCA-ER camera, with the exception of worms expressing the FLP-3::mCherry::pHluorin fusion, which were imaged using a Nikon Eclipse T*i* microscope and a Princeton Instrument Pixis 1024 camera. Images were analyzed using ImageJ. Fluorescence intensities were quantified using a selected region of interest (ROI) from which we subtracted a background of equal size from a nearby region. The dorsal nerve cord was imaged near where the posterior gonad arm turns. For quantification of the FLP-3::mCherry::pHluorin fusion fluorescence intensities, the "Subtract background" option of ImageJ was used prior to selecting ROIs as above. For immunohistochemistry, worms were washed off plates in PBS 1X and transferred to a 1.5 mL tube. Animals were washed three times and frozen in liquid nitrogen in about 150 µL of PBS 1X. Aliquots were thawed and pressed between two glass slides and placed on dry ice for 10 min. Glass slides were pulled apart and covered in ice-cold methanol in 50 mL tubes. Worms were washed off glass slides using a Pasteur pipette, and the glass slides were

removed from the tube. Tubes were centrifuged 5 min at 3700 rpm. Worms were retrieved using a Pasteur pipette and transferred to a clean 1.5 mL tube. Methanol was removed. Worms were incubated in acetone for 5 min on ice. Worms were rehydrated three times in PBS 1X and incubated overnight at 4 °C with rabbit monoclonal anti-GFP antibody (1:100) (Invitrogen) and mouse monoclonal anti-SNB-1 (1:100) antibody or mouse anti-UNC-17 (1:100) antibody (gift from J. Rand). Secondary antibodies were goat anti-rabbit and anti-mouse antibodies coupled with Alexa 594 and Alexa 488 (1:2500), respectively (Invitrogen). Images were acquired using a Zeiss Axioskop II.

Primary hippocampal and cortical neuron cultures: All manipulations were performed in accord with the guidelines of the MIT Institutional Animal Care and Use Committee. Primary neuron cultures were prepared from embryonic day 15 (E15) mice. Hippocampus or cortex was dissected and treated with papain (Worthington) and DNaseI (Sigma) for 10 min at 37 °C and triturated with a fire-polished Pasteur pipette. Cells were plated at the density of 5×10^4 cells / cm^2 on coverslips or plastic plates that were pre-coated with alpha-laminin and poly-D-lysine and cultured in Neurobasal medium supplemented with B-27.

Immunocytochemistry and immunohistochemistry of mouse neurons: For immunocytochemistry, mouse cultured neurons were fixed with 4% paraformaldehyde in PBS for 10 min, permeabilized and blocked with 5% goat serum and 0.3% Triton X-100 in PBS for 1 hour. After incubation with primary antibodies overnight at 4 °C and with secondary antibodies for 1 hour at room temperature, coverslips were mounted with Fluoromount-G (Electron

Microscopy Sciences). z-stack images were taken using a Nikon PCM 2000 or C2 confocal microscope with a 60x oil objective (N.A. 1.4) at 0.5 μm z-intervals.

For immunohistochemistry, VGAT-Venus mice were perfused with 4% paraformaldehyde in PBS, cryoprotected in 30% sucrose and sectioned at 60 μm on a freezing microtome. Sagittal sections were permeabilized and blocked in 5% goat serum and 1% Triton X-100 in PBS. Sections were incubated with primary antibodies overnight at 4 °C and secondary antibodies for 2 hours at room temperature, and mounted with Fluoromount-G. z-stack images were taken using a Nikon PCM 2000 confocal microscope with a 10x objective (N.A. 0.5) at 10 μm z-intervals. The figures presented are projections from these confocal z-stacks. Image analysis was performed by ImageJ software. Antibodies used were: mVPS50/CCDC132 (rabbit, Sigma), Chromogranin C (mouse, Abcam), neuropeptide Y (sheep, Millipore), GFP (rat, Nacalai), NeuN (mouse, Millipore), GM130 (mouse, BD Biosciences), Golgin-97 (mouse, Santa Cruz), TGN-43 (sheep, Serotec). Secondary antibodies were: goat anti-mouse, anti-rabbit, anti-rat or anti-sheep conjugated with Alexa 488, Alexa 543 or Alexa 633 (Invitrogen).

Transfection and confocal imaging of SypHy: Cultured cortical neurons were co-transfected with SypHy and shRNA or control plasmids using Lipofectamine 2000 (Invitrogen) at DIV (days *in vitro*) 5-7 and imaged using a Nikon PCM 2000 or C2 confocal microscope with a 60x water objective (N.A. 1.0) at DIV 10-14. Imaging was performed using a modified Tyrode's solution containing 150 mM NaCl, 4 mM KCl, 2 mM $MgCl_2$, 2 mM $CaCl_2$, 10 mM glucose, and 10 mM HEPES (pH 7.4). 50 μM AP-5 and 10 μM CNQX were added to prevent excitotoxicity. A modified Tylode solution substituting 50 mM NaCl with 50 mM NH_4Cl was used to confirm the expression level of SypHy, as described previously [41].

Statistical tests: For colocalization experiments, Pearson's correlation coefficients were obtained using the Coloc2 plugin in ImageJ. An ROI was drawn to include the cell bodies and dendrites. Bar graph comparisons were performed using Student's t test, and multiple comparisons were corrected using the Holm-Bonferroni method.

Additional experimental procedures are available in the Supplemental Information.

Author Contributions

N.P., Y.M., A.F., D.T.O., C.L.P., M.A., M.C.-P. and H.R.H. designed the experiments and analyzed the data. N.P., Y.M., C.L.P., M.A., M.C.-P. and H.R.H. wrote the manuscript. N.P., Y.M., A.F., D.T.O., C.L.P. and M.A. performed the experiments. Correspondence and requests for materials should be addressed to H.R.H. (horvitz@mit.edu).

Acknowledgments

We thank R. Droste for determining DNA sequences; N. An for strain management; G. Miesenböck, L. Lagnado, Y. Yanagawa, A. Miyawaki, P. Chartrand, K. Miller, J. Rand, J.T. August, M. Nonet and Developmental Studies Hybridoma Bank for reagents; and D. Denning, D. Ma, N. Bhatla and S. Luo for discussions. N.P. was supported by a postdoctoral fellowship from the Natural Sciences and Engineering Research Council of Canada (NSERC). A.F. was supported by a NIH NRSA postdoctoral fellowship. This work was supported by NIH grant GM024663 to H.R.H and by a grant from the Simons Foundation to the Simons Center for the Social Brain at MIT to H.R.H. and M.C.-P. H.R.H. is the David H. Koch Professor of Biology at MIT and an Investigator of the Howard Hughes Medical Institute. The authors declare no competing financial interests.

References

1. Sawin, E. R., Ranganathan, R., and Horvitz, H. R. (2000). *C. elegans* locomotory rate is modulated by the environment through a dopaminergic pathway and by experience through a serotonergic pathway. Neuron *26*, 619–631.

2. Ranganathan, R., Sawin, E. R., Trent, C., and Horvitz, H. R. (2001). Mutations in the *Caenorhabditis elegans* serotonin reuptake transporter MOD-5 reveal serotonin-dependent and -independent activities of fluoxetine. J. Neurosci *21*, 5871–5884.

3. Ailion, M., Hannemann, M., Dalton, S., Pappas, A., Watanabe, S., Hegermann, J., Liu, Q., Han, H.-F., Gu, M., Goulding, M. Q., et al. (2014). Two Rab2 Interactors Regulate Dense-Core Vesicle Maturation. Neuron *82*, 167–180.

4. Swaab, D. F. (2004). Neuropeptides in hypothalamic neuronal disorders. Int. Rev. Cytol. *240*, 305–375.

5. Sakurai, T. (2007). The neural circuit of orexin (hypocretin): maintaining sleep and wakefulness. Nature Reviews Neuroscience *8*, 171–181.

6. Hall, D. H., and Hedgecock, E. M. (1991). Kinesin-related gene *unc-104* is required for axonal transport of synaptic vesicles in *C. elegans*. Cell *65*, 837–847.

7. Nonet, M. L. (1999). Visualization of synaptic specializations in live *C. elegans* with synaptic vesicle protein-GFP fusions. Journal of Neuroscience Methods *89*, 33–40.

8. Matsumoto, Y., Imai, Y., Sugita, Y., Tanaka, T., Tsujimoto, G., Saito, H., and Oshida, T. (2010). CCDC132 is highly expressed in atopic dermatitis T cells. Mol Med Report *3*, 83–87.

9. Wang, Y., Kakizaki, T., Sakagami, H., Saito, K., Ebihara, S., Kato, M., Hirabayashi, M., Saito, Y., Furuya, N., and Yanagawa, Y. (2009). Fluorescent labeling of both GABAergic and glycinergic neurons in vesicular GABA transporter (VGAT)–Venus transgenic mouse. Neuroscience *164*, 1031–1043.

10. Park, J. J., Gondré-Lewis, M. C., Eiden, L. E., and Loh, Y. P. (2011). A distinct *trans*-Golgi network subcompartment for sorting of synaptic and granule proteins in neurons and neuroendocrine cells. J Cell Sci *124*, 735–744.

11. Avery, L., Bargmann, C. I., and Horvitz, H. R. (1993). The *Caenorhabditis elegans unc-31* gene affects multiple nervous system-controlled functions. Genetics *134*, 455–464.

12. Speese, S., Petrie, M., Schuske, K., Ailion, M., Ann, K., Iwasaki, K., Jorgensen, E. M., and Martin, T. F. J. (2007). UNC-31 (CAPS) is required for dense-core vesicle but not synaptic vesicle exocytosis in *Caenorhabditis elegans*. J. Neurosci. *27*, 6150–6162.

13. Edwards, S. L., Charlie, N. K., Richmond, J. E., Hegermann, J., Eimer, S., and Miller, K. G. (2009). Impaired dense core vesicle maturation in *Caenorhabditis elegans* mutants lacking *rab2*. J Cell Biol *186*, 881–895.

14. Sumakovic, M., Hegermann, J., Luo, L., Husson, S. J., Schwarze, K., Olendrowitz, C., Schoofs, L., Richmond, J., and Eimer, S. (2009). UNC-108/RAB-2 and its effector RIC-19 are involved in dense core vesicle maturation in *Caenorhabditis elegans*. J Cell Biol *186*, 897–914.

15. Sulston, J., Dew, M., and Brenner, S. (1975). Dopaminergic neurons in the nematode *Caenorhabditis elegans*. J. Comp. Neurol *163*, 215–226.

16. Sze, J. Y., Victor, M., Loer, C., Shi, Y., and Ruvkun, G. (2000). Food and metabolic signalling defects in a *Caenorhabditis elegans* serotonin-synthesis mutant. Nature *403*, 560–564.

17. Alkema, M. J., Hunter-Ensor, M., Ringstad, N., and Horvitz, H. R. (2005). Tyramine Functions Independently of Octopamine in the *Caenorhabditis elegans* Nervous System. Neuron *46*, 247–260.

18. Kass, J., Jacob, T. C., Kim, P., and Kaplan, J. M. (2001). The EGL-3 proprotein convertase regulates mechanosensory responses of *Caenorhabditis elegans*. J. Neurosci. *21*, 9265–9272.

19. Fares, H., and Grant, B. (2002). Deciphering endocytosis in *Caenorhabditis elegans*. Traffic *3*, 11–19.

20. Sieburth, D., Madison, J. M., and Kaplan, J. M. (2007). PKC-1 regulates secretion of neuropeptides. Nat Neurosci *10*, 49–57.

21. Toei, M., Saum, R., and Forgac, M. (2010). Regulation and isoform function of the V-ATPases. Biochemistry *49*, 4715–4723.

22. Moriyama, Y., Maeda, M., and Futai, M. (1992). The Role of V-ATPase in neuronal and endocrine systems. J Exp Biol *172*, 171–178.

23. Morel, N. (2003). Neurotransmitter release: the dark side of the vacuolar-H+ATPase. Biology of the Cell *95*, 453–457.

24. Jansen, E. J. R., Hafmans, T. G. M., and Martens, G. J. M. (2010). V-ATPase-mediated granular acidification is regulated by the V-ATPase accessory subunit Ac45 in POMC-producing cells. Mol. Biol. Cell *21*, 3330–3339.

25. Ernstrom, G. G., Weimer, R., Pawar, D. R. L., Watanabe, S., Hobson, R. J., Greenstein, D., and Jorgensen, E. M. (2012). V‐ATPase V1 sector is required for corpse clearance and neurotransmission in *Caenorhabditis elegans*. Genetics *191*, 461–475.

26. Pujol, N., Bonnerot, C., Ewbank, J. J., Kohara, Y., and Thierry-Mieg, D. (2001). The *Caenorhabditis elegans unc-32* gene encodes alternative forms of a vacuolar ATPase a subunit. J. Biol. Chem. *276*, 11913–11921.

27. Miesenböck, G., De Angelis, D. A., and Rothman, J. E. (1998). Visualizing secretion and synaptic transmission with pH-sensitive green fluorescent proteins. Nature *394*, 192–195.

28. Miesenböck, G. (2012). Synapto-pHluorins: genetically encoded reporters of synaptic transmission. Cold Spring Harb Protoc *2012*, pdb.ip067827.

29. Nonet, M. L., Holgado, A. M., Brewer, F., Serpe, C. J., Norbeck, B. A., Holleran, J., Wei, L., Hartwieg, E., Jorgensen, E. M., and Alfonso, A. (1999). UNC-11, a *Caenorhabditis elegans* AP180 Homologue, Regulates the Size and Protein Composition of Synaptic Vesicles. Molecular Biology of the Cell *10*, 2343 –2360.

30. Granseth, B., Odermatt, B., Royle, S. J., and Lagnado, L. (2006). Clathrin-mediated endocytosis is the dominant mechanism of vesicle retrieval at hippocampal synapses. Neuron *51*, 773–786.

31. Koivusalo, M., Welch, C., Hayashi, H., Scott, C. C., Kim, M., Alexander, T., Touret, N., Hahn, K. M., and Grinstein, S. (2010). Amiloride inhibits macropinocytosis by lowering submembranous pH and preventing Rac1 and Cdc42 signaling. J Cell Biol *188*, 547–563.

32. Huttlin, E. L., Ting, L., Bruckner, R. J., Gebreab, F., Gygi, M. P., Szpyt, J., Tam, S., Zarraga, G., Colby, G., Baltier, K., et al. (2015). The BioPlex Network: A Systematic Exploration of the Human Interactome. Cell *162*, 425–440.

33. Wan, C., Borgeson, B., Phanse, S., Tu, F., Drew, K., Clark, G., Xiong, X., Kagan, O., Kwan, J., Bezginov, A., et al. (2015). Panorama of ancient metazoan macromolecular complexes. Nature *525*, 339–344.

34. Schindler, C., Chen, Y., Pu, J., Guo, X., and Bonifacino, J. S. (2015). EARP is a multisubunit tethering complex involved in endocytic recycling. Nat Cell Biol *17*, 639–650.

35. Gillingham, A. K., Sinka, R., Torres, I. L., Lilley, K. S., and Munro, S. (2014). Toward a Comprehensive Map of the Effectors of Rab GTPases. Developmental Cell *31*, 358–373.

36. Sadakata, T., Washida, M., Iwayama, Y., Shoji, S., Sato, Y., Ohkura, T., Katoh-Semba, R., Nakajima, M., Sekine, Y., Tanaka, M., et al. (2007). Autistic-like phenotypes in Cadps2-knockout mice and aberrant CADPS2 splicing in autistic patients. J Clin Invest *117*, 931–943.

37. Sadakata, T., and Furuichi, T. (2010). Ca(2+)-dependent activator protein for secretion 2 and autistic-like phenotypes. Neurosci. Res *67*, 197–202.

38. Gai, X., Xie, H. M., Perin, J. C., Takahashi, N., Murphy, K., Wenocur, A. S., D'arcy, M., O'Hara, R. J., Goldmuntz, E., Grice, D. E., et al. (2012). Rare structural variation of synapse and neurotransmission genes in autism. Mol Psychiatry *17*, 402–411.

39. Ma, D. K., Vozdek, R., Bhatla, N., and Horvitz, H. R. (2012). CYSL-1 interacts with the O2-sensing hydroxylase EGL-9 to promote H2S-modulated hypoxia-induced behavioral plasticity in *C. elegans*. Neuron *73*, 925–940.

40. Ringstad, N., and Horvitz, H. R. (2008). FMRFamide neuropeptides and acetylcholine synergistically inhibit egg-laying by *C. elegans*. Nat Neurosci *11*, 1168–1176.

41. Ashby, M. C., Rue, S. A. D. L., Ralph, G. S., Uney, J., Collingridge, G. L., and Henley, J. M. (2004). Removal of AMPA receptors (AMPARs) from synapses is preceded by transient endocytosis of extrasynaptic AMPARs. J. Neurosci. *24*, 5172–5176.

Figure Legends

Figure 1: VPS-50 regulates the behavioral state of *C. elegans*. A) The locomotory behavior of *C. elegans* is modulated by the presence of food and past feeding experience. Well-fed wild-type animals move more slowly on a bacterial lawn (red bars) than in the absence of bacteria (blue bars), and food-deprived animals (green bars) slow even more than well-fed animals [1]. *vps-50* mutants (*n3925* and *n4022*) moved as if they were food-deprived even when well-fed, and this behavioral defect was rescued by a transgene expressing a GFP-tagged wild-type copy of *vps-50* from its endogenous promoter. $n = 6$ plates for the wild type; $n = 3$ plates for all other genotypes. Mean ± SD. B) *vps-50* mutants show normal pumping rates, indicating that they do not have a feeding defect. C) *vps-50* mutants develop at a rate similar to that of wild-type animals. We followed synchronized animals after recovery from L1 arrest. All wild-type and *vps-50* mutant worms observed had a developed vulva after 44 hours; 12/12 wild-type animals were gravid after 49 hours, while 11/12 *vps-50* mutants were gravid after 49 hours. D) Analyses of the *in utero* retention time of eggs, assayed by the distribution of the developmental stages of newly laid eggs. *vps-50* mutants retained eggs *in utero* for an abnormally long period of time, as seen by a shift to later stages of their newly laid eggs. The egg-laying defect of *vps-50* mutants was rescued by transgenes expressing *vps-50* under its endogenous promoter or a pan-neuronal promoter but not under a body-wall muscle promoter. See also Figure S1.

Figure 2: VPS-50 functions in neurons. A) Fluorescence and Nomarski micrographs of regions of *C. elegans* transgenic animals expressing VPS-50::GFP (*nIs388*) using the *vps-50* promoter. *vps-50* was expressed in most if not all neurons. Occasional expression was observed in some pharyngeal muscles. VNC: ventral nerve cord. [#]To enhance visualization, we used *unc-104(e1265)* mutant animals to increase the fluorescence level in cell bodies. Scale bars: 10 μm. B) *vps-50* functions in neurons to regulate locomotion. *vps-50* was expressed pan-neuronally (*Prab-3*) and in body-wall muscles (*Pmyo-3*) to identify its site of action. Pan-neuronal expression of *vps-50*, or of its murine homolog *mVps50*, rescued the locomotion defect of *vps-50(n4022)* animals. $n = 3$ plates for all genotypes. C) *vps-50* functions in cholinergic neurons to regulate locomotion on food. *vps-50* was expressed in cholinergic neurons (*Punc-17*), in GABAergic neurons (*Punc-47*) and in a subset of sensory neurons (*Ptax-2*) to identify its site of action. $n = 5$ plates for the wild type and *vps-50(n4022)*; $n = 3$ plates for all other genotypes. (B

and C) Significance is defined by comparison to the equivalent state for *vps-50(n4022)* mutants. Means ± SDs. D) The localization of VPS-50::GFP to synapse-rich areas of the nerve ring depends on UNC-104/KIF1A, a molecular motor that transports synaptic vesicles and their associated proteins to synapses. Immunohistochemistry against GFP and synaptobrevin (SNB-1) and DAPI staining are shown. The dotted line indicates the synapse-rich nerve ring, and clusters of neuronal cell bodies are marked. Scale bar, 10 μm.

Figure 3: mVPS50 is widely expressed in the mammalian brain neurons. Anti-VPS50 antibodies specifically recognize mVPS50 (see Fig. S2A-B for validation of the anti-mVPS50 antibody). A) mVPS50 is enriched in brain tissue. Protein extracts from dissected adult mouse tissues were analyzed for mVPS50 expression by immunoblotting. B) mVPS50 is expressed in most brain regions, with strong expression in cortex and hippocampus. C) mVPS50 is expressed in the mouse cortex throughout postnatal (P) development. Protein extracts from dissected mouse cortex were analyzed for mVPS50 expression at different developmental stages. D) mVPS50 is expressed broadly in the mouse hippocampal neurons. Transgenic mice that express VGAT-Venus in inhibitory neurons were used for immunohistochemical studies of sagittal hippocampal slices [9]. The dentate gyrus and CA3 are shown. The mVPS50 immunostaining overlaps with neuron specific marker NeuN including both Venus-positive inhibitory neurons and Venus-negative excitatory neurons. Scale bar: 100 μm. See also Figure S2.

Figure 4: mVPS50 Associates with Synaptic and Dense-Core Vesicles. A) mVPS50 does not colocalize with the *cis*-Golgi apparatus (GM130) in mouse primary cultured cortical neurons. B) mVPS50 partially colocalizes with the *trans*-Golgi apparatus (Golgin-97) in mouse primary cultured cortical neurons. C) mVPS50 partially colocalizes with Chromogranin C-containing dense-core vesicles (ChrC) in mouse primary cultured cortical neurons. D) mVPS50 partially colocalizes with neuropeptide Y-containing dense-core vesicles (NPY) in mouse primary cultured cortical neurons. Endogenous mVPS50, GM130, Golgin-97, ChrC and NPY were detected by immunofluorescence. Scale bar for A-B: 10 μm. Scale bar for C-D: 5 μm. E) mVPS50 significantly cofractionates with the synaptic vesicle protein synaptophysin and the neuropeptide Chromogranin C. Extracts from adult mouse cortex were fractionated, and fractions were probed by immunoblotting for mVPS50, the NMDA glutamate receptor subunit GluN1, the postsynaptic density protein PSD-95, the neuropeptide Chromogranin C, the synaptic vesicle membrane protein synaptophysin, the cytoplasmic V-ATPase A and H subunit (the mammalian homolog of *C. elegans* VHA-15) and the vesicle coat protein clathrin heavy chain. F) mVPS50 is a soluble protein. The synaptic vesicle and cytosol (LS1) fraction from adult mouse cortex was further fractionated using sucrose gradient centrifugation, and fractions were probed by immunoblotting. See also Figure S3.

Figure 5: *vps-50* disruption reduces neuropeptide levels and impairs neuropeptide processing. A) Modulation of locomotion in response to the presence of food and past feeding experience. Like *vps-50* mutants, *unc-31* (CADPS2) and *rab-2* (Rab2) mutants, which are defective in dense-core vesicle release and maturation, respectively, behave as if they had been food-deprived even when well-fed; *egl-3* (PC2) mutants are more similar to wild-type animals. *n* = 4 plates for wild type; *n* = 3 plates for all other genotypes. B). Mutant animals defective in the synthesis of biogenic amines (*cat-2*: dopamine, *tph-1*: serotonin, *tdc-1*: tyramine and octopamine) behave differently when well-fed or food-deprived, unlike *vps-50* mutants. *n* = 10 plates for wild type; *n* = 3 plates for all other genotypes. C) *vps-50* mutants, like *rab-2* mutants, show reduced FLP-3::Venus neuropeptide levels in the *C. elegans* dorsal nerve cord. *unc-31* and *egl-3* mutants show elevated neuropeptide levels at synapses. D) *vps-50* mutants do not significantly accumulate FLP-3::Venus neuropeptides in neuronal cell bodies. E) *vps-50* mutants have reduced levels of FLP-3::Venus neuropeptides in coelomocytes. F) *vps-50* mutants do not have a dense-core vesicle maturation defect identical to that of *rab-2* mutants based on the dense-core vesicle marker IDA-1::GFP in the *C. elegans* dorsal nerve cord. G) *vps-50* mutants, like *rab-2* mutants, abnormally accumulate IDA-1::GFP in ventral nerve cord cell bodies. H) *vps-50* mutants have reduced levels of the neuropeptide FLP-3 as well as reduced FLP-3 processing. Immunoblots of *C. elegans* protein extracts showing the levels of processed and unprocessed neuropeptide FLP-3::Venus and the constant levels of the synaptobrevin reporter mCherry::SNB-1. The transgene *ceIs61* expressed both FLP-3::Venus and mCherry:SNB-1 from the *unc-129* promoter. Mutants for the proprotein convertase 2 homolog EGL-3 had no detectable fully processed FLP-3 neuropeptides. I) *vps-50* mutants show reduced NLP-21::Venus neuropeptide levels in the *C. elegans* dorsal nerve cord. Scale bars: 5 μm. Bar graphs A and B, means ± SDs. Bar graphs C-G & I, *n* values (number of animals) are indicated on bars, representative fluorescence micrographs and quantification are shown, means ± SEMs. See also Figure S4.

Figure 6: Disruption of *vps-50* in *C. elegans* or of its murine homolog *mVps50* in mouse cultured neurons similarly impair synaptic vesicle acidification. A) VPS-50 can associate with the V-ATPase subunit VHA-15 in the yeast two-hybrid assay. Growth occurred on media lacking histidine (dark triangle). B) *vps-50* mutants have a synaptic vesicle acidification defect. Representative micrographs and quantification of synaptopHluorin (SpH) fluorescence levels. SpH fluorescence is quenched by acidic pH; thus, increased fluorescence levels correspond to increased pH. Mutants defective in the V-ATPase complex subunit gene *unc-32* were used as an acidification-defective control [25]. C) *vps-50* mutants did not have elevated levels of synaptobrevin SNB-1 at synapses, indicating that the higher SpH (a SNB-1::pHluorin fusion) fluorescence levels observed in *vps-50* and *unc-32* mutants were not caused by elevated levels of SpH at synapses. Representative fluorescence micrographs and quantification of mCherry::SNB-1 levels at synapses. D) Knockdown of *mVps50* in mouse primary cultured cortical neurons led to a synaptic vesicle acidification defect. Quantification of SypHy (synaptophysin-pHluorin

fusion) fluorescence levels with or without knockdown of *mVps50*. Higher fluorescence levels correspond to higher pH. SypHy expression levels in wild-type and *mVps50* knocked-down neurons are similar, as addition of NH_4Cl to increase the intravesicular pH to 7.4 led to similar SypHy fluorescence levels in both. E) *vps-50* mutants have a dense-core vesicle acidification defect. pHluorin and mCherry fluorescence intensities were quantified from FLP-3_{1-5}::mCherry::pHluorin reporter. An increased pHluorin/mCherry fluorescence ratio indicates increased pH. Mutants defective in the V-ATPase complex subunit gene *unc-32* were used as an acidification-defective control. F) Knockdown of *mVps50* in mouse primary cultured cortical neurons reduces the amount of V-ATPase (V1) subunits A and B in the synaptosomal fraction. Levels of V-ATPase soluble subunits A and B were quantified in total protein extracts and in synaptosomal fractions in wild-type and *mVps50* knockdown primary cultured neurons. $n = 6$. Scale bars: 5 μm. Bar graphs, *n* values (number of animals or neurons) are indicated on bars, means ± SEMs. See also Figure S5.

Fig 1.

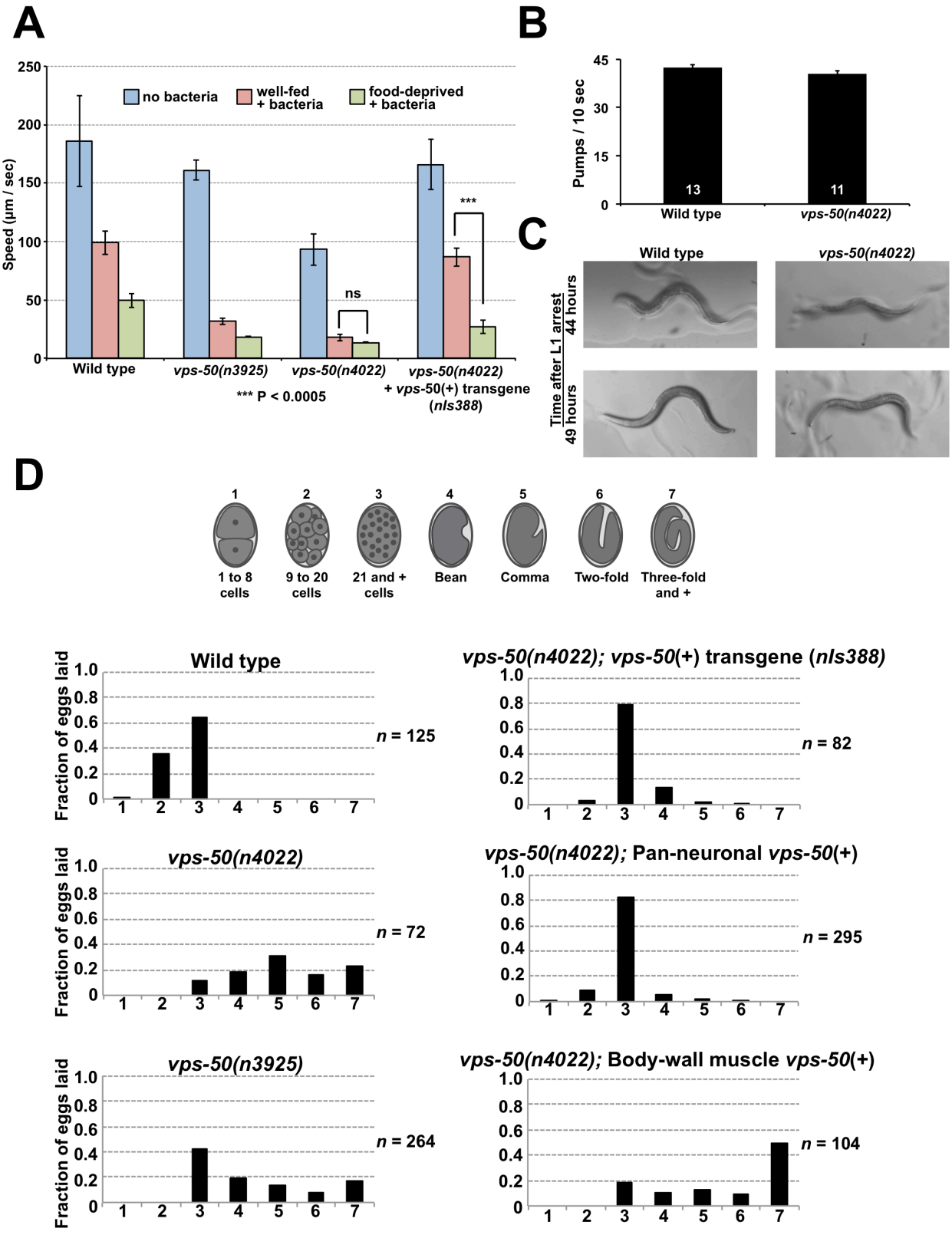
A
Speed (µm / sec)
no bacteria
well-fed + bacteria
food-deprived + bacteria
Wild type
vps-50(n3925)
vps-50(n4022)
vps-50(n4022) + vps-50(+) transgene (nIs388)
*** P < 0.0005
ns
***
B
Pumps / 10 sec
13
11
Wild type
vps-50(n4022)
C
Wild type
vps-50(n4022)
Time after L1 arrest
44 hours
49 hours
D
1 to 8 cells
9 to 20 cells
21 and + cells
Bean
Comma
Two-fold
Three-fold and +
Fraction of eggs laid
Wild type
n = 125
vps-50(n4022)
n = 72
vps-50(n3925)
n = 264
vps-50(n4022); vps-50(+) transgene (nIs388)
n = 82
vps-50(n4022); Pan-neuronal vps-50(+)
n = 295
vps-50(n4022); Body-wall muscle vps-50(+)
n = 104

Fig 2.

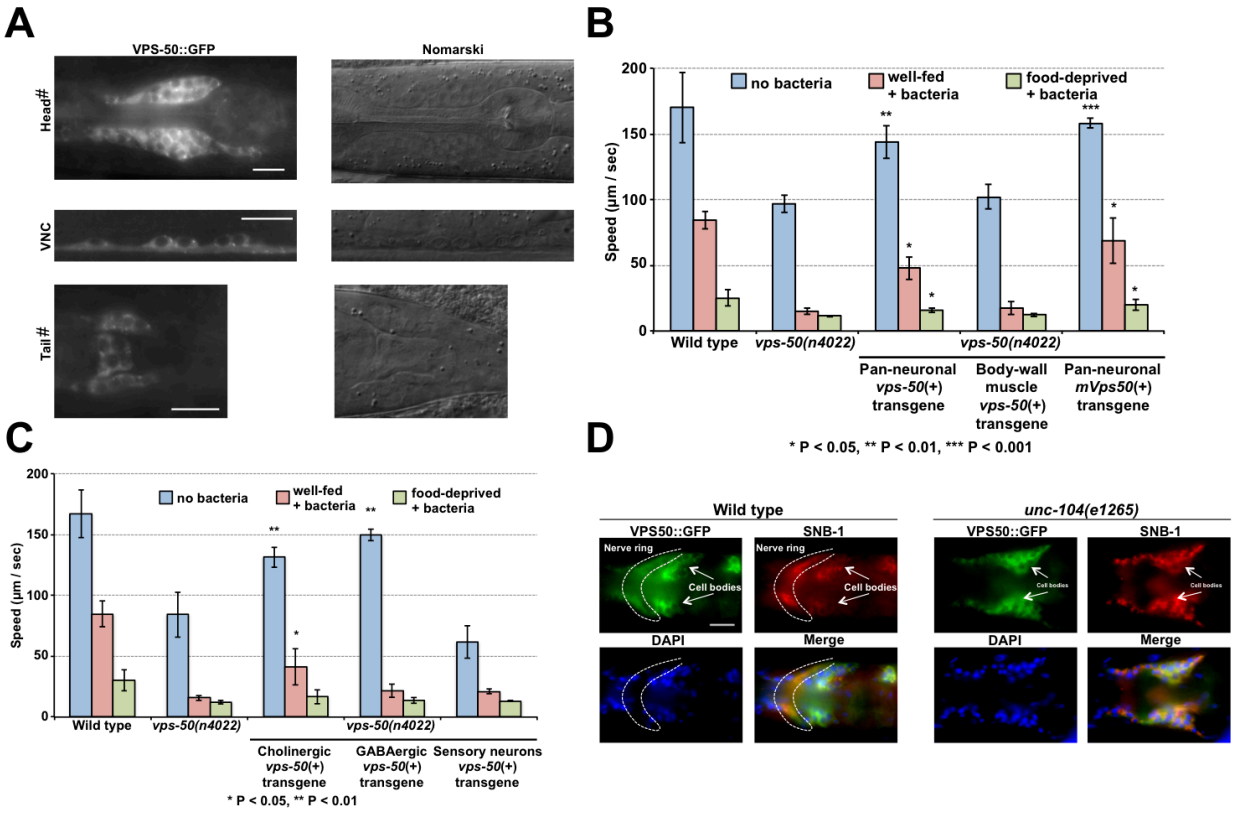
A
VPS-50::GFP
Nomarski
Head#
VNC
Tail#
B
Speed (µm / sec)
no bacteria
well-fed + bacteria
food-deprived + bacteria
Wild type
vps-50(n4022)
vps-50(n4022)
Pan-neuronal vps-50(+) transgene
Body-wall muscle vps-50(+) transgene
Pan-neuronal mVps50(+) transgene
* P < 0.05, ** P < 0.01, *** P < 0.001
C
Speed (µm / sec)
no bacteria
well-fed + bacteria
food-deprived + bacteria
Wild type
vps-50(n4022)
vps-50(n4022)
Cholinergic vps-50(+) transgene
GABAergic vps-50(+) transgene
Sensory neurons vps-50(+) transgene
* P < 0.05, ** P < 0.01
D
Wild type
unc-104(e1265)
VPS50::GFP
SNB-1
Nerve ring
Cell bodies
DAPI
Merge

Fig 3.

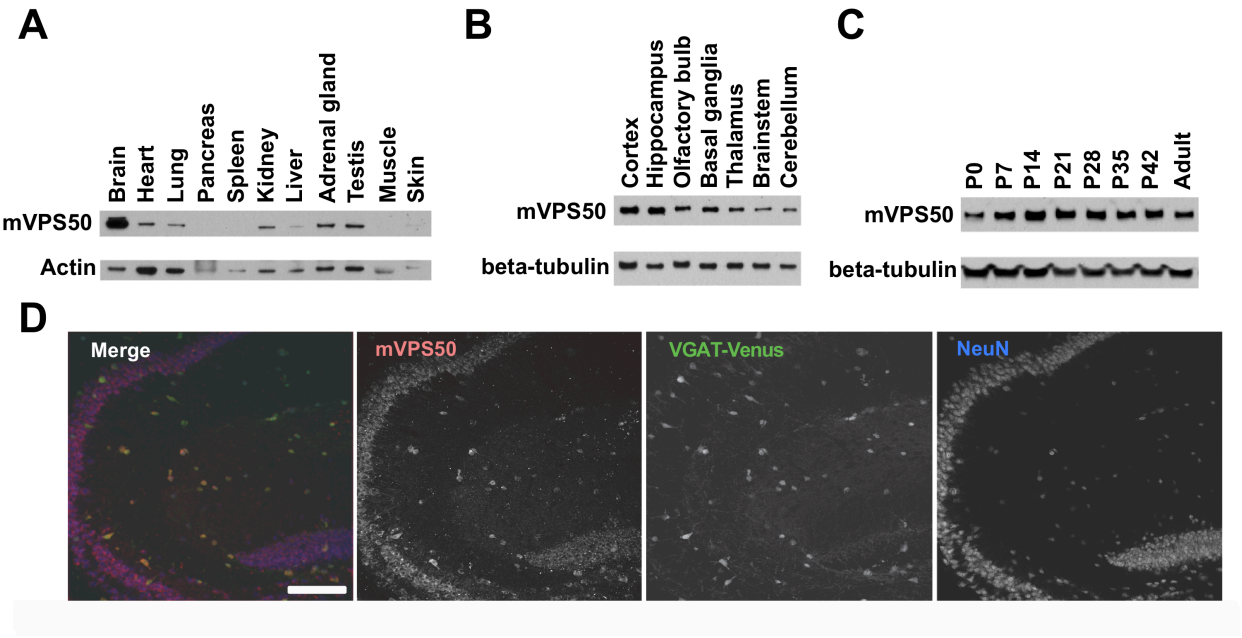
A
Brain
Heart
Lung
Pancreas
Spleen
Kidney
Liver
Adrenal gland
Testis
Muscle
Skin
mVPS50
Actin
B
Cortex
Hippocampus
Olfactory bulb
Basal ganglia
Thalamus
Brainstem
Cerebellum
mVPS50
beta-tubulin
C
P0
P7
P14
P21
P28
P35
P42
Adult
mVPS50
beta-tubulin
D
Merge
mVPS50
VGAT-Venus
NeuN

Fig 4.

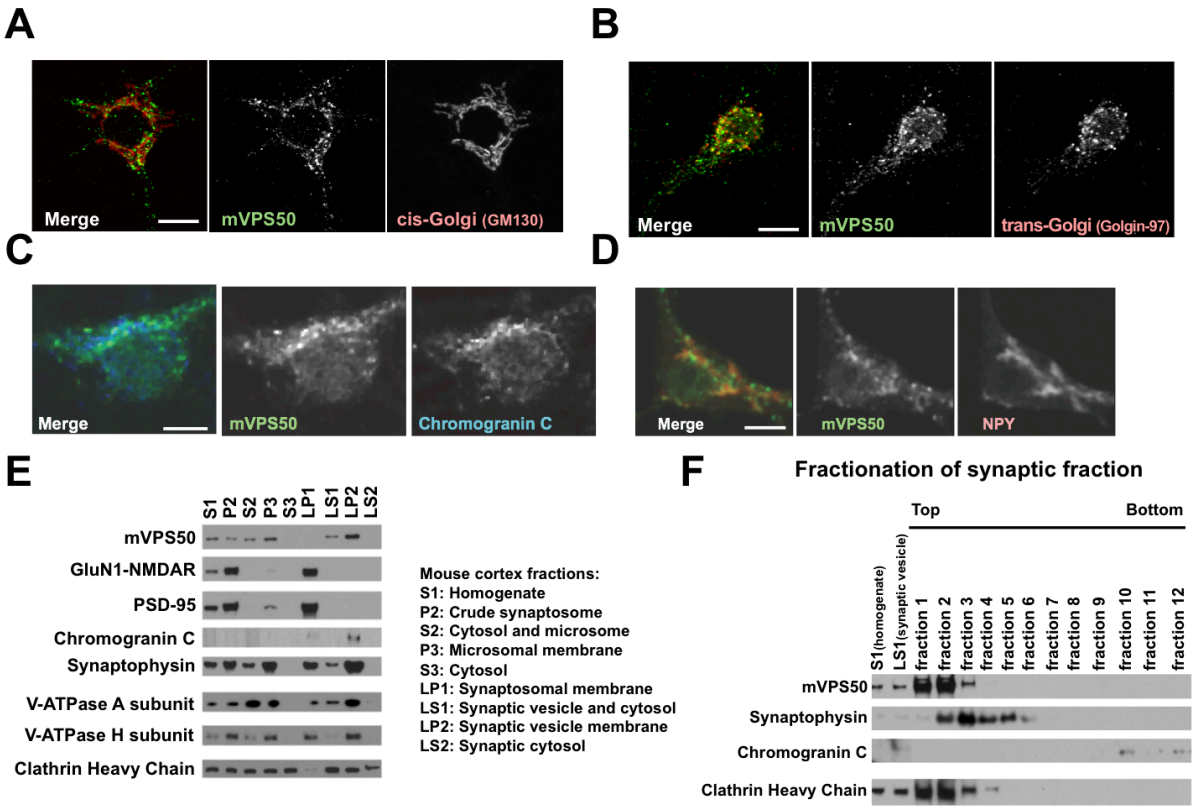
A
Merge
mVPS50
cis-Golgi (GM130)
B
Merge
mVPS50
trans-Golgi (Golgin-97)
C
Merge
mVPS50
Chromogranin C
D
Merge
mVPS50
NPY
E
S1
P2
S2
P3
S3
LP1
LS1
LP2
LS2
mVPS50
GluN1-NMDAR
PSD-95
Chromogranin C
Synaptophysin
V-ATPase A subunit
V-ATPase H subunit
Clathrin Heavy Chain
Mouse cortex fractions:
S1: Homogenate
P2: Crude synaptosome
S2: Cytosol and microsome
P3: Microsomal membrane
S3: Cytosol
LP1: Synaptosomal membrane
LS1: Synaptic vesicle and cytosol
LP2: Synaptic vesicle membrane
LS2: Synaptic cytosol
F
Fractionation of synaptic fraction
Top
Bottom
S1 (homogenate)
LS1 (synaptic vesicle)
fraction 1
fraction 2
fraction 3
fraction 4
fraction 5
fraction 6
fraction 7
fraction 8
fraction 9
fraction 10
fraction 11
fraction 12
mVPS50
Synaptophysin
Chromogranin C
Clathrin Heavy Chain

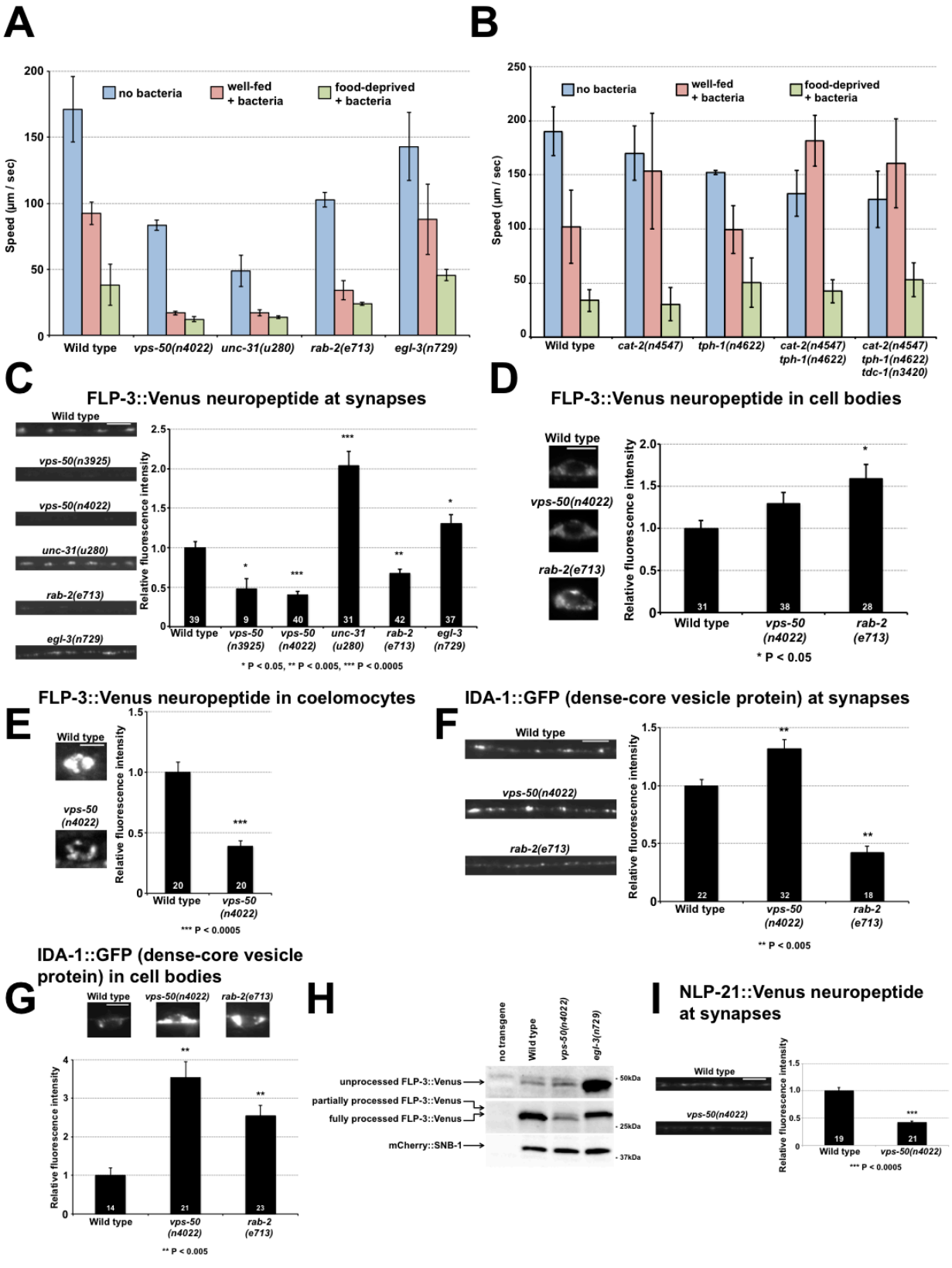
A
Speed (µm / sec)
no bacteria
well-fed + bacteria
food-deprived + bacteria
Wild type
vps-50(n4022)
unc-31(u280)
rab-2(e713)
egl-3(n729)
B
Speed (µm / sec)
no bacteria
well-fed + bacteria
food-deprived + bacteria
Wild type
cat-2(n4547)
tph-1(n4622)
cat-2(n4547) tph-1(n4622)
cat-2(n4547) tph-1(n4622) tdc-1(n3420)
C
FLP-3::Venus neuropeptide at synapses
Wild type
vps-50(n3925)
vps-50(n4022)
unc-31(u280)
rab-2(e713)
egl-3(n729)
Relative fluorescence intensity
Wild type
vps-50 (n3925)
vps-50 (n4022)
unc-31 (u280)
rab-2 (e713)
egl-3 (n729)
* P < 0.05, ** P < 0.005, *** P < 0.0005
D
FLP-3::Venus neuropeptide in cell bodies
Wild type
vps-50(n4022)
rab-2(e713)
Relative fluorescence intensity
Wild type
vps-50 (n4022)
rab-2 (e713)
* P < 0.05
E
FLP-3::Venus neuropeptide in coelomocytes
Wild type
vps-50 (n4022)
Relative fluorescence intensity
Wild type
vps-50 (n4022)
*** P < 0.0005
F
IDA-1::GFP (dense-core vesicle protein) at synapses
Wild type
vps-50(n4022)
rab-2(e713)
Relative fluorescence intensity
Wild type
vps-50 (n4022)
rab-2 (e713)
** P < 0.005
G
IDA-1::GFP (dense-core vesicle protein) in cell bodies
Wild type
vps-50(n4022)
rab-2(e713)
Relative fluorescence intensity
Wild type
vps-50 (n4022)
rab-2 (e713)
** P < 0.005
H
no transgene
Wild type
vps-50(n4022)
egl-3(n729)
unprocessed FLP-3::Venus
partially processed FLP-3::Venus
fully processed FLP-3::Venus
mCherry::SNB-1
50kDa
25kDa
37kDa
I
NLP-21::Venus neuropeptide at synapses
Wild type
vps-50(n4022)
Relative fluorescence intensity
Wild type
vps-50(n4022)
*** P < 0.0005

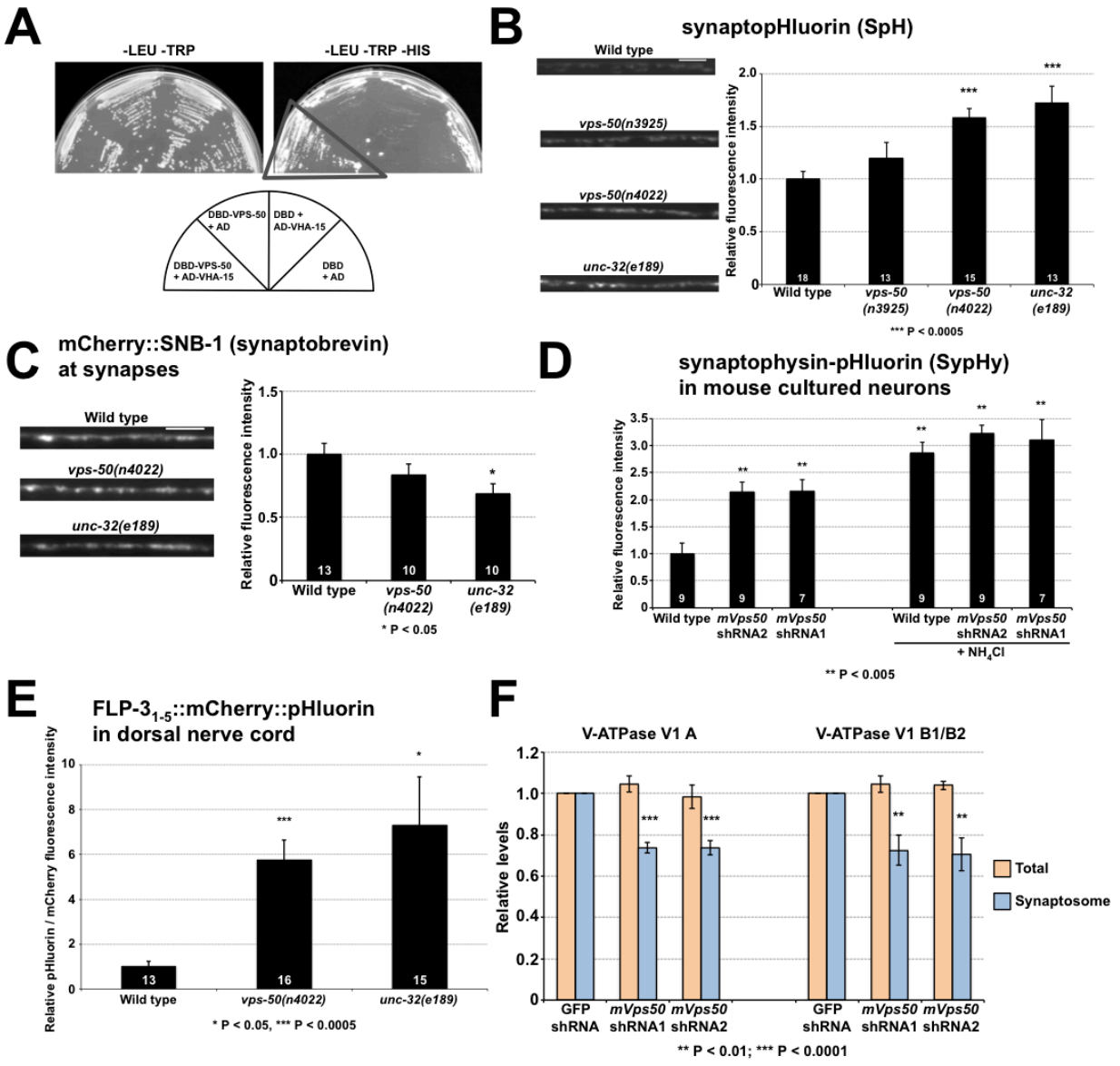
A
-LEU -TRP
-LEU -TRP -HIS
DBD-VPS-50 + AD
DBD + AD-VHA-15
DBD-VPS-50 + AD-VHA-15
DBD + AD
B
synaptopHluorin (SpH)
Wild type
vps-50(n3925)
vps-50(n4022)
unc-32(e189)
Relative fluorescence intensity
Wild type
vps-50 (n3925)
vps-50 (n4022)
unc-32 (e189)
*** P < 0.0005
C
mCherry::SNB-1 (synaptobrevin) at synapses
Wild type
vps-50(n4022)
unc-32(e189)
Relative fluorescence intensity
Wild type
vps-50 (n4022)
unc-32 (e189)
* P < 0.05
D
synaptophysin-pHluorin (SypHy) in mouse cultured neurons
Relative fluorescence intensity
Wild type
mVps50 shRNA2
mVps50 shRNA1
+ NH4Cl
** P < 0.005
E
FLP-3 1-5::mCherry::pHluorin in dorsal nerve cord
Relative pHluorin / mCherry fluorescence intensity
Wild type
vps-50(n4022)
unc-32(e189)
* P < 0.05, *** P < 0.0005
F
V-ATPase V1 A
V-ATPase V1 B1/B2
Relative levels
GFP shRNA
mVps50 shRNA1
mVps50 shRNA2
Total
Synaptosome
** P < 0.01; *** P < 0.0001

Figure S1:

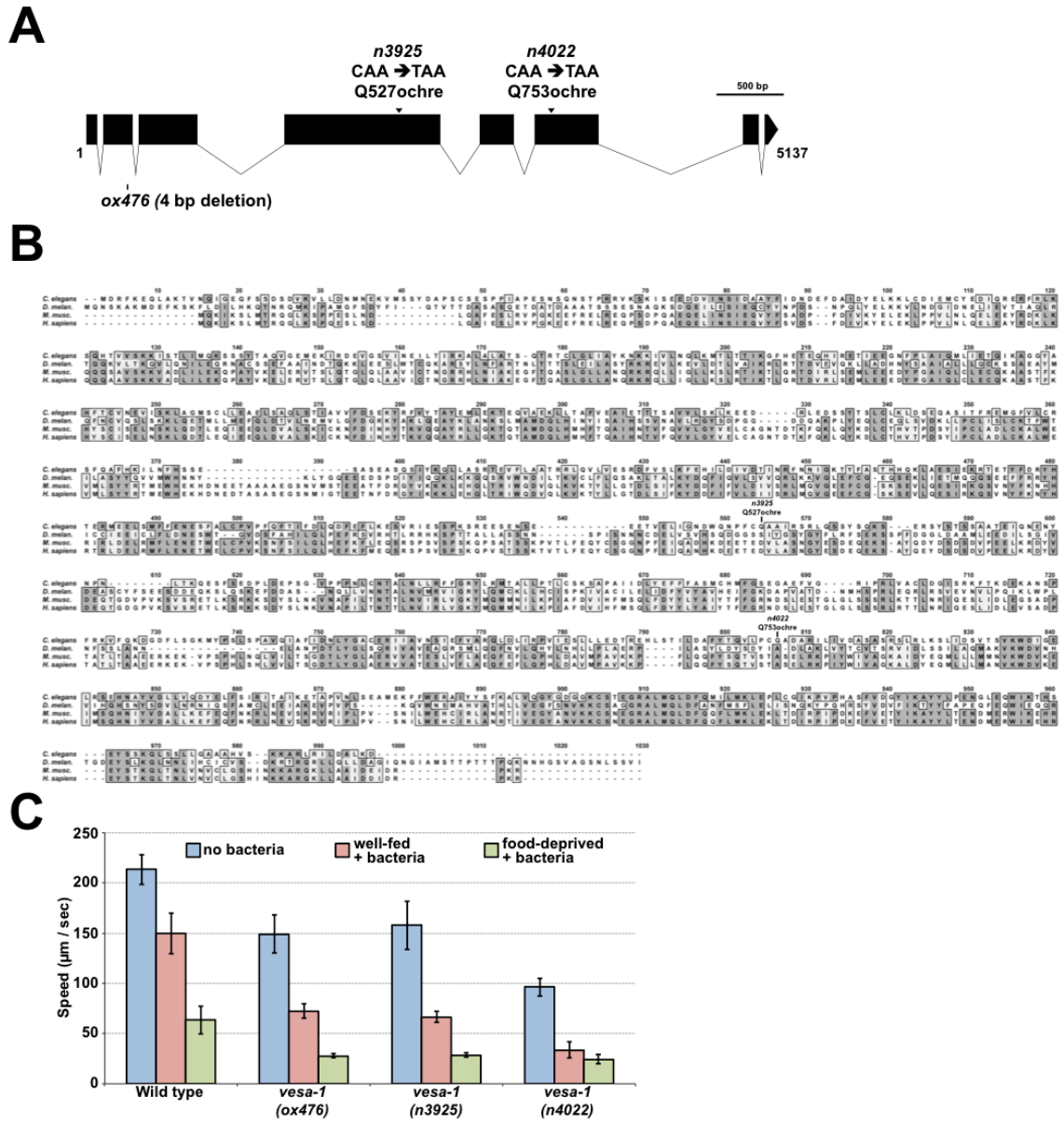

Figure S1 (related to Figure 1): (A) Schematic of *vps-50* exon-intron gene structure. *vps-50(ox476)* is a 4 bp deletion of nucleotides 304-307, *vps-50(n3925)* is a C-to-T mutation resulting in a Q527ochre change, and *n4022* is a C-to-T mutation resulting in a Q753ochre change. Translation of *vps-50* results in a 938 amino acid protein. Graph was generated using www.wormweb.org/exonintron. *n4022* and *n3925* are both nonsense alleles. (B) VPS-50 is conserved from worms to humans. Disrupted sites of *n3925* and *n4022* mutants are indicated. Sequence alignment of worm (*C. elegans*), fly (*D. melanogaster*), mouse

(*M. musculus*) and human (*H. sapiens*) sequences is shown. Dark gray boxes mark identical residues, and light gray boxes mark similar residues. (C) Modulation of locomotion in response to the presence of food and past feeding experience. Speeds of *C. elegans* in the absence of food (blue bars), well-fed in the presence of food (red bars) and food-deprived returned to food (green bars). *vps-50(ox476)* and *vps-50(n3925)* similarly cause a weaker locomotion defect than that of *vps-50(n4022)* mutants. It is possible that *vps-50(ox476)* and *vps-50(n3925)* are incomplete loss-of-function mutants, while *vps-50(n4022)* might be a molecular null mutation: an uncloned shorter isoform of *vps-50* might still be present in *ox476* and *n3925* mutants. Alternatively, *ox476* and *n3925* might be null alleles, and *n4022* might be non-null but have a phenotype stronger than that of null mutants. That *n4022* can be recued by the expression of *vps-50* shows that its stronger phenotype is not caused by a mutation in another gene.

Figure S2:

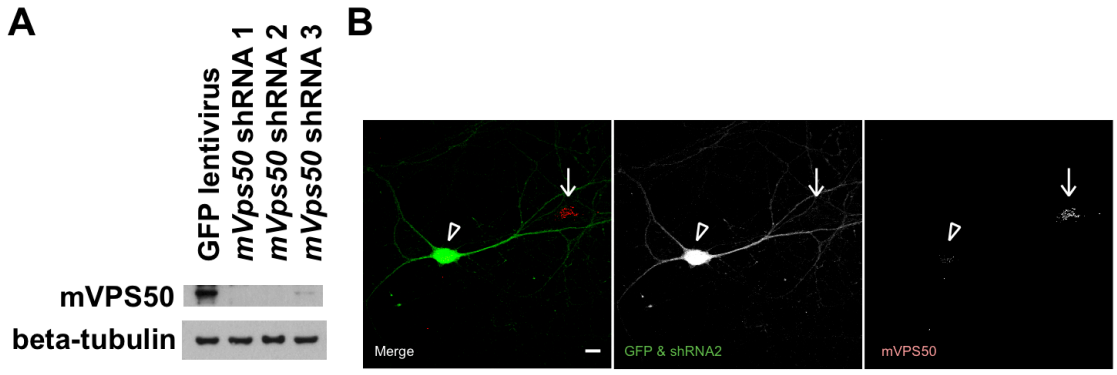

Figure S2 (related to Figure 3): (A) Immunoblotting analysis of mVPS50 using an antibody against the human VPS50 protein. Protein extracts from mouse primary cultured cortical neurons infected with GFP lentivirus (control) or shRNA lentiviruses against *mVps50* were analyzed by immunoblotting using an anti-VPS50 antibody. (B) Immunohistochemistry of mouse primary cultured cortical neurons infected with lentiviruses that coexpress GFP and an shRNA against *mVps50* using an anti-VPS50 antibody. Cells that express GFP do not express mVPS50 and *vice versa*. Arrowhead points to a GFP-positive cell (expressing the *mVps50* shRNA) in which mVPS50 signal is barely detectable. Arrow points to a GFP-negative cell (not expressing the *mVps50* shRNA) where mVPS50 is detected. Scale bar: 10 μm.

Figure S3:

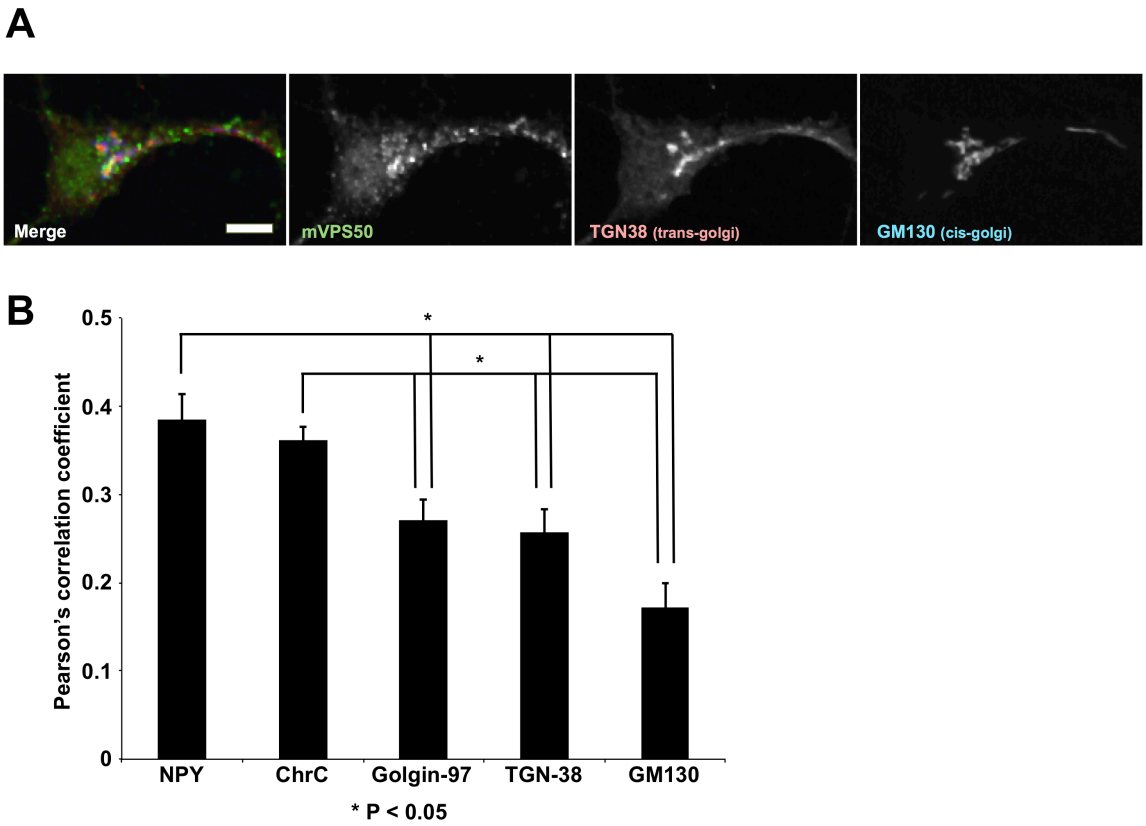

Figure S3 (related to Figure 4): (A) mVPS50 partially colocalized with the *trans*-Golgi marker TGN38 in mouse primary cultured cortical neurons. Endogenous mVPS50 and the *cis*-Golgi matrix protein GM130 and *trans*-Golgi protein TGN38 were detected by immunofluorescence. Scale bar: 5 μm. (B) Quantification of the colocalization between mVPS50 and Neuropeptide Y (NPY), Chromogranin C (ChrC), Golgin-97, TGN-38 or GM130. mVPS50 colocalizes more with neuropeptides NPY or ChrC than with *trans*-Golgi markers Golgin-97 or TGN-38, or with the *cis*-Golgi marker GM130. Significance was analyzed using Student's t test. Multiple comparisons were corrected using the Holm-Bonferroni method.

Figure S4:

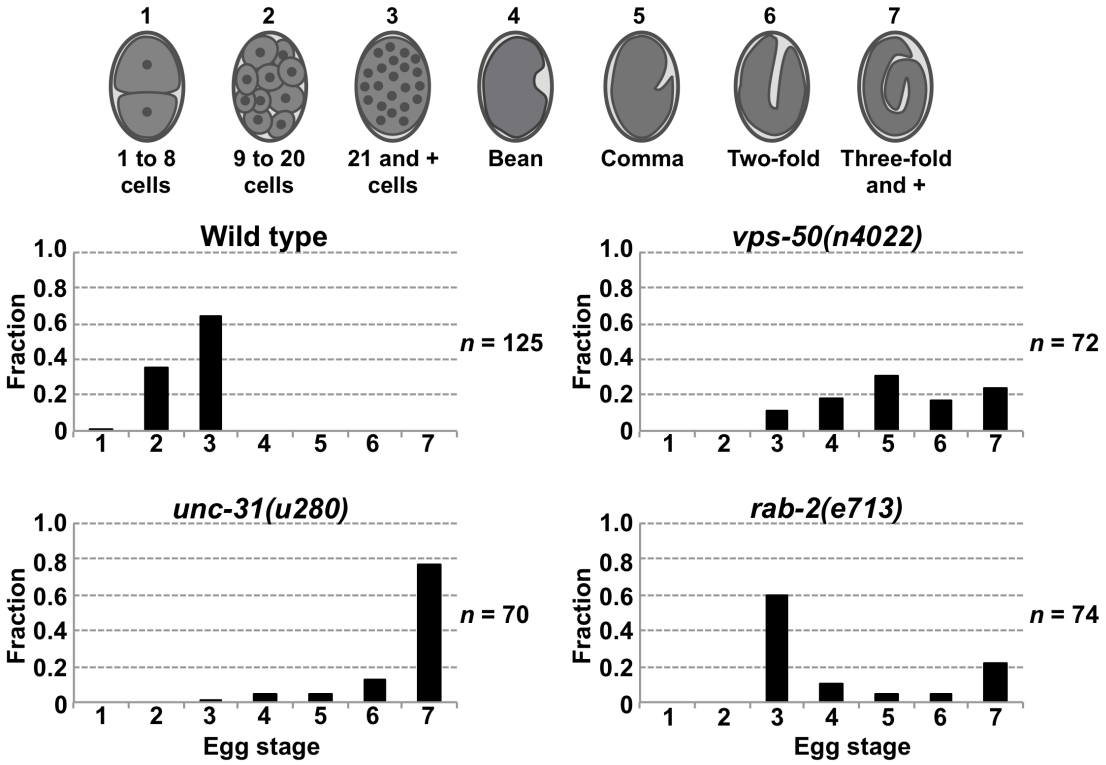

Figure S4 (related to Figure 5): Analyses of the *in utero* retention time of eggs, assayed by the distribution of the developmental stages of newly laid eggs. Like *vps-50* mutants, *unc-31* and *rab-2* mutant animals retain eggs *in utero* longer than do wild-type animals. (Wild type and *vps-50(n4022)* data are the same as in Figure 1D).

Figure S5:

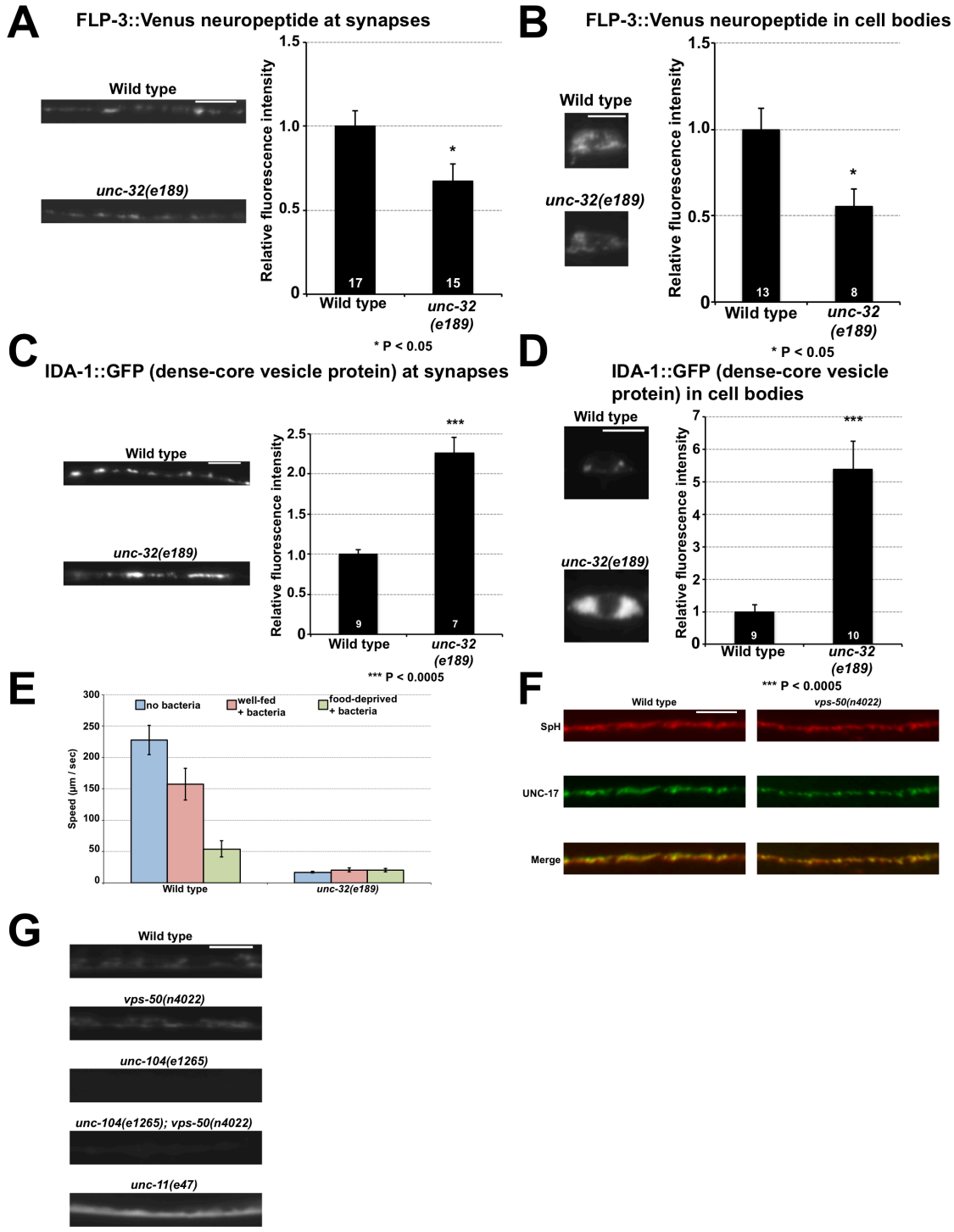

Figure S5 (related to Figure 6): Disruption of synaptic vesicle acidification leads to defects similar to those of *vps-50* mutants. Disruption of the V-ATPase complex subunit gene *unc-32* led to low levels of

the FLP-3::Venus neuropeptide reporter (A) at synapses in the dorsal nerve cord and (B) in neuronal cell bodies in the ventral nerve cord. Representative fluorescence micrographs and quantification of FLP-3::Venus. Like *vps-50* mutants, *unc-32* mutants have increased levels of the dense-core vesicle marker IDA-1::GFP (C) at synapses and (D) in neuronal cell bodies. Representative fluorescence micrographs (left) and quantification of the dense-core vesicle marker IDA-1::GFP (right) in the *C. elegans* dorsal nerve cord and cell bodies. Scale bars: 5 μm. Bar graphs, *n* values (number of animals) are indicated on bars, means ± SEMs. Significance was analyzed using Student's t test. (E) *unc-32* mutants have generally impaired locomotion. Modulation of locomotion in response to the presence of food and past feeding experience. Speeds in the absence of food (blue bars), well-fed in the presence of food (red bars) and food-deprived returned to food (green bars). (F) SpH localizes to synapses. SpH colocalizes with the vesicular acetylcholine transporter UNC-17 in both wild-type and *vps-50* mutant animals. SpH and endogenous UNC-17 localization were analyzed by immunohistochemistry. (G) Transport of SpH to dorsal cord synapses requires the molecular motor UNC-104/KIF1A in both wild-type and *vps-50* mutant animals. Unlike *vps-50* mutants, *unc-11*/AP180 mutants fail to recycle SpH, leading to its diffusion along the plasma membrane. Scale bars: 10 μm.

SUPPLEMENTAL EXPERIMENTAL PROCEDURES

***C. elegans* strains:** *C. elegans* was cultured as described previously at room temperature (~22.5 °C) [S1]. The wild-type strain was Bristol N2. Mutants used were: LGI: *mod-5(n3314)*, *rab-2(e713)*, *unc-11(e47)*; LGII: *unc-104(e1265)*, *cat-2(n4547)*, *tph-1(n4622)*, *tdc-1(n3420)*; LGIII: *unc-32(e189)*, *vps-50(ox476)*, *vps-50(n3925)*, *vps-50(n4022)*, *unc-64(e246)*; LGIV: *unc-31(u280)*; LGV: *egl-3(n729)*; LGX: *lin-15AB(n765)*; Transgenes: *ceIs61(II)*[$P_{unc-129}$*::flp-3::Venus,* $P_{unc-129}$*::RFP:snb-1,* P_{ttx-3}*::RFP]*, *ceIs72*[$P_{unc-129}$*::ida-1::GFP,* P_{ttx-3}*::RFP]*, *nEx*[P_{unc-17}*::flp-3*$_{1-5}$*::mCherry::pHluorin*; P_{myo2}*::mCherry*], *nIs388*[P_{vps-50}*::vps-50::GFP; lin-15(+)]*, *nIs463*[P_{unc-17}*::SpH; lin-15(+)]*, *nIs468*[P_{vps-50}*::GFP; lin-15(+)]*, *nIs490*[P_{rab-3}*::vps-50::GFP; lin-15(+)]*, *nIs517*[P_{unc-17}*::vps-50::GFP; lin-15(+)]*, *nIs521*[P_{rab-3}*::mVps50::GFP; lin-15(+)]*, *nIs522*[P_{unc-47}*::vps-50::GFP; lin-15(+)]*, *nIs523*[P_{myo-3}*::vps-50::GFP; lin-15(+)]*, *nIs613*[P_{tax-2}*::vps-50::GFP; lin-15(+)]*, *nuIs183*[$P_{unc-129}$*::nlp-21::Venus*; P_{myo2}*::NLS::GFP*].

Isolation of *vps-50* mutants: To isolate mutants that behave as if they had been food-deprived even when well-fed, *mod-5(n3314)* animals were used as a sensitized background, because in the food-deprived state their locomotion is significantly slower than that of wild-type worms [S2]. *mod-5(n3314)* animals were mutagenized using EMS, and mutagenized parental (P_0) animals were transferred to Petri plates and grown at 20°C for four days. Adult F_1 progeny were bleached, and eggs were collected and allowed to hatch in S Basal medium in the absence of food to synchronize development. These F_2 progeny were grown to adulthood and assayed for behavioral responses to food. Specifically, animals were transferred to the center of a ring-shaped *E. coli* lawn, and the animals were allowed to move for 30 min. Animals that moved to the inner ring of the lawn and then stopped moving (i.e., could move but stopped moving after encountering *E. coli*) were picked and retested and then examined for coordinated locomotion in the absence of food to ensure that they were capable of coordinated locomotion and not simply paralyzed. *vps-50* mutations were outcrossed from the *mod-5(n3314)* background for further characterization.

Protein interaction assays: For the GST pull-down experiments, GST fusion proteins were purified as described previously [S3]. Worm protein extracts were prepared using a mortar and pestle cooled in liquid nitrogen. Eluted proteins were separated on 4-20% Mini-PROTEAN TGX precast gels (Bio-Rad) and stained with SYPRO Ruby (Invitrogen). Mass spectrometry was performed by the Swanson Biotechnology Center at MIT. For the yeast two-hybrid assay, *vps-50* was cloned in vector pGBKT7, giving a fusion with the Gal4p DNA-binding domain (DBD), and *vha-15* was cloned into vector pGADT7, giving a fusion with the Gal4p activation domain (AD) (Clontech). Plasmids were transformed in strain pJ69-4a, and interaction was assayed by growth in the absence of histidine.

Subcellular fractionation: All buffers contained a protease inhibitor cocktail (Roche), and all procedures were performed on ice or at 4 °C. Subcellular fractionation was performed as described [S4, S5]. The cortexes collected from 2-month old male C57BL/6 mice or mouse primary cultured neurons were homogenized in 0.32 M sucrose and 4 mM HEPES (pH 7.4) and centrifuged at 1,000 g for 10 min to remove the nuclear pellet and debris. The supernatant (S1) was centrifuged at 10,000 g for 10 min to obtain a crude synaptosomal fraction (P2). The supernatant, cytosolic and microsomal fraction (S2) was centrifuged at 165,000 g for 2 hours to obtain the cytosolic supernatant (S3) and the microsomal fraction (P3). The crude synaptosomal fraction (P2) was lysed by hypo-osmotic shock and centrifuged at 25,000 g for 20 min to obtain the synaptosomal membrane fraction (LP1). The resulting supernatant synaptic vesicular and cytosolic fraction (LS1) was centrifuged at 165,000 g for 2 hours to obtain the synaptic vesicular membrane fraction (LP2) and the supernatant fraction (LS2).

Isolation of synaptic and dense-core vesicle fractions was performed using sucrose density gradient centrifugation. The synaptic vesicle fraction (LS1) was prepared from the cortex of adult male mice as described above and layered onto a sucrose gradient (0.6 M – 1.6 M) and centrifuged at 100,000 g for 2 hours at 4 °C. The 12 fractions were collected from the top and analyzed by western blotting.

Antibodies used were: mVPS50/CCDC132 (rabbit, Sigma), PSD-95 (mouse, NeuroMab), GluN1 (mouse, BD Biosciences), beta tubulin (rabbit, Abcam), beta actin (mouse, Sigma), clathrin heavy chain (mouse,

BD Biosciences), Chromogranin C (mouse, Abcam), synaptophysin (rabbit, Invitrogen and mouse, Sigma), V-ATPase V1 A subunit (rabbit, Proteintech), V-ATPase V1 B1/2 subunit (mouse, Santa Cruz) V-ATPase V1 H subunit (mouse, Santa Cruz). The secondary antibodies were: goat anti-mouse or anti-rabbit conjugated with HRP (Pierce and Jackson Immunoresearch).

Immunoblotting of *C. elegans* proteins: Proteins were extracted by heating animals in 1X loading buffer at 95 °C for 20 min. The soluble fraction was separated on an AnyKD Mini-PROTEAN TGX precast gel (Bio-Rad) and transferred to Hybond-ECL nitrocellulose (GE Healthcare). Membranes were incubated first with a monoclonal mouse anti-GFP antibody (1:1,000) (Roche) and second with goat anti-mouse-HRP antibody (1:10,000) (Sigma) for detection of FLP-3::Venus. Membranes were stripped and blotted with a polyclonal rabbit anti-RFP antibody (1:1,000) (Clontech) and second with goat anti-rabbit-HRP antibody (1:60,000) (Sigma) for detection of mCherry::SNB-1.

Construction of the lentiviral *mVps50* shRNA vector: The lentiviral shRNA plasmid pLL 3.7 (gift from Carlos Lois, University of Massachusetts, Worcester, MA) was modified to enhance neuronal expression of GFP or mCherry by replacing the CMV promoter with the human synapsin 1 promoter [S6, S7]. The following oligonucleotides encoding short hairpin RNAs (shRNAs) were inserted under the U6 promoter between HpaI and XhoI sites.

shRNA1:

tGCTTCCTCCTGTTCTCAATCTcgaaAGATTGAGAACAGGAGGAAGCttttttc

tcgagaaaaaaGCTTCCTCCTGTTCTCAATCTttcgAGATTGAGAACAGGAGGAAGCa

shRNA2:

tggCTATTACTTGTATGCCATATAcgaaTATATGGCATACAAGTAATAGttttttc

tcgagaaaaaaCTATTACTTGTATGCCATATAttcgTATATGGCATACAAGTAATAGcca

shRNA3:

tggATAGCATTGAACAAGTCTATTcgaaAATAGACTTGTTCAATGCTATttttttc

tcgagaaaaaaATAGCATTGAACAAGTCTATTttcgAATAGACTTGTTCAATGCTATcca

All three shRNAs were validated for *mVps50* knockdown efficiency, and shRNA1 and shRNA2 were used for further experiments.

Lentivirus Production: Lentiviruses were produced as previously described [S8]. Briefly, human embryonic kidney 293T (HEK 293T) cells were transfected using Lipofectamine 2000 (Invitrogen) with lentiviral shRNA plasmid, pCMV-dR8.91 plasmid and pCMV-VSV-G plasmid at 20, 15, and 10 µg of DNA per 15 cm plate. 48 hours after transfection, culture medium was collected and centrifuged at 2,000 g for 10 min. Supernatants were filtered through a 0.45-µm filter and centrifuged at 83,000 g for 1.5 hours, and the resulting pellets were resuspended in PBS. The titer of lentivirus was between 5×10^4 and 1×10^5 infectious units per µL.

SUPPLEMENTAL REFERENCES

[S1] Brenner, S. (1974). The genetics of *Caenorhabditis elegans*. Genetics *77*, 71–94.

[S2] Ranganathan, R., Sawin, E. R., Trent, C., and Horvitz, H. R. (2001). Mutations in the *Caenorhabditis elegans* serotonin reuptake transporter MOD-5 reveal serotonin-dependent and -independent activities of fluoxetine. J. Neurosci *21*, 5871–5884.

[S3] Paquin, N., Ménade, M., Poirier, G., Donato, D., Drouet, E., and Chartrand, P. (2007). Local activation of yeast *ASH1* mRNA translation through phosphorylation of Khd1p by the casein kinase Yck1p. Molecular Cell *26*, 795–809.

[S4] Huttner, W. B., Schiebler, W., Greengard, P., and Camilli, P. D. (1983). Synapsin I (protein I), a nerve terminal-specific phosphoprotein. III. Its association with synaptic vesicles studied in a highly purified synaptic vesicle preparation. J Cell Biol *96*, 1374–1388.

[S5] Dunah, A. W., and Standaert, D. G. (2001). Dopamine D1 receptor-dependent trafficking of striatal NMDA glutamate receptors to the postsynaptic membrane. J. Neurosci. *21*, 5546–5558.

[S6] Rubinson, D. A., Dillon, C. P., Kwiatkowski, A. V., Sievers, C., Yang, L., Kopinja, J., Rooney, D. L., Zhang, M., Ihrig, M. M., McManus, M. T., et al. (2003). A lentivirus-based system to functionally silence genes in primary mammalian cells, stem cells and transgenic mice by RNA interference. Nature Genetics *33*, 401–406.

[S7] Dittgen, T., Nimmerjahn, A., Komai, S., Licznerski, P., Waters, J., Margrie, T. W., Helmchen, F., Denk, W., Brecht, M., and Osten, P. (2004). Lentivirus-based genetic manipulations of cortical neurons and their optical and electrophysiological monitoring *in vivo*. PNAS *101*, 18206–18211.

[S8] Lois, C., Hong, E. J., Pease, S., Brown, E. J., and Baltimore, D. (2002). Germline transmission and tissue-specific expression of transgenes delivered by lentiviral vectors. Science *295*, 868–872.